Universidade do Minho
Escola de Engenharia

Cristina Correia

Engineering osteochondral tissues with human adipose tissue derived stem cells under precise biomechanical and biochemical *in vitro* environments

Janeiro de 2012

Engineering osteochondral tissues with human adipose tissue derived stem cells under precise biomechanical and biochemical *in vitro* environments
Cristina Correia
UMinho | 2012

Universidade do Minho
Escola de Engenharia

Cristina Correia

Engineering osteochondral tissues with human adipose tissue derived stem cells under precise biomechanical and biochemical *in vitro* environments

Tese de Doutoramento em Engenharia Biomédica

Trabalho realizado sob a orientação do
Professor Rui Luís Gonçalves dos Reis
e do
Doutor Rui Pedro Romero Amandi de Sousa

Janeiro de 2012

To Rui Duarte and my Family

What did you learn today?

A. Correia

Acknowledgments

People. Who challenged me to do better. Who brought out the best of me. Who reprehended me when I did wrong, and who complimented me for what I did right. Who taught me best in both cases.

For the past four years I was fortunate enough to have had extraordinary people who made this journey special, all achievements possible, and to whom I deeply acknowledge today.

Professor Rui L. Reis, my supervisor and mentor. Who provided me the opportunities and the freedom at his lab to explore my ideas, and to grow as a scientist. Professor Rui, thank you for being the example and inspiration for what is determination, ambition, conquer and stringency – the dimension and quality of 3B's are proof of these.

Doctor Rui A. Sousa, my co-supervisor and adviser. Who was always there, on daily basis. For the good and the bad. Who reminded me every now and then, not to crack under pressure! Thank you Rui for your scientific support and advice, for sharing your thoughts and perspectives, and for being tough on me whenever needed. Also, thank you for feeding my entrepreneurial enthusiasm, and for your friendship.

Professor Gordana Vunjak-Novakovic, my foreign supervisor and "scientific mother". Thank you for receiving me in your lab with arms wide open. Thank you for caring for my needs in both scientific and personal ways. With you and your lab I learned so much and matured. You are an extraordinary women, who I deeply admire.

To all three, I am limitlessly grateful for the opportunity to work and live in the prestigious Columbia University, among the best and the brightest, at the unstoppable New York City. I got impregnated in that city's life. I could have never loved it more. There, I was fortunate to meet extraordinary people:

Sarindr "Ick" Buhrimatana and Warren Grayson, I am so grateful to you for all the energy, time and patience you spent with me. For all the knowledge you shared. For caring. You were fundamental for all my achievements at the lab.

Darja Marolt, George Eng and Ryan Eton, thank you for supporting me whenever I struggled. Thank you for sharing your time, your ideas, your opinions, and your stories! Nebo, Jenny, Quentin, Ivan, Leo, Danny, Supansa, Shelby, Nina, Elisa, Yi, Xi, Jung, Petros, Jesse, Kacey and Mikail. In your own personal way, thanks for making each day at the lab, fun days, creative days, enjoyable days! I had a great time with all of you.

Professor David Kaplan and Professor Jeff Gimble, I am very grateful for your help with silk scaffolds and adipose stem cells. Besides providing me the tools to work, you also shared with me the time and knowledge, discussed issues, asked me the tough questions and made me grow as scientist. Thank you so much.

Financially, I want to thank the Portuguese Foundation for Science and Technology (FCT) for providing me the PhD grant (SFRH / BD / 42316 / 2007), as well as funding from the American National Institute of Health (NIH) for GVN's lab (DE161525 and EB02520), which allowed all this to happen.

At 3B's, I want to deeply acknowledge the amazing *lab rats* with whom I shared moments, either debating science, asking advices or helping to look for magnets, antibodies, or pipetors… either having a drink, playing soccer, running races, enjoying concerts or a step of dance… I most deeply thank you for your time, your joy, your energy, your smile, your wisdom, your care, your friendship and camaraderie.

To my wonderful friends Rita Duarte and Sofia Caridade, my deepest thanks for your strong friendship; for always being there for the rescue and relief on the worst moments, and for the hugs and smiles on the best! You are true friends!

Daniela Coutinho, Vitor Espirito Santo, Isa Monteiro and Ana Mendes – war companions!!! I am so grateful for having you there, making this battle easier to fight ☺ so many doubts, so many complaints… but also lots of jokes and good mood!

Yan, it was awesome working with you! Silk gave us some disappointments but we were relentless and achieved our goals! Thank you so much for all your help.

My special thanks to João Oliveira who was tireless on helping me giving my first steps in the lab, and Luísa Pereira, with whom I shared the ups and downs of adipose stem cell isolation – it was great working with you. Yet, I also want acknowledge so many bright people who were always available to clarify and discuss doubts, share knowledge, and help around in the lab – thank you: Ana Frias, Tírcia Santos, Rogério Pirraco, Mariana Cerqueira, Marta Silva, Rui Pereira, Ana Martins, Ana Rita Pinto, Helena Lima, Elena Popa, Silvia Mihaila, Pedro Carvalho, Albino Martins, Wojciech Szymczyk, Tommaso Rada, Dennis Link and Joana Correia.

Ana Leite, Miguel Oliveira, Vitor Correlo, Alexandra Marques and António Salgado, thank you for sharing your advices, knowledge and friendship.

To the technical office: Liliana, Cláudia, Adriano and Filipe, and lately Ana, thank you for being very professional and never failing on me for whatever and whenever I needed (and I know I must've been a pain at certain times). And the MT: Patrícia, Ana, Cristiana, Joana, Virgínia, Berta, Fátima, Ariana and Tânia – thank you for all the support on every bureaucratic issue, making paperwork easy to deal with.

I want to address my specific acknowledgments to Professor Nuno Neves and Hospital S. Marcos – Braga, for providing cartilage tissue, as well Doctor Emílio Valls and Clínica Luso-Espanhola – Porto, for providing lipoaspirate, used in my experiments.

To all co-authors and everyone who contributed (even the slightest!) for the successful experiments, published and submitted papers, oral and poster communications, my overwhelming acknowledgments.

Outside of the lab, I want thank my extraordinary friends for their vital friendship and support. My big thankful hug to *Marias* Diana, Patricia, Joana, Claudia, Hugo, Bruno, Rafael and Renatha, *NewYorkers* Neide, Raquel, Julie, Lamas and Ibrahim, and my long-lasting childhood friends Marisa, Filipe, Beta, Márcio and Doriza.

Last, but firstly, my family.

My eternal thanks to all my family at New York, for all you gave me during my stay – that year wouldn't have been as good without you. To my beloved grandparents who, among their ageing difficulties were vigorous on providing their support.

My mother and father, sisters Susana and Andrea and my brother John are my solid ground and pillars. Thank you, in your specific personal way, all the love and support you gave that made me who I am today.

Rui Duarte. My Love, to you I address my deepest acknowledgments. Thank you for your resilience and comprehension; thank you for being tireless and vigorous on supporting me throughout this long and winding road. Thank you for giving me the energy I needed. Thank you for your unconditional Love. To you I dedicate this thesis.

Engineering osteochondral tissues with human adipose tissue derived stem cells under precise biomechanical and biochemical *in vitro* environments

Abstract

With the continuous increase in life expectancy, health problems tend to arise, whereas joint ailments are among the most prevalent. The knee joint, in particular, is subjected to serious illnesses that range from articular cartilage injuries, osteochondral lesions and osteoarthritis. Joint pathologies globally affect population of all ages and gender, resulting in reduced quality of life due to limited activity and increased expenditures, either directly (treatment, private expenditure), or indirectly (lost productivity, lost earnings). In this context, the need for new therapies and products that could satisfy the growing clinical requirements will rise in the future. Tissue engineering and regenerative medicine, as a rapidly emerging field, is expected to provide valuable solutions.

Osteochondral lesions are articular cartilage lesions where the underlying bone is also damaged. A tissue engineering approach needs to address the cartilage component, composed by a hydrated soft tissue layer, and the bone compartment, composed by a stiff, complex and vascularized tissue.

In this thesis we propose complementary approaches to evolve current state of the art, and move a step further in the development of functional solutions for cartilage, bone and/or osteochondral regeneration. Our rationale was based on the use of human adipose stem cells (hASC) as a single cell source to engineer all tissue compartments, by taking advantage of its characteristics: 1) hASC have intrinsic capacity to differentiate into the chondrogenic, osteogenic and endothelial lineages; 2) hASC can be obtained from adipose tissue collected by dedicated or non-dedicated liposuction procedures, repeatedly and abundantly; 3) hASC are isolated by enzymatic digestion, yielding high cell number, which may avoid or minimize cell expansion. Furthermore, we explored the use of precise biomechanical and biochemical environments specific for each engineered tissue, in order to improve cell differentiation and matrix deposition. Specifically, hydrostatic pressure stimulation was employed for cartilage engineering, while flow perfusion and inherent shear stress were investigated in bone development context. In order to vascularize engineered bone, a specific spatio-temporal regulation of growth factors and cells were thoroughly explored.

To this end, five experimental studies were performed. The first studied focused on the development of two bioreactor devices aimed at generating hydrostatic pressure (HP) for dynamic culturing of cartilage tissue. We hypothesized that the formation of engineered cartilage could be augmented by applying such physiologic stimuli to chondrogenic cells (human nasal chondrocytes - HNC) or stem cells (human adipose stem cells - hASC), cultured in gellan gum hydrogels, by varying both frequency and magnitude of loading. In the HNC study, the best tissue development was achieved for pulsatile HP regimen, while in the hASC study, the best cartilage outcomes were obtained for physiologic loading (5 MPa), as evidenced by gene expression of aggrecan, collagen type II and sox-9, metachromatic staining of cartilage matrix and immunolocalization of collagens.

The next step aimed to evaluate the effects of scaffold architecture and biomechanics, in order to optimize silk scaffolds for bone tissue engineering. Silk scaffolds were fabricated using different solvents (aqueous vs. hexafluoro-2-propanol - HFIP), pore sizes (250-500μm vs. 500-1000μm) and structures (lamellar vs. spherical pores). Given the great potential of hASC for cell-based therapies and tissue engineering, in particular bone tissue, silk scaffold and hASCs are two promising components, which have not been previously investigated in combination. The porous HFIP silk scaffold with 400-600 μm pores performed better than any other scaffold, while the lamellar scaffolds performed better than spherical-pore scaffolds.

We further used this HFIP-silk scaffold as cell support for dynamic culturing studies, where the effects of pulsatile perfusion on *in vitro* bone expression by human adipose stem cells (hASCs) was assessed. We hypothesized that the formation of engineered bone could be augmented by replicating physiologic stimuli – pulsatile interstitial flow - to cells cultured in porous scaffolds using bioreactors with medium perfusion. This was confirmed, once the best tissue development was achieved for the sequence of 2 weeks of steady flow and 3 weeks of pulsatile flow, as evidenced by gene expression, construct compositions, histomorphologies and biomechanical properties.

Further challenge was to vascularize the engineered bone grafts. Even more demanding was to use the same cell source – hASC. From a clinical perspective, it would be ideal to engineer vascularized bone grafts starting from one single cell harvest obtained from the patient. We hypothesized that a sequential application of osteogenic and endothelial growth factors to hASC cultured on biomaterial scaffolds (HFIP-silk scaffold), with different timing of addition of fresh cells could support the development of bone-like tissue containing an integrated vascular

network. Three strategies were evaluated by changing spatio-temporal cues, but only one of the combinations, in particular the osteo-induction of hASC seeded to silk scaffold for 3 weeks, followed by addition of fibrin-encapsulated hASC to which vasculogenic cues were provided for 2 weeks, resulted in the most promising outcomes towards vascularized bone grafts.

The final experimental design focused on the development of an *in vitro* model for studies of heterotypic cellular interactions that couple blood vessel formation with osteogenesis by using human umbilical vein endothelial cells (HUVECs) and human bone marrow mesenchymal stem cells (hMSCs). In this study, we hypothesized that the sequential application of growth factors, to firstly induce the formation of stable vasculature and subsequently initiate osteogenic differentiation, could provide a biologically-inspired *in vitro* model of bone vascularization. Two important findings resulted from these studies: (*i*) vascular development needs to be induced prior to osteogenesis, and (*ii*) the addition of additional hMSCs at the osteogenic induction stage improves both tissue outcomes, and anastomosis of vascular networks with the host (SCID mice) vasculature.

Taken altogether, the results obtained during the accomplishment and completion of this thesis prove the successful use of human adipose stem cells for osteochondral tissue engineering, as mechanically responsive cell source, which, in combination with appropriate growth factors, generate both cartilage and bone compartments. Besides the success obtained with dynamic culturing, it was proven that hASC have great potential to be used as single cell source for the development of vascularized bone grafts.

Desenvolvimento de tecidos osteocondrais com células estaminais do tecido adiposo sob condições precisas de estimulação biomecânica e bioquímica

Resumo

Com o aumento contínuo da esperança média de vida, tem ocorrido um aumento progressivo de problemas de saúde, estando as doenças articulares entre as mais prevalentes. A articulação do joelho, em particular, está sujeita a doenças graves, que vão desde lesões focais da cartilagem articular, lesões osteocondrais e osteoartrite. As patologias do joelho afetam globalmente a população de todas as idades e género, resultando numa redução significativa da qualidade de vida devido às limitações de atividade, assim como devido a despesas acrescidas, seja direta (tratamento, despesas privadas), ou indiretamente (perda de produtividade, perda de lucros). Neste contexto, a necessidade de novas terapias e produtos que possam satisfazer as crescentes exigências clínicas tende a aumentar. A engenharia de tecidos e medicina regenerativa, como área em rápida expansão, é estimada que possa fornecer soluções valiosas.

As lesões osteocondrais são lesões da cartilagem articular onde o osso subjacente é também danificado. Numa abordagem de engenharia de tecidos seria necessário abordar tanto a componente da cartilagem, composto por uma camada de tecido mole altamente hidratado, como o compartimento ósseo, composto por um tecido rígido, complexo e vascularizado.

Nesta tese, propomos algumas abordagens para evoluir o estado da arte atual, assim como avançar um passo no desenvolvimento de soluções funcionais para o osso, cartilagem e / ou regeneração osteocondral. Para tal, usamos células estaminais humanas derivadas do tecido adiposo (TA) (hASC), como fonte celular única para a engenharia de todos os compartimentos do tecido, tirando partido das suas características: 1) as hASC têm capacidade intrínseca para se diferenciar nas linhagens condrogénica, osteogénica e endotelial, 2) as hASC podem ser obtidas de TA recolhido em cirurgia de lipoaspiração, em abundância e repetidamente; 3) as hASC são isoladas através de uma digestão enzimática fácil e rápida, resultando num elevado número de células, evitando ou minimizando a expansão celular. Adicionalmente, exploramos o uso de ambientes biomecânicos e bioquimicamente precisos e específicos para cada tecido a ser desenvolvido, de modo a melhorar a diferenciação celular e deposição de matriz. De forma específica, a estimulação através de pressão hidrostática foi utilizada para o desenvolvimento de cartilagem, enquanto a perfusão de fluxo e inerente tensão de corte foram

investigados no contexto do desenvolvimento ósseo. A fim de vascularizar o enxerto ósseo desenvolvido, foram exploradas condições específicas de regulação espaço-temporal de células e fatores de crescimento.

Para este propósito, cinco estudos experimentais foram realizados. O primeiro estudo focado no desenvolvimento de dois bioreatores visou gerar pressão hidrostática (HP) para a cultura dinâmica do tecido cartilaginoso. Consideramos como hipótese que a formação de cartilagem poderia ser aumentada através da aplicação de tais estímulos fisiológicos, tanto em células primárias (condrócitos) (septo nasal humano - HNC) ou células-estaminais (células estaminais do tecido adiposo humano - hASC), cultivadas em hidrogéis de goma gelana, variando a frequência e magnitude de carga. No estudo HNC, o melhor desenvolvimento de tecido foi conseguido para o regime de HP pulsátil, enquanto que no estudo hASC, os melhores resultados foram obtidos através da aplicação de níveis fisiológicos de HP (5 MPa), como evidenciado pela expressão genética de agrecano, colagénio tipo II e sox-9, assim como através da coloração metacromática da matriz da cartilagem e imunolocalização de colagénios.

O próximo passo pretendia avaliar os efeitos da arquitectura e propriedades biomecânicas de suportes, a fim de otimizar suportes de seda para a engenharia de tecido ósseo. Suportes de seda foram fabricados usando diferentes solventes (aquoso vs hexafluoro-2-propanol - HFIP), tamanhos de poros (250-500μm versus 500-1000μm) e estruturas (poros lamelar versus esférica). Dado o grande potencial de hASC para terapias celulares e engenharia de tecidos, em especial do tecido ósseo, os suportes de seda e hASC constituem dois componentes promissores, que ainda não foram previamente investigados em combinação. O suporte composto por seda-HFIP, com poros esféricos de 400-600 μm, demonstrou melhor desempenho do que qualquer outro suporte, enquanto os suportes com estrutura lamelar demonstraram melhor desempenho do que os suportes com poros esféricos.

Este suportes de seda-HFIP foram posteriormente utilizados para os estudos de cultura dinâmica, onde foram avaliados os efeitos da perfusão pulsátil sobre a expressão óssea por hASC. Consideramos como hipótese que a formação de osso poderia ser aumentada através da replicação de estímulos fisiológicos - fluxo intersticial pulsátil - para as células cultivadas em suportes porosos utilizando bioreatores com perfusão do meio de cultura. Esta hipótese foi confirmada, uma vez que o melhor desenvolvimento de tecido foi obtido para a sequência de 2

semanas de fluxo constante e 3 semanas de fluxo pulsátil, como evidenciado pela expressão genética, composição do enxerto, histomorfologias e propriedades biomecânicas.

O desafio seguinte consistia em vascularizar os enxertos ósseos desenvolvidos. Mais exigente foi o uso da mesma fonte celular - hASC. Numa perspectiva clínica, o ideal seria desenvolver enxertos ósseos vascularizados a partir de uma colheita celular única obtida do paciente. Consideramos como hipótese que uma aplicação sequencial de fatores de crescimento endoteliais e osteogénicos em hASC cultivadas em biomateriais (suportes de seda-HFIP), com diferentes períodos de adição de células frescas, poderia beneficiar o desenvolvimento de osso contendo uma rede vascular integrada. Três estratégias foram avaliadas mas apenas uma das combinações forneceu resultados promissores para o desenvolvimento de enxerto ósseo vascularizado, em particular a osteo-indução das hASC aderidas ao suporte de seda durante 3 semanas, seguido pela adição de hASC encapsuladas em fibrina, às quais foram fornecidas fatores vasculogénicos durante 2 semanas.

O desenho experimental final concentrou-se no desenvolvimento de um modelo *in vitro* para estudo de interações celulares heterotípicas que combinem formação de vasos sanguíneos com osteogénese, usando células endoteliais do cordão umbilical humano (HUVECs) e células-estaminais mesenquimatosas da medula óssea humana (hMSCs). Neste estudo, testamos a hipótese da aplicação sequencial de fatores de crescimento, em primeiro lugar, induzir a formação de vasos estáveis e, posteriormente, iniciar a diferenciação osteogénica, poder fornecer um modelo *in vitro* de vascularização óssea, biologicamente inspirado. Duas conclusões importantes resultaram deste estudo: (i) o desenvolvimento vascular necessita de ser induzida antes da osteogénese, e (ii) a adição de hMSCs adicionais na fase de indução osteogénica melhora os resultados do tecido, assim como a anastomose das redes vasculares com a vasculatura do animal recetor (ratinhos SCID).

Analisados em conjunto, os resultados obtidos durante a realização e conclusão desta tese provam o sucesso do uso de células estaminais do tecido adiposo humano para engenharia de tecidos osteocondrais, como fonte de células mecanicamente sensíveis às distintas forças de estimulação biomecânica, que, em combinação com os fatores de crescimento adequados, desenvolveram os compartimentos cartilagíneo e ósseo. Além do sucesso obtido com a cultura dinâmica, foi comprovado que as hASC apresentam grande potencial para serem utilizadas como fonte celular única para o crescimento de enxertos ósseos vascularizados.

Table of Contents

A

A/B	Antibiotic / Antimycotic
Abs	Absorbance
AC	Air Chamber
AC	Articular Cartilage
ACT	Autologous Chondrocyte Transplantation
Agrc	Aggrecan
ANOVA	ANalysis Of VAriance
AP	Alkaline Phosphatase
ASC	Adipose Stem Cells
AT	Adipose Tissue

B

bFGF	basic Fibroblast Growth Factor
BMP	Bone Morphogenic Protein
BMSC	Bone Marrow Stem Cell
BMPC	Bone Marrow Progenitor Cell
bp	Base pairs
BSP	Bone Sialoprotein
BV	Bone Volume
BV/TV	Bone Volume per Tissue Volume

C

Ca^{2+}	Calcium
CC	Culture Chamber
CCB	Concentric Cylinder Bioreactor
cDNA	complementary Deoxyribonucleic Acid
CFU-F	colony forming units-fibroblast
cm	centimeter
CO_2	Carbon Dioxide
Col I	Collagen type I
Col II	Collagen type II
COMP	Cartilage oligomeric matrix protein
CPBS	Chitosan-poly(butylene succinate)

D

DAB	3,3'-DiAminoBenzidine
DCB	Decellularized bone
DEPC	Diethylpyrocarbonate
DF	Dermal Fibroblasts
dH_2O	Distilled water
DMB	1,9-DimethylMethyleneBlue
DMEM	Dulbecco's Modified Eagle Medium
DNA	Deoxyribonucleic Acid
dsDNA	double stranded Deoxyribonucleic Acid
dyn/cm^2	Dyne per square centimeter

E

ECM	ExtraCellular Matrix
EDTA	Ethylenediaminetetraacetic acid
EGM	Endothelial Growth Media
ELB	Erythrocyte Lysis Buffer
EPC	Endothelial Progenitor Cell
ERK	Extracellular signal-regulated kinase
ESC	Embryonic Stem Cell
EthD-1	Ethidium homodimer-1

F

FBS	Fetal Bovine Serum
FEC	Fetal Epiphyseal Cartilage

G

g	Centrigual force
g/mL	gram per milliliter
GAG	Glycosaminoglycan

GAPDH	glyceraldehyde-3-phosphate dehydrogenase
GE	Gene expression
GEA ID	Gene expression assay identification
GF	Growth Factor
GG	Gellan gum
GPa	Giga Pascal

H

h	hour
HA	Hydroxyapatite
HA	Hyaluronic Acid / Hyaluronan
HAS	Hyaluronan Synthase
hASC	human Adipose Stem Cell
HDMEC	Human Dermal Microvascular Endothelial Cells
HHPB	High Hydrostatic Pressure Bioreactor
hMSC	human Mesenchymal Stem Cell
H&E	Hematoxylin & Eosin
H_2O	Water
H_2O_2	Hydrogen peroxide
HCl	Hydrochloric acid
HEPES	(4-(2-hydroxyethyl)-1-piperazineethanesulfonic acid)
HFIP	Hexafluoro-2-propanol
HNC	Human Nasal Chondrocytes
HOP	Human OsteoProgenitors
HP	Hydrostatic Pressure
HPB	Hydrostatic Pressure Bioreactor
HUVEC	Human Umbilical Vein Endothelial Cells
Hz	Hertz

I

i.d.	inner diameter
IGF	Insulin Growth Factor
IHC	ImmunoHistoChemistry
IL-1ß	Interleukin-1 beta
ITS	Insulin, human Transferrin, and Selenous acid

J

JWR	Japanese White Rabbits

K

kDa	Kilo Daltons

L

LHPB	Low Hydrostatic Pressure Bioreactor
LiBr	Lithium bromide

M

m	meter
M	Molar
M199	Culture medium
MC	Meniscal Cells
µCT	micro Computed Tomography
µg	micrograms
µg/mL	microgram per milliliter
µL	microliter
µm/s	micrometers per second
mg	milligrams
mg/kg	milligram per kilogram
mg/mL	milligram per milliliter
mg/mm^3	milligram per cubic millimeter
min	Minutes
mL	milliliter
mM	milli Molar
mm	millimeter
MMA	Methyl-methacrylate
MPa	Mega Pascal
mRNA	messenger Ribonucleic Acid

MSC	Mesenchymal Stem Cells
MTS	Mechanical Testing System
MTS	3-(4,5-dimethylthiazol-2-yl)-5(3-carboxymethoxyphenyl)-2(4-sulfofenyl)-2H-tetrazolium

N

n	total number of data points
N	Normal (concentration)
n/a	not applicable
Na_2CO_3	Sodium carbonate
NaCl	Sodium Chloride
NaCl	Sodium Chloride
NaOH	Sodium Hydroxide
NC	Nasal Cartilage
ng	nanogram
ng/mL	nanogram per milliliter
NHS	Normal Horse Serum
nm	nanometer
NO	Nitric Oxide
NOD	Nonobese diabetic

O

ºC	Degree Celsius
Ob	Osteoblasts
OC	Osteoarthritic chondrocytes
OC	Osteochondral
OCN	Osteocalcin
OCPC	Ortho-cresolphthalein complexone
OD	Optical Density
OM	Osteogenic Media
OPN	Osteopontin

P

p	probability value
PBS	Phosphate Buffer Saline
PBT	Poly(butylene terephthalate)
PDMS	Polydimethylsiloxane
PDS	Polydioxanon
PEG	Poly(ethylene glycol)
PEGT	Poly(ethylene glycol terephthalate)
Pen/Strep	Penincilin/Streptomicin
PF	Pulsatile Flow
PG	Proteoglycans
PGA	Poly(Glycolic Acid)
PGE_2	Prostaglandin E2
PGE_2S	Prostaglandin E2 synthase
PHP	Pulsatile Hydrostatic Pressure
PLC	Programmable Logic Computer
PLCL	Poly(lactic-co-ε-caprolactone)
PLGA	Poly(lactic-co-glycolic acid)
PLLA	Poly(L-lactic acid)
PMMA	Poly(methyl methacrylate)
pNPP	p-nitrophenyl phosphate
PRG4	Proteoglycan 4

Q

qRT-PCR	quantitative Reverse Transcription Polymerase Chain Reaction

R

RNA	Ribonucleic Acid
rpm	Rotations per minute
RSB	Rotating Shaft Bioreactor
RT	Room Temperature

S

SCID	Severe Combined ImmunoDeficiency
sec	seconds
SEM	Scanning Electron Microscopy
SF	Silk fibroin
SF	Skin Fibroblasts

SF	Spinner Flask
SF	Steady Flow
sGAG	sulphated Glycosaminoglycan
SHP	Steady Hydrostatic Pressure
Sox-9	SRY (sex determining region Y)-box 9
SPC	Synovium-derived progenitor cells
SS	Stainless Steel
SVF	Stromal Vascular Fraction
SZP	Superficial Zone Protein

T

TCA	TriChloroacetic Acid
T-CUP	Tissue Culture Under Perfusion
TGF-ß	Transforming growth factor beta
TIMP-3	Tissue inhibitor metalloproteinase-3
TE	Tissue Engineering
TERM	Tissue Engineering and Regenerative Medicine
TV	Tissue Volume

U

U/mL	Units per milliliter
UV	Ultra Violet

V

VEGF	Vascular endothelial growth factor
VOI	Volume of Interest
v/v	volume per volume
vWF	von Willebrand Factor

W

wt	Weight
w/v	weight per volume
w/w	wet weight
WWB	Wavy Wall Bioreactor

List of Figures

List of Tables

Short Curriculum vitae

Cristina Correia was born on July 25th 1985 at Miami, USA. She moved to Portugal at the age of eight, and was raised at Vila Verde, Braga.

From 2003-2007 Cristina studied Applied Biology at University of Minho, graduating with a final grade of 16 (0-20). As her senior research internship she developed the project entitled "Design and construction of new expression vector to clone and produce genetically engineered biomaterials based on the sequence of elastin and silk fibroin", at the Biology Departament of University of Minho, under the supervision of Margarida Casal, PhD., concluding with a final grade of 18 (0-20).

At January 2008 she started her PhD program in Biomedical Engineering at the 3B's Research Group, University of Minho, under supervision of Professor Rui L. Reis and co-supervision of Rui Amandi de Sousa. Her research project focuses on osteochondral tissue engineering using adipose stem cells and dynamic culturing. Under the scope of this project, she developed research work in collaboration with Professor Gordana Vunjak-Novakovic at the Laboratory for Stem Cells and Tissue Engineering, Columbia University – New York, USA, for 13 months (January 2010 - February 2011).

During her PhD project, Cristina has acquired good knowledge and experience with cell isolation, culture and characterization of primary cells, such as chondrocytes and umbilical vein endothelial cells, as well as stem cells from different sources, such as bone marrow and adipose tissue. She developed and worked with several bioreactors for cartilage and bone tissue engineering, therefore has gathered great skills on dynamic culturing of cell-scaffold constructs.

She has participated in several teams for preparation of grant proposals, both at National level – Portuguese Foundation for Science and Technology (FCT) and National Strategic Reference Framework (QREN); and European level - Framework Programme VII (FP7).

As a result of her research work, Cristina attended several of the most important international conferences in the field of Biomaterials, Tissue Engineering and Regenerative Medicine with oral communications (4) and poster presentations (7). Presently, she is the first author of 7 papers in international journals.

List of Publications

The work performed during this PhD work resulted in the following publications:

INTERNATIONAL JOURNALS WITH REFEREE

1. Correia C, Pedro AJ, Oliveira JT, Sousa RA and Reis RL, 2008, *Hydrostatic pressure culture system for human chondrocyte cultivation and stimulation in gellan gum hydrogel disks*, Tissue Engineering Part A, 14 (5): 860-861

2. Correia C, Grayson WL, Park M, Hutton D, Zhou B, Guo XE, Niklason L, Sousa RA, Reis RL and Vunjak-Novakovic G, 2011, *In vitro model of vascularized bone: synergizing vascular development and osteogenesis*, PLoS ONE, 6(12): e28352.

3. Correia C, Grayson WL, Eton R, Gimble JM, Sousa RA, Reis RL, Vunjak-Novakovic G, 2011, *Human adipose stem cells can serve as a single cell source for the in vitro cultivation of vascularized bone grafts,* Journal of Tissue Engineering and Regenerative Medicine – in press.

4. Correia C, Bhumiratana S, Yan LP, Oliveira AL, Gimble JM, Rockwood D, Kaplan DL, Sousa RA, Reis RL, Vunjak-Novakovic G, 2011, *Development of silk-based scaffolds for tissue engineering of bone from human adipose derived stem cells* - submitted.

5. Correia C, Bhumiratana S, Sousa RA, Reis RL, Vunjak-Novakovic G, 2011, *Sequential application of steady and pulsatile medium perfusion enhanced the formation of engineered bone* - submitted.

6. Correia C, Pereira AL, Duarte ARC, Pedro AJ, Frias AM, Oliveira JT, Sousa RA and Reis RL, 2011, *Dynamic culturing of cartilage tissue: the significance of hydrostatic pressure* - submitted.

7. Correia C, Sousa RA and Reis RL, 2011, *Dynamic culturing for cartilage tissue engineering: a retrospective analysis* - submitted.

8. Correia C, Sousa RA and Reis RL, 2011, *Engineering bone: current considerations* - submitted.

9. Yan LP, Silva-Correia J, Correia C, Caridade SG, Fernandes EM, Mano JF, Oliveira JM, Oliveira AL, Reis RL, 2011, *Macro/micro Porous Silk Fibroin/Nano-sized Calcium Phosphate Scaffolds for Bone Tissue Engineering Applications,* Acta Biomaterialia (2011), 8(1):289-301

NATIONAL AND INTERNATIONAL CONFERENCES

Oral Communications

1. Correia C, Bhumiratana S, Yan LP, Oliveira AL, Gimble JM, Rockwood D, Kaplan DL, Sousa RA, Reis RL and Vunjak-Novakovic G, *Development of silk-based scaffolds for tissue engineering of bone from human adipose derived stem cells*, 9th International Symposium on Frontiers in Biomedical Polymers, Funchal, Portugal, May 2011

2. Correia C, Grayson WL, Park M, Hutton D, Guo XE, Niklason L, Sousa RA, Reis RL and Vunjak-Novakovic G, *Co-operative induction of vascular and osteogenic lineages in engineered bone grafts*, TERMIS-EU 2011, Granada, Spain, June 2011

3. Correia C, Bhumiratana S, Sousa RA, Vunjak-Novakovic G and Reis RL, *Engineering osteochondral tissue by human adipose stem cells using biomechanical and biochemical stimuli*, 2011 School of Engineering Week - University of Minho, Guimarães, Portugal, October 2011

4. Correia C, Sousa RA, Reis RL*, Co-cultures and dynamic culture of cells*, 2nd 3B's symposium on biomaterials and stem cells in regenerative medicine, AvePark – Guimarães, Portugal, January 2012

5. Correia C, Sousa RA, Reis RL, *MACI: State of the art,* 2nd National Meeting of Orthopaedic Services, Cartilage: Lesions and treatments, Guimarães, Portugal, March 2012

Poster Presentations

1. Correia C, Pedro AJ, Oliveira JT, Sousa RA and Reis RL, Hydrostatic pressure culture system for human chondrocyte cultivation and stimulation in gellan gum hydrogel disks, TERMIS-EU 2008, Porto, Portugal, June 2008

2. Correia C, Deus FD, Pedro AJ, Oliveira JT, Sousa RA and Reis RL, *A Cartilage Tissue Engineering perspective: The effect of hydrostatic pressure and flow perfusion on ATDC-5 proliferation and ECM deposition using soft and semi-rigid scaffolds*, R&D day of University of Minho's School of Engineering week, Guimarães, Portugal, October 2008

3. Correia C, Deus FD, Pedro AJ, Oliveira JT, Sousa RA and Reis RL, *Chondrogenic cell line differentiation using soft and semi-rigid scaffolds under hydrostatic pressure and perfusion stimuli*, InVENTScience - 6th Marie Curie Cutting Edge InVENTS Conference on Stem cells: from the Petri dish to the clinical application, Alvor, Portugal, October 2008

4. Correia C, Sousa RA and Reis RL, *The effect of hydrostatic pressure on cartilage development*, R&D day of University of Minho's School of Engineering week, Guimarães, Portugal, October 2009

5. Correia C, Sousa RA, Reis RL and Vunjak-Novakovic G, *Human adipose derived cells can serve as a single cell source for the in vitro cultivation of vascularized bone grafts*, Aegean Conferences - 4th International Conference on Tissue Engineering, Chania, Greece, May 2011

6. Correia C, Bhumiratana S, Sousa RA, Reis RL and Vunjak-Novakovic G, *Pulsatile fluid flow enhances engineered bone development by human adipose derived stem cells*, 4th Joint ESAO-IFAO Congress 2011, Porto, Portugal, October 2011

7. Correia C, Bhumiratana S, Sousa RA, Vunjak-Novakovic G and Reis RL, *Engineering osteochondral tissue by human adipose stem cells using biomechanical and biochemical stimuli*, 2011 School of Engineering Week - University of Minho, Guimarães, Portugal, October 2011

8. Yan LP, Silva-Correia J, Correia C, Caridade SG, Oliveira JM, Oliveira AL, Mano JF and Reis RL, Characterization and cytotoxicity of macro/micro porous silk and silk/nano-CaP scaffolds for bone tissue engineering applications, The 9th World Biomaterials Congress, Chengdu, China, June 2012

Awards and Recognitions

1. Best Oral Communication

   Correia C, Bhumiratana S, Sousa RA, Vunjak-Novakovic G and Reis RL, *Engineering osteochondral tissue by human adipose stem cells using biomechanical and biochemical stimuli*, 2011 School of Engineering Week - University of Minho, Guimarães, Portugal, October 2011

2. Peer Nomination and Finalist

   PAPS-LBC Leadership Award 2010 - Portuguese American Post-Graduate Society – Leadership Business Consulting - Leadership Award, New York, USA, April 2011

The present thesis is divided in six sections and nine chapters. The first section is composed of two review papers, gathering relevant bibliographic references and significant research done in osteochondral tissue engineering while positioning the work developed in this thesis among current state-of-the-art. The second section explains the materials and methods used for experimental work described in further sections three, four and five. Finally, the major conclusions achieved within this thesis are addressed in section six. A brief description of each section is summarized below:

Section 1.

Chapter I is composed by a comprehensive review paper where dynamic culturing is thoroughly explored in the context of cartilage tissue engineering. Besides focusing on the improvement of cartilage tissue outcomes by dynamic culturing, this review also explores the mechanisms by which stem cells and primary cells respond to distinct biomechanical forces, and how these forces are applied to tissue engineered constructs through appropriate bioreactor devices. Shear stress, direct or indirect compression, flow perfusion and the generation of hydrostatic pressure are the forces of biomechanical interest for the development of cartilage tissues with adequate properties, and therefore explored in this review.

Chapter II contains a concise review of the most recent achievements on tissue engineering of bone, with specific highlights on major outcomes attained by dynamic culturing with flow perfusion, as major force governing osteocyte mechanotransduction. Mechanisms of mechanotransduction and mechanobiology of bone are also addressed. Furthermore, insights on latest findings regarding vascularization of bone are discussed.

Section 2.

Chapter III explains in great detail all materials and methods used in the experimental work described in further sections of this thesis.

Section 3.

Chapter IV presents the design and validation of two bioreactor devices for dynamic culturing of cartilage tissue, by generation of hydrostatic pressure (HP). The response of human nasal chondrocytes (HNC) and human adipose stem cells (hASC) to such physiologic

stimuli was addressed. Cells were encapsulated in gellan gum hydrogels, and cultured in distinct regimens of loading frequency and magnitude.

Section 4.

Chapter V describes the performance of silk scaffolds for bone tissue engineering by human adipose stem cells. Different pore sizes and pore structure, as well as two types of solvents were tested, resulting in distinct scaffold architecture and biomechanics. hASC osteogenic differentiation and bone-tissue outcomes were evaluated.

Chapter VI reports major findings regarding the effects of pulsatile perfusion on bone development by human adipose stem cells (hASCs) cultivated on the HFIP-silk scaffold selected from previous study. Sequence application of steady and pulsatile flows were tested in order to understand the importance of osteogenic pre-differentiation of hASC to respond to the proposed mechanical stimulation.

Section 5.

Chapter VII demonstrates the potential of hASC as single cell source for the development of vascularized bone grafts. Three major strategies, and seven experimental groups were evaluated by changing location and timing of construct nourishment with cells and growth factors.

Chapter VIII describes a co-culture study using human umbilical vein endothelial cells (HUVECs) and human bone marrow mesenchymal stem cells (hMSCs) for growth of vascularized bone *in vitro*, and further validation by anastomosis of engineered networks with SCID mice vasculature.

Section 6.

Chapter IX highlights major conclusions and future perspectives regarding the set of studies presented in this thesis. More than addressing a complete analysis of the progress beyond state-of-the-art, future perspectives are provided regarding osteochondral tissue engineering and the exploitation of adipose stem cells in this context.

Section 1.

CHAPTER I

Dynamic culturing for cartilage tissue engineering: a retrospective analysis

---

This chapter is based on the following publication: Correia C, Sousa RA and Reis RL, 2011, *Dynamic culturing for cartilage tissue engineering: a retrospective analysis* - submitted.

Abstract

Clinical experience has demonstrated with clear evidence that excessive loading may significantly contribute to joint wear, while controlled loading is a requirement for healthy cartilage growth and maintenance. The high incidence of joint injuries in addition with the very low capacity of cartilage self-repair, leads to major potential applications for cartilage tissue engineering. Through the past decades, tissue engineering research has advanced from standard static culturing towards the development of new tools aiming to mimic the dynamic biomechanical processes that occur at articular cartilage *in vivo*.

Tensile and shear forces, direct or indirect compression, flow perfusion or the generation of hydrostatic pressure are forces of biomechanical interest to be generated in bioreactor devices, for the development of cartilage tissues with adequate properties. In this regard, high quality research has been made to understand how cells respond to mechanical stimulation, and in which manner can these forces be used to enhance cell proliferation, increase extracellular matrix deposition, or even to tune mesenchymal stem cell differentiation towards the chondrogenic lineage. This review intends to provide a retrospective critical analysis of the overall output obtained through the triangle relationship between cells, scaffolds and bioreactor devices.

1. INTRODUCTION

It has been extensively stated that joint ailments are a major health drawback affecting population worldwide that are age-wide and lifetime enduring. Traumatic injuries, degenerative or rheumatic diseases are the main causes of these ailments. Analyzing United States statistics at 2005, we can see that between the age of 18 and 64, fractures or joint injury are responsible for 10-20‰ of activity limitation, and arthritis or other musculoskeletal disease are responsible for 20, 58 and 98‰ of limitation among 18-44, 45-54 and 55-64 years old, respectively [1]. Most articular cartilage defects are caused by trauma, which can occur by a single impact or repeated micro trauma [2]. On the other hand, degenerative or rheumatic diseases are the main causes of joints cartilage degradation. Arthritis is a complex disorder that comprises more than 100 different disease patterns [3] and can affect people at any stage of life. It is characterized by inflammation of one or more joints [4], which consequently results in stiffness, swelling and persistent joint pain, including hip, knee, ankle, shoulder, elbow, hand or wrist joint pain. In addition to the patients' reduced quality of life, the socio-economic

consequences of arthritic diseases (incapacity to work and early retirement), together with health care costs, are noticeably high [5].

However, currently no therapeutic approach have experienced wide clinical acceptance. The successful outcome of the treatment, which ideally should be the formation of a durable repair tissue that provides symptomatic relief and allows for normal physical activity, depends highly on the exact nature of the cartilage defect, such as size, location and associated pathologies. On what concerns knee articular cartilage, there are currently several surgical treatment approaches, namely arthroscopic lavage and debridement [6, 7]; microfracture [7-10] and mosaicplasty [11-14]. However, in a best-case scenario these approaches render only a temporary effect, being their long time therapeutic effect still questionable. Autologous chondrocyte transplantation (ACT) represented the first generation cell based therapy for cartilage repair [15-17]. However, even this therapy presents several performance drawbacks [18-21], and is not available for osteoarthritic patients. New and better solutions are clearly needed to repair cartilage tissue defects.

Among the three major types of cartilage present in the human body, articular cartilage (AC) is the one found in most synarthroidal and diarthroidal joints. Due to the specific cartilage composition and structure, firstly characterized as a hypocellular connective tissue with complete lack of blood vessels, lymphatic vessels, and neurons, which normally nourish other parts of the body, cartilage is not able to regenerate when injured [22, 23]. Focusing on this minimal healing capacity, cartilage repair is undoubtedly a potentially significant application field for Tissue Engineering.

It is well known that articular cartilage is affected *in vivo* as well as *in vitro* by several, very distinct, biomechanical forces that are responsible to maintain its structure and function. These include tensile or shear forces [24-26], fluid perfusion, compression [27-29] or hydrostatic pressurization, which is known to be the predominant mechanical signal governing normal articular cartilage [30-33] The application of mechanical stimuli to foster tissue development during culturing, as a complement to the use of growth factors solely, is a scientific and experimental challenge. In this regard, bioreactor devices have been developed in order to construct functional cartilage tissues. In this domain, extensive research has been performed in order to overcome the research-scale product designs and to dynamically engineer reproducible, safe and economically competitive *ex vivo* biologically functional tissues. In a cartilage tissue engineering approach, bioreactors, yet, form only one of the vertices of a very strict triangle relationship, of which cells and scaffolds constitute the remaining two.

Fundamental studies have predominantly evaluated bovine articular explants or isolated chondrocytes, while more recent studies have evaluated normal or osteoarthritic human chondrocytes' response to load under distinct protocols of load amplitude, frequency and duration. Biomechanical stimuli have also been applied to adult stem cells, namely bone marrow mesenchymal stem cells, with the aim of tailoring these multipotent cells into the chondrogenic lineage.

This review addresses the use of bioreactors in the context of cartilage tissue engineering, with special emphasis to dynamic culturing of cells using three-dimensional (3D) scaffolds under different biomechanical contexts.

2. CARTILAGE BIOLOGY

Three major types of cartilage are found in the human body [34]: elastic cartilage, fibrocartilage and hyaline cartilage. Their differences reside essentially in the structure and biochemical composition of their extracellular matrix (ECM). These characteristics result in diverse mechanical properties and physical occurrences within the body [22, 34].

Hyaline cartilage is the most widespread cartilage in the human body. Macroscopically it appears as a white and slightly bluish tissue with a smooth surface, which can be found in the nose, the trachea, bronchi and most joints (synarthrodial and diarthrodial joints) [23, 35, 36]. In synchondroidal joints, it builds up a continuous connection between bones, e.g., between the ribs and sternum, in the intervertebral discs, or in the epiphyseal junction of the femur. In diarthrodial joints, hyaline cartilage covers the contact zones of two interlocked bones, where it functions to transmit high stresses generated in these joints and is so-called articular cartilage [22]. *Articular cartilage* (AC) is the most common and well-studied hyaline cartilage. It appears as a hydrated soft tissue layer with a thickness of 0.5 to 5 mm covering the ends of all synovial joints (ankle, knee, hip, shoulder, elbow, wrist, and finger) [37]. It has four important roles: 1) to transmit compressive forces across the joint; 2) to allow motion in the joint with minimal friction and wear; 3) to redistribute contact stresses over a larger area and 4) to protect the underlying bone. AC is constituted by a well organized biphasic system. The liquid phase is comprised by water and electrolytes, and ranges 80% of wet weight, while the solid phase is constituted both by cellular and acellular components that give rise to a porous-permeable composite material. This solid phase is organized at a well-defined multi-scale, hierarchical level [37]:

Micro-scale 10^{-7}-10^{-4} m: at this level, chondrocytes occupy 2% of the total volume. These singular cells synthesize and secrete extracellular matrix (ECM) which by itself occupies 20% wet weight of the acellular fraction;

Ultra-scale 10^{-8}-10^{-6} m: Collagen molecules are the major participants at this scale, accounting for 50–80% of the dry weight of articular cartilage [37]. Among all types of collagen, type II accounts for 90-95% of total collagen found in AC. It is displaced in a three-dimensional arrangement, forming fibrils, which non-covalently immobilizes the highly hydrated, negatively charged, proteoglycans (PGs) aggrecan and versican [36].

Nano-scale 10^{-10}-10^{-9} m: Glycosaminoglycans (GAGs) chains participate at this level. Chondroitin sulfate and keratan sulfate are covalently attached to the aggrecan protein backbone. Additionally at this nano-scale, ions such as Na^+, Ca^{2+}, SO_3^-, COO^- are responsible for AC swelling, for governing osmotic pressure of cartilage, and consequently contribute for its compressive stiffness [37].

3. MECHANOBIOLOGY OF ARTICULAR CARTILAGE (AC)

AC comprises a specific structure which outcomes in unique functional and mechanical properties (table I) [37-39]. Movement between two bones occurs with minimal friction and wear. The joint surfaces have remarkably low coefficients of friction - it has been reported to range from 0.005 to 0.04 in some joints, which allow the surfaces to glide over each other smoothly [37]. Cartilage is capable of distributing load over its surface, halving contact stresses, therefore assuring stability and functioning of the joint. Furthermore, cartilage is an anisotropic tissue [31, 40] and well suited to withstand demanding loads, responding to load in a viscoelastic manner [41, 42], by varying its stiffness according to the imposed strain rate [37]. This outstanding load-bearing capacity of articular cartilage is mainly assured by its extracellular structure, making it possible to withstand loads up to 10 times the body weight [31, 37]. Collagen type II is an important protein on what concerns stiffness and strength of AC [43]. Collagen fibers, composed by three α-helix chains, include intermolecular crosslinks which contribute for the tensile strength of collagen fibrils [44]. On the other hand, collagen type IX mediates the inter-fibrillar connections by covalent linkages to the surface of collagen type II fibril [45]. Collagen type IX is, in addition to collagen type II, a marker for differentiated chondrocytes, and, a requirement for a mechanically functional extracellular network [46]. Proteoglycans provide compressive stiffness to the tissue while their highly negatively charged glycosaminoglycans chains afford ACs' swelling capacity [37].

Table I – Mechanical performance of articular cartilage extracellular matrix. Compiled from references [37-39]

MECHANICAL FEATURES	RANGE VALUE
Compressive modulus	< 1.5 MPa
Shear modulus	< 0.5 MPa
Tensile equilibrium modulus	1- 18 MPa
Permeability coefficient	10^{14} - 10^{15} $m^4/N.s$
Poisson's ratio	0 - 0.42

At joints, such as the hip or the knee, AC is subjected to intermittent cyclic stress that can either be compressive or shear (Figure 1). Compressive stress is supported by the incompressible fluid component, where water is driven out on loading. On the opposite, shear load is supported by the matrix network and results deformation. An excessive shear stress can result in cartilage degradation through the disruption of the cartilage fiber network, which results in wear and fibrillation. Intermittent hydrostatic pressure is so essential for cartilage homeostasis that joint immobilization or decreased loading results in cartilage thinning. Since 95% of total applied joint load is supported by interstitial fluid pressurization, hydrostatic pressure is a fundamental mechanical stimulus governing the normal functioning articular cartilage (Figure 1) [37].

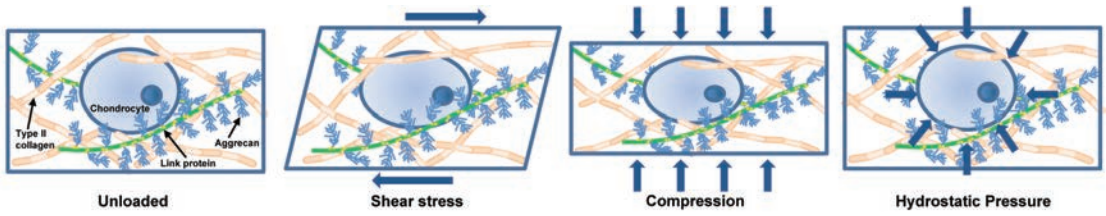

Figure 1 – Basic forces acting on articular cartilage during loading. Adapted from [37]

4. CELL MECHANOTRANSDUCTION

State of the art knowledge makes obvious the influence of mechanical forces on cartilage and chondrocyte metabolism. However, the underlying machinery by which cells sense and respond under the influence of mechanical signal is, to a certain extent, still concealed. Nevertheless, within this process, five players have been identified [27, 47-52]:

a) Physicochemical Effects – Under load, cartilage suffers deformation to some extent, which activate a host of changes in extracellular matrix. Some effects created during cartilage loading include increased interstitial fluid flow, electrical potential variation, increased osmotic pressure, and decreased pH [27, 47].
b) Ion Pumps and Channels - Signal transduction occurs by the flow of ions into and out of the cell. Intracellular Ca^{2+} waves and stretch-activated Ca^{2+} channels in the plasma membrane have been implicated in several studies of chondrocyte mechanotransduction [48, 49].
c) Integrins - Cell-matrix interactions are strictly mediated by integrins. They are exceptionally positioned to act as cellular mechanosensors, performing as the primary bridge between the ECM and the actin cytoskeleton [50].
d) Cytoskeleton - When subjected to load, the cytoskeleton, a potential force transducer in cells, can undergo numerous changes due to its structural role. These changes include deformation, reorganization, assembly, and disassembly. Additionally, it has been reported that the levels of actin, vimentin, and tubulin vary along separate regions in cartilage, which may somehow be correlated to the distinct load distribution across the tissue [51, 52].
e) Nuclear Deformation - Deformation of nuclei may be a pathway for transducing mechanical signalling into changes in gene expression. Upon deformation of the nucleus, the nuclear pore complex may be physically modified, or change the accessibility of genomic DNA for transcription [50].

Understanding these complex mechanotransduction pathways by which chondrocytes interpret and respond to load is of critical importance for cartilage tissue engineers who are currently attempting to develop mechanically functional tissues through dynamic cell culturing.

5. ENGINEERING CARTILAGE TISSUE BY DYNAMIC CULTURING

In tissue engineering, different bioreactors [53-56] have been developed in order to provide control over the physicochemical culturing parameters during cell or tissue culture. These devices are intended to standardize and automate the major processes of cell culturing, and to provide a solid basis for subsequent scaling-up into clinical applications. In the scope of cartilage tissue engineering, two important features are important during the development of a bioreactor:

1- To assure high nutrient transport and to provide an adequate hydrodynamic environment in order to accelerate and improve the *in vitro* growth of the tissue*;*
2- To mimic the biomechanical environment experienced by cartilage *in vivo* that results from the motion of joints and the forces resulting from surrounding muscles and tendons, in order to promote chondrocyte differentiation and tissue maturation.

By recognizing the importance of these parameters in cartilage tissue engineering, the so-called dynamic culturing has been developed leading to a significant advantage when compared with static culturing. In the last years, a great number of studies have explored the effects of different types of forces exerted over articular cartilage during joint movement, including shear stress, direct and indirect compression, flow perfusion or hydrostatic pressure. The experimental design of these studies vary extensively regarding the force parameters applied (duration, magnitude and frequency), the type of specimen employed such as the use of explants or isolated cells, the anatomic provenience of such cells and lately the use of three-dimensional supports for cell attachment and growth, i.e., scaffolds.

This review attempts to cover the advances in dynamic cell culturing in the context of cartilage tissue engineering during the last years. For this, a dynamic bibliographic search was performed using *ISI Web of Knowledge*^{SM} (Thomson Reuters, USA) and *Scopus* (Elsevier, The Netherlands) databases. Taking into account the tissue engineering perspective given to this review, emphasis was given to studies based on the combined use of bioreactors with tissue engineering scaffolds, in detriment of experimental studies focusing solely on the effects of mechanical stimuli over tissue explants or cell monolayers.

When analyzing the different types of mechanical stimuli investigated, it is possible to detect a trend in terms of experimental investigation. Figure 2 displays the research data published since 1993 by type of mechanical stimuli investigated (shear, perfusion, compression and hydrostatic pressure). The noticeable trend in the figure is the progressive importance of studies aimed at understanding the effect of stimuli such as compression, flow perfusion and shear stress in chondrocyte mechanotransduction and mechanosensation, as opposed to studies focusing on hydrostatic pressure.

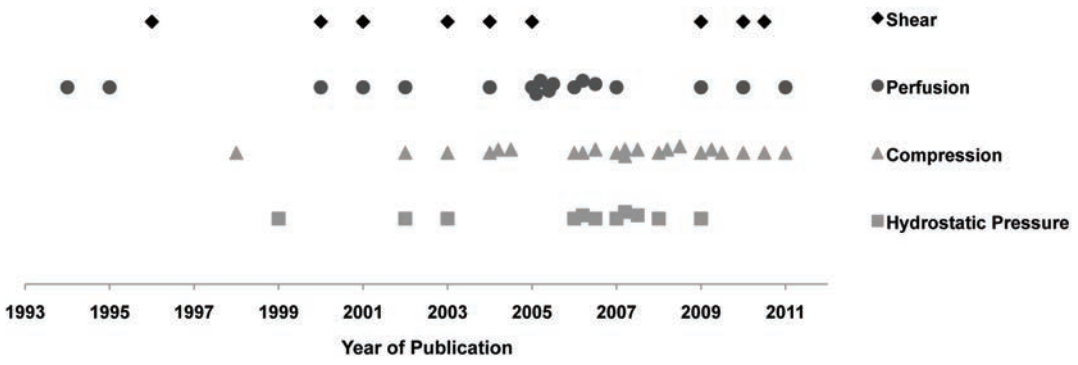

Figure 2 – Time distribution of research studies published between 1993 and 2011 on the effect of mechanical stimulation of cells in the context of cartilage tissue engineering. From *ISI Web of Knowledge*[SM] (Thomson Reuters, USA) and *Scopus* (Elsevier, The Netherlands) databases.

5.1. SHEAR STRESS STIMULI

Shear stress is a stress state where the stress is parallel or tangential to a face of the material, as opposed to normal stress, where the stress is perpendicular to the face (Figure 1). When joint movements occur, cartilage has to resist shear force generated by the synovial fluid pressurization alongside its surface. The shear modulus for articular cartilage ranges from 0.20 to 0.40 MPa, indicating a low rigidity, which facilitates adaptation of the tissue to different shapes in an equivoluminal manner [37] . Cartilage responds by deforming without changes in volume neither in pressure gradient nor fluid flow. The deeper and calcified zones of cartilage are not able to react flexibly to the shear stress; therefore, it is the upper zone of cartilage that reacts flexibly to this force, being able to shift vertically up to 15° [57]. The collagen macromolecules are responsible for the resistance against shear stress, in a magnitude that is directly proportional to its concentration [57]. Research work has been developed in the context of cartilage tissue engineering to assess the effect of shear force over chondrocyte metabolism. Table II highlights the experimental setup used for these studies and summarizes the respective outcomes. On what concerns the type of cells investigated in this context, chondrocyte primary cultures have been those mostly used, namely human chondrocytes (nasal or articular), bovine and murine articular chondrocytes. Stem cells have scarcely been investigated in this context, whereas only Ohyabu *et al* (2009) [58] evaluated the effects of shear stress on the chondrogenic differentiation of Japanese White Rabbits' bone marrow stem cells.

Regarding type of scaffolds employed, microcarriers have been extensively used in these studies. Frondoza *et al* (1996) [59] tested four types of microcarriers: Cytodex™ 1 and 2: 180 μm and 155 μm size beads of dextran; Cytodex™ 3, 175 μm size beads of denatured pig skin type I collagen-coated dextran [59], and Cellagen™, 100-400~μm size beads of collagen type I [59, 60]. Poly(glycolic acid) (PGA) scaffolds and other poly(α-hydroxy esters) such as poly(L-lactic acid) (PLLA) and the co-polymer poly(lactic-co-glycolic acid) (PLGA) were also employed to develop cartilage constructs under shear stress conditions. Poly(α-hydroxy esters) have been widely adopted in this research context due to their biodegradability and clinical approval by FDA (Food and Drug Administration) [61-64]. Chitosan, a natural polysaccharide, was studied for cartilage TE due to its structural similarity with glycosaminoglycans [65]

It is evident that the combination of different experimental approaches and cell models reduces comparability of reported data and contributes to variability of findings. Frondoza stated that Cellagen™ microcarriers showed to be the most suitable for chondrocyte culturing, obtaining a 20-fold cell multiplication after 2 weeks of culture, with production of extracellular matrix components, namely collagen type II [59]. Experiments using nasal chondrocytes, in culture medium for 8 days, resulted in the expression of high levels of collagen type II mRNA, together with low levels of collagen type I mRNA. Aggrecan mRNA was detectable, and levels of *de novo* $^{35}SO_4$ incorporation were high [60]. These results were accompanied by a change in cell morphology, once chondrocytes at the surface of microcarriers appeared spherical. Levels of messenger RNA transcripts of the ß-1 integrin gene (possibly responsible for mechanotransduction) were high and its protein product was detectable by immunostaining. Based on these results, Bouchet *and co-workers* [60] stated that the ability to respond to a mechanical stimulus may be a characteristic of chondrocytes, irrespective of their source.

Table II – Experimental studies developed in order to evaluate the effect of shear stress over cartilage biosynthesis. Compiled from references [58-63, 65, 66]

Specie	Cell type	Scaffold	Bioreactor	Conditions*	Major results / Key findings	Ref.
Human	OC	Cytodex™ and Cellagen™ microcarriers	Spinner Flask (SF)	$2x10^2$ cells/cm^2 60 rpm 2 weeks	Best results for Cellagen™: 20-fold cell multiplication; Collagen type II production	[59]
Human	NC	Cellagen™	Spinner	$4x10^3$ cells/cm^2	High levels of β-1 integrin, collagen	[60]

		microcarrier	Flask (SF)	60 rpm 8 days	type II and aggrecan mRNA expression	
Human	DF	Gelatine microcarrier	Spinner Flask (SF)	$18x10^6$ cells/g 20 rpm 12 weeks	Increased aggrecan production	[66]
Bovine	AC	CPBS (5 mm cube)	Rotator	$6.5x10^5$ cells/ scaffold 60 rpm 4 weeks	Enhancement of GAG production	[65]
Bovine	AC	PGA fibrous mesh (10x5mm)	Spinner Flask (SF)	$7x10^6$ cells/ scaffold 80, 120, 160 rpm 42 days	Presence of mixing rather than its intensity is more determinant in GAG and collagen synthesis	[63]
Bovine	AC	PGA disc (5x2mm)	Wavy-walled bioreactor (WWB)	$5x10^6$ cells/ scaffold 50 rpm 4 weeks	30% higher cell population 60% higher production of extracellular matrix (as compared to spinner flask)	[61]
Bovine	AC	PLLA disc (10x1.9mm)	Concentric cylinder bioreactor (CCB)	3.75, 5.0, 6.25 $x10^6$ cells/ scaffold 19, 38, 76 rpm 4 weeks	Robust collagen and GAG deposition at higher cell density GAG decrease for high rotations	[64]
JWR	BM-SC	Collagen I sponge	Rotating Wall Vessel (RWV)	$3x10^6$ cells/cm^3 3 weeks	Increase in GAG content Increase in compression strength of the construct	[58]
Murine	AC	PLGA disc (7.5x3.5mm)	Rotating shaft bioreactor (RSB)	$3x10^6$ cells/ scaffold 2, 5,10 rpm 4 weeks	Small variations in cell number for different velocities Culture at 10 rpm showed aerobic cell metabolism, higher collagen synthesis but lower GAG content	[62]
Murine	AC	PLGA disc (7.5x3.5mm)	Rotating shaft bioreactor (RSB)	$6x10^6$ cells/ scaffold 10 rpm 3 weeks	Increased cell number to $1.1x10^7$ cells/ scaffold Increase of ECM components: 3.1 mg GAG/construct 7.0 mg collagen/construct	[62]

* Conditions: cell density, rotation conditions, culturing period

AC – Articular chondrocytes; BM-SC – Bone Marrow Stem Cells; CPBS - chitosan-poly(butylene succinate); DF – Dermal Fibroblasts; GAG – Glycosaminoglycan; mRNA – messenger Ribonucleic Acid; JWR – Japanese White Rabbits; NC – Nasal chondrocytes; OC – Osteoarthritic chondrocytes; PGA – Poly(glycolic acid); PLGA – Poly(lactic-co-glycolic acid); PLLA – poly(L-lactic acid); rpm – rotations per minute

On what concerns studies using spinner flasks (SF), Gooch *et al* (2001) [63] studied the effects of shear stress at different intensities over calf articular chondrocytes on PGA scaffolds. On the third day of culture, the mixing intensity was set to nine different levels, by varying the length and rotation of the stirrer. Constructs exposed to mixing contained higher fractions of collagen, synthesized and released more glycosaminoglycans (GAG), but exhibited lower GAG content. The presence or absence of mixing was the primary determinant of the GAG and collagen content in the constructs, while the intensity of the mixing was not so important [63]. Bovine chondrocytes were dynamically seeded into PLLA scaffolds and cultured for 4 weeks at different cell seeding densities (up to 6.25 x 10^6 cells / construct) and different shear stresses (between 19, 38, and 76 rpm). Dynamically cultured constructs with the highest cell density contained up to 15 x 10^6 cells, 2 mg GAG, and 3.5 mg collagen per construct and exhibited morphology similar to that of native cartilage. Cartilage constructs exhibited robust matrix collagen and GAG deposition [64]. The concentric cylinder bioreactor produced constructs with low variance in terms of chondrocyte number and collagen content, but larger variance in terms of GAG content upon 28 days of culture. Although higher rotations increased collagen content, significantly decrease in GAG composition was observed for longer culture periods [64].

A parallel study performed using the rotating shaft bioreactor (RSB) [62] reports the culture of chondrocyte based constructs under medium and gas perfusion under different rotating speeds (up to 10 rpm). The chondrocyte density after 4 weeks exhibited small variations within the distinct groups, but in contrast, the average values of the molar ratio of lactate production to glucose consumption were lowered to ~1.26 under the highest rotating speed, which reveals an aerobic metabolism. This culture condition additionally resulted in higher collagen synthesis and GAG release, but lower GAG content [62]. Modification of the culture method by cultivating initially the constructs at 10 rpm during 3 weeks followed by one additional week of culture at 2 rpm, led to a 100% increase in GAG content relatively to the control. The doubling in cell seeding density resulted in 40% maximum increase in cell number attained after the first week of culture, but resulted in the best culture conditions in terms of GAG and collagen contents per construct: 3.1 and 7.0 mg/construct, respectively [62].

The wavy-walled bioreactor (WWB) provided efficient attachment of bovine articular chondrocytes to PGA scaffolds, and these chondrocytes proliferated and remained metabolically active, synthesizing extracellular matrix over a period of 4 weeks [61]. In comparison with SF, WWB supported increased cell proliferation and deposition of glycosaminoglycans and collagen in a range of 1.3 to 1.6 fold higher. Upon 4 weeks of culture, the wet weight of constructs cultivated in WWB was similar to that of SF. However, the former were 60% heavier due to equally higher incorporation of extracellular matrix and 30% higher cell population [61].

Shear stress states have proven to be used successfully to culture cartilage constructs that resemble native tissue and exhibit improved matrix deposition relative to conventional static cultures. However, the ideal parameters to be applied to specific cultures are yet to be elucidated.

5.2. PERFUSION OF CULTURING MEDIA

Perfusion systems have been designed to mimic forces experienced by chondrocytes during joint motion, and used to investigate *in vitro* maturation of cartilage constructs [67]. *In vivo,* chondrocytes encounter internal stress in the form of osmotic pressure, and external stress, as hydrostatic pressure, during joint motion [67]. In perfusion bioreactors, medium flow through the pores of scaffolds benefits cell proliferation and differentiation by two ways: by enhancing nutrient transport to the bulk of the scaffold and by providing cell mechanical stimulation via fluid shear. Perfusion can be additionally used for seeding cells into scaffolds, by promoting cell transport throughout the porous interior of scaffolds. Hydrodynamic stress imposed on cells within scaffolds upon perfusion is intrinsically dependent on scaffold microstructure and on bioreactor configuration [68]. Several groups have gathered efforts to study the effect of fluid perfusion over cell / scaffold constructs using flow perfusion systems. Such efforts are shortly summarized in Table III. The effect of flow perfusion on cell-based constructs has been investigated in combination with a large variety of scaffolds. In this context, very high levels of porosity are mostly desirable to minimize pressure drop upon media perfusion. PGA scaffolds have been investigated due to its intrinsic characteristics and processability into very high porous structures (up to 97%) [69-72]. Other commercially available scaffolds, such as Degrapol® [68, 73], Polyactive™ foams [74] and Calcibon® carriers [75] have been used in this context, due to their particular characteristics, off-the-shelf availability and standardization. Collagen sponges [67, 76], alginate and agarose gels [77, 78] were also investigated as a

physical support during medium perfusion despite their low porosity and interconnectivity. As previously mentioned, chitosan has been proven a great scaffold for cartilage TE and was also used for perfusion studies [53, 79]. Silk fibroin, protein obtained from *Bombix mori* silkworm, when prepared into a sponge, provides a great structure for cartilage tissue development, and adequate for perfusion bioreactor studies [80].

Table III – Experimental studies developed in order to evaluate the effect of fluid perfusion over cartilage biosynthesis. Compiled from references [67-81]

Specie	Cell type	Scaffold	Bioreactor	Conditions*	Major results /Key findings	Ref.
Human	ESC	Silk sponge (8x3mm)	Custom-made perfusion bioreactor	$1x10^6$cells/mL 1mL/min 4 weeks	Dynamically cultured constructs showed higher amounts of GAGs, DNA, total collagen and collagen type II as well as 3.7-fold higher mechanical stiffness	[80]
Human	ASC	PGA disc (5x15mm)	Re-circulation bioreactor	2 or $4x10^7$cells/ scaffold 0.2 mL/min 5 weeks	Highest levels of collagen II and GAG measured in bioreactor culture with initial seeding density of $4x10^7$cells/ scaffold	[81]
Human	AC	Copolymer vicryl+ PDS	Minucells and Minutissue	1 mL/h, on/off 30' 2 weeks	Abundant proteoglycans and collagen fibrils formation	[82]
Human	AC	DegraPol® (16x2mm)	Closed-loop re-circulation system	$1.5x10^6$cells/ scaffold 0.5 mL/min 4 weeks	2-fold increase of cell viability Biosynthetic activity demonstrated only in the bioreactor-cultured constructs	[73]
Human	AC	Collagen sponge (10x4mm)	Direct perfusion bioreactor	$1x10^6$ cells/ sponge 0.1, 0.3, 1 mL/ min 1 week	No high levels of proliferation or synthesis of new matrix was measured when perfusion rates increased	[67]
Human	FEC	PGA disc (4.75x2.15 mm)	Glass tube perfusion bioreactor	$4.4x10^6$ or $8x10^6$ cells/mL 0.2 mL/min 5 weeks	Constructs contained GAG concentrations similar to those measured in ex vivo AC Total collagen and collagen type II levels were substantially lower than those in adult tissue	[71]
Bovine	AC	PLLA/PGA	Custom-	$2.5x10^6$ cells/	Increased content of DNA (118%)	[72]

		(12.7x1mm)	made perfusion bioreactor	scaffold 400 μm/s 4 weeks	Increased content of GAG (184%) and hydroxyproline (155%)	
Bovine	AC	Collagen sponges (7x1.5mm)	Custom-made perfusion bioreactor	3x10^6 cells/ scaffold 0.33 mL/min 15 days	sGAG accumulation, ^{35}S-sulfate incorporation, and aggrecan plus collagen type II gene expression were all down-regulated when compared to non-perfused culture	[76]
Bovine	AC	Collagen sponge (10x4mm)	Direct perfusion bioreactor	1x10^7 cells/ sponge 0.1, 0.3, 1 mL/ min 1 week	Reduction in cell number and GAG content was measured when perfusion rates increased	[67]
Bovine	AC	Collagen sponge (10x4mm)	Direct perfusion & Free flow	1x10^7 cells/ sponge 0.1 mL/min 1 week	Non-significant change in the number of cells in the free flow system and direct perfusion GAG content was elevated by 25% only under free flow	[67]
Bovine	AC	Agarose gel (1μl)	Perfusion Micro-bioreactor	4x10^6 cells/ mL 1 μL /h 6 days	Increase in lactate production rate GAG production rate unaltered	[77]
Bovine	AC	Degrapol® (3,4,5,8x 1mm)	Direct perfusion bioreactor	8x10^4 cell/ mm^3 0.5 mL/min 2 weeks	1.7-fold increase in DNA content 2.9-fold increase in the mean content in sGAG	[68]
Bovine	AC	Agarose & alginate hydrogel (6x1.1mm)	Custom-made perfusion bioreactor	4x10^6 cells/ mL 0.025 mL/h 7 days	No difference in cell viability was observed Only alginate constructs under perfusion culture accumulated more GAG and collagen	[78]
Bovine	AC	Polyactive™ foam (4x8mm)	T-CUP	1x10^6 cells/ scaffold 0.4mm/s 14 days	Abundant extracellular matrix rather uniformly distributed and positively stained for GAG	[74]
Ovine	AC	PGA (10x2mm)	Poly-carbonate vessel connected to media bag	4x10^6 cells/ scaffold 0.05 or 0.8 mL/min	Higher DNA content; 40% increase of sGAG synthesis and deposition	[70]

				9 days		
Porcine	AC	Calcibon® (4.55x2mm)	Flow chamber with integrated aeration	$1x10^5$ cells/ mL 0.5 mL/min 3 weeks	Lower ratio of GAG/DNA Constructs of both culture methods contained high amount of collagen II	[75]
Murine	ATDC5 cell line	Chitosan (BMP-loaded) (10x2mm)	RCMW™	$4x10^4$ cells/ mL 2.25 mL/min 4 weeks	Chondrogenic phenotype preserved without hypertrophic morphology Neo-formed tissue matrix was built	[79]
Rabbit	AC	PGA (20x10mm)	Poly-carbonate vessel connected to a media bag	$4x10^6$ cells/ scaffold 50 µL/min 28 days	Immunostaining positive reactivity for type II collagen and chondroitin sulfate; Collagen and GAG values showed to be 15% and 25% dry weight	[69]

* Conditions: cell density, perfusion conditions, culturing period

AC - Articular chondrocytes; ASC – Adipose stem cells; DNA – Desoxiribonucleic acid; ESC – Embryonic stem cells; FEC - Fetal epiphyseal cartilage; sGAG – sulphated Glycosaminoglycan; PDS- polydioxanon; PGA – poly(glycolic acid); PLLA - poly(L-lactic acid); T-CUP - Tissue-Culture Under Perfusion

The latest studies investigating perfusion for cartilage TE have looked into differentiation of human stem cells. Both embryonic (ESCs) [80] and adult stem cells [81] (obtained from adipose tissue – Adipose stem cells (ASC)) were explored, and promising outcomes were achieved: Tigli and colleagues (2011) [80] observed greater cartilage-like tissue development when ESCs were dynamically cultured, and Mahmoudifar *et al* (2010) [81] also verified that perfusion culturing improved ASCs chondrogenic differentiation and cartilage matrix deposition. The many research studies on the effect of perfusion on cell response led to some discrepancies. Proteoglycan and collagen formation together with an increase in cell number seem to be prevalent in most of dynamic culturing studies. Nevertheless, the magnitude of these variations varies to a large extent. Dunkelman *et al* (1995) [69] stated that 4 weeks of culture under perfusion yielded a significant production of glycosaminoglycans (GAGs), but no significant collagen type II deposition was detected. Secretion of chondroitin sulfate and hydroxyproline has been shown to be highly promoted under perfusion, as demonstrated by several studies [69, 70, 72, 74]. However, the influence of perfusion on chondrogenesis is not obvious. The culture of bovine articular chondrocytes in collagen sponges inhibited chondrogenesis as demonstrated by Mizuno *et al* (2001) [76]. Concordant with these results, Freyria *et al* (2005) [67] reported a reduction in bovine cell number and GAG content when perfusion rates were increased. Additionally, the experiments performed by Nagel-Heyer *et al*

(2005) [75] with articular chondrocytes from adult mini-pigs demonstrated that the constructs cultured in 12-well-plates had a higher amount of extracellular matrix, as quantified by the content of GAG and total proline, when compared to those from the bioreactor. The work developed by Raimondi *et al* (2004) [73] did not assess cartilage biosynthesis, but has shown that full thickness-perfused constructs, maintained a higher degree of cell viability (human articular chondrocytes), when compared both to surface-perfused constructs and to static controls. However, human articular chondrocytes cultured by Freyria *et al* (2005) [67] under perfusion for 1 week resulted in a decline in cell number and GAG content. The application of miniaturization to 3D cell culturing for reducing chemical gradients in both the culture environment and the construct proved to be successful by increasing lactate production rate of bovine articular chondrocytes encapsulated in agarose. Nevertheless, no improvement was observed in GAG production rate [77].

When analyzing cell viability of bovine articular chondrocytes encapsulated in alginate or agarose and cultured under perfused or static conditions, Xu and co-workers (2006) [78] found no significant difference. Upon 12 days of culture, alginate based constructs cultured under perfusion released and accumulated more GAG and collagen as compared to the remaining conditions. Other study evaluated the bovine articular chondrocytes response to increasing values of shear flow (up to 12-fold increase in the level of applied shear) and observed that the total increase for DNA and sGAG content was about 1.7-fold and 2.9-fold. In contrast, the sGAG/DNA ratio showed a tendency to decrease for increasing shear levels [68]. At last, Mahmoudifar *et al* (2005) [71] operated the bioreactor with periodic medium flow reversal instead of unidirectional flow. This improvement in perfusion culturing resulted in increases in GAG and collagen levels when composite scaffolds were employed.

Taken altogether, the reported data suggests that the protocol defined for perfusion culture requires a high level of optimization in order to achieve an appropriate balance between cell viability, cell proliferation, extracellular matrix production and deposition. From the reported literature, a certain level of culturing prior perfusion appears to be required, as the efficacy of physical stimulation has been demonstrated to depend on presence and amount of extracellular matrix at the construct. The many discrepancies among the reported data may result from the large number of experimental combinations that result from the vast number of bioreactor configurations, dynamic conditions applied, scaffolds used and cells investigated.

5.3. COMPRESSION FORCES

In vivo, when articular cartilage is subjected to a uniaxial compression force the internal hydrostatic pressure increases within the joint. Daily activities cause intermittent loading that introduces very high cyclic hydrostatic pressure at the joint and the cartilage itself. Cartilage can be regarded as a combination of two phases: a fluid phase and a solid one. Compressive loading is counteracted by the stressing of the solid phase and by the pressurization of the interstitial fluid that behaves itself as an incompressible solid. Although pressurization tends to push out the fluid from the solid phase, the squeezing out is limited by the low hydraulic permeability of the matrix. In this regard, proteoglycans (PGs) have an important role resisting compression, as the hydraulic permeability is inversely correlated with the respective charge density. In addition, physical restraining of adjacent tissues also opposes fluid flow from the matrix. Upon increasing deformation, the fluid phase is further squeezed out from the tissue, causing the progressive loading of the cartilage matrix and a concomitant decrease in porosity, which further decreases fluid permeability [42, 83-86]. The removal of the compressive force originates hydrostatic tension in the cartilage matrix that promotes fluid migration back to the solid phase and restoration of the matrix volume.

Table IV summarizes the reported results from several experimental studies aimed at investigating the effect of static and dynamic compressive cycling over tissue engineered constructs.

In terms of the type of cell investigated, bovine articular chondrocytes remain the preferable type of cell studied. Cells from human origin are less represented. Human nasal chondrocytes have been successfully compared with healthy articular chondrocytes, which may suggest the potential heterologous use of these cells for articular regeneration [87]. Just like previous studies adopting perfusion or shear forces, stem cells of both animal and human origin have been investigated.

Table IV – Experimental studies developed in order to evaluate the effect of compression over cartilage biosynthesis. Compiled from references [29, 87-107]

Specie	Cell type	Scaffold	Bioreactor	Conditions*	Major results /Key findings	Ref.
Human	MSC	Fibrin+ Poly-urethane scaffold (8x4mm)	Ceramic hip ball	$5x10^6$ cells/scaffold 25º ball oscillation, 1 Hz. Dynamic	Chondrogenesis of hMSCs promoted by mechanical load through TGF-ß pathway by up-regulating TGF-ß gene expression and protein	[102]

				compression of 10-20% strain amplitude 1 h/day, 7 days 2 weeks	synthesis	
Human	AC	PEGT/ PBT foam Poli Active™ (8x1mm)	Poly-sulfone chamber with compression platen	$5x10^6$ cells/scaffold 6 cycles of 2h, 5% amplitude, 5% offset, 0.1 Hz, + 10h without deformation 3 days	Response of AC does not depend directly upon the stage of cell differentiation, but rather on the ECM surrounding the cells	[89]
Human	AC + NC	Hyaff®-11 (6x2mm)	Chamber with compression platen	$3.7x10^6$ cells/scaffold 30 minutes; 7.5% or 15% strain offset; 0.1 Hz; every 2nd day 10 days	Increased synthesis of GAG, PG and collagen type II at NC constructs AC constructs were less responsive than NC to all loading regimens	[87]
Human	AC + NC	Poly-urethane foam (8x4mm)	Ceramic hip ball	$10x10^6$ cells/scaffold 30 minutes; 60ºamplitude rotation;10% offset; 0.1 Hz; every 2nd day 10 days	32.9-fold increase in the mRNA expression of SZP but not HAS-1 and HAS-2 on NC constructs, in comparison with AC constructs	[87]
Bovine	AC	PGA disc (10x2mm)	Stainless steel porous platens	$2x10^4$ cells/scaffold Unconfined 10, 30, 50%static deformation 24h	Synthesis of both sGAG and total protein were suppressed by 35% and 57%, respectively, by static compression at an amplitude of 50%	[29]
Bovine	AC	PGA disc (10x2mm)	Stainless steel porous platens	$2x10^4$ cells/scaffold Unconfined 5% amplitude; 10 & 50% offset; 0.001 & 0.1 Hz 24h	Most dramatic effects observed at 0.1 Hz and 50% compression amplitude: 99% and 179% synthesis increase of total protein and sGAG, respectively	[29]
Bovine	AC	PGA disc (5x2mm)	Poly-sulfone chamber with	$5x10^6$ cells/scaffold 1 h/day;	Round cell morphology GAG and type II collagen	[92]

			compression platen	Unconfined 10% compressive strain or dynamic 7% strain at 0.3 Hz 37 days	accumulated in the face side, as compared to the lateral side of the scaffold	
Bovine	AC	Poly-urethane disc (8x4mm)	Biaxial Pin-on-Ball	$25x10^6$ cells/scaffold 2x 1h/day; Unconfined 5, 10, 20% compressive strain; 60º amplitude rotation; 0.1 Hz 3 days	COMP gene clearly promoted by relative surface motion Stimulation of ECM production was reduced and/or inhibited	[101]
Bovine	AC	PEG hydrogel (10x4mm)	Chamber with compression piston	$30x10^6$ cells/mL 1.5 h/day, 15% deformation, 1 Hz 2 weeks	37% increase in sGAG levels No differences between PEG and PEG-fibrinogen culturing	[96]
Bovine	AC	Poly-urethane disc (8x4mm)	Ceramic hip ball	$1x10^7$ cells/scaffold 2x/day; Unconfined 10-20% strain amplitude; 7.5º scaffold oscillation; 25º ball oscillation; 0.1 Hz 5 days	PRG4, collagen type II and COMP mRNA expression levels increased by ball oscillation Aggrecan and TIMP-3 mRNA expression levels upregulated by multi-directional articular motion	[98]
Bovine	AC	Poly-urethane disc (8x4mm)	Ceramic hip ball	$10x10^6$ cells/scaffold 2x 1h/day; Unconfined 10-20% strain amplitude 3 days	Most pronounced mRNA up-regulations observed for PRG4 expression in deep zone and HAS2 expression in superficial zone cells Full thickness chondrocytes experienced the greatest effect on HAS1 mRNA expression and HA release	[99]
Bovine	AC	Agarose hydrogel (4x1.5mm)	Chamber with compression platen	$20x10^6$ cells/mL Unconfined 10% deformation: 1 or 2h at 1 Hz; or 1h at 0.33, 1 or 3 Hz 72h	Increase in aggrecan promoter activity and decrease in collagen II promoter activity with increasing duration of loading	[93]

Bovine	BMSC	Agarose hydrogel (4x1.5mm)	Chamber with compression platen	$20x10^6$ cells/mL 3h/day; Unconfined 10% deformation; 1 Hz 5 days + 23 days free swelling	Increase in short-term aggrecan transcriptional activity Increase in GAG deposition in long-term culture	[93]
Bovine	AC	Poly-urethane disc (8x4mm)	Ceramic hip ball	$10x10^6$ cells/scaffold 1h/day; Confined 10-20% amplitude strain; 0.5 Hz 28 days	Increase of type II collagen gene expression; No influence on aggrecan mRNA levels Low O_2 and mechanical stimuli may synergistically act towards cell phenotype stabilization	[100]
Porcine	AC	Chitosan (6x4mm)	Chamber with compression piston	$2x10^6$ cells/scaffold 4x/day; Unconfined 5-15% strain amplitude; 0.1 Hz, 45 / 315' on/off, 3 weeks	Enhanced mRNA levels for aggrecan 5-fold and 2-fold increased deposition of proteoglycan and collagen type II, respectively	[97]
Canine	AC	PLLA (4x2.6mm)	Commercial bioreactor (Enduratec, Bose, Minnesota, USA)	$1x10^6$ cells/scaffold 10% strain amplitude; 1 Hz; 1h / 7h on/off, 2 weeks	Higher chondrocyte viability was obtained in the scaffolds cultured under dynamic loading	[103]
Canine	AC	Agarose gel (Ø4mm)	Chamber with compression platen	$30x10^6$ cells/mL 3h/day, 5 days/week; Deformational loading: Unconfined compression, 10% strain amplitude; 1 Hz Sliding contact loading: 0.5 Hz, 10% deformation 56 days	Loaded constructs exhibited increased mechanical properties relatively to free-swelling control No differences were observed among groups regarding DNA, GAG and collagen content	[104]
Rabbit	BMSC	Agarose gel (8x1.5mm)	Chamber with compression platen	$10x10^6$ cells/mL 5% compressive sinusoidal strain;	Cyclic compressive loading alone promotes chondrogenic differentiation of BMSC	[95]

				1Hz 14 days		
Rabbit	BMSC	PLCL (Ø9mm) with or without fibrin	Compressio n bioreactor	2x10^6 cells/scaffold Continuous compressive deformation, 5% strain; 0.1 Hz 10 days	Dynamic culture and 3D environment created by PLCL+fibrin gel encouraged BMSCs to differentiate into chondrocytes, maintain their phenotypes and enhance GAGs production	[105]
Rabbit	AC	PLCL sponge (9x3mm)	Chamber with compression piston	1x10^6 cells/scaffold Unconfined 10% compressive strain; 0.1 Hz 24h	Proximal region of the COL2A1 gene promoter mediates the dynamic compression-induced transcriptional activation of the human COL2A1 gene in chondrocytes	[90]
Rabbit	AC	PLCL sponge (9x3mm)	Chamber with compression platen	1-5x10^6 cells/scaffold Unconfined 10% strain amplitude; 0.01, 0.05, 0.1, 0.5 Hz 6 days	Improved production and release of sGAG at continuous dynamic compression High mRNA expression of type II collagen at 0.1 Hz	[91]
Rabbit	AC	PLCL (5x3mm)	Chamber with compression platen	2x10^6 cells/scaffold 5% strain; 0.1 Hz 24 days	Unhealthy lacunae shapes and hypertrophy forms were observed in implants	[94]
Rabbit	AC	Chitosan/ gelatin scaffolds (Ø6mm)	PMMA plate with compressive pins	8x10^6 cells/mL 40% compressive strain; 0.1 Hz 6h/day 3 weeks	Increased cell proliferation and deposition of GAG	[106]
Murine	AC	Collagen type I gel	Cell Stretcher System NS 500	1x10^6 cells/mL 0, 10, 60, 120 min/day Cyclic compression: 5% strain amplitude, 0.33Hz, 2.35 kPa peak stress; 1 loading session / day 1 week	Dynamic compression reactivated the dedifferentiated chondrocytes Growth factors did not play a synergistic role when applied with loading	[107]

Murine	ESC	Collagen gel (Ø96well-plate)	Weight over culture plate lid	$2.25x10^6$ cells/mL Unconfined 20-30% deformation 10 days	2- to 3-fold increase in collagen type II & aggrecan expression; Sox9 was up-regulated while IL-1β, was down-regulated	[88]

* Conditions: cell density, compression conditions, culturing period

AC - Articular chondrocytes; BMSC – Bone marrow stromal cells; COMP – Cartilage oligomeric matrix protein; ECM – Extracellular matrix; ESC – Embrionic Stem Cells; sGAG – sulphated Glycosaminoglycan; HA – Hyaluronan; HAS (1 and 2) – Hyaluronan synthase (1 and 2); IL-1β - Interleukin-1 beta; NC- Nasal chondrocytes; PBT - poly(butylene terephthalate); PEG - poly(ethylene glycol); PEGT - poly(ethylene glycol terephthalate); PGA – Poly(glycolic acid); PLCL - poly(lactide-co-ε-caprolactone); PLLA – Polylactic acid; PMMA - Poly(methyl methacrylate); PRG4 – Proteoglycan 4; SZP – Superficial zone protein; TIMP-3 – Tissue inhibitor metalloproteinase-3

In the reported studies, several bioreactor configurations were adopted to exert compressive load over cell/scaffold constructs. For instance, static compressive forces were applied by exerting a constant force on the top of the construct through the use of a fixed weight [88] or through constant mechanical constringent of the construct by fixating it between two platens and a radial ring. Using this last configuration, static and dynamic compression were possible to be applied depending on the relative positioning of the bottom platen [29, 87, 89-91]. Other studies adopted similar bioreactor configurations by means of applying compression force of a mechanical spectrometer, separated from the culture chamber by a membrane, through an indenter positioned over the constructs [92-95]. The work developed by Fehrenbacher *et al* (2006) [97] and Schmidt *et al* (2006) [96] used the lid of the bioreactor as a manifold for stainless steel pistons positioned above six growth chambers. During the loading experiments, the lid was attached to a pneumatic actuator which induced cyclic, linear displacement of the lid causing the compression of the culture chambers [96, 97]. An alternative device is commercially available, consisting of a ceramic hip ball (32 mm in diameter) that is pressed against the construct. The motion generated at the interface could be (a) rotation of the sample holder around the main axis of the construct; (b) oscillation of the ball around an axis perpendicular to the main axis of the construct, and (c) oscillation in both axes in phase difference [87, 98-101]. This device has provided interesting results. Grad and colleagues exposed resorbable porous polyurethane scaffolds seeded with bovine articular chondrocytes to dynamic compression using this system [98], and reported increased proteoglycan 4 (PRG4), collagen type II and cartilage oligomeric matrix protein (COMP) mRNA expression levels for ball oscillation, and upregulation of aggrecan and tissue inhibitor of

metalloproteinase-3 (TIMP-3) mRNA expression levels for multidirectional articular motion. Ball oscillation also increased the release of PRG4, COMP, and hyaluronan (HA) into the culture media [98]. Li *et al* (2007) [99] went further to investigate the effect of surface motion on gene expression of proteoglycan 4 (PRG4), hyaluronan synthases (HAS1, HAS2), as well as on release of hyaluronan (HA) and proteoglycan 4 (PRG4) by chondrocytes from different zones of bovine articular cartilage (superficial zone, deep zone, full thickness, and 1:1 superficial/deep ratio mix chondrocytes) seeded into polyurethane scaffolds. Mechanical loading enhanced mRNA levels for all cell types, with most pronounced upregulation observed for the PRG4 expression for deep zone cells and HAS2 expression for superficial zone cells. The effect of the biochemical and biomechanical environment appeared to be additive, resulting in highest mRNA levels for the top sections of the constructs. Bioreactor stimulation also enhanced the HA release for all cell populations. Full thickness chondrocytes experienced the greatest effect on HAS1 mRNA expression and HA release, indicating that the interaction between cell populations influences HA synthesis as compared to subpopulations alone [99]. The combination of low oxygen and mechanical stimuli using this bioreactor, may act synergistically with respect to the stabilization of the chondrogenic phenotype [100]. Demarteau and his group [89] achieved outstanding results. They concluded that GAG synthesis, accumulation, and release induced by dynamic compression were not correlated with the expression of collagen type II mRNA, suggesting that the response of human articular chondrocytes to dynamic compression does not depend directly on the stage of cell differentiation but, instead, on the quantity and composition of the matrix surrounding the cells at the time of stimulus [89].

In order to understand if a scaffold containing biological motifs, such as fibrinogen, would enhance mechanotransduction, Schmidt and colleagues [96] incorporated these motifs in PEG hydrogels scaffolds, but concluded that this approach did not enhance chondrocyte metabolism more than mechanical stimulation. The effect of strain stimulation on the total GAG (normalized per construct) was significant both for PEG-fibrinogen and PEG constructs [96].

Rabbit articular chondrocyte-seeded PLCL sponges, subjected to 24 h of continuous dynamic compression, showed that type II collagen mRNA expression level was significantly increased as compared with static controls [90], while loaded at 0.1 Hz, 5% strain for 24 days resulted in unhealthy lacunae shapes and hypertrophy forms were observed [94]. Porcine articular chondrocytes loaded in chitosan-biocomposites displayed enhanced mRNA levels for COL2A1 and aggrecan and accumulated significantly more proteoglycan and collagen type II per cell as compared to unloaded controls [97]. Continuous dynamic compression improved the

production of sGAG of rabbit articular chondrocytes cultured in SPCL scaffolds, most of which was released into the culture medium upon loading. At the frequency of 0.1 Hz was observed the highest mRNA expression for type II collagen. Small dependency on frequency was observed for aggrecan expression. Conversely, an intermittent loading (24-h cycle of loading and unloading) or short loading and unloading duration per cycle-compression regime maintained high levels of mRNA expression [91].

On what concerns stem cells, Takahashi *et al* (1998) [88] demonstrated that static compressive load promotes chondrogenesis during embryonic limb bud mesenchymal cell differentiation and Huang and colleagues [95] showed that rabbit bone marrow mesenchymal stem cells exhibited chondrogenic gene expression when subjected to cyclic compressive loading. Mauk *et al* (2007) [93] cultured both bovine bone marrow stem cells and articular chondrocytes, and observed that, in chondrocyte culture, aggrecan promoter activity increased with increasing duration of loading, particularly in the outer annulus region, while type II collagen promoter activity decreased. The role of mechanical compression in directing chondrogenic differentiation of MSCs was traduced by an increase in short-term aggrecan transcriptional activity and by GAG deposition in the long-term [93]. Human MSCs subjected to dynamic compression increased TGF-ß gene expression and protein synthesis, which led Li and colleagues (2010) [102] to postulate that mechanical load promotes chondrogenesis of hMSCs through TGF-ß pathway.

Compression is not always favorable for cartilage biosynthesis. 50% static compression has been reported to suppress the total synthesis of protein and sGAG [29]. However, the simple variation from static to dynamic compression has resulted in an increase of these cartilage components [29]. Seidel *et al* (2004) [92] also noticed that mechanical compression contributed to a decrease of GAG content for prolonged culture time, and had little effect on the composition, morphology and mechanical properties at the core of construct discs but resulted in variation of properties at the periphery and face sides of the same on what concerns GAG and collagen type II retention [92]. The conditions defined by Wimmer *et al* (2004)[101] using elliptical displacement trajectories similar to the motion paths occurring *in vivo* resulted in the promotion of COMP gene, (an early marker in chondrogenesis), but resulted in a reduction or inhibition of extracellular matrix production .

5.4. HYDROSTATIC PRESSURE ENVIRONMENT

Pressures on normal human acetabular cartilage have been collected from two implanted instrumented femoral head hemiprostheses [108]. Despite significant differences in subjects' gender, morphology, mobility, and coordination, *in vivo* pressure measurements from both subjects covered similar ranges, with maximums of 5–6 MPa for gait, and as high as 18 MPa for other movements. This unique *in vivo* data is consistent with corresponding cadaver experiments and model analyses. The collective results, *in vitro* data, model studies, and now corroborating *in vivo* data, support the self-pressurizing ''weeping'' theory of synovial joint lubrication [108]. The last biomechanical force described in the context of cartilage tissue engineering is hydrostatic pressure. Table V summarizes scientific research performed on the effect of hydrostatic pressure in cartilage biosynthesis.

Animal articular chondrocytes are usually the preferred cell source in these studies (equine [109], bovine [110-112], porcine [113], caprine [114], etc). Human osteoarthritic chondrocytes have also been investigated, but its relevance is doubtful as hydrostatic pressure within the normal physiological range appears to have an apoptotic effect over these cells [115], while low pressure loadings seem to provide increased collagen type II and aggrecan gene expression [116]. Human bone marrow derived stem cells cultured at 1 MPa loading and 1 Hz frequency enhanced in vitro differentiation in the presence of differentiation factors. This loading regime has been suggested to play a critical role during cartilage development and regeneration in vivo [117].

Table V – Experimental studies developed in order to evaluate the effect of hydrostatic pressure over cartilage biosynthesis. Compiled from references [109-120]

Specie	Cell type	Scaffold	Bioreactor	Conditions*	Major results /Key findings	Ref.
Human	OC	HYAFF®-11 (7x3mm)	Vessel connected to a MTS	$1x10^6$ cells/ scaffold 5 MPa;1 Hz 4h	Increased proportion of apoptotic cells in cartilage constructs	[115]
Human	OC	Collagen-I gel (1.5 mL)	Polymethyl methacrylate tube	$2x10^5$ cells/mL 40 kPa; 0.0125 Hz 14 days	Increased collagen-II and aggrecan gene expression Enhancement of proteoglycan content in media	[116]

Human	BMSC	Helistat® (12.5x12.5x5 mm)	SS pressure vessel connected to a MTS	$5x10^5$ cells/ scaffold 1 MPa; 1 Hz; 4h/day 10 days	Increase in mRNA expression of aggrecan, collagen-II and sox9 No change in mRNA expression of Runx2 or TGF-b1	[117]
Bovine	AC	Collagen sponge (7x1.5mm)	Pressure/ perfusion culture system	$3x10^6$ cells/ scaffold 2.8 MPa; 0.015 Hz 15 days	3.1-fold and 2.7-fold increase in accumulation of sGAG with 0 and 0.015 Hz, respectively	[110]
Bovine	AC	Agarose gel (0.44 mL)	Piston+ pressure chamber	$2x10^6$ cells/mL 5 MPa;1 Hz 4h	11% increase in GAG synthesis 4-fold increase in aggrecan mRNA	[111]
Bovine	AC	Agarose gel (0.44 mL)	Piston+ pressure chamber	$2x10^6$ cells/mL 5 MPa 4h	ERK pathway inhibited: may be a negative regulator of sox9 mRNA expression	[111]
Equine	AC	PGA fibrous mesh (1x1x5mm)	Semi-continuous perfusion/ compression system	$5x10^6$ cells/ scaffold 6,87MPa, 5s on/15s off, 20 min/4h 5 weeks	Concentration of sGAG in constructs from juvenile cells was found to be 10x greater than concentrations in control	[109]
Ovine	AC	Alginate beads	Cyclic hydrostatic load generating machine	$2.5x10^4$ cells/ bead 1.2 & 2.4 MPa, 0 & 0.66 Hz 4h	Increase in GAG content Improved cells ultrastructure and cell–matrix interactions	[113]
Porcine	AC	Alginate beads	Compressed air loading device	0.3 MPa, 1' on/off 7days	25% increase in GAG/DNA ratio; 65% increase in collagen-II/ collagen-I ratio	[113]
Rabbit	MC	PLLA (1.5x3mm)	Water-filled SS chamber connected to an Instron via a water-	$0.7x10^6$ cells/ scaffold 10 MPa for 1	10 MPa, 0 Hz stimulus enhanced: total collagen/scaffold, total GAG/scaffold, instantaneous modulus and relaxation modulus	[119]

			driven SS piston	h every 3 days; 0, 0.1 or 1 Hz 4 weeks		
Rabbit	AC	Alginate beads	Oil pressure apparatus	$4x10^6$ cells/mL 10 or 50 MPa 12 or 24h	Duration and magnitude of loading increased apoptotic cells in non-pre-cultured group	[118]
Rabbit	AC SPC BMPC SF	Alginate beads	SS pressure vessel with pump and cylinder valve	$4x10^6$ cells/mL 1, 5 MPa, 0.5 Hz 1h	SPCs under 5 MPa : enhanced mRNA expression of proteoglycan, collagen type II and sox9; enhanced production of sox9 protein and GAG	[119]

* Conditions: cell density, hydrostatic pressure conditions, culturing period

AC - Articular chondrocytes; BMPC – Bone marrow-derived progenitor cells; BMSC – Bone marrow stem cells; ERK- Extra-cellular signal-regulated kinase; sGAG – sulphated Glycosaminoglycan; MC – Meniscus cells; MTS – Mechanical Testing System; OC – Osteoarthritic chondrocytes; PGA - PoliGlycolic Acid; PLLA – Polylactic acid; SF – Skin fibroblasts; SPC – Synovium –derived progenitor cells; SS – Stainless Steel; TGF-ß1 – Transforming growth factor beta1

In general, customized loading reactors are used to apply hydrostatic pressure to cell/scaffold constructs. These reactors have in common the possibility of applying physiological relevant pressures and frequencies that range between 3 to 10 MPa, and 0 to 1 Hz, respectively [37]. In many bioreactors, a computer controlled mechanical testing system or actuator is generally used to apply the desired load into a culture chamber [109-111, 114, 116]. Other devices use compressed air to generate load [108, 112] or oil pressurized apparatus [118]. Additionally, pressure can also be imposed through the fluid medium via the axial movement of a piston [113]. It is interesting to notice that, although hydrostatic pressurization of a cell/scaffold construct is especially suitable to use with any kind of scaffold structure, the majority of studies have used gels and beads based constructs.

A global analysis of Table V demonstrates that hydrostatic pressure has a beneficial effect over cartilage extracellular matrix biosynthesis. Sulfated glycosaminoglycan (sGAG) concentration in pressurized constructs from juvenile bovine cells have been reported to be 10 times greater [109] than concentrations in non-pressurized and adult cell derived constructs. Toyoda *et al*

(2003) [110] also observed that constant pressurization yielded better outputs. Bovine articular chondrocytes loaded with 5 MPa constantly for 4 hours caused an 11% increase in GAG synthesis, which was associated with large proteoglycans, and a 4-fold increase in levels of aggrecan mRNA comparatively to unloaded ACs. The intermittence and magnitude of the hydrostatic pressure appears to be an important parameter. Intermittent pressurization at near 7 MPa enhanced the production of collagen, suggesting that there may be a minimum level of pressure necessary to stimulate collagen formation [109]. In comparison with the control group, the incorporation of [35S]-sulfate into glycosaminoglycans (GAGs) was 3.1-fold and 2.7-fold greater when constant and cyclic HP, respectively, were applied for 15 days at 2.8 MPa [109].
A significant increase in the ratio of glycosaminoglycan (GAG) to DNA was found to be 25% higher for intermittent 0.3 MPa loading as compared to the corresponding static control. A 65% higher ratio of collagen type II to I compared to the static control was also observed [113].
Controversial results were observed by Sharma and colleagues (2007) [114]. Compared with unloaded cells, cyclic loading increased the glycosaminoglycan content of cells at 1.2 and 2.4 MPa in cellular matrix and further removed matrix whereas it decreased at similar static loads. Both 1.2 and 2.4 MPa cyclic load levels inhibited metalloprotease specific activity in cellular matrix but increased it at static loading. Transmission electron microscopy data showed improved cells ultra structure and cell–matrix interactions under cyclic load whereas these deteriorated under static loadings. The study suggests that cyclic loading has a positive effect on chondrocytes metabolism and morphology whereas static load has a degenerative effect [113]. Mio *et al* (2007) [112] developed a more fundamental study. ERK (Extra-cellular signal-Regulated Kinase) pathway was hypothesized to participate in hydrostatic pressure-induced mechanotransduction in chondrocytes. An inverse relationship between ERK phosphorylation and *Sox9* expression was observed after loading. Quantification of Western blot analysis showed a significant decrease in ERK phosphorylation to 72% relatively to the control, while, in contrast, analysis of *Sox9* expression showed a significant increase of 278% compared to the control as a result of pressure application [111]. Hydrostatic pressure may therefore modulate the negative effect on ERK pathway in chondrocytes and contribute towards cell homeostasis by stimulating *Sox9* mRNA expression [111].

6. CELL SOURCES USED IN DYNAMIC CULTURING STUDIES

Since the emerging of Tissue Engineering as a research field [121], very distinct cell sources have been used by researchers in order to understand the influence of biomechanical

phenomena in cartilage tissue development. In order to analyze the progresses in this area, Figure 3 displays the cell sources used in the aforementioned studies along time. We can observe that animal-origin chondrocytes were the most used, followed by human chondrocytes, however, a turnover to the study of stem cells, both of human and animal origin, has been occurring during the last 3-4 years.

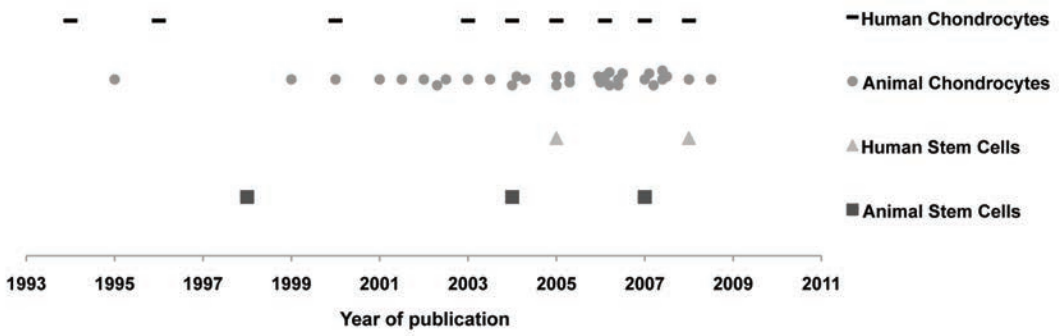

Figure 3 – Cell sources used in dynamic culturing studies to assess the effect of biomechanical forces in cartilage tissue engineering, from 1993 to 2011. From *ISI Web of Knowledge*^{SM} (Thomson Reuters, USA) and *Scopus* (Elsevier, The Netherlands) databases

Additionally, Figure 4 displays the cell source used with each four dynamic culturing methods covered in this review. Animal origin chondrocytes, mostly from bovine articular cartilage, have been the most widely studied cell source. These cells have been dynamically cultured under shear stress, flow perfusion, direct or indirect, confined or unconfined compression, or under hydrostatic pressure. So far, human chondrocytes, either obtained from the nasal septum or from the articular joints (healthy or osteoarthritic) have been investigated, ensuing very satisfactory outputs. Human stem cells have scarcely been exploited in this context, despite their great capacity to differentiate into the chondrogenic lineage, and clinical potential. It would be of interest to assess the effect of dynamic culturing on aspects such as chondrogenic differentiation and correspondent extracellular matrix production, secretion and deposition. Bone marrow derived stem cells' behavior has been recently studied under dynamic culturing, with some promising results. Other stem cell sources, such as adipose tissue, have solely been investigated under perfusion culturing.

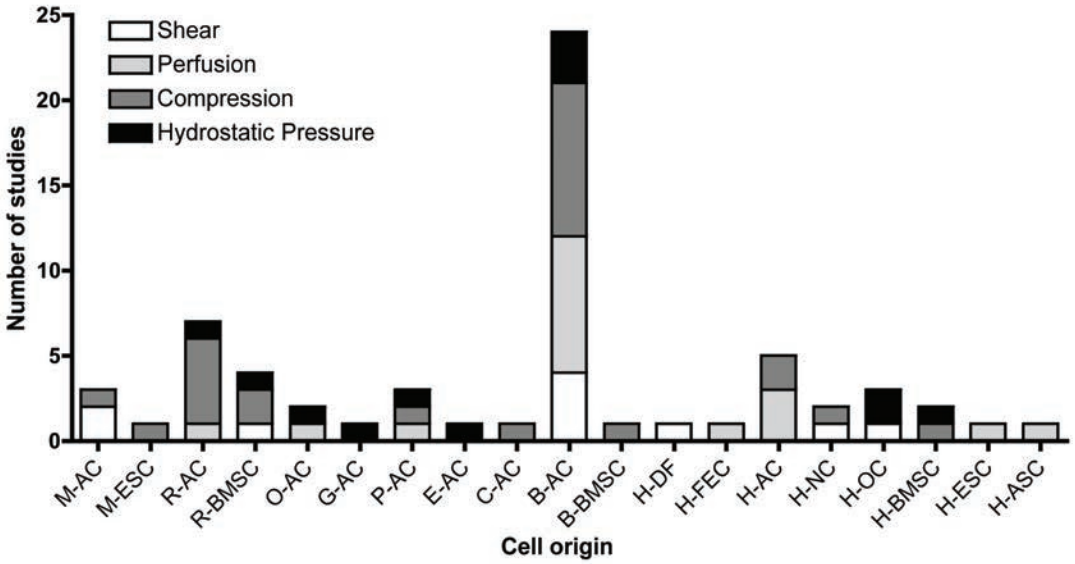

Figure 4 – Correlation between cell source and mechanical stimuli under study.

(BAC-Bovine Articular Chondrocytes; BBMSC-Bovine Bone Marrow Stem Cells; CAC-Canine Articular Chondrocytes; EAC-Equine Articular Chondrocytes; GAC-Goat Articular Chondrocytes; HAC-Human Articular Chondrocytes; HASC-Human Aipose Stem Cells; HDF-Human Dermal Fibroblasts; HESC-Human Embryonic Stem Cells; HNC-Human Nasal Chondrocytes; HOC-Human Osteoarthritic Chondrocytes; HBMSC-Human Bone Marrow Stem Cells; MAC-Murine Articular chondrocytes; MESC-Murine Embryonic Stem Cells; OAC-Ovine Articular Chondrocytes; PAC-Porcine Articular Chondrocytes; RAC-Rabbit Articular Chondrocytes; RBMSC-Rabbit Bone Marrow Stem Cells; RMC-Rabbit Meniscus Cells)

7. FINAL REMARKS

Extensive and high quality research has been made in order to understand how chondrogenic cells, or stem cells, sense, detect and respond to mechanical loading of distinct nature in 3D constructs. The major aim has been to identify how this stimulation regulates and/or influences cartilage tissue homeostasis, what are the mechanotransduction molecules and pathways involved, and take advantage of this knowledge to engineer *de novo* tissue *in vitro.* Current strategies have provided remarkable outputs, however new and relevant routes should be taken to engineer functional tissue for cartilage lesions repair. Some approaches could include:

The stimulation of cells with physiologically-relevant levels of loading;

The integration of multiple forces, mimicking the human articular joint;

The combination of hypoxia with mechanical loading.

Acknowledgments

We gratefully acknowledge funding support by the Portuguese Foundation for Science and Technology to CCorreia (PhD grant SFRH/BD/42316/2007).

References

1. Statistics, N.C.f.H., *Health, United States, 2007 - With Chartbook on Trends in the Health of Americans*. 2007, Hyattsville, MD: U.S. Government Printing Office - Washington, DC 20402.
2. Erggelet, C., Mandelbaum, B.R., *Principles of Cartilage Repair*. 2008, Germany: Steinkopff Verlag.
3. CDC, *Centers for Disease Control and Prevention.* http://www.cdc.gov/arthritis/index.htm, 2012.
4. Wright, S.H., *Inflammatory arthritis.* Adv NPs PAs, 2011. 2(11): p. 29-30, 32.
5. Cheng YJ, et al., *Prevalence of doctor-diagnosed arthritis and arthritis-attributable activity limitation — United States, 2007–2009.* National Center for Health Statistics, 2010. 59(39): p. 1261–1265.
6. Gibson, J.N., et al., *Arthroscopic lavage and debridement for osteoarthritis of the knee.* J Bone Joint Surg Br, 1992. 74(4): p. 534-7.
7. Lutzner, J., et al., *Surgical options for patients with osteoarthritis of the knee.* Nat Rev Rheumatol, 2009. 5(6): p. 309-16.
8. Steadman, J.R., W.G. Rodkey, and J.J. Rodrigo, *Microfracture: surgical technique and rehabilitation to treat chondral defects.* Clin Orthop Relat Res, 2001(391 Suppl): p. S362-9.
9. Gill TJ, Asnis PD, and B. EM, *The treatment of articular cartilage defects using the microfracture technique.* J Orthop Sports Phys Ther. , 2006 36(10): p. 728-38.
10. Williams, R.J., 3rd and H.W. Harnly, *Microfracture: indications, technique, and results.* Instr Course Lect, 2007. 56: p. 419-28.
11. Hangody, L., et al., *Mosaicplasty for the treatment of articular cartilage defects: application in clinical practice.* Orthopedics, 1998. 21(7): p. 751-6.
12. Bader, S. and A. Miniaci, *Mosaicplasty.* Orthopedics, 2011. 34(9): p. e491-3.
13. Robert, H., *Chondral repair of the knee joint using mosaicplasty.* Orthop Traumatol Surg Res, 2011. 97(4): p. 418-29.
14. Nam, D., et al., *Traumatic osteochondral injury of the femoral head treated by mosaicplasty: a report of two cases.* HSS J, 2010. 6(2): p. 228-34.
15. Brittberg, M., et al., *Treatment of deep cartilage defects in the knee with autologous chondrocyte transplantation.* N Engl J Med, 1994. 331(14): p. 889-95.
16. Gillogly, S.D., M. Voight, and T. Blackburn, *Treatment of articular cartilage defects of the knee with autologous chondrocyte implantation.* J Orthop Sports Phys Ther, 1998. 28(4): p. 241-51.
17. Erggelet, C., M.R. Steinwachs, and A. Reichelt, *The operative treatment of full thickness cartilage defects in the knee joint with autologous chondrocyte transplantation.* Saudi Med J, 2000. 21(8): p. 715-21.
18. Minas, T., et al., *Increased failure rate of autologous chondrocyte implantation after previous treatment with marrow stimulation techniques.* Am J Sports Med, 2009. 37(5): p. 902-8.
19. Harris, J.D., et al., *Autologous chondrocyte implantation: a systematic review.* Journal of Bone and Joint Surgery-American Volume, 2010. 92(12): p. 2220-33.
20. Harris, J.D., et al., *Failures, re-operations, and complications after autologous chondrocyte implantation--a systematic review.* Osteoarthritis Cartilage, 2011. 19(7): p. 779-91.
21. Panagopoulos, A., L. van Niekerk, and I. Triantafillopoulos, *Autologous Chondrocyte Implantation for Knee Cartilage Injuries: Moderate Functional Outcome and Performance in Patients With High-impact Activities.* Orthopedics, 2012. 35(1): p. e6-e14.
22. Buckwalter JA, H.E., Rosenberg L, Coutts R, Adams M, Eyre D, *Articular cartilage: composition and structure*. Injury and repair of the musculoskeletal soft tissues, ed. B.J. Woo SL. 1988, Park Ridge: American Academy of Orthopaedic Surgeons.
23. Buckwalter, J.A. and H.J. Mankin, *Articular cartilage: tissue design and chondrocyte-matrix interactions.* Instr Course Lect, 1998. 47: p. 477-86.
24. Zhu, W., et al., *Viscoelastic shear properties of articular cartilage and the effects of glycosidase treatments.* J Orthop Res, 1993. 11(6): p. 771-81.
25. Smith, R.L., et al., *Effects of fluid-induced shear on articular chondrocyte morphology and metabolism in vitro.* J Orthop Res, 1995. 13(6): p. 824-31.

26. Lane Smith, R., et al., *Effects of shear stress on articular chondrocyte metabolism.* Biorheology, 2000. 37(1-2): p. 95-107.
27. Gray, M.L., et al., *Mechanical and physiochemical determinants of the chondrocyte biosynthetic response.* J Orthop Res, 1988. 6(6): p. 777-92.
28. Guilak, F., et al., *The effects of matrix compression on proteoglycan metabolism in articular cartilage explants.* Osteoarthritis Cartilage, 1994. 2(2): p. 91-101.
29. Davisson, T., et al., *Static and dynamic compression modulate matrix metabolism in tissue engineered cartilage.* J Orthop Res, 2002. 20(4): p. 842-8.
30. Hu, J.C. and K.A. Athanasiou, *The effects of intermittent hydrostatic pressure on self-assembled articular cartilage constructs.* Tissue Eng, 2006. 12(5): p. 1337-44.
31. Bachrach, N.M., V.C. Mow, and F. Guilak, *Incompressibility of the solid matrix of articular cartilage under high hydrostatic pressures.* Journal of Biomechanics, 1998. 31(5): p. 445-451.
32. Urban, J.P., *The chondrocyte: a cell under pressure.* Br J Rheumatol, 1994. 33(10): p. 901-8.
33. Hall, A.C., J.P. Urban, and K.A. Gehl, *The effects of hydrostatic pressure on matrix synthesis in articular cartilage.* J Orthop Res, 1991. 9(1): p. 1-10.
34. Gray, H. and H.V. Carter, *Anatomy: Descriptive and Surgical*. 1858, London: John W. Parker and Son.
35. Möricke, K., *Binde- und Stützgewebe.* Biologie Menschen, 1997. 14: p. 106–125.
36. Buckwalter, J., *Cartilage*, in *Encyclopedia of human biology*, R. Dulbecco, Editor. 1997. p. Vol 2. 431-445.
37. Mow, V.C., A. Ratcliffe, and A.R. Poole, *Cartilage and diarthrodial joints as paradigms for hierarchical materials and structures.* Biomaterials, 1992. 13(2): p. 67-97.
38. Athanasiou, K.A., et al., *Interspecies Comparisons of Insitu Intrinsic Mechanical-Properties of Distal Femoral Cartilage.* Journal of Orthopaedic Research, 1991. 9(3): p. 330-340.
39. Netti, P. and L. Ambrosio, *Articular Cartilage*, in *Integrated Biomaterials Science*, B. R, Editor. 2002, Kluwer Academic / Plenum Publishers: New York. p. 381-402.
40. Farquhar, T., P.R. Dawson, and P.A. Torzilli, *A microstructural model for the anisotropic drained stiffness of articular cartilage.* J Biomech Eng, 1990. 112(4): p. 414-25.
41. Hayes, W.C. and L.F. Mockros, *Viscoelastic properties of human articular cartilage.* Journal of Applied Physiology, 1971. 31(4): p. 562-8.
42. Cohen, N.P., R.J. Foster, and V.C. Mow, *Composition and dynamics of articular cartilage: structure, function, and maintaining healthy state.* J Orthop Sports Phys Ther, 1998. 28(4): p. 203-15.
43. Eyre, D.R., *The collagens of articular cartilage.* Semin Arthritis Rheum, 1991. 21(3 Suppl 2): p. 2-11.
44. Nimni, M.E., *Collagen: Biochemistry*, in *Biomechanics and Biotechnology*, M.E. Nimni, Editor. 1988, CRC Press: Boca Raton, Fl, USA.
45. Eyre, D.R., et al., *Collagen Type-Ix - Evidence for Covalent Linkages to Type-Ii Collagen in Cartilage.* Febs Letters, 1987. 220(2): p. 337-341.
46. Eyre, D., *Collagen of articular cartilage.* Arthritis Res, 2002. 4(1): p. 30-5.
47. Guilak, F., G.R. Erickson, and H.P. Ting-Beall, *The effects of osmotic stress on the viscoelastic and physical properties of articular chondrocytes.* Biophys J, 2002. 82(2): p. 720-7.
48. D'Andrea, P., et al., *Intercellular Ca2+ waves in mechanically stimulated articular chondrocytes.* Biorheology, 2000. 37(1-2): p. 75-83.
49. Yellowley, C.E., et al., *Effects of fluid flow on intracellular calcium in bovine articular chondrocytes.* Am J Physiol, 1997. 273(1 Pt 1): p. C30-6.
50. Shieh, A.C. and K.A. Athanasiou, *Principles of cell mechanics for cartilage tissue engineering.* Ann Biomed Eng, 2003. 31(1): p. 1-11.
51. Idowu, B.D., et al., *Confocal analysis of cytoskeletal organisation within isolated chondrocyte sub-populations cultured in agarose.* Histochemical Journal, 2000. 32(3): p. 165-174.
52. Langelier, E., et al., *The chondrocyte cytoskeleton in mature articular cartilage: structure and distribution of actin, tubulin, and vimentin filaments.* J Histochem Cytochem, 2000. 48(10): p. 1307-20.

53. da Silva, M.L.A., et al., *Chondrogenic differentiation of human bone marrow mesenchymal stem cells in chitosan-based scaffolds using a flow-perfusion bioreactor.* Journal of Tissue Engineering and Regenerative Medicine, 2011. 5(9): p. 722-732.
54. Goncalves, A., et al., *Effect of flow perfusion conditions in the chondrogenic differentiation of bone marrow stromal cells cultured onto starch based biodegradable scaffolds.* Acta Biomater, 2011. 7(4): p. 1644-52.
55. Oliveira, J.T., et al., *A cartilage tissue engineering approach combining starch-polycaprolactone fibre mesh scaffolds with bovine articular chondrocytes.* J Mater Sci Mater Med, 2007. 18(2): p. 295-302.
56. VunjakNovakovic, G., et al., *Effects of mixing on the composition and morphology of tissue-engineered cartilage.* Aiche Journal, 1996. 42(3): p. 850-860.
57. Schulz, R.M. and A. Bader, *Cartilage tissue engineering and bioreactor systems for the cultivation and stimulation of chondrocytes.* Eur Biophys J, 2007. 36(4-5): p. 539-68.
58. Ohyabu, Y., et al., *Cartilage tissue regeneration from bone marrow cells by RWV bioreactor using collagen sponge scaffold.* Materials Science & Engineering C-Biomimetic and Supramolecular Systems, 2009. 29(4): p. 1150-1155.
59. Frondoza, C., A. Sohrabi, and D. Hungerford, *Human chondrocytes proliferate and produce matrix components in microcarrier suspension culture.* Biomaterials, 1996. 17(9): p. 879-88.
60. Bouchet, B.Y., et al., *Beta-1 integrin expression by human nasal chondrocytes in microcarrier spinner culture.* J Biomed Mater Res, 2000. 52(4): p. 716-24.
61. Bueno, E.M., B. Bilgen, and G.A. Barabino, *Wavy-walled bioreactor supports increased cell proliferation and matrix deposition in engineered cartilage constructs.* Tissue Eng, 2005. 11(11-12): p. 1699-709.
62. Chen, H.C., et al., *A novel rotating-shaft bioreactor for two-phase cultivation of tissue-engineered cartilage.* Biotechnol Prog, 2004. 20(6): p. 1802-9.
63. Gooch, K.J., et al., *Effects of mixing intensity on tissue-engineered cartilage.* Biotechnol Bioeng, 2001. 72(4): p. 402-7.
64. Saini, S. and T.M. Wick, *Concentric cylinder bioreactor for production of tissue engineered cartilage: effect of seeding density and hydrodynamic loading on construct development.* Biotechnol Prog, 2003. 19(2): p. 510-21.
65. Alves da Silva, M.L., et al., *Chitosan/polyester-based scaffolds for cartilage tissue engineering: assessment of extracellular matrix formation.* Acta Biomater, 2010. 6(3): p. 1149-57.
66. Sommar, P., et al., *Engineering three-dimensional cartilage- and bone-like tissues using human dermal fibroblasts and macroporous gelatine microcarriers.* Journal of Plastic Reconstructive and Aesthetic Surgery, 2010. 63(6): p. 1036-1046.
67. Freyria, A.M., et al., *Optimization of dynamic culture conditions: effects on biosynthetic activities of chondrocytes grown in collagen sponges.* Tissue Eng, 2005. 11(5-6): p. 674-84.
68. Raimondi, M.T., et al., *The effect of hydrodynamic shear on 3D engineered chondrocyte systems subject to direct perfusion.* Biorheology, 2006. 43(3-4): p. 215-22.
69. Dunkelman NS, Z.M., LeBaron RG, Pavelec R, Kwan M, Purchio AF, *Cartilage production by rabbit articular chondrocytes on polyglycolic acid scaffolds in a closed bioreactor system.* Biotech Bioeng, 1995. 46: p. 299–305.
70. Davisson, T., R.L. Sah, and A. Ratcliffe, *Perfusion increases cell content and matrix synthesis in chondrocyte three-dimensional cultures.* Tissue Eng, 2002. 8(5): p. 807-16.
71. Mahmoudifar, N. and P.M. Doran, *Tissue engineering of human cartilage in bioreactors using single and composite cell-seeded scaffolds.* Biotechnol Bioeng, 2005. 91(3): p. 338-55.
72. Pazzano, D., et al., *Comparison of chondrogensis in static and perfused bioreactor culture.* Biotechnol Prog, 2000. 16(5): p. 893-6.
73. Raimondi, M.T., et al., *The effect of media perfusion on three-dimensional cultures of human chondrocytes: integration of experimental and computational approaches.* Biorheology, 2004. 41(3-4): p. 401-10.
74. Timmins, N.E., et al., *Three-dimensional cell culture and tissue engineering in a T-CUP (tissue culture under perfusion).* Tissue Eng, 2007. 13(8): p. 2021-8.
75. Nagel-Heyer, S., et al., *Bioreactor cultivation of three-dimensional cartilage-carrier-constructs.* Bioprocess Biosyst Eng, 2005. 27(4): p. 273-80.

76. Mizuno, S., F. Allemann, and J. Glowacki, *Effects of medium perfusion on matrix production by bovine chondrocytes in three-dimensional collagen sponges.* J Biomed Mater Res, 2001. 56(3): p. 368-75.
77. Wu, M.H., et al., *Development of PDMS microbioreactor with well-defined and homogenous culture environment for chondrocyte 3-D culture.* Biomed Microdevices, 2006. 8(4): p. 331-40.
78. Xu, X., et al., *Influence of perfusion on metabolism and matrix production by bovine articular chondrocytes in hydrogel scaffolds.* Biotechnology and Bioengineering, 2006. 93(6): p. 1103-1111.
79. Tigli, R.S. and M. Gumusderelioglu, *Chondrogenesis on BMP-6 Loaded Chitosan Scaffolds in Stationary and Dynamic Cultures.* Biotechnol Bioeng, 2009. 104(3): p. 601-610.
80. Tigli, R.S., et al., *Chondrogenesis in perfusion bioreactors using porous silk scaffolds and hESC-derived MSCs.* Journal of Biomedical Materials Research Part A, 2011. 96A(1): p. 21-28.
81. Mahmoudifar, N. and P.M. Doran, *Chondrogenic differentiation of human adipose-derived stem cells in polyglycolic acid mesh scaffolds under dynamic culture conditions.* Biomaterials, 2010. 31(14): p. 3858-3867.
82. Sittinger, M., et al., *Engineering of cartilage tissue using bioresorbable polymer carriers in perfusion culture.* Biomaterials, 1994. 15(6): p. 451-6.
83. Grodzinsky AJ, U.J., *Physical regulation of metabolism in cartilaginous tissues: relation to extracellular forces and flows*, in *Interstitium connective tissue and lymphatics*, G.L. RK Reed, JL Bert, P Winlove, N McHale, Editor. 1995, Portland Press: London. p. 67–84.
84. Setton, L.A., et al., *Biomechanical factors in tissue engineered meniscal repair.* Clin Orthop Relat Res, 1999(367 Suppl): p. S254-72.
85. Eckstein, F., et al., *In vivo morphometry and functional analysis of human articular cartilage with quantitative magnetic resonance imaging--from image to data, from data to theory.* Anat Embryol (Berl), 2001. 203(3): p. 147-73.
86. Soltz, M.A. and G.A. Ateshian, *Experimental verification and theoretical prediction of cartilage interstitial fluid pressurization at an impermeable contact interface in confined compression.* J Biomech, 1998. 31(10): p. 927-34.
87. Candrian, C., et al., *Engineered cartilage generated by nasal chondrocytes is responsive to physical forces resembling joint loading.* Arthritis Rheum, 2008. 58(1): p. 197-208.
88. Takahashi, I., et al., *Compressive force promotes sox9, type II collagen and aggrecan and inhibits IL-1beta expression resulting in chondrogenesis in mouse embryonic limb bud mesenchymal cells.* J Cell Sci, 1998. 111 (Pt 14): p. 2067-76.
89. Demarteau, O., et al., *Dynamic compression of cartilage constructs engineered from expanded human articular chondrocytes.* Biochem Biophys Res Commun, 2003. 310(2): p. 580-8.
90. Xie, J., Z.Y. Han, and T. Matsuda, *Mechanical compressive loading stimulates the activity of proximal region of human COL2A1 gene promoter in transfected chondrocytes.* Biochemical and Biophysical Research Communications, 2006. 344(4): p. 1192-1199.
91. Xie, J., et al., *Mechanical loading-dependence of mRNA expressions of extracellular matrices of chondrocytes inoculated into elastomeric microporous poly (L-lactide-co-epsilon-caprolactone) scaffold.* Tissue Engineering, 2007. 13(1): p. 29-40.
92. Seidel, J.O., et al., *Long-term culture of tissue engineered cartilage in a perfused chamber with mechanical stimulation.* Biorheology, 2004. 41(3-4): p. 445-58.
93. Mauck, R.L., et al., *Regulation of cartilaginous ECM gene transcription by chondrocytes and MSCs in 3D culture in response to dynamic loading.* Biomechanics and Modeling in Mechanobiology, 2007. 6(1-2): p. 113-125.
94. Jung, Y., et al., *Cartilaginous tissue formation using a mechano-active scaffold and dynamic compressive stimulation.* Journal of Biomaterials Science-Polymer Edition, 2008. 19(1): p. 61-74.
95. Huang, C.Y., et al., *Effects of cyclic compressive loading on chondrogenesis of rabbit bone-marrow derived mesenchymal stem cells.* Stem Cells, 2004. 22(3): p. 313-23.
96. Schmidt, O., et al., *Immobilized fibrinogen in PEG hydrogels does not improve chondrocyte-mediated matrix deposition in response to mechanical stimulation.* Biotechnol Bioeng, 2006. 95(6): p. 1061-9.

97. Fehrenbacher, A., et al., *Long-term mechanical loading of chondrocyte-chitosan biocomposites in vitro enhanced their proteoglycan and collagen content.* Biorheology, 2006. 43(6): p. 709-720.
98. Grad, S., et al., *Effects of simple and complex motion patterns on gene expression of chondrocytes seeded in 3D scaffolds.* Tissue Engineering, 2006. 12(11): p. 3171-3179.
99. Li, Z., et al., *Different response of articular chondrocyte subpopulations to surface motion.* Osteoarthritis and Cartilage, 2007. 15(9): p. 1034-1041.
100. Wernike, E., et al., *Effect of reduced oxygen tension and long-term mechanical stimulation on chondrocyte-polymer constructs.* Cell and Tissue Research, 2008. 331(2): p. 473-483.
101. Wimmer, M.A., et al., *Tribology approach to the engineering and study of articular cartilage.* Tissue Engineering, 2004. 10(9-10): p. 1436-1445.
102. Li, Z., et al., *Mechanical load modulates chondrogenesis of human mesenchymal stem cells through the TGF-beta pathway.* J Cell Mol Med, 2010. 14(6): p. 1338-1346.
103. El-Ayoubi, R., et al., *Design and Dynamic Culture of 3D-Scaffolds for Cartilage Tissue Engineering.* Journal of Biomaterials Applications, 2011. 25(5): p. 429-444.
104. Bian, L.M., et al., *Dynamic Mechanical Loading Enhances Functional Properties of Tissue-Engineered Cartilage Using Mature Canine Chondrocytes.* Tissue Engineering Part A, 2010. 16(5): p. 1781-1790.
105. Jung, Y., et al., *The effects of dynamic and three-dimensional environments on chondrogenic differentiation of bone marrow stromal cells.* Biomedical Materials, 2009. 4(5).
106. Wang, P.Y., et al., *Dynamic Compression Modulates Chondrocyte Proliferation and Matrix Biosynthesis in Chitosan/Gelatin Scaffolds.* Journal of Biomedical Materials Research Part B-Applied Biomaterials, 2009. 91B(1): p. 143-152.
107. Ando, K., et al., *Effect of dynamic compressive loading and its combination with a growth factor on the chondrocytic phenotype of 3-dimensional scaffold-embedded chondrocytes.* Acta Orthopaedica, 2009. 80(6): p. 724-733.
108. Morrell, K.C., et al., *Corroboration of in vivo cartilage pressures with implications for synovial joint tribology and osteoarthritis causation.* Proc Natl Acad Sci U S A, 2005. 102(41): p. 14819-24.
109. Carver, S.E. and C.A. Heath, *Increasing extracellular matrix production in regenerating cartilage with intermittent physiological pressure.* Biotechnol Bioeng, 1999a. 62(2): p. 166-74.
110. Mizuno, S., et al., *Hydrostatic fluid pressure enhances matrix synthesis and accumulation by bovine chondrocytes in three-dimensional culture.* J Cell Physiol, 2002. 193(3): p. 319-27.
111. Toyoda, T., et al., *Hydrostatic pressure modulates proteoglycan metabolism in chondrocytes seeded in agarose.* Arthritis Rheum, 2003. 48(10): p. 2865-72.
112. Mio, K., J. Kirkham, and W.A. Bonass, *Possible role of extracellular signal-regulated kinase pathway in regulation of Sox9 mRNA expression in chondrocytes under hydrostatic pressure.* J Biosci Bioeng, 2007. 104(6): p. 506-9.
113. Heyland, J., et al., *Redifferentiation of chondrocytes and cartilage formation under intermittent hydrostatic pressure.* Biotechnology Letters, 2006. 28(20): p. 1641-1648.
114. Sharma, G., R.K. Saxena, and P. Mishra, *Differential effects of cyclic and static pressure on biochemical and morphological properties of chondrocytes from articular cartilage.* Clin Biomech (Bristol, Avon), 2007. 22(2): p. 248-55.
115. Wenger, R., et al., *Hydrostatic pressure increases apoptosis in cartilage-constructs produced from human osteoarthritic chondrocytes.* Front Biosci, 2006. 11: p. 1690-5.
116. Gavenis, K., et al., *Effects of cyclic hydrostatic pressure on the metabolism of human osteoarthritic chondrocytes cultivated in a collagen gel.* Artif Organs, 2007. 31(2): p. 91-8.
117. Wagner, D.R., et al., *Hydrostatic pressure enhances chondrogenic differentiation of human bone marrow stromal cells in osteochondrogenic medium.* Ann Biomed Eng, 2008. 36(5): p. 813-20.
118. Nakamura, S., et al., *Hydrostatic pressure induces apoptosis of chondrocytes cultured in alginate beads.* Journal of Orthopaedic Research, 2006. 24(4): p. 733-739.
119. Gunja, N.J. and K.A. Athanasiou, *Effects of hydrostatic pressure on leporine meniscus cell-seeded PLLA scaffolds.* Journal of Biomedical Materials Research Part A, 2010. 92A(3): p. 896-905.

120. Sakao, K., et al., *Induction of chondrogenic phenotype in synovium-derived progenitor cells by intermittent hydrostatic pressure.* Osteoarthritis Cartilage, 2008. 16(7): p. 805-14.
121. Langer, R. and J.P. Vacanti, *Tissue engineering.* Science, 1993. 260(5110): p. 920-6.

CHAPTER II

Engineering bone: current considerations

This chapter is based on the following publication: Correia C, Sousa RA and Reis RL, 2011, Engineering bone: current considerations - submitted.

Abstract

Bone failure associated with aging, disease or trauma, is a limiting health drawback causing physical disability, pain and increased health costs. Due to the epidemic of musculoskeletal disease occurring worldwide the United Nations has endorsed the past decade as the Bone and Joint Decade [1]. Great effort was made to fight bone ailments in many lines of action, and Tissue Engineering, as an emerging field, greatly evolved to offer new functional therapeutic approaches to this application area. In the context of bone tissue engineering, autologous or allogenic cells can be used in combination with suitable biomaterial scaffolds and bioreactors aimed at providing biomechanical stimulation and environmental control. In this review, major outcomes attained by means of using dynamic culturing under flow perfusion, as major force governing osteocyte mechanotransduction are highlighted. Some insights on latest findings regarding vascularization of bone are discussed.

1. INTRODUCTION

In 2011, the average life expectancy in Europe and United States was estimated as 78.82 and 78.37 years, respectively, corresponding to an 8 year increase relatively to 1970 [2]. Associated with aging phenomena, progressive increases in health problems, as those related with bone failure and internal organ failure being the most common, are creating a large economic and social impacts. There is clinical need to regenerate functional bone due to congenital defects such as hemimelia [3] and growing defects [4]; injury in cases of non-union fractures [5] or acute fractures (boneless) [6], and disease-related, namely after tumoral resection [7] or hip arthroplasty revision surgery [8], among others. Given this, it is believed that the field of tissue engineering and regenerative medicine can provide an invaluable contribution to the treatment of a large variety of bone related conditions. The present review aims to highlight the latest developments in bone tissue engineering by focusing on *in vitro* development of robust bone grafts of clinical-relevant dimension by using dynamic culturing, and specifically by flow stimulation; as well as to draw attention to the latest accomplishments on vascularization of those engineered tissues by spatio-temporal nourishment and culturing of cells (Figure 1).

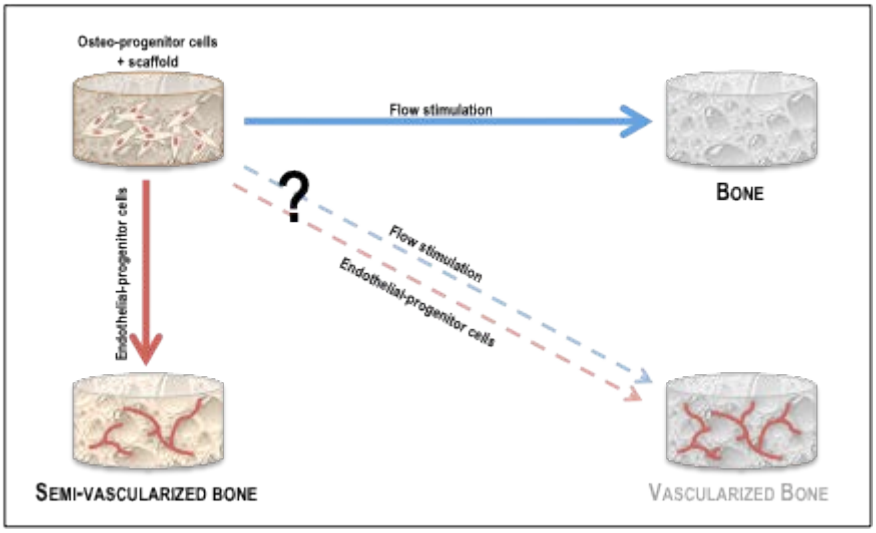

Figure 1 – Schematic representation of possible approaches for engineering bone grafts. Current approaches begin with the use of a scaffold as support for osteo-progenitor cells to grow bone tissue. To improve bone-related outcomes, flow stimulation is applied to cell-scaffold construct obtaining robust mineralized matrix. On the other hand, to attempt growing vascularized bone, combination of endothelial progenitor cells with cell-scaffold construct results in the development of blood vessels within a bone-like graft. Moreover, could both approaches be combined in order to engineer a fully developed and functional vascularized bone graft?

2. BONE BIOLOGY

Bone is a dynamic and greatly vascularized support tissue, with the ability to adapt its mass and morphology to functional demand, owning a distinct capacity to heal and remodel itself without scar [9]. Bone is composed of three distinct cell types [9, 10]: support cells, including the matrix-producing osteoblasts located at the bone surface and the highly specialized osteocytes at the lacuno-canalicular porosities; and the remodeling cells, that include the tissue-resorbing osteoclasts, located at the Howship's lacunae. Along with these cells, calcified bone is composed 70% by weight (wt.) by an inorganic mineral generically referred to as hydroxyapatite [$Ca_{10}(PO_4)_6(OH)_2$], and 25-30% wt. by a non-mineral matrix comprised of type I collagen (~94%)[11] and non-collagenous proteins, such as osteocalcin, osteopontin, osteonectin and bone sialoprotein [9].

At the macroscopic physiology level, the bones of an adult skeleton have a basic structure composed ~80% wt. by an outer cortical or compact zone, ~20% wt. by an inner trabecular or spongy zone, a periosteum and an endosteum [12, 13]. Cortical bone only 10% porous, so it forms a rigid outer shell that resists deformation, while the inner trabecular network provides

strength by acting as a complex system of internal supports [10, 13]. Compact bone contains osteocytes, canaliculi and blood vessels, and its layers of matrix are highly organized forming osteons (Haversian systems). On the other hand, cancellous bone is 50-90% porous, composed by a trabecular meshwork occupied by bone marrow [12]. This porosity makes cancellous bone 10 times weaker than cortical bone [12, 14].

3. MECHANOBIOLOGY OF BONE AND CELL MECHANOTRANSDUCTION

Gravity and locomotion generate mechanical loads responsible by stimulating bone remodeling and consequently maintaining its excellent performance. Nowadays, it is common knowledge that a sedentary lifestyle or prolonged periods of inactivity reduce mechanical stimulation of bone, resulting in net bone loss due to lower tissue formation and higher tissue resorption. While osteoblasts synthesize bone matrix, osteocytes are the major mechanotransducing cell in bone [15, 16]. When mechanically stimulated, osteocytes express multiple paracrine factors, which stimulate osteoblast function and decrease osteoclast activity [9, 17]. Those factors include majorly nitric oxide (NO), prostaglandin E_2 (PGE_2), and insulin-like growth factor (IGF) [15]. This mechanical stimulation is majorly driven by flow – the most widely accepted model of osteocyte mechanotransduction [15, 18-21]. Compressive forces acting on the bone stimulate flow of interstitial fluid through lacuno-canalicular porosities where osteocytes reside [21]. Consequently, shear stresses generated are predicted to range 8 – 30 dyn/cm^2, analogous to vascular wall shear stress [22]. More detailed studies performed on the geometry of the lacuno-canalicular porosity propose that flow is sensed by osteocyte's processes rather than by cell body [22, 23]. While osteocytes are the major cell responsible for sensing mechanical loading in bone, these signals are transmitted by putative mechanotransducers that include mechanosensitive ion channels and integrin adhesions. A rapid and transient increase in intracellular calcium is stimulated by shear stress, which leads to the paracrine factor NO and PGE_2 production [17, 21]. More recently, it has been shown that PGE_2 also plays an important role in mediating the activation of β-catenin signaling pathway in response to the fluid flow shear stress [16]. For more details on the molecular interactions regulating osteoblast functioning and bone remodeling we advise reading Robling *et al.* 2006 [19] and Papachroni *et al.* 2009 [24].

4. ENGINEERING BONE BY DYNAMIC CULTURING – FLOW AS MAJOR MODEL OF OSTEOCYTE MECHANOTRANSDUCTION

The bone tissue engineering has been extensively exploring *in vitro* mechanical stimulation, as a tool for promoting the development of bone-like tissue. Bioreactor systems designed for cultivating bone tissue attempt to elongate, compress or deflect cells grown on different substrates. However, as previously stated, flow is the major inducer of osteocyte mechanotransduction, therefore special focus is given solely to the latest studies exploring the effect of fluid flow on bone biosynthesis in a tissue engineering perspective. Table I presents experimental work published in the last 3 years concerning this subject.

Table I - Experimental studies developed in order to evaluate the effect of fluid flow over bone biosynthesis. Compiled from references [25-32]

Specie	Cell type	Scaffold	Conditions*	Major results /Key findings	Ref.
Human	BMSC	Bovine DCB (TMJ–shaped)	$1x10^6$ cells/mL 1.8 mL/min 5 weeks	Confluent layers of lamellar bone (by SEM), increased volume of mineralized matrix (μCT), formation of osteoids (histologically)	[25]
Human	BMSC	PET	$1.9x10^6/cm^3$ 0.1 ml/min 35 days	Increased differentiation in perfusion cultured shown by lower CFU-F ability and decreased expressions of stem-cell genes of Rex-1 and Oct-4, and higher expression level of osteonectin gene	[26]
Human	BMSC	Bovine DCB	$3x10^7$ cells/mL 80, 400, 800, 1200, 1800 μm/s 5 weeks	Flow velocity increase affected cell morphology, cell–cell interactions, matrix production, composition and expression of osteogenic genes Flow velocities 400 and 800 μm/s yielded the best osteogenic responses	[33]
Human	BMSC	Silk-HA	$3x10^7$ cells/mL 400 μm/s 5,10 weeks	Formation of bone-like structures; 4-fold or 8-fold increase in equilibrium Young's modulus (at 5 or 10 weeks, respectively) in correlation with the initial HA content in scaffolds.	[28]
Rat	BMSC	SPCL	$5x10^5$ cells/scaffold 1 mL/min 8 or 16 days	All data corroborate that lipase coupled with flow perfusion improved osteogenic differentiation of MSCs and enhanced ECM mineralization	[29]

Human	Ob	CG	$4x10^6$ cells/scaffold 1 mL/min; 1h every 7h, 24h 28 days	Flow perfusion bioreactor improved construct homogeneity and enhanced osteogenic phenotype over static controls No difference in the compressive modulus between bioreactor and static groups	[30]
Human	SVF	HA	$1.2x10^7$ cells/scaffold 1 mL/min 5 days + 8 weeks *in vivo*	Endothelial and mesenchymal progenitors formed capillary networks, which anastomosed with host vasculature 1 week after implantation Maintenance of endothelial/mesenchymal SVF cell fractions is crucial to generate osteogenic constructs with enhanced engraftment capacity	[31]
Human	ASC	Bovine DCB	$1.5x10^6$ cells/scaffold 400 μm/s 5 weeks	Medium perfusion markedly improved distribution of cells and bone matrix deposition in engineered constructs	[32]

ASC – adipose stem cell; BMSC – bone marrow mesenchymal stem cell; CFU-F - colony forming units-fibroblast; CG – collagen-glycosaminoglycan; DCB – decellularized bone; ECM- extracellular matrix; HA – Hydroxyapatite; μCT – micro computed tomography; Ob – osteoblasts; PET - poly(ethylene terephthalate); SEM - Scanning electron microscopy; SPCL - starch and poly(e-caprolactone); SVF – stromal vascular fraction; TMJ - temporomandibular joint.

As it can be observed in Table I, the majority of studies investigating effect of fluid flow over bone biosynthesis used human bone marrow mesenchymal stem cells (hMSC). These cells have extraordinary osteogenic differentiation potential [34, 35], and respond positively to flow by increasing osteogenic differentiation [26, 33] and bone-tissue outcomes [28, 33], either directly by responding to shear stress applied at its surface or indirectly by benefiting from improved exchange of gas and nutrients through construct. Moreover, hMSC respond differently to distinct levels of flow - high velocities do not necessarily promote increased bone outcomes [33]. For the first time, a viable human bone graft of clinical relevant dimension, was engineered by using hMSC and a ‘‘biomimetic’’ scaffold-bioreactor system, which have been designed specifically for this purpose [25]. In spite of these achievements, these studies did not explore modifications in mechanotransduction molecules, such as NO, PGE_2 or IGF, which would be of major interest to understand how hMSC respond to applied flow, and possibly to define opportunities for better benefiting from such response when developing bone grafts. In addition, in native bone, cells experience fluctuating shear forces that are induced by pulsatile interstitial flow associated with habitual loading, which makes physiological flow not static. It

would be interesting to attempt mimicking this dynamic nature of flow for *in vitro* bone tissue development. Lastly, Frohlich and co-workers [32] demonstrated that hASC also respond to fluid flow, by enhancing bone matrix deposition, although flow by itself was not enough to induce osteogenic differentiation in hASC - osteogenic supplements were required for such purpose. This questions if either the magnitude of shear stress was too low (approximately 0.01 Pa), or the nature of flow not the ideal (steady, unidirectional shear vs. oscillating flow). Another important question regards the importance of phenotype pre-commitment of hASCs when mechanically stimulated, in order to assure that cells sense, interpret and respond to shear stress [32]. Accurate answers should be given to these questions, so that hASC's potential (as further discussed) could be enhanced towards the engineering of functional and clinically relevant bone grafts.

5. BONE VASCULARIZATION

The vascularized component of engineered bone graft is critical for its survival and function after *in vivo* implantation. This major concern has led to the development of several studies in order to 1) achieve a vascularized bone graft and 2) understand the cross-talk between bone and vascular cells. Table II summarizes most recent findings in this domain.

Table II – Co-culture and single-cell approaches for bone vascularization. Compiled from references [36-42]

Co-culture approach		Scaffold	*In vitro* evaluation	*In vivo* evaluation	Ref.
HDMEC $1.3x10^5$	HOb $0.2x10^5$	Silk fibroin nets	7 and 14 days [43]	SCID mice, subcutaneous 14 days *in vitro* pre-formed microcapillary anastomosed with host vasculature	[36]
HUVEC (1:2)	HOP (1:2)	Alginate micro-spheres	Dynamic culturing, 3 weeks Upregulation of AP and OCN GE and increased mineralization deposits; Increased VEGF secretion	SCID mice, femur defect 3 and 6 weeks Mineralization significantly increased when HOPs were co-immobilized with HUVECs	[37]
HUVEC (1:1)	hMSC (1:1)	n/a	DMEM + M199 (1:1 v/v), 3 weeks Promotion of osteogenic differentiation and significant increase on hMSC proliferation	n/a	[38]
HUVEC $1x10^6$	hMSC $2.5x10^5$	Collagen-fibronectin	hMSC osteoinduction, 1 week	SCID mice, subcutaneous 8 weeks	[39]

(4:1)	(4:1)	gel + PLGA scaffold	Scaffolds were then seeded with collagen-fibronectin gel containing HUVEC and MSC and implanted subcutaneously in SCID mice	HUVECs formed tube-like structures and networks 4–7 days after implantation; anastomosis occurred by day 11; At 4 weeks, network was mature and mineralization occured	
cEPC	cMSC	Collagen fiber mesh scaffold	n/a	SCID mice, subcutaneous 12 weeks Co-implanted EPCs increased neovascularization; Bone area was greater in the MSC+EPC group	[40]
HUVEC $1x10^5$ + $2x10^5$	hMSC $1x10^6$	Fibrin/ Matrigel + Tutobone	hMSC osteoinduction, 3 days	SCID mice, orthotopic calvarial defect, 6 weeks HUVECs formed complex 3D networks of perfused neovessels; MSCs supported bone formation	[41]
Single-cell approach					
hASC $1x10^6$ cells/cm^2	-	Hydroxy-apatite scaffold	Co-differentiation, 3 weeks M199 + osteogenic and endothelial GF	Nude rats, calvarial defect, 3 weeks ASC adhesion, distribution, proliferation and GE demonstrated a full osteogenic and vasculogenic commitment *in vitro* and *in vivo*	[42]

AP – alkaline phosphatase; cEPC – canine endothelial progenitor cells; cMSC - canine mesenchymal stem cells; DMEM - Dulbecco's Modified Eagle's medium; GE – gene expression; GF – growth factors; hASC – human adipose stem cells; HDMEC - human dermal microcapillary endothelial cells; hMSC - human mesenchymal stem cells; HOb – human osteoblasts; HOP- human osteoprogenitors; HUVEC - human umbilical vein endothelial cells; M199 – medium; n/a – non applicable; OCN – osteocalcin; PLGA - poly(DL -lactide-co-glycolide); SCID – severe combined immunodeficiency; VEGF - vascular endothelial growth factor; v/v - volume/volume

A clear trend is observed by analyzing Table II: in the last three years, HUVECs and hMSC interactions have been the most thoroughly explored in order to respectively develop vascular and osteogenic compartments. This is an evolution relatively to earlier studies, well reviewed by Santos and Reis 2010 [44] when HDMECs and human osteoblasts (hOb) were the most used cell sources.

HUVECs are a key cell source on what concerns the formation of functional vascular structures. While HDMEC develop microvascular structures, HUVECs are capable of forming

large blood vessels, which is a beneficial characteristic on aiming to engineer stable functional vascularized bone grafts.

hMSC are a more advantageous cell type than hOb, once MSCs have the potential to undergo two main roles: 1) as osteogenic progenitors, forming mineralized bone matrix [34, 35]; and 2) as pericytes, responsible for stabilizing vascular networks. In this regard, recent publications have been supporting this fact, majorly when MSC are co-cultured with mature endothelial cells [39, 41]. Data summarized in Table II may support this vision: in most studies, better outcomes for both tissue compartments were obtained when endothelial cells were co-immobilized/co-implanted with osteo-progenitors [37, 40].

The close interaction between MSCs and HUVECs in co-culture systems is yet target of extensive research [38, 39, 41]. A reliable *in vitro* model composed of these cells, could become a great tool to clarify and specify the molecular mechanisms that regulate inter-cellular interactions, relevant not only in the scope of engineering vascularized bone grafts, but also to provide a platform to study disease conditions and/or developmental processes.

On the other hand, given the final therapeutic aim, hASC present a clear lead over the HUVEC-hMSC approach, once the same cell source is used to fully develop the vascularized bone graft. hASC have proven to be no less capable of osteogenic differentiation and bone tissue development than bone-marrow MSC [32, 45], which confirms as a promising alternative for cell based therapies of bone [46]. In addition, hASC have demonstrated its intrinsic potential for endothelial differentiation and capillary formation [47-49]. As mentioned in table II, when nourished with a cocktail of both osteogenic and vasculogenic growth factors, hASC show to commit to both lineages, by expressing correspondent specific markers, such as osteopontin, osteonectin, osteocalcin, and collagen type I, for bone; and CD31, von Willebrand Factor and VEGF, for vasculogenesis [42]. Besides this potential, hASC present other key characteristics such as:

a. Adipose tissue (AT) is harvested from the patient by either dedicated or non-dedicated procedures. AT can be obtained repeatedly in large quantities under local anesthesia and with a minimum of patient discomfort;
b. Can be used used in an autologous manner, but still presents a high potential for allogeinic purposes;
c. Adipose tissue yields very high cell numbers, as compared to bone-marrow harvest procedures [50].

Although hASC present such attractive characteristics, the major challenge - to fully engineer functional bone and vessels concurrently - is yet to be achieved.

6. Conclusions and Future Perspectives

In this concise review, we have highlighted several aspects, namely the need to fulfill current clinical demands of bone grafts, the basics of bone biology, as well as the biomechanical mechanisms by which bone tissue remodels and maintains its specific architecture. Under this transversal scope we have further addressed the most recent studies on dynamic engineering of bone grafts using flow perfusion (and inherently shear stress – the major force type governing osteocyte mechanotransduction).

While hMSC remains the major cell source studied under this domain during the past three years; hASC have emerged as an alternative and promising cell source for exploitation. In fact, hASC have proved its potential for development of both osteogenic compartment and blood vessel network, which would enable the engineering of a functional tissue graft from a unique cell source. Taken these two approaches together we believe and suggest that flow can also be used to mechanically stimulate endothelial / stem cells in order to induce better vasculature within the engineered bone, and reduce the overall culturing period time.

Acknowledgments

We gratefully acknowledge funding support by the Portuguese Foundation for Science and Technology to CCorreia (PhD grant SFRH/BD/42316/2007).

References

1. Hazes, J. and A. Woolf, *The bone and joint decade 2000-2010.* J Rheumatol, 2000. 27: p. 1-3.
2. CIA. *The World Factbook*. 2011.
3. Weber, M., *New classification and score for tibial hemimelia.* J Child Orthop, 2008. 2(3): p. 169-75.
4. Dayer, R., et al., *Tibial aplasia-hypoplasia and ectrodactyly in monozygotic twins with a discordant phenotype.* J Pediatr Orthop, 2007. 27(3): p. 266-9.
5. Tare, R.S., et al., *Skeletal stem cells and bone regeneration: translational strategies from bench to clinic.* Proc Inst Mech Eng H, 2010. 224(12): p. 1455-70.
6. Argintar, E., S. Edwards, and J. Delahay, *Bone morphogenetic proteins in orthopaedic trauma surgery.* Injury, 2011. 42(8): p. 730-4.
7. De Biase, P., et al., *Scaffolds combined with stem cells and growth factors in healing of pseudotumoral lesions of bone.* Int J Immunopathol Pharmacol, 2011. 24(1 Suppl 2): p. 11-5.
8. Mall, N.A., et al., *The fate of grafting acetabular defects during revision total hip arthroplasty.* Clin Orthop Relat Res, 2010. 468(12): p. 3286-94.
9. Sommerfeldt, D.W. and C.T. Rubin, *Biology of bone and how it orchestrates the form and function of the skeleton.* Eur Spine J, 2001. 10 Suppl 2: p. S86-95.
10. Salgado, A.J., et al., *Adult stem cells in bone and cartilage tissue engineering.* Curr Stem Cell Res Ther, 2006. 1(3): p. 345-64.
11. Viguet-Carrin, S., P. Garnero, and P.D. Delmas, *The role of collagen in bone strength.* Osteoporos Int, 2006. 17(3): p. 319-36.
12. Buckwalter JA, G.M., Cooper RR, Recker R, *Bone Biology.* J Bone Jt Surg, 1996. 77(A): p. 1256-89.
13. Sikavitsas, V.I., J.S. Temenoff, and A.G. Mikos, *Biomaterials and bone mechanotransduction.* Biomaterials, 2001. 22(19): p. 2581-93.
14. Currey, J., *The mechanical properties of materials and the structure of bone.*, in *The mechanical adaptations of bones*. 1984, Princeton University Press: Princeton. p. 3-37.
15. Orr, A.W., et al., *Mechanisms of mechanotransduction.* Developmental Cell, 2006. 10(1): p. 11-20.
16. Kamel, M.A., et al., *Activation of beta-catenin signaling in MLO-Y4 osteocytic cells versus 2T3 osteoblastic cells by fluid flow shear stress and PGE(2): Implications for the study of mechanosensation in bone.* Bone, 2010. 47(5): p. 872-881.
17. Raisz, L.G., *Physiology and pathophysiology of bone remodeling.* Clin Chem, 1999. 45(8 Pt 2): p. 1353-8.
18. Fritton, S.P. and S. Weinbaum, *Fluid and Solute Transport in Bone: Flow-Induced Mechanotransduction.* Annual Review of Fluid Mechanics, 2009. 41: p. 347-374.
19. Robling, A.G., A.B. Castillo, and C.H. Turner, *Biomechanical and molecular regulation of bone remodeling.* Annual Review of Biomedical Engineering, 2006. 8: p. 455-498.
20. Mullender, M., et al., *Mechanotransduction of bone cells in vitro: mechanobiology of bone tissue.* Med Biol Eng Comput, 2004. 42(1): p. 14-21.
21. Burger, E.H. and J. Klein-Nulend, *Mechanotransduction in bone--role of the lacuno-canalicular network.* FASEB J, 1999. 13 Suppl: p. S101-12.
22. Weinbaum, S., S.C. Cowin, and Y. Zeng, *A Model for the Excitation of Osteocytes by Mechanical Loading-Induced Bone Fluid Shear Stresses.* Journal of Biomechanics, 1994. 27(3): p. 339-360.
23. Anderson, E.J., et al., *Nano-microscale models of periosteocytic flow show differences in stresses imparted to cell body and processes.* Annals of Biomedical Engineering, 2005. 33(1): p. 52-62.
24. Papachroni, K.K., et al., *Mechanotransduction in osteoblast regulation and bone disease.* Trends in Molecular Medicine, 2009. 15(5): p. 208-216.
25. Grayson, W.L., et al., *Engineering anatomically shaped human bone grafts.* Proc Natl Acad Sci U S A, 2010. 107(8): p. 3299-304.
26. Zhao, F., et al., *Perfusion affects the tissue developmental patterns of human mesenchymal stem cells in 3D scaffolds.* J Cell Physiol, 2009. 219(2): p. 421-9.

27. Grayson, W.L., et al., *Optimizing the medium perfusion rate in bone tissue engineering bioreactors.* Biotechnol Bioeng, 2010.
28. Bhumiratana, S., et al., *Nucleation and growth of mineralized bone matrix on silk-hydroxyapatite composite scaffolds.* Biomaterials, 2011. 32(11): p. 2812-20.
29. Martins, A.M., et al., *Combination of enzymes and flow perfusion conditions improves osteogenic differentiation of bone marrow stromal cells cultured upon starch/poly(epsilon-caprolactone) fiber meshes.* J Biomed Mater Res A, 2010. 94(4): p. 1061-9.
30. Keogh, M.B., et al., *Three Hours of Perfusion Culture Prior to 28 days of Static Culture, Enhances Osteogenesis by Human Cells in a Collagen GAG Scaffold.* Biotechnology and Bioengineering, 2011. 108(5): p. 1203-1210.
31. Guven, S., et al., *Engineering of large osteogenic grafts with rapid engraftment capacity using mesenchymal and endothelial progenitors from human adipose tissue.* Biomaterials, 2011. 32(25): p. 5801-5809.
32. Frohlich, M., et al., *Bone Grafts Engineered from Human Adipose-Derived Stem Cells in Perfusion Bioreactor Culture.* Tissue Engineering Part A, 2010. 16(1): p. 179-189.
33. Grayson, W.L., et al., *Optimizing the Medium Perfusion Rate in Bone Tissue Engineering Bioreactors.* Biotechnology and Bioengineering, 2011. 108(5): p. 1159-1170.
34. Bruder, S.P., N. Jaiswal, and S.E. Haynesworth, *Growth kinetics, self-renewal, and the osteogenic potential of purified human mesenchymal stem cells during extensive subcultivation and following cryopreservation.* J Cell Biochem, 1997. 64(2): p. 278-94.
35. Cheng, S.L., et al., *Differentiation of human bone marrow osteogenic stromal cells in vitro: induction of the osteoblast phenotype by dexamethasone.* Endocrinology, 1994. 134(1): p. 277-86.
36. Unger, R.E., et al., *The rapid anastomosis between prevascularized networks on silk fibroin scaffolds generated in vitro with cocultures of human microvascular endothelial and osteoblast cells and the host vasculature.* Biomaterials, 2010. 31(27): p. 6959-6967.
37. Grellier, M., et al., *The effect of the co-immobilization of human osteoprogenitors and endothelial cells within alginate microspheres on mineralization in a bone defect.* Biomaterials, 2009. 30(19): p. 3271-8.
38. Bidarra, S.J., et al., *Phenotypic and proliferative modulation of human mesenchymal stem cells via crosstalk with endothelial cells.* Stem Cell Res, 2011. 7(3): p. 186-97.
39. Tsigkou, O., et al., *Engineered vascularized bone grafts.* Proceedings of the National Academy of Sciences of the United States of America, 2010. 107(8): p. 3311-3316.
40. Usami, K., et al., *Composite implantation of mesenchymal stem cells with endothelial progenitor cells enhances tissue-engineered bone formation.* J Biomed Mater Res A, 2009. 90(3): p. 730-41.
41. Koob, S., et al., *Bone formation and neovascularization mediated by mesenchymal stem cells and endothelial cells in critical-sized calvarial defects.* Tissue Eng Part A, 2011. 17(3-4): p. 311-21.
42. Gardin, C., et al., *In vitro concurrent endothelial and osteogenic commitment of adipose-derived stem cells and their genomical analyses through CGH array: novel strategies to increase the successful engraftment of tissue engineered bone grafts.* Stem Cells and Development, 2011. in press.
43. Unger, R.E., et al., *Tissue-like self-assembly in cocultures of endothelial cells and osteoblasts and the formation of microcapillary-like structures on three-dimensional porous biomaterials.* Biomaterials, 2007. 28(27): p. 3965-3976.
44. Santos, M.I. and R.L. Reis, *Vascularization in Bone Tissue Engineering: Physiology, Current Strategies, Major Hurdles and Future Challenges.* Macromolecular Bioscience, 2010. 10(1): p. 12-27.
45. Schaffler, A. and C. Buchler, *Concise review: adipose tissue-derived stromal cells--basic and clinical implications for novel cell-based therapies.* Stem Cells, 2007. 25(4): p. 818-27.
46. Gimble, J.M., F. Guilak, and B.A. Bunnell, *Clinical and preclinical translation of cell-based therapies using adipose tissue-derived cells.* Stem Cell Research & Therapy, 2010. 1.

47. Fischer, L.J., et al., *Endothelial Differentiation of Adipose-Derived Stem Cells: Effects of Endothelial Cell Growth Supplement and Shear Force.* Journal of Surgical Research, 2009. 152(1): p. 157-166.
48. Scherberich, A., et al., *Adipose tissue-derived progenitors for engineering osteogenic and vasculogenic grafts.* J Cell Physiol, 2010. 225(2): p. 348-53.
49. Keerl, S., et al., *PDGF and bFGF Modulate Tube Formation in Adipose Tissue-Derived Stem Cells.* Annals of Plastic Surgery, 2010. 64(4): p. 487-490.
50. Aust, L., et al., *Yield of human adipose-derived adult stem cells from liposuction aspirates.* Cytotherapy, 2004. 6(1): p. 7-14.

Section 2.

CHAPTER III

Materials and Methods

This chapter describes the materials used and the experimental methods employed in the set of studies described in this thesis. Although each individual chapter contains a brief specific materials and methods section, this chapter will provide additional information about the procedures used and how they were performed, as well as more details about the materials chosen for the experimental development of both cartilage and vascularized bone tissue.

1. MATERIALS

1.1. GELLAN GUM

Gellan gum (GG) is a high molecular weight polysaccharide obtained by microbial fermentation *of Sphingomonas elodea*, an anaerobic, non-pathogenic gram-negative bacterium [1]. GG is a water-soluble gelling agent commonly used in food and pharmaceutical industry, due to its processing into transparent gels resistant to heat and acid stress. The general chemical structure of GG is presented in Figure 1, initially described by Moorhouse et al. [2] Its structure is composed of tetrasaccharide (1,3-β-D-glucose, 1,4-β–D-glucuronic acid, 1,4-β-D-glucose, 1,4-α-L-rhamnose) repeating units, containing one carboxyl side group. The thickness and hardness of the GG is determined by acetyl groups present in the gellan gum obtained from the microbial culture: with acetyl groups, the gel is soft and elastic; without acetyl groups, firmer gels are obtained [3]. Both are commercially available, being the later the most common. Both form thermo-reversible gels with different mechanical properties in the presence of metallic ions and upon temperature decrease. In addition to food and pharmaceutical applications, GG has proven its potential application in Tissue Engineering and Regenerative Medicine field. Once GG presents a thermo-sensitive behavior, with gelation close to body temperature, its application as an injectable formulation for repair of cartilage defects is promising. In our group, Oliveira JT *et al* [4-6] firstly described its use as a biomaterial for cartilage regeneration, proving deposition of cartilaginous extracellular matrix *in vitro* and *in vivo* by articular chondrocytes, nasal chondrocytes and adipose-derived stem cells. Furthermore, Correia JS *et al* increased structural and mechanical integrity of GG hydrogel by modifying the polymer with specific functional groups (i.e. methacrylates). Free radical polymerization occurs in the presence of a photo-initiator and upon exposure to UV light [7]. The studies performed in the scope of this thesis (chapter IV) were developed with non-modified gellan gum, purchased from Sigma-Aldrich - Gelzan™ CM, Cat # G1910.

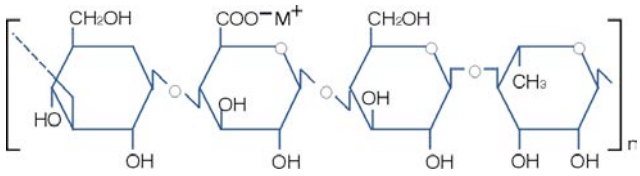

Figure 1. Molecular structure of gellan gum. Consists of a linear repeating tetrasaccharide unit (n) composed of glucose, rhamnose and glucuronic acid. www.kelco.com

1.2. SILK FIBROIN

Silkworm silk fibroin (SF) has been used in textile production for centuries, and in the last decades it has found wide clinical use as biomedical sutures. SF extracted from the silkworm *Bombix mori* cocoon (Figure 2A), consists primarily of two protein components: fibroin and sericins (Figure 2B). Fibroin is the structural protein of the silk fibers composed of heavy and light chain polypeptides of 350 and 25 kDa, respectively, connected by a disulfide link [8]. It is a protein dominated in composition by the amino acids glycine, alanine and serine, which form antiparallel ß-sheets in the spun fibers, leading to the stability and mechanical features of the fibers [9, 10]. Sericins are the water-soluble glue-like proteins that bond the fibroin fibers together [11]. The highly repetitive primary sequence that characterizes fibrous proteins such as silk, lead to significant homogeneity in secondary structure (ß-sheets), which allow silk fibroin to exhibit extraordinary strength, ranging 15–17 GPa [12]. Because of this impressive mechanical performance, in combination with its biocompatibility and biodegradability characteristics, silk fibroin provides an important set of material options for biomaterials and scaffolds for tissue engineering [12-16]. In particular for bone tissue engineering, silk fibroin has been studied thoroughly in order to achieve an ideal scaffold [17-22]. In this thesis, silk fibroin scaffolds were used in chapters V, VI and VII.

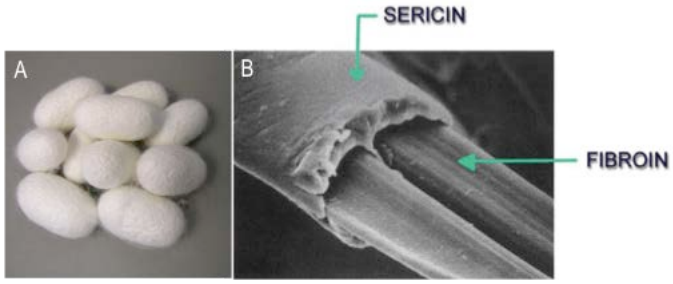

Figure 2 – A – *Bombix mori* silk cocoon, B – Silk fiber composed by fibroin and outer layer of sericin. www.dermasilk.com.

1.3. BOVINE TRABECULAR BONE

Trabecular bone was obtained from the subchondral region of carpometacarpal joints of 2-week to 4-month old bovine calves. Demineralized bone matrix is an osteo-inductive biomaterial due to the presence of bone-derived growth factors [23]. As a result, various forms of demineralized bone matrix, bone morphogenetic proteins, and bone graft substitutes are commonly used in clinical applications for bone repair [24]. Decellularized bone (DCB), per se, provide the osteoinductive growth factors in addition to mechanical and architectural properties, making these suitable for bone tissue engineering purposes. DCB scaffolds have been employed for bone tissue-engineering applications [24, 25], and will be used in chapter V as a gold standard, and chapter VIII as part of the *in vitro* model developed.

2. SCAFFOLDS PRODUCTION

2.1. GELLAN GUM HYDROGELS

Gellan gum hydrogel was produced according to the procedure described by Oliveira JT *et al* [26, 27]. Briefly, powdered gellan gum (Gelzan™ Sigma G1910) was dissolved in distilled water under constant stirring at room temperature into a 1.5% (w/v) solution. This solution was progressively heated up to 90ºC, temperature at which complete and homogenous dissolution of the material was obtained. After 20-30 min, temperature was progressively decreased to 37-40ºC, for cell encapsulation. PBS (Sigma P4417) was added to GG solution at 1:20 (v/v) ratio. Before gelation, GG solution was cast into a cylindrical mould and PBS was used as a cross-linking agent to stabilize the hydrogel structure. Discs with 4 mm diameter and 2 mm height were cut using a scalpel, and used in experiments described in chapter IV.

2.2. SILK FIBROIN SCAFFOLDS

Silk fibroin from silkworm (*Bombix mori*) cocoons was extracted with 0.02 M sodium carbonate (Na_2CO_3) solution, rinsed in distilled water, dissolved in a 9.3 M lithium bromide (LiBr) solution and dialyzed for 48h against distilled water in benzoylated dialysis tubing (Sigma D7884). Dissolved silk fibroin was centrifuged for 20 min at 9000 rpm (4ºC). The resulting solution was determined by weighing the remaining solid after drying, yielding a 6-wt % aqueous silk fibroin solution.

2.2.1. AQUEOUS-BASED POROUS SCAFFOLDS

Aqueous-derived silk fibroin porous sponges were prepared by salt leaching methods. NaCl salt was sieved with metal mesh to obtain particle size of 250–500 μm (Aq-250), or 500–1000 μm (Aq-500), and added into silk fibroin aqueous solution at a 2:1 (w/v) ratio, in disk-shaped containers. The container was covered and left at room temperature. After 24h, the container was immersed in water to extract NaCl salt for 2 days with water changes. Discs with 4 mm diameter and 2 mm height were cored and used in experiments described in chapter V.

2.2.2. AQUEOUS-BASED LAMELLAR SCAFFOLDS

Aqueous-derived silk fibroin lamellar scaffolds (Aq-Lam) were prepared by pouring silk fibroin aqueous solution into silicon tubing (6 mm i.d.), frozen at -80ºC, lyophilized for 1 day, and autoclaved to induce the formation of the β-sheet structure and insolubility in aqueous solution. 4 mm diameter and 2 mm height discs were cored and used in experiments described in chapter V.

2.2.3. HFIP-DERIVED POROUS SCAFFOLDS

HFIP-derived silk fibroin scaffolds (HFIP-400) were prepared as previously described [28], and used in chapters V, VI and VII. Silk fibroin aqueous solution was lyophilized and further dissolved with HFIP, resulting in a 17-wt % HFIP-derived silk fibroin solution. Granular NaCl (400–600 μm) were added to 2 mL of silk fibroin in HFIP at 2:1 (w/v) ratio. The containers were covered overnight to reduce evaporation of HFIP and to provide sufficient time for homogeneous distribution of the solution. Subsequently, the solvent was evaporated at room temperature for 3 days. The matrices were then treated in 90% (v/v) methanol for 30 min, to induce the formation of the β-sheet structure, followed by immersion in water for 2 days to remove the NaCl.

2.3. DECELLULARIZED BONE SCAFFOLDS

Trabecular bone cylinders (4 mm diameter) were cored from the subchondral region of carpometacarpal joints of bovine calves, and washed with a high velocity stream of water to remove bone marrow from pore spaces. Scaffolds were further washed for 1h in phosphate-buffered saline (PBS) with 0.1% ethylenediamine tetraacetic acid (EDTA) at room temperature (RT), followed by sequential washes in hypotonic buffer (10 mM Tris and 0.1% EDTA)

overnight at 4º C, in detergent (10 mM Tris and 0.5% sodium dodecyl sulfate) for 24 h at RT, and in enzyme solution (100 U/mL DNAse, 1 U/mL RNAse, and 10 mM Tris) for 6 h at 37º C, to fully remove cellular material. Scaffolds were then rinsed in PBS, freeze-dried, and cut into 2 mm thick cylindrical plugs. The scaffolds within the density range of 0.28–0.38 mg/mm^3 (calculated based on the dry weights and exact dimensions) were selected for experiments of chapters V and VIII.

3. Cell isolation and expansion

3.1. Isolation and expansion of Human Nasal Chondrocytes

Transphenoidal biopsy was collected from patients undergoing neurosurgery. The patients had signed an informed consent document approved by the Ethical Committee of Hospital S. Marcos, Braga, Portugal. Nasal cartilage was dissected and digested with collagenase type II, according to protocol described elsewhere [29]. Briefly, the tissue was washed with sterile PBS (Sigma P4417), diced into 2-3 mm thickness cubes, immersed in 20 mL trypsin-EDTA solution (Invitrogen 25300-062) and incubated for 30 minutes at 37ºC in a rotator. Tripsin-EDTA solution was removed and 20 mL of collagenase type II (2 mg/mL, Sigma C6885) was added and allowed to incubate for 15h at 37ºC in a rotator. The digested tissue was filtered and the cell suspension centrifuged at 1200 rpm for 8 minutes. The cell pellet was washed twice with PBS and cells counted with a hemocytometer using the viability stain trypan blue (Sigma). Chondrocytes were expanded with chondrogenic expansion medium composed by D-MEM high glucose (Sigma D5671), 1% non-essential amino-acids (1xMEM Invitrogen 11140-035); 20 mM L-alanyl-L-glutamine (Sigma G8541); 1% antibiotic/antimicotic 100x (15240-062 Gibco); 10 mM HEPES (Sigma H4034); 10% Fetal Bovine Serum (Biochrom, Germany, Heat inactivated 30 min., 57ºC), supplemented with basic fibroblast growth factor (b-FGF) 10 ng/mL (Peprotek 100-18B, UK). Chondrocytes were expanded until passage 3 and detached from the culture flask with trypsin-EDTA (Invitrogen 25300-062) and used in studies of chapter V.

3.2. Isolation and expansion of Human Adipose Stem Cells

Human adipose stem cells (hASCs) were isolated from liposuction aspirates of subcutaneous adipose tissue (AT), donated with written consent by patients undergoing elective liposurgery. AT was distributed into 50 mL falcon tubes to which PBS (1:1) was added, and vigorously agitated. The mixture was centrifuged 200g for 5 minutes at RT and infranatants discarded. 1

mL of collagenase solution 0.2 U/mL (Collagenase NB 4 Standard grade, SERVA Electrophoresis, Cat. No. 17454) was added per gram of washed AT, shaked vigorously and incubated at 37ºC for 45 min in a water bath with agitation at 200 rpm. Digested AT was further centrifuged at 1200g, 3minutes, RT and supernatants discarded. The remaining pellet was suspended with erythrocyte lysis buffer (ELB) and further centrifuged at 400g, 10 min, RT. Supernatant was discarded and pellet suspended in alpha-MEM media (GIBCO 12000-063) for filtering through a cell strainer. The stromal vascular fraction (SVF) was plated in cell culture plates, and adhered cells were further were expanded to the third passage in high-glucose Dulbecco's modified Eagle's medium (DMEM) (GIBCO 11965) supplemented with 10% fetal bovine serum (FBS) (GIBCO 26140), penicillin–streptomycin (1%) (GIBCO 15140) and 1 ng/mL basic fibroblast growth factor (bFGF) (Peprotech 100-18B). p0 cells were examined for surface marker expression using flow cytometry and used in experiments described in chapters IV, V, VI and VII. The presence of specific antigens such as CD105, CD45, CD34, CD73 and CD90 were analyzed, as previously published [30, 31]. hASCs were tested for their differentiation capacity into the osteogenic, chondrogenic and adipogenic lineages.

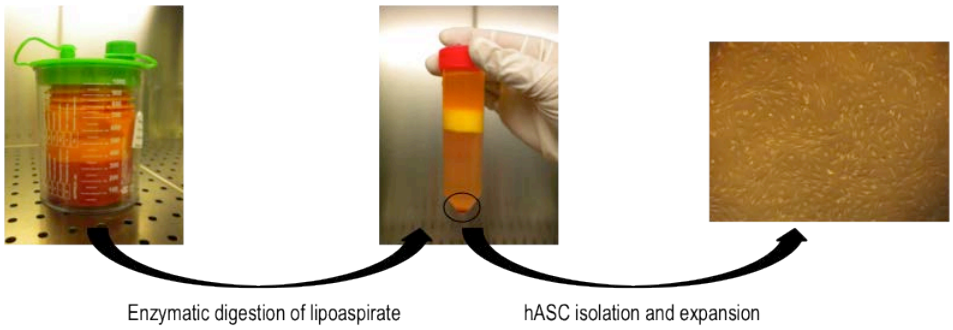

Figure 3. Major steps performed for isolation of human adipose stem cells.

3.3. Expansion of Human Bone Marrow Stem Cells

Bone marrow-derived human mesenchymal stem cells (MSCs) were isolated from the mononuclear fraction of a bone marrow aspirate obtained from a commercial source (Cambrex, CA) based on their attachment to tissue culture plastics [25], expanded in high glucose DMEM supplemented with 10 % FBS, 1 % Pen–Strep and 1 ng/mL basic fibroblast growth factor (bFGF) to the 3rd passage. These cells have been characterized for their ability to differentiate into osteogenic, chondrogenic, and adipogenic phenotypes *in vitro* and for their ability to give

rise to new bone formation *in vitro* and *in vivo* [22, 25, 32]. These expanded MSCs were used in the experiments described in chapter VIII.

3.4. Expansion of Human Umbilical Vein Endothelial Cells

Fresh umbilical veins were obtained from the neonatal unit at Columbia University following an approved IRB protocol (IRBAAAC4839). To isolate human umbilical vein endothelial cells (HUVECs), the vein was flushed with HEPES buffer to remove residual blood and treated with trypsin for 15 minutes to remove the endothelial cells. Cells were flushed from the vein with HEPES and collected in centrifuge tubes. The suspension was centrifuged at 300 g for 5 minutes and the supernatant was discarded. Cells were resuspended in EGM and cultured in tissue culture flasks. Non-adherent cells were washed out after 1 day. When the HUVECs grew to confluence, they were trypsinized, counted and cryopreserved. For experiments described in chapter VIII HUVECs were expanded in EGM media to passage four.

4. *In vitro* studies

4.1. Cartilage tissue development by Hydrostatic Pressure Stimulation

Two original easy-to-use devices were developed to generate hydrostatic pressure forces, which uniformly load constructs in culture (chapter IV). The High Hydrostatic Pressure Bioreactor (HHPB) was designed to generate physiological amplitudes of hydrostatic pressure (up to 10 MPa), and the Low Hydrostatic Pressure Bioreactor (LHPB) was projected to load culturing constructs with lower HP amplitudes (up to 0.5 MPa). Both devices enclose particular key characteristics, such as:

a. Possibility to perform long term culturing, up to several weeks;
b. Culture of multiple 3D constructs within a high range of dimensions;
c. Tunable loading parameters: pressure amplitudes may range 0 - 0.4 MPa (for LHPB) and 1.5 - 10 MPa (for HHPB); frequency may range between 0 - 1 Hz;
d. Operation of devices inside standard biohazard hoods, and CO_2 incubators at 37ºC, in complete sterile conditions;
e. LHPB is disposable, composed by standard, off-the-shelf components, while HHPB is reusable, composed by sterilizable stainless steel components.

4.1.1. HIGH HPB

The High-HPB system consists of a stainless steel device (15 cm diameter x 18 cm height), composed of a culture chamber (CC), an air chamber (AC) and a piston. The air pressure driven piston creates hydrostatic pressure in the culture chamber, where constructs reside in culturing media. As filtered compressed house air enters the air chamber, piston is pushed up. Ratio of AC and CC area is 15:1. A pressure transducer (0-16 MPa, Swagelok, USA), with digital display is connected to the lid of the culture chamber providing real time pressure reading. Pulsatile pressurization is controlled by a Programmable Logic Controller unit (PLC – OMRON CPM1A-30CDR-A-V1, Netherlands), and solenoid valve (Camozzi A331-1C2, Italy). When non-pressurized, culture media is replenished through the culture chamber by a peristaltic pump (Ismatec, USA), from a standard 50 mL schott bottle, with an adapted air filter.

4.1.2. LOW HPB

The Low-HPB system is composed by a 30 mL luer-lok polypropylene syringe (BD Biosciences), where the rubber piston is used as a physical division between the culture media and compressed air, used as mechanism of compression. An aluminum adapter is connected at the top of the syringe, together with a semi-rigid nylon tube (Legris) to conduct filtered compressed house air inside the chamber. At the bottom of the syringe, Pharmed BPT tubing (Masterflex, USA) is connected to allow gas exchange. PLC and solenoide valve used with HHPB allow controlled pulsatile pressurization of the culture media. Media is replenished through the Pharmed BPT tubing, using a syringe to avoid complex manipulation.

4.1.3. CELL ENCAPSULATION

Gellan gum hydrogel was produced according to the procedure published by Oliveira JT *et al* (2010) [26, 27] and described in section 2.1. Powder GG, autoclave-sterilized was dissolved in distilled water at 1.5% (w/v). When temperature of GG solution was decreased to 37-40ºC, a cell-suspension prepared at a final concentration of $10x10^6$ cells/mL of PBS was added at 1:20 ratio (v/v) under constant stirring. Cylindrical discs were made with a mould and PBS was used as a cross-linking agent to stabilize the hydrogel structure. Discs with 4 mm diameter and 2 mm height were cut using a borer.

4.2. Bone tissue development by Pulsatile Perfusion

4.2.1. Perfusion Bioreactor

The perfusion bioreactor system used in chapter VI has been widely used in bone tissue engineering studies [22, 32-34]. It has the dimensions of a 10-cm glass Petri dish, and the glass cover of this dish serves as the removable bioreactor cover. It allows culturing multiple scaffolds (4 to 10 mm in diameter and up to 4 mm high) and imaging capabilities. Scaffolds are placed into six wells arranged in a radial pattern, press-fit in place into a layer of polydimethylsiloxane (PDMS). Each bioreactor enabled simultaneous cultivation and uniform perfusion of the six scaffolds. Culture medium enters the bioreactor through a central port from where it flows to the center of the bioreactor and is evenly distributed into six channels leading to the scaffolds. A multi-channel peristaltic pump (Ismatec, USA) is used to maintain re-circulating flow. The flow rate was determined by the cross-sectional area of the tube as the length of the column of fluid being pumped and the rate of pumping remained constant among groups. Figure 4 displays the bioreactor design [33].

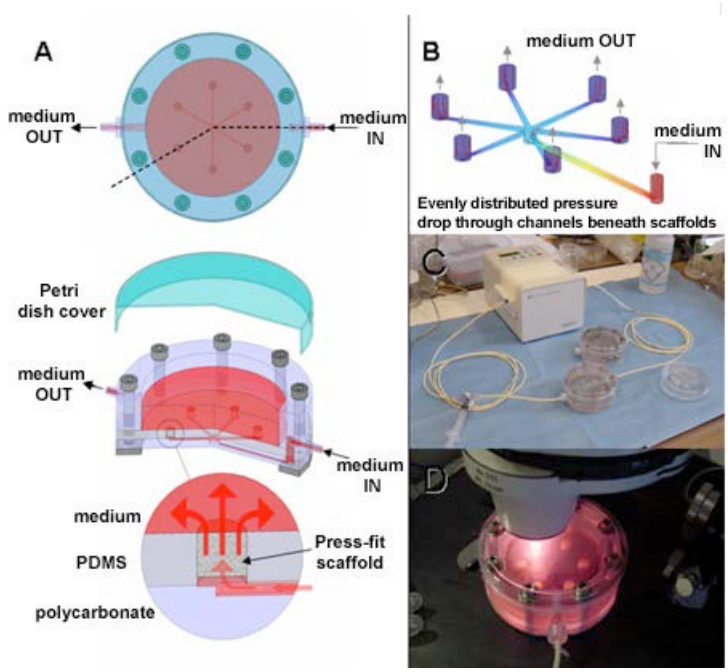

Figure 4 – Perfusion bioreactor: (A) Schematic presentation of the perfusion bioreactor system. (B) Computational Fluid Dynamics simulation of flow through channels indicating uniform flow to all six wells. (C) Complete experimental set-up. (D) Imaging of tissue constructs in situ.

4.2.2. CELL SEEDING

For perfusion studies performed in chapter VI, HFIP-derived silk fibroin scaffolds were sterilized in 70% (v/v) ethanol overnight, washed in PBS and incubated in culture media prior to seeding. Expanded hASCs at passage 4 were suspended at $30x10^6$ cells/mL. A 40 μL aliquot of cell suspension was pipetted to the top of blot-dried scaffods, pipetted up and down to ensure even distribution of cells. After 15 minutes in the incubator, scaffolds were rotated 180º, and 10 μL of cell-free medium was added to prevent these to dry. This process was repeated four times, to allow uniform cell distribution, after which, osteogenic media (low glucose DMEM, 10% FBS, 1% penicillin–streptomycin, 10 mM sodium-b-glycerophosphate, 10 mM HEPES, 100 nM dexamethasone and 50 μg/mL ascorbic acid-2-phosphate) was added. Scaffolds were then cultured in static conditions (well-plate) for 3 days to allow cell attachment.

4.3. SILK SCAFFOLD SCREENING

In chapter V, the four formulations of silk scaffolds described in 2.2, were cultured with human adipose stem cells (hASC), in order to assess bone tissue development. All scaffolds were sterilized in 70% ethanol overnight, washed in PBS and incubated in culture medium prior to seeding. Expanded P4 hASC were suspended in culture medium at $30x10^6$ cells/mL. A 20 μL aliquot of cell suspension was pipetted into blot-dried scaffolds, and pipetted up and down to ensure even distribution of cells. After 15 minutes in the incubator, scaffolds were rotated 180º, and 10 μL of cell-free medium was added to maintain hydration. This process was repeated four times, to achieve uniform cell distribution, after which, osteogenic media (low glucose DMEM, 10% FBS, 1% penicillin–streptomycin, 10 mM sodium-ß-glycerophosphate, 10 mM HEPES, 100 nM dexamethasone and 50 μg/mL ascorbic acid-2-phosphate) was added and cultured for 7 weeks.

4.4. VASCULARIZED BONE DEVELOPMENT: SCREENING GROWTH FACTOR COCKTAILS

4.4.1. HASC AS SINGLE CELL SOURCE FOR ENGINEERING VASCULARIZED BONE

In chapter VII, hASC were used to engineer vascularized bone *in vitro.* Expanded hASC were suspended at $20x10^6$ cells/mL. A 20 μL aliquot of cell suspension was pipetted to the top of blot-dried HFIP-derived silk scaffolds, pipetted up and down to ensure even distribution of cells. After 15 minutes in the incubator, scaffolds were rotated 180º, and 10 μL of cell-free medium was added to prevent these to dry. This process was repeated four times, to allow uniform cell

distribution, after which, constructs were incubated overnight to allow cell attachment (Fig.1). These hASCs, attached to silk fibroin scaffolds are intended for bone formation. At day 1, fibrinogen (Sigma F8630) was prepared at a concentration of 5 mg/mL and thrombin (Sigma T6200-1KU) was used at 10 Units/mL. Expanded hASCs intended to form vasculature network were encapsulated in fibrin at a density of $20x10^6$ cells/mL. Thrombin was added to cross-link the gel, giving a final fibrin concentration of 4 mg/mL. Before cross-linking occurred, 20 µl of cell/gel suspension was pipetted into blot-dried scaffolds to allow uniform cell seeding throughout the scaffolds. Before the gels became cross-linked fully, they were aspirated under a light vacuum so that they coated the walls of the scaffolds, but did not fill the pore spaces. This step was performed on groups 1 to 5 at day 1, and on groups 6 and 7 only after 3 weeks of osteogenic culture.

Seven experimental groups were defined. Two of these were 'controls':

Group 1 where constructs were cultured in osteogenic medium (OM), which consisted of low glucose DMEM, 10% FBS, 1% Pen–Strep supplemented with osteogenic factors (all purchased from Sigma-Aldrich): 100 nM dexamethasone, 10 mM sodium-β-glycerophosphate, 10 mM HEPES and 50 µg/mL ascorbic acid-2-phosphate, for 5 weeks, to evaluate osteogenic differentiation and bone tissue development;

Group 2, where endothelial growth media was used (EGM) (Lonza CC-3162), to evaluate endothelial differentiation and vascular tissue development. Five further groups were chosen for growing vascularized bone constructs.

In Group 3, both osteogenic and vasculogenic supplements were provided simultaneously throughout the total period of culture - constructs were cultured for 5 weeks in a cocktail medium composed by EGM and OM at 1:1 ratio (cocktail group).

Further, two sequential approaches were established: a) to induce vasculogenesis prior to osteogenesis (groups 4 and 5), and b) reverse the process, and induce osteogenesis prior to vasculogenesis (groups 6 and 7).

At group 4, constructs were cultured in EGM for 2 weeks and in cocktail medium for remaining 3 weeks (EGM|cocktail). Constructs at group 5, were cultured exactly as in Group 4 except that fresh hASCs were added into scaffold pore spaces at this 2-week time point. This is indicated as EGM|cocktail+ASC. In Group 6 and 7, we 'reversed' the process and induced osteogenic differentiation first. In these groups, hASCs were only seeded into the scaffolds and cultured in osteogenic media for 3 weeks. Subsequently, hASCs in fibrin were added to the constructs and cultured either in EGM media (Group 6 - OM|EGM), either in cocktail medium (Group 7 - OM|cocktail).

4.4.2. HUVEC-MSC CO-CULTURE AS AN *IN VITRO* MODEL OF VASCULARIZED BONE

In chapter VIII, a co-culture of HUVECs and MSCs was used to engineer vascularized bone *in vitro.* To induce bone formation, 20 µl suspension of MSCs at a density of 10×10^6 cells/mL was seeded into blot-dried decellularized bone scaffolds, divided into five groups, and incubated overnight to allow cell attachment.

At day 1, solutions of fibrinogen (5 mg/mL) and thrombin (10 Units/mL) were prepared. In Groups 1 – 4, HUVECs and MSCs, intended to form stable vasculature network, were encapsulated in fibrin at a 2:1 ratio and a density of 30×10^6 cells/mL. Thrombin was added to crosslink the gel, giving a final fibrin concentration of 4 mg/mL. Before crosslinking occurred, 20 µl of cell/gel suspension was pipetted into blot-dried scaffolds to allow uniform cell seeding throughout the scaffolds. Before the gels became fully cross-linked, they were aspirated under a light vacuum so that the fibrin gel coated the walls of the scaffolds, but did not fill the pore spaces. In Group 5, this same step was performed on MSC-seeded scaffolds after 4 weeks of osteogenic culture.

Five experimental groups were established to study vascularized bone constructs, including three main groups and two controls.

Group 1 (control for osteogenic conditions) utilized osteogenic medium (OM) throughout the culture, containing low glucose DMEM, 10% FBS, 1% Pen–Strep supplemented with osteogenic factors: 100 nM dexamethasone, 10 mM sodium-β-glycerophosphate, and 50 µg/mL ascorbic acid-2-phosphate, supplemented with BMP-2 (at 10 ng/mL) for 6 weeks.

Group 2 (control for vasculogenic conditions) utilized endothelial growth medium (EGM) throughout the culture.

Group 3 utilized EGM for 2 weeks and then a cocktail medium composed by EGM and OM at 1:1 ratio (EGM|cocktail) for 4 weeks.

Group 4 was designed exactly as Group 3 except that osteo-induced MSCs were added into scaffold pore spaces at the 2-week time point (EGM|cocktail+MSC).

In Group 5, MSCs only were seeded into the scaffolds and cultured in osteogenic medium for 4 weeks, at which point HUVECs and MSCs in fibrin were added to the constructs and cultured in cocktail medium for an additional 2 weeks (OM|cocktail).

5. *IN VIVO* STUDIES

5.1. SUB-CUTANEOUS IMPLANTATION OF ENGINEERED VASCULARIZED BONE IN NUDE MICE

NOD/SCID mice (Nonobese diabetic / severe combined immune deficiency, NOD.CB17-*Prkdc*^{scid}/NCrHsd, Harlan) were used as *in vivo* model for subcutaneous implantation of engineered vascularized bone grafts, in chapter VIII. Mice were anaesthetized by a subcutaneous injection of ketamine (80-100 mg/kg) and xylazine (5-10mg/kg). Analgesia was provided with buprenorphine (0.05-0.1 mg/kg). Constructs were implanted into separate subcutaneous dorsal pockets (one construct per pocket, two pockets per animal) according to an approved Columbia University Institutional Animal Care & Use Committee (IACUC) protocol.

6. BIOLOGICAL CHARACTERIZATION

6.1. CELL VIABILITY AND PROLIFERATION

6.1.1. MTS ASSAY

Cell metabolic activity was assessed through MTS (3-(4,5-dimethylthiazol-2-yl)-5(3-carboxymethoxyphenyl)-2(4-sulfofenyl)-2H-tetrazolium) assay (VWR G3580). This substrate is bioreduced by dehydrogenase enzymes, active in live cells, into a brown formazan product. The intensity of colour, measured at OD 490 nm, is directly related to number of viable cells. In chapter V, constructs were washed in PBS and incubated with MTS solution prepared in serum-free culture medium without phenol red, at 37ºC for 3h. After incubation, 100 µL were transferred in triplicate into a 96-well plate for optical density (OD) measurement at 490 nm.

6.1.2. LIVE/DEAD ASSAY

The LIVE/DEAD assay provides a two-color fluorescence cell viability assay based on the simultaneous determination of live and dead cells. Live cells are distinguished by the enzymatic conversion of the cell-permeant calcein AM to the intensely fluorescent calcein (ex/em ~495 nm/~515 nm), while dead cells are detected by fluorescence of ethidium homodimer (EthD-1) or propidium iodide (ex/em ~495 nm/~635 nm) that enters cells with damaged membranes binding to nucleic acids. LIVE/DEAD assay was used to evaluate cell viability. In chapter IV, live cells (indicated by calcein AM, Invitrogen C3099) and dead cells (indicated by propidium iodide, Alfagene P1304MP) were imaged through a Zeiss Axioimage (RZ1M) florescence microscope (Germany). In chapters V, VI, VII and VIII, LIVE/DEAD Viability/Citotoxicity kit

(Molecular Probes, OR/USA) was used to evaluate cell viability. Live cells (indicated by calcein AM) and dead cells (indicated by ethidium homodimer-1) were observed and imaged through a confocal microscope (Leica, Germany). Optical surfaces were taken from the surface up until 160 μm deep, with 10 μm intervals. All images are presented as vertical projections.

6.1.3. DNA QUANTIFICATION

Quantitating double-stranded DNA (dsDNA) is a very accurate method to assess number of cells, once these two parameters are directly correlated. In tissue engineering experimentation, this method may be used to assess cell-seeding efficiency into proposed culturing scaffolds (chapter V), as well as to determine cell proliferation along construct development (chapters IV – VIII). Quant-iT™ PicoGreen® dsDNA reagent is an ultrasensitive fluorescent nucleic acid stain, therefore used thoroughly in all experimental studies described in this thesis. Briefly, constructs were harvested, washed in PBS, cut in half and weighed. Samples were digested with Proteinase K enzyme. 1 mL of proteinase K digestion buffer (10 mM Tris, 1 mM EDTA, 0.1% Triton X-100, 0.1 mg/mL proteinase K) was added to samples and incubated overnight at 56ºC. After centrifugation at 3000g, 10 minutes, the supernatants were removed, diluted, pippeted in duplicate into a 96-well plate and 1:1 ratio of picogreen solution (Quant-iT™ PicoGreen ® dsDNA Kit, Invitrogen) was added. Sample fluorescence was measured with fluorescent plate reader at excitation ~480 nm, emission ~520 nm. Lambda DNA was used to prepare the standard curve. Based on previous studies where DNA content of hASCs was determined, a conversion factor of 5 pg DNA per cell was used.

6.2. HISTOLOGICAL ANALYSIS

6.2.1. SOFT TISSUE HISTOLOGY

In chapter IV, 10% formalin was used to fix samples for 1 day, and further dehydrated with graded ethanol washes. Samples were embedded in paraffin, sectioned to 5 μm and mounted on glass slides. To proceed to distinct stainings, sections were deparaffinized with Clearite and rehydrated with a graded series of ethanol washes.

Safranin O and Alcian Blue staining were performed to detect articular cartilage extracellular matrix components, such as mucopolysaccharides and glycosaminoglycans. Briefly, safranin O staining was performed with Weigert's iron hematoxylin, 10 min followed by running in tap water for 10 min. Slides were then immersed in 0.02% fast green solution, 5 min and rinsed 10-15 sec in 1% acetic acid. Finally, samples were stained with 0.1% safranin O solution for 5 min.

Regarding alcian blue stain, slides were immersed 30 min in 0.01 g/mL alcian blue solution, and washed in running tap water for 2 min. A counterstain with nuclear fast red (0.5%) was performed for 5 min. Upon staining, sections were washed in running tap water, dehydrated with a graded series of ethanol, cleared with Clearite and mounted with resinous mounting media (Entellan® Merck & Co., Inc. USA).

In chapter V, samples were fixed in 4% formaldyhyde solution for 1 day. Bone scaffolds were decalcified with immunocal solution (Decal Chemical, Tallman, NY) for 1 day, and further dehydrated with graded ethanol washes, concurrently with remaining silk constructs. Samples were embedded in paraffin, sectioned to 5-μm slices and mounted on glass slides. For staining, sections were deparaffinized with CitriSolv and rehydrated with a graded series of ethanol washes. Samples were stained using standard hematoxylin and eosin.

6.2.2. HARD TISSUE HISTOLOGY

Hard tissue histology was performed in samples harvested from subcutaneous implantation in NOD SCID mice, described in chapter VIII. In order to assess new bone formation, contructs were not decalcified and further processed according to hard tissue histology methods: constructs were fixed in 10% formalin for 1 day and dehydrated with sequential washes in 70 % ethanol (2 days), 100 % ethanol (2 days with twice daily solution changes), and toluene (2 days with once daily solution change). Constructs were then washed in activated methyl methacrylate (MMA) with daily changes of MMA solution for four days at 4 °C, and then placed at 32 °C until the MMA cured. Plastic-embedded sections were sectioned to 8 μm on a Leica hard tissue microtome. Staining for the new osteoid formation was done using the traditional Goldner's Masson trichrome stain (table I and II):

Table I – Protocol for Goldner's Masson trichrome stain

Staining step	Time (minutes)
Weigert's Hematoxylin	30
Rinse tap water	2
Ponceau working solution	5
Acetic acid 0.2%	3
Phosphotungstic-Phosphomolybdic acid	10
Acetic acid 0.2%	3
Light green	13
70%, 95%, 100% Ethanol	2 (2x each)

Table II – Composition of solutions used in Goldner's Masson trichrome stain

Weigert's Hematoxylin	
Solution A	
Hematoxylin	1 g
95% Ethyl alcool	100 mL
Solution B	
Ferric chloride 29% aq. solution	4 mL
Distilled water	95 mL
Hydrochloric acid (concentrated)	1 mL
Working solution:	
Mix equal amount of A and B. Use immediately.	
(Shelf life of A and B is 8 months.)	

0.2% Acetic acid	
Glacial acetic acid	2 mL
Distilled water	1 L
(Shelf life is indefinite.)	

Phosphotungstic-Phosphomolybdic acid	
Phosphotungstic acid	5 g
Phosphomolybdic acid	5 g
Distilled water	100 mL
(Shelf life is 1-2 months.)	

Ferric chloride 29% aqueous solution	
Ferric chloride, anhydrous	1.5 g
Distilled water	99 mL
Hydrochloric acid (concentrated)	1 mL
(Shelf life is 8 months.)	

Masson Fuchsin Ponceau Orange G Stock	
Ponceau 2R	2 g
Acid Fuchsin	1 g
Orange G	2 g
0.2 % Acetic acid	300 mL
Working solution:	
Stock solution of F-P-O	10 mL
0.2 % Acetic acid	90 mL
(Shelf life of F-P-O stock is 9-12 months.)	

Light green	
Light green stain	0.1 g
0.2 % Acetic acid	100 mL
(Shelf life is 6 months.)	

6.2.3. IMMUNOHISTOCHEMISTRY

Immunohistochemistry (IHC) is a method for demonstrating the presence and location of proteins in tissue sections, enabling the observation of processes in the context of intact tissue. IHC staining performed with antibodies that recognize the target protein. Antibodies are highly specific, binding only to the protein of interest in the tissue section. The engineered tissue developed in the context of this thesis, was evaluated by detecting the antibody-antigen interaction using a chromogenic detection, where an enzyme conjugated to the antibody cleaves a substrate, producing a colored precipitate at the location of the protein.

In chapters V, VI and VII, silk fibroin scaffolds were to engineer bone tissue, while gellan gum hydrogels were used to engineer cartilage tissue in chapter IV. In these chapters, samples were fixed in 10% formalin for 1 day, embedded in paraffin, sectioned to 5 μm and mounted on glass slides. In chapter V and VIII, where decellularized bone scaffolds were also used to engineer bone tissue. In order to perform soft tissue histology, samples were decalcified for 2 days with Immunocal solution (Decal Chemical, Tallman, NY, USA) before embedding in

paraffin. When starting IHC procedure, sections were deparaffinized with CitriSolv and rehydrated in a graded series of ethanol washes. Antigen retrieval was performed by heat-induced method using a microwave and Citrate Buffer (0.1M Citric acid and 0.1M Sodium citrate), 20 min. Once horseradish peroxidase enzyme conjugate is used for protein detection, suppression of any endogenous peroxidase activity was performed by incubating sections 30 min in H_2O_2 0.3% RT with agitation, to decrease background staining (false positives).

After washing with PBS+0.025% Triton-X, normal horse serum - NHS (20 min, RT) was applied to reduce non-specific binding of primary antibody. Excess serum was blot, before incubation with diluted primary antibody (table III) overnight at 4ºC (in moist chamber). Negative controls were performed by omitting the primary antibody incubation step.

Sections were further washed with PBS+0.025% Triton-X before incubation with biotin-labeled secondary antibody, 30 min, RT, after which, VECTASTAIN ABC reagent was applied. This is an avidin-biotinylated enzyme complex (ABC) that will bind to the biotinylated secondary antibody (Vectastain Universal Elite ABC Kit, PK-6200 Vector Laboratories).

Finally, the tissue antigen is localized by incubation (5-10 min) with peroxidase substrate solution (3, 3'- diaminobenzidine), yielding a brown stain (DAB substrate kit SK-4100 Vector Laboratories). Counterstaining of cell nuclei was further performed with haematoxylin (2 min). Sections were lastly dehydrated, cleared in CitriSolv and mounted in organic mounting media.

Table III – Primary anti-bodies used for immunohistochemistry in chapters IV - VIII

Target protein	Primary Antibody	Dilution	Company / Ref	Chapter
Collagen II (Col II)	Rabbit anti-human polyclonal antibody	1:50	Abcam / ab34712	IV
Collagen I (Col I)	Rabbit anti-human polyclonal antibody	1:200	Abcam / ab292	IV
CD31	Rabbit anti-human monoclonal antibody	1:250	Millipore / 04-1074	VII, VIII
von Willebrand Factor (vWF)	Rabbit anti-human polyclonal antibody	1:200	Sigma-Aldrich / F3520	VII, VIII
Collagen I (Col I)	Mouse anti-human monoclonal antibody	1:500	Abcam / ab6308	V, VIII
Osteopontin (OPN)	Rabbit anti-human polyclonal antibody	1:750	Chemicon / ab1870	V - VII
Bone Sialoprotein (BSP)	Rabbit anti-human polyclonal antibody	1:1000	Millipore / ab1854	V - VIII

6.3. BIOCHEMICAL QUANTIFICATION

6.3.1. GLYCOSAMINOGLYCAN QUANTIFICATION

Glycosaminoglycans (GAGs) chains participate at the nano-scale level of cartilage. Chondroitin sulfate and keratan sulfate are covalently attached to the aggrecan protein backbone. In addition with ions such as Na^+, Ca^{2+}, SO_3^-, COO^-, are responsible for AC swelling, for governing osmotic pressure of cartilage, and consequently contribute for its compressive stiffness [35].
The 1,9-dimethylmethylene blue (DMB) metachromatic assay was used as standard procedure to quantify GAG deposition in cartilage tissue, engineered among experiments described at chapter IV. This reagent entangles mechanically with GAGs present in solution, generating a peak shift at OD 525-530 nm. To this end, engineered constructs were added to 1 mL of papain digestion buffer (1.5 mg/mL L-cysteine hydrochloride, 0.125 mg/mL papain in PBE buffer – table IV) and incubated overnight at 60ºC for digestion. After centrifugation at 10000g, 5 minutes, 10 µL of supernatant was removed and pippeted in duplicate into a 96-well plate. Chondroitin 6-sulfate C sodium salt was used to prepare the standard curve. Dilutions of a 50 µg/mL stock solution were pipetted in duplicate to the 96-well plate. 250 µL of DMB solution (table IV) was added and sample absorbance was immediately measured using a microplate reader at OD 530 nm.

Table IV – Solutions used for glycosaminoglycan quantification assay

PBE buffer	
Na_2HPO_4	3.265 g
NaH_2PO_4	3.240 g
EDTA-Na_2 500mM	5 mL
Distilled water	450 mL
	(Adjust pH to 6.5)

DMB solution	
Solution A	
NaCl	0.59 g
Glycine	0.76 g
Distilled water	225 mL
Solution B	
DMB	4 mg
100% Ethanol	1.25mL
Mix both. Adjust pH to 3.0. Complete to 250 mL.	
(Shelf life is 3-6 months.)	

6.3.2. CALCIUM QUANTIFICATION

Mineralized matrix is a key outcome for bone development. The direct quantification of mineral in engineered bone grafts is a fundamental tool to assess progression of osteogenic differentiation. Total calcium assessment can be performed by its direct combination with ortho-

cresolphthalein complexone (OCPC) to form a stable color reaction. In this assay, calcium is disassociated from proteins in an acid solution, followed by its direct reaction with OCPC. In a subsequent alkaline medium, the Ca-OCPC complex turns purple, which is measured at 575 nm. The amount of calcium in solution is directly proportional to the color intensity developed by the reaction. In chapters V, VI, VII, one-half of constructs were incubated in 1 mL TCA 5% (trichloroacetic acid 5% v/v) and calcium was extracted by disintegrating the construct using steel balls and MinibeadBeater™ (Biospec, Bartlesville, OK/USA) (3x 25000 rpm, 10 seconds each). Samples were further incubated 30 min, RT after which a centrifugation step was performed for 10 min, 3000g. 10 µL of each sample were pippeted in duplicate into a 96-well plate, as well as Calcium standard prepared. 100 µL of calcium color and base reagent (1:1 v/v) were added and incubated in the dark at RT for 5 min. Sample optical density was measured at 575 nm using a microplate reader. Calcium content and standard were quantified using StanbioTotal Calcium Liquicolor® (Stanbio Laboratory/USA).

6.3.3. ALKALINE PHOSPHATASE QUANTIFICATION

Progression of osteogenic differentiation may be determined by alkaline phosphatase (AP) activity, a cell surface protein bound to the plasma membrane through phosphatidylinositol phospholipid complexes [36]. High AP activity is associated with the active formation of mineralized matrix. In chapters V and VII AP activity was determined by adding cell lysis solution to one-half of each scaffold, and these were disintegrated using steel balls and MinibeadBeater™. After centrifugation, 50 µL of supernatant were incubated with 50 µL *p*NPP (p-nitrophenyl-phosphate) substrate solution, at 37ºC for 20 min. Colourless *p*NPP is hydrolyzed by alkaline phosphatase produced by cells (at pH 10.5, 37ºC), to form yellow-coloured free *p*-nitrophenol. The reaction was stopped with 50 µL of stop solution, and absorbance was read at 405 nm in a microplate reader. p-Nitrophenol at known concentrations was used to prepare the standard curve. All solutions were components of SensoLyte® *p*NPP Alkaline Phosphatase Complete Kit (Cell Biolabs, CBA-302).

6.4. MICRO COMPUTED TOMOGRAPHY (µCT) ANALYSIS

The microstructure of engineered bone grafts can be qualitatively and quantitatively evaluated using a high-resolution µCT scanner, providing several bone morphometric parameters, and a visual distribution of mineral throughout the sample. BV/TV ratio is one of the most important

parameters. Total volume (TV) of the volume-of-interest (VOI) is measured in both 2d and 3d. The 2d measurement is simply the total number of voxels of (solid and space) in the VOI times the voxel volume. Bone Volume (BV) on the other hand, is the total volume of binarised objects within the VOI, measured in both 2d and 3d. Given this, the BV/TV ratio corresponds to the proportion of the VOI occupied by binarised solid objects. In chapters V, VI and VIII μCT was performed using the protocol described by Liu et al [37]. Samples were aligned in a 2 mL screw-cap centrifuge tube, which was clamped in the specimen holder of a vivaCT40 system (SCANCO Medical AG, Basserdorf, Switzerland). The 2 mm length of the scaffold was scanned at 21 μm isotropic resolution. A global thresholding technique, which only detects mineralized tissue, was applied to obtain the bone volume (BV) of samples.

6.5. Scanning Electron Microscopy (SEM) imaging

Scanning Electron Microscopy (SEM) analysis provides images of the surface of a sample by scanning with a high energy beam of electrons. SEM was used in chapter V, to analyze the distribution, level and morphology of cell attachment on the surface of the scaffolds, as well as to analyze scaffold structure. To keep samples in their natural state, special methods of fixation and stabilization of the cells on the scaffolds are necessary. Samples were washed in PBS and then fixed in 2% gluteraldehyde in sodium cacodylate buffer for 2 h. Constructs were washed in buffer and freeze-dried overnight. Before imaging, samples were coated with gold and palladium and imaged in SEM machine (JEOL, JAPAN).

6.6. Mechanical Properties evaluation

Mechanical properties of the scaffold and consequent engineered tissue after culture, is of crucial importance for its integration upon implantation in lesion site. In chapters V and VI, Stiffness upon compression was determined under unconfined compression in wet conditions using a modification of an established protocol [38]. An initial tare load of 0.2 N was applied and was followed by a stress-relaxation step where specimens were compressed at a ramp velocity of 1% per second up to 10% strain and maintained at the position for 1800 s. The equivalent Young's modulus was obtained from the equilibrium forces measured at 10% strain.

6.7. Quantitative Real-Time PCR Analysis

The fluorescence-based quantitative real-time PCR (polymerase chain reaction), is a methodology to detect and measure minute amounts of nucleic acids in a wide range of samples from numerous sources. In chapters IV, VI and VII, gene expression of specific chondrogenic, osteogenic and endothelial markers were quantified to assess cell differentiation stage and consequent tissue development. Slight protocol variations were performed in each chapter.

For RNA extraction, constructs in chapter IV were added to 800 µL of TRIzol® (Invitrogen 15596-026) and disintegrated by mortar and pestle, using liquid nitrogen to maintain samples cold. Suspensions were centrifuged at 12,000 g for 10 min at 4°C to remove tissue debris and extracted with chloroform (JMGS C/4960/17). Colorless aqueous phase, containing RNA was removed and mixed with equal volume of isopropanol (Laborspirit 33539). Suspensions were again centrifuged at 12,000 g for 8 min at 4°C, supernatant discarded, and RNA pellet washed with 75% ethanol. Samples were centrifuged at 7,500 g for 5 min at 4°C, supernatant removed, pellet air-dried, and dissolved with RNAase-free water (Invitrogen 10977035). RNA was quantified using Nanodrop® ND-1000. Approximately 1 µg of RNA was reversely transcribed with random hexameres using qScript™ cDNA Synthesis Kit (Quanta Biosciences 95047). Collagen type II, aggrecan, Sox-9 and the housekeeping gene glyceraldehyde-3-phosphatedehydrogenase (GAPDH) expression were quantified using PerfeCTa™ SYBR® Green FastMix™ (Quanta Biosciences 95072) and the Eppendorf realplex4 System. Primer sequences and amplicon size are described on table V. The expression data were normalized to GAPDH and presented as average values for each group (n=3 ± standard deviation).

In Chapters VI and VII, a different method was used. For RNA extraction, one-half of constructs were added to 800 µL of TRIzol® (Invitrogen 15596-026, USA) and disintegrated by using steel balls and MinibeadBeater™ (Biospec, Bartlesville, OK/USA), maintaining samples in ice. Suspensions were centrifuged at 12,000 g for 10 min at 4°C to remove tissue debris and extracted with chloroform (Sigma C2432). Colorless aqueous phase, containing RNA was removed and mixed with equal volume of isopropanol (Sigma I9516). Suspensions were again centrifuged at 12,000 g for 8 min at 4°C, supernatant discarded, and RNA pellet washed with 75% ethanol. Samples were centrifuged at 7,500 g for 5 min at 4°C, supernatant removed, pellet air-dried, and dissolved with DEPC-water (Applied Biosystems AM 9920). RNA was quantified using Nanodrop® ND-1000. Approximately 1 µg of RNA was reversely transcribed

with random hexameres using High Capacity cDNA Reverse Transcription Kit (Applied Biosystems 4368814). Osteopontin (OPN), bone sialoprotein (BSP), prostaglandin E2 synthase (PGE_2S), CD31, von Willebrand factor (vWF) and the housekeeping gene glyceraldehyde-3-phosphatedehydrogenase (GAPDH) expression were quantified using a 7500 Fast Real-Time PCR System (Applied Biosystems, USA). Gene expression assay ID, probe and amplicon size and are described on table V. All TaqMan® Gene Expression Assays were purchased from Applied Biosystems.

The expression of each gene was normalized to GAPDH value of corresponding sample and relative gene expression was quantified according to the Livak method, considering that normalized expression ratio = $2^{-\Delta\Delta Ct}$. Average values for each group were presented.

Table V – Primers and Gene Expression Assays used in quantitative RT-PCR analysis

Gene	Primers	GEA ID	Amplicon	Chapter
Collagen II (Col II)	F: 5'GACAATCTGGCTCCCAAC	-	257 bp	IV
	R: 5'ACAGTCTTGCCCCACTTA			
Aggrecan (Agrc)	F: 5'TGAGTCCTCAAGCCTCCTGT	-	129 bp	IV
	R: 5'TGGTCTGCAGCAGTTGATTC			
Sox-9	F: 5'TACGACTACACCGACCACCA	-	256 bp	IV
	R: 5'TTAGGATCATCTCGGCCATC			
GAPDH	F: 5'ACAGTCAGCCGCATCTTCTT	-	94 bp	IV
	R: 5'ACGACCAAATCCGTTGACTC			
Prostaglandin E2 synthase (PGE_2S)	-	Hs00228159_m1	66 bp	VI
Osteopontin (OPN)	-	Hs00167093_m1	65 bp	VI
Bone Sialoprotein (BSP)	-	Hs00173720_m1	95 bp	VI
CD31	-	Hs00169777_m1	65 bp	VII
von Willebrand Factor (vWF)	-	Hs00169795_m1	70 bp	VII
GAPDH	-	Hs99999905_m1	122 bp	VI, VII

bp – base pairs; GEA – gene expression assay; GAPDH - Glyceraldehyde 3-phosphate dehydrogenase

7. STATISTICAL ANALYSIS

Data are presented as average (n=3) ± standard deviation. Statistical significance was determined using analysis of variance (ANOVA) followed by Tukey's HSD (honestly significant difference) test using Prism software (Prism 4.0c, GraphPad Software Inc., San Diego, CA, USA). $p < 0.05$ were considered statistically significant

References

1. Jansson, P.E., B. Lindberg, and P.A. Sandford, *Structural Studies of Gellan Gum, an Extracellular Polysaccharide Elaborated by Pseudomonas-Elodea.* Carbohydrate Research, 1983. 124(1): p. 135-139.
2. Moorhouse, R., et al., *Ps-60 - New Gel-Forming Polysaccharide.* Abstracts of Papers of the American Chemical Society, 1980. 179(Mar): p. 22-Carb.
3. Grasdalen, H. and O. Smidsrod, *Gelation of Gellan Gum.* Carbohydrate Polymers, 1987. 7(5): p. 371-393.
4. Oliveira J.T. , L.M., R. Picciochi, P.B. Malafaya, R.A. Sousa, R. Fernandes, N.M. Neves, J.F. Mano, R.L. Reis, *Gellan gum: a new biomaterial for cartilage tissue engineering applications.* Journal of Biomedical Materials Research Part A, 2009. accepted for publication.
5. Oliveira, J.T., et al., *Injectable Gellan Gum Hydrogels with Autologous Cells for the Treatment of Rabbit Articular Cartilage Defects.* Journal of Orthopaedic Research, 2010. 28(9): p. 1193-1199.
6. Oliveira, J.T., et al., *Gellan gum injectable hydrogels for cartilage tissue engineering applications: in vitro studies and preliminary in vivo evaluation.* Tissue Eng Part A, 2010. 16(1): p. 343-53.
7. Silva-Correia, J., et al., *Gellan gum-based hydrogels for intervertebral disc tissue-engineering applications.* J Tissue Eng Regen Med, 2010.
8. Tanaka, K., et al., *Determination of the site of disulfide linkage between heavy and light chains of silk fibroin produced by Bombix mori.* Biochimica Et Biophysica Acta-Protein Structure and Molecular Enzymology, 1999. 1432(1): p. 92-103.
9. Asakura, T., et al., *Heterogeneous structure of silk fibers from Bombyx mori resolved by C-13 solid-state NMR spectroscopy.* Journal of the American Chemical Society, 2002. 124(30): p. 8794-8795.
10. He, S.J., R. Valluzzi, and S.P. Gido, *Silk I structure in Bombyx mori silk foams.* International Journal of Biological Macromolecules, 1999. 24(2-3): p. 187-195.
11. Mondal, M., K. Trivedy, and S. Nirmal Kumar, *The silk proteins, sericin and fibroin in silkworm, Bombyx mori Linn., - a review.* Caspian Journal of Environmental Sciences, 2007. 5(2): p. 63-76.
12. Altman, G.H., et al., *Silk-based biomaterials.* Biomaterials, 2003. 24(3): p. 401-16.
13. Altman, G.H., et al., *Silk matrix for tissue engineered anterior cruciate ligaments.* Biomaterials, 2002. 23(20): p. 4131-4141.
14. Kang, J.H., J.M. Gimble, and D.L. Kaplan, *In Vitro 3D Model for Human Vascularized Adipose Tissue.* Tissue Engineering Part A, 2009. 15(8): p. 2227-2236.
15. Lovett, M., et al., *Silk fibroin microtubes for blood vessel engineering.* Biomaterials, 2007. 28(35): p. 5271-5279.
16. Wang, Y.Z., et al., *In vitro cartilage tissue engineering with 3D porous aqueous-derived silk scaffolds and mesenchymal stem cells.* Biomaterials, 2005. 26(34): p. 7082-7094.
17. Sofia, S., et al., *Functionalized silk-based biomaterials for bone formation.* Journal of Biomedical Materials Research, 2001. 54(1): p. 139-148.
18. Meinel, L., et al., *Engineering bone-like tissue in vitro using human bone marrow stem cells and silk scaffolds.* Journal of Biomedical Materials Research Part A, 2004. 71A(1): p. 25-34.
19. Fini, M., et al., *The healing of confined critical size cancellous defects in the presence of silk fibroin hydrogel.* Biomaterials, 2005. 26(17): p. 3527-3536.
20. Kim, H.J., et al., *Influence of macroporous protein scaffolds on bone tissue engineering from bone marrow stem cells.* Biomaterials, 2005. 26(21): p. 4442-4452.
21. Kim, H.J., et al., *Bone tissue engineering with premineralized silk scaffolds.* Bone, 2008. 42(6): p. 1226-1234.
22. Bhumiratana, S., et al., *Nucleation and growth of mineralized bone matrix on silk-hydroxyapatite composite scaffolds.* Biomaterials, 2011. 32(11): p. 2812-20.
23. Urist, M.R., R.J. DeLange, and G.A. Finerman, *Bone cell differentiation and growth factors.* Science, 1983. 220(4598): p. 680-6.

24. De Long, W.G., et al., *Bone, grafts and bone graft substitutes in orthopedic trauma surgery - A critical analysis.* Journal of Bone and Joint Surgery-American Volume, 2007. 89A(3): p. 649-658.
25. Grayson, W.L., et al., *Engineering anatomically shaped human bone grafts.* Proc Natl Acad Sci U S A, 2010. 107(8): p. 3299-304.
26. Oliveira JT , S.R., Reis RL, *Gellan Gum Based Hydrogels for Regenerative Medicine and Tissue Engineering Applications, Its System, and Processing Devices Devices / Hidrogéis À Base De Goma Gelana Para Utilização Em Medicina Regenerativa e Engenharia De Tecidos, Seu Sistema E Dispositivos De Processamento*, in *INPI, EPO, submitted*.
27. Oliveira, J.T., et al., *Gellan gum: A new biomaterial for cartilage tissue engineering applications.* Journal of Biomedical Materials Research Part A, 2010. 93A(3): p. 852-863.
28. Kim, U.J., et al., *Three-dimensional aqueous-derived biomaterial scaffolds from silk fibroin.* Biomaterials, 2005. 26(15): p. 2775-2785.
29. Crawford, A., Dickson, S. C., ed. *Chondrocyte Isolation, Expansion and Culture on Polymer Scaffolds*. Methods in Molecular Biology, ed. A.P. Hollander, P. V. Hatton Vol. 238, Biopolymer Methods in Tissue Engineering. 2004, Humana Press Inc.: Totowa, NJ.
30. McIntosh, K., et al., *The immunogenicity of human adipose-derived cells: Temporal changes in vitro.* Stem Cells, 2006. 24(5): p. 1246-1253.
31. Mitchell, J.B., et al., *Immunophenotype of human adipose-derived cells: Temporal changes in stromal-associated and stem cell-associated markers.* Stem Cells, 2006. 24(2): p. 376-385.
32. Grayson, W.L., et al., *Optimizing the Medium Perfusion Rate in Bone Tissue Engineering Bioreactors.* Biotechnology and Bioengineering, 2011. 108(5): p. 1159-1170.
33. Grayson, W.L., et al., *Effects of initial seeding density and fluid perfusion rate on formation of tissue-engineered bone.* Tissue Eng Part A, 2008. 14(11): p. 1809-20.
34. Frohlich, M., et al., *Bone Grafts Engineered from Human Adipose-Derived Stem Cells in Perfusion Bioreactor Culture.* Tissue Engineering Part A, 2010. 16(1): p. 179-189.
35. Mow, V.C., A. Ratcliffe, and A.R. Poole, *Cartilage and diarthrodial joints as paradigms for hierarchical materials and structures.* Biomaterials, 1992. 13(2): p. 67-97.
36. Hofmann, S., D. Kaplan, and G. Vunjak-Novakovic, *Tissue Engineering of Bone*, in *Culture of Cells for Tissue Engineering*, V.-N. G and F. RI, Editors. 2006, John Wiley & Sons, Inc.: New Jersey. p. 323-373.
37. Liu, X.W.S., et al., *Quantification of the roles of trabecular microarchitecture and trabecular type in determining the elastic modulus of human trabecular bone.* Journal of Bone and Mineral Research, 2006. 21(10): p. 1608-1617.
38. Mauck, R.L., et al., *Functional tissue engineering of articular cartilage through dynamic loading of chondrocyte-seeded agarose gels.* Journal of Biomechanical Engineering-Transactions of the Asme, 2000. 122(3): p. 252-260.

Section 3.

CHAPTER IV

Dynamic culturing of cartilage tissue: the significance of hydrostatic pressure

---

This chapter is based on the following publication: Correia C, Pereira AL, Duarte ARC, Pedro AJ, Frias AM, Oliveira JT, Sousa RA and Reis RL, 2011, *Dynamic culturing of cartilage tissue: the significance of hydrostatic pressure* - submitted.

Abstract

Human articular cartilage functions under a wide range of mechanical loads in synovial joints, where hydrostatic pressure (HP) is the prevalent actuating force. We hypothesized that the formation of engineered cartilage can be augmented by applying such physiologic stimuli to chondrogenic cells or stem cells, cultured in hydrogels, using custom-designed hydrostatic pressure bioreactors. To test this hypothesis, we investigated the effects of distinct hydrostatic pressure regimens on cartilage formation *in vitro* by either human nasal chondrocytes (HNC) or human adipose stem cells (hASCs) encapsulated in gellan gum (GG) hydrogels. To this end, we varied the frequency of low HP, by applying pulsatile (PHP) or steady (SHP) load to HNC-GG constructs over a period of 3 weeks, and evaluated their effects on cartilage tissue engineering outcomes. HNC ($10x10^6$ cells/mL) were encapsulated in GG hydrogels (1.5%) and cultured in chondrogenic medium under three regimens for 3 weeks: (1) 0.4 MPa Pulsatile HP; (2) 0.4 MPa Steady HP; and (3) Static. Subsequently, we applied the pulsatile regimen to hASC-GG constructs and varied the amplitude of loading, by generating both low (0.4 MPa) and physiologic (5 MPa) HP levels. hASC ($10x10^6$ cells/mL) were encapsulated in GG hydrogels (1.5%) and cultured in chondrogenic medium under three regimens for 4 weeks: (1) 0.4 MPa Pulsatile HP; (2) 5 MPa Pulsatile HP; and (3) Static. In the HNC study, the best tissue development was achieved by the pulsatile HP regimen, while in the hASC study, greater chondrogenic differentiation and matrix deposition were obtained for physiologic loading, as evidenced by gene expression of aggrecan, collagen type II and sox-9, metachromatic staining of cartilage ECM and immunolocalization of collagens. We thus propose that both HNC and hASC detect and respond to physical forces, thus resembling joint loading, by enhancing cartilage tissue development in a frequency- and amplitude-dependant manner.

1. INTRODUCTION

Hydrostatic pressure has long been considered a variable influencing chondrocyte activity, since 1985 when Lippiello and co-workers [1] firstly evaluated the *in vitro* metabolic response of articular cartilage (AC) explants (both bovine and human) to different levels of hydrostatic pressure – 75 to 375 psi (0.5 - 2.5 MPa). Data suggested that AC chondrocytes have the capacity to rapidly and differentially transform mechanical signals derived from application of HP into metabolic events, which are also determined by the magnitude of the applied force [1].
With the emerging of Tissue Engineering as an independent research field, and the understanding that chondrocytes are mechanically sensitive cells [2, 3], great efforts have been

made to comprehend how hydrostatic pressure and other mechanical stimuli relevant for articular cartilage, such as compression [4-7] and shear [8-12], may improve the development of cartilage tissue *in vitro*. *In vivo,* articular cartilage is exposed to a wide range of static and dynamic mechanical loads, ranging amplitudes of about 5–6 MPa for gait, and as high as 18 MPa for other movements such as running or jumping [13, 14]. In accordance to the biphasic model of cartilage [15], the solid components of the extracellular matrix support shear stress, while the incompressible interstitial water is responsible for withstanding compressive loading, by driving out of the tissue. In view of this, 95% of overall applied joint load is supported by interstitial fluid pressurization, so hydrostatic pressure is the prevailing mechanical signal governing normal articular cartilage homeostasis [2, 16]. Most studies [17-27] have focused on the effects of hydrostatic pressure stimuli on chondrocyte-mediated synthesis and degradation of cartilage matrix macromolecules, such as proteoglycans, collagens, non-collagenous proteins and glycoproteins. Articular chondrocytes, usually from animal source, respond positively to pulsatile (0.0125–1 Hz) HP loadings ranging 0.3–5 MPa, by increasing glycosaminoglycan synthesis and deposition, as well as expression of healthy AC markers such as collagen type II, aggrecan and sox-9 transcription factor [17-19, 22, 23]. However, when high HP magnitudes are applied, in the order of 50 MPa, cell apoptosis is observed [21]. The same outcome was observed when culturing human osteoarthritic chondrocytes under physiologically normal pressure magnitudes (5 MPa) [20]. In our study, we consider two clinically relevant cell sources as potentially responsive to HP dynamic culturing: Human nasal chondrocytes (HNC) have demonstrated to respond to physical forces resembling joint loading [28], therefore this cell source was used as proof-of-principle. Nasal cartilage tissue is characterized as hyaline cartilage, containing differentiated chondrocytes which express the extracellular matrix molecules typical of articular cartilage [29, 30], and are responsive to physical forces resembling joint loading [28]. Nasal septum cartilage may be obtained under local anesthesia, through a procedure considered to be less invasive as compared to localized tissue harvesting from non-load-bearing areas of the joint. This last biopsy procedure is the one normally employed when treating articular cartilage lesions using cell-based therapies such as autologous chondrocyte implantation or matrix-induced chondrocyte implantation [31, 32]. We aim to understand whether HNC respond to hydrostatic pressure loading, and consequently improve *in vitro* cartilage tissue development. Furthermore, and considering a more challenging approach, adipose tissue derived stem cells (ASCs) appear to be a promising alternative cell source for cell based therapies [33-35], as well as for cartilage tissue regeneration [36-39] due to their excellent features. ASCs may be easily isolated from adipose tissue, proliferate quickly,

and their chondrogenic differentiation potential have been proven [40-42]. This known, we additionally hypothesize if hASC respond to biomechanical stimuli, particularly hydrostatic pressure, and if this could be employed to enhance and ameliorate cartilage tissue development *in vitro*, with the aim of reducing time-to-therapy, and ultimately increasing graft implantation success. To achieve these outcomes, two custom-designed bioreactors were developed allowing long term culturing, and control of loading parameters. In this study we evaluated the effects of loading amplitude (0.4 and 5 MPa) and frequency (pulsatile versus steady pressurization). Assays of the produced tissues evaluated the significance of these treatments on cartilage tissue development, as compared to a static culture condition (control condition).

2. MATERIALS AND METHODS

2.1. DEVELOPMENT OF HYDROSTATIC PRESSURE BIOREACTORS (HPB)

Two original easy-to-use devices were developed in order to generate hydrostatic pressure forces, which uniformly load constructs in culture. The High Hydrostatic Pressure Bioreactor (HHPB) was designed to generate physiological amplitudes of hydrostatic pressure (up to 10 MPa), and the Low Hydrostatic Pressure Bioreactor (LHPB) was projected to load culturing constructs with shorter HP amplitudes (up to 0.5 MPa). Both devices enclose particular key characteristics, such as:

a) Possibility to perform long term culturing, up to several weeks;
b) Culture of multiple 3D constructs within a high range of dimensions;
c) Tunable loading parameters: pressure amplitudes may range 0 - 0.4 MPa (for LHPB) and 1.5 - 10 MPa (for HHPB); frequency may range between 0 - 1 Hz;
d) Operation of devices inside standard biohazard hoods, and CO_2 incubators at 37ºC, in complete sterile conditions;
e) LHPB is disposable, composed by standard, off-the-shelf components, while HHPB is reusable, composed by sterilizable stainless steel components.

2.1.1. HIGH-HPB

The High-HPB system (Fig.1A and 1B) consists of a stainless steel device (15 cm diameter x 18 cm height), composed of a culture chamber (CC), an air chamber (AC) and a piston. The air pressure driven piston creates hydrostatic pressure in the culture chamber, where constructs reside in culturing media. As filtered compressed house air enters the air chamber, piston is

pushed up. Ratio of AC and CC area is 15:1, so that 15x the applied pressure is generated in the upper CC. A pressure transducer (0-16 MPa, Swagelok, USA), with digital display is connected to the lid of the culture chamber providing real time pressure reading. Pulsatile pressurization is controlled by a Programmable Logic Controller unit (PLC – OMRON CPM1A-30CDR-A-V1, Netherlands), and solenoid valve (Camozzi A331-1C2, Italy). When non-pressurized, culture media is replenished through the culture chamber by a peristaltic pump (Ismatec, USA), from a standard 50 mL schott bottle, with an adapted air filter.

2.1.2. Low-HPB

The Low-HPB system (Fig.1D and 1E) is composed by a 30 mL luer-lok polypropylene syringe (BD Biosciences), where the rubber piston is used as a physical division between the culture media and compressed air, used as mechanism of compression. An aluminum adapter is connected at the top of the syringe, together with a semi-rigid nylon tube (Legris) to conduct filtered compressed house air inside the chamber. At the bottom of the syringe, Pharmed BPT tubing (Masterflex, USA) is connected to allow gas exchange. PLC and solenoide valve used with HHPB allow controlled pulsatile pressurization of the culture media. Media is replenished through the Pharmed BPT tubing, using a syringe to avoid complex manipulation.

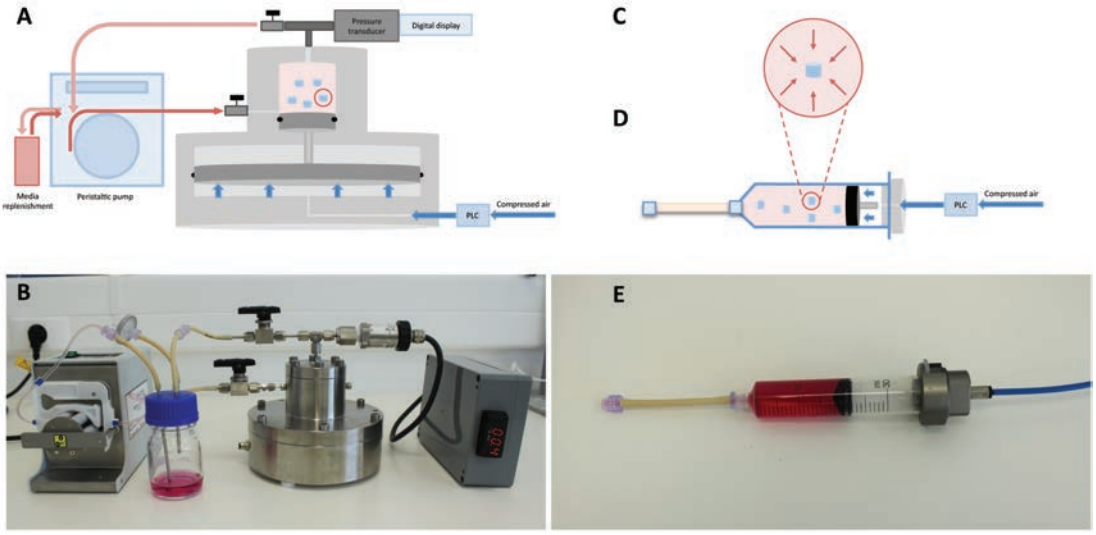

Figure 1. Custom-designed hydrostatic pressure bioreactors. A) Schematic representation of High Hydrostatic Pressure Bioreactor (HHPB); B) Photograph of High Hydrostatic Pressure Bioreactor (HHPB); C) Schematic representation of HP forces applied to cell encapsulated gellan gum construct; D) Schematic representation of Low Hydrostatic Pressure Bioreactor (LHPB); E) Photograph of Low Hydrostatic Pressure Bioreactor (LHPB).

2.2. ISOLATION, EXPANSION AND CELL ENCAPSULATION IN GELLAN GUM HYDROGELS

2.2.1. HUMAN NASAL CHONDROCYTES (HNC)

A transphenoidal biopsy was collected from patients undergoing neurosurgery. All patients signed an informed consent document approved by the Ethical Committee of Hospital S. Marcos (Braga, Portugal). Nasal cartilage was dissected and digested with collagenase type II, according to a protocol described elsewhere [43]. Briefly, the tissue was washed with sterile PBS (Sigma P4417), diced into 2-3 mm thickness cubes, immersed in 20 mL trypsin-EDTA solution (Invitrogen 25300-062, USA) and incubated for 30 minutes at 37ºC in a rotator. Tripsin-EDTA solution was removed and 20 mL of collagenase type II (2 mg/mL, Sigma C6885, USA) was added and allowed to incubate for 15h at 37ºC in a rotator. The digested tissue was filtered and the cell suspension centrifuged at 1200 rpm for 8 minutes. The cell pellet was washed twice with PBS and cells counted with a hemocytometer using the viability stain trypan blue (Sigma). Chondrocytes were expanded with chondrogenic expansion medium composed by D-MEM high glucose (Sigma D5671), 1% non-essential amino-acids (1xMEM Invitrogen 11140-035); 20 mM L-alanyl-L-glutamine (Sigma G8541); 1% antibiotic/antimicotic 100x (15240-062 Gibco, USA); 10 mM HEPES (Sigma H4034); 10% Fetal Bovine Serum (Biochrom, Germany, Heat inactivated 30 min., 57ºC), supplemented with basic fibroblast growth factor (b-FGF) 10 ng/mL (Peprotek 100-18B, United Kingdom). Chondrocytes were expanded until passage 3 and detached from the culture flask with trypsin-EDTA Solution (Invitrogen 25300-062).

2.2.2. HUMAN ADIPOSE DERIVED STEM CELLS (HASCS)

hASCs were isolated according to previously described methods [44] from liposuction aspirates of subcutaneous adipose tissue (AT), donated with written consent by patients undergoing elective liposurgery. Briefly, AT was washed with PBS (1:1 v/v), centrifuged 200g for 5 minutes at RT and infranatants discarded. 1 mL of collagenase solution 0.2 U/mL (Collagenase NB 4 Standard grade, SERVA Electrophoresis, Cat. No. 17454) was added per gram of washed AT, shaked vigorously and incubated at 37ºC for 45 min in a water bath with agitation at 200 rpm. Digested AT was further centrifuged at 1200g, 3minutes, RT, supernatants discarded and the pellet (correspondent to the stromal vascular fraction - SVF) was plated in cell culture plates. Adhered cells (adipose stem cells – hASC) were further expanded to the third passage in high-glucose Dulbecco's modified Eagle's medium (DMEM) (GIBCO 11965) supplemented with 10% fetal bovine serum (FBS) (GIBCO 26140), penicillin–streptomycin (1%) (GIBCO 15140)

and 1 ng/mL basic fibroblast growth factor (bFGF) (Peprotech 100-18B). p0 cells were examined for surface marker expression using flow cytometry. The presence of specific antigens such as CD105, CD45, CD34, CD73 and CD90 were analyzed, as previously published [44, 45]. hASCs were tested for their differentiation capacity into the osteogenic, chondrogenic and adipogenic lineages.

2.3. CELL ENCAPSULATION IN GELLAN GUM HYDROGELS

Gellan gum (GG) is a water-soluble gelling agent commonly used in food and pharmaceutical industry, due to its processing into transparent gels resistant to heat and acid stress. The thickness and hardness of the GG is determined by acetyl groups present: with acetyl groups, the gel is soft and elastic; without acetyl groups, firmer gels are obtained [46]. Both form thermo-reversible gels with different mechanical properties in the presence of metallic ions and upon temperature decrease. Once GG presents a thermo-sensitive behavior [47-49], with gelation close to body temperature, its application as an injectable formulation, for repair of cartilage defects, is promising [50-53].

Gellan gum hydrogel was produced according to the procedure described by Oliveira JT, Reis RL *et al* (2009)[50, 54]. Briefly, powdered gellan gum (Gelzan^{TM} Sigma G1910) was dissolved in distilled water into a 1.5% solution, and heated up to 90ºC. Temperature was subsequently decreased down to 37-40ºC, for cell encapsulation at a final concentration of $10x10^6$ cells/mL. Cylindrical discs were made with a mould and phosphate buffer saline (PBS) (Sigma P4417) was used as a cross-linking agent to stabilize the hydrogel structure.

2.4. BIOREACTOR CULTIVATION OF TISSUE CONSTRUCTS

2.4.1. HNC STUDY

The experimental design is outlined in Figure 2. Human nasal chondrocytes encapsulated in gellan gum hydrogel (HNC-GG) were cultured up to 3 weeks in three conditions (Fig.2A and 2B): 1) Pulsatile Hydrostatic Pressure (PHP) – culture medium pressurized between 0.1 MPa and 0.4 MPa, at a frequency of 0.1 Hz, 3 hours/day, 5 days/week; 2) Steady Hydrostatic Pressure (SHP) – culture medium pressurized at 0.4 MPa for 3 hours/day, 5 days/week; 3) Static culturing (Static) - Constructs were cultured at atmospheric pressure conditions (0.1 MPa) during the total culturing period. Equal individual devices were used for each culturing regime.

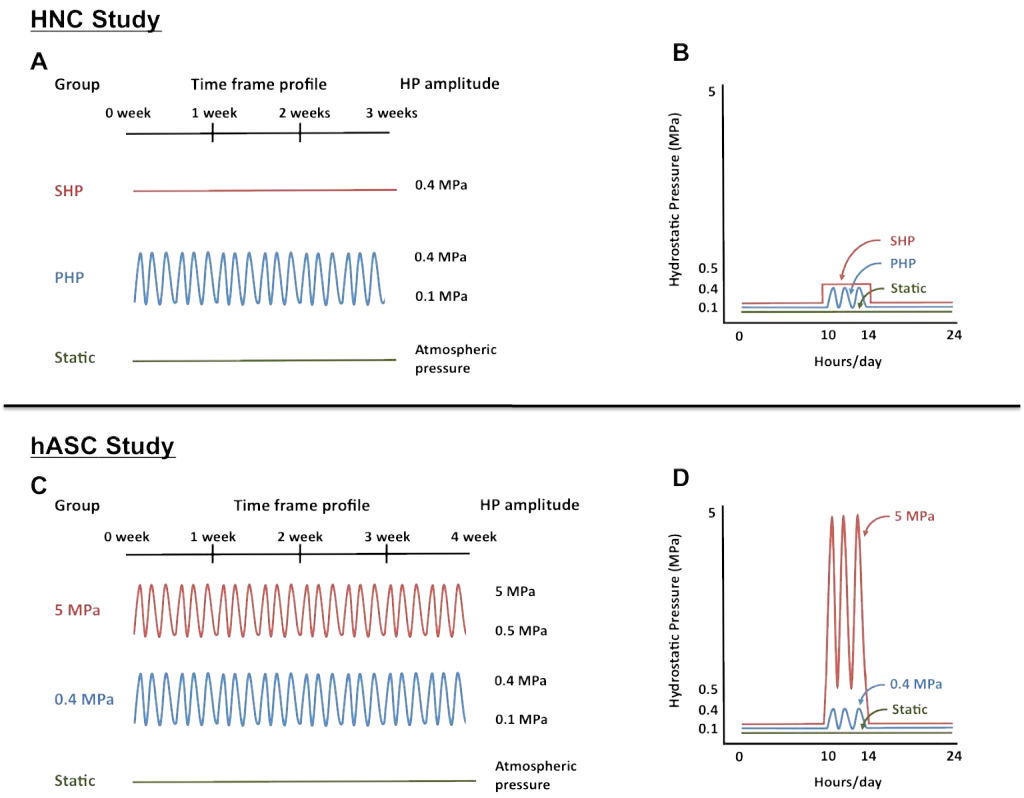

Figure 2. Hydrostatic Pressure (HP) profiles applied to constructs. HNC study: A) HP profile applied along 3 weeks of culture (SHP – Steady Hydrostatic Pressure; PHP – Pulsatile Hydrostatic Pressure); B) Daily HP profile applied to constructs. hASC study: C) HP profile applied along 4 weeks of culture; D) Daily HP profile applied to constructs.

2.4.2. hASC STUDY

Human adipose stem cells (hASC) encapsulated in gellan gum hydrogel (hASC-GG) were cultured up to 4 weeks in three conditions (Fig.2C and 2D): 1) High Hydrostatic Pressure (5 MPa) - culture medium pressurized between 0.5 MPa and 5 MPa, at a frequency of 0.5 Hz, 4 hours/day, 5 days/week; 2) Low Hydrostatic Pressure (0.4 MPa) - culture medium pressurized at 0.4 MPa, at a frequency of 0.5 Hz, 4 hours/day, 5 days/week; Static culturing (Static) - constructs were cultured at atmospheric pressure conditions during the total culturing period.

2.5. CELL VIABILITY AND PROLIFERATION ASSESSMENT

Cell viability was evaluated by a LIVE/DEAD assay. Live cells (indicated by calcein AM, Invitrogen C3099) and dead cells (indicated by propidium iodide, Alfagene P1304MP, Portugal) were imaged through a Zeiss Axioimage (RZ1M) florescence microscope (Germany). Cell metabolic activity was assessed through MTS (3-(4,5-dimethylthiazol-2-yl)-5(3-

carboxymethoxyphenyl)-2(4-sulfofenyl)-2H-tetrazolium) assay (VWR G3580). Constructs were washed in PBS and incubated with MTS solution at 37ºC for 3h, after which 100 µL were transferred to a 96-well plate for optical density (OD) measurement at 490 nm. OD is directly proportional to the cellular activity, being a measure of mitochondrial activity.

2.6. BIOCHEMICAL CHARACTERIZATION

Constructs were harvested, washed in PBS, cut in half and weighed. For DNA assay, one-half was added to 1 mL of proteinase K digestion buffer (10 mM Tris, 1 mM EDTA, 0.1% Triton X-100, 0.1 mg/mL proteinase K) and incubated overnight at 56ºC for digestion. After centrifugation at 3000g, 10 minutes, the supernatants were removed, diluted, pippeted in duplicate into a 96-well plate and 1:1 ratio of picogreen solution (Quant-iT™ PicoGreen ® dsDNA Kit, Invitrogen) was added. Sample fluorescence was measured with fluorescent plate reader at excitation ~480 nm, emission ~520 nm. Lambda DNA was used to prepare the standard curve. For glycosaminoglycan (GAG) quantification, one-half of constructs was added to 1 mL of papain digestion buffer (100 mM Sodium Phosphate Buffer, 10 mM Na_2EDTA, 1.5 mg/mL L-cysteine hydrochloride, 0.125 mg/mL papain) and incubated overnight at 60ºC for digestion. After centrifugation at 10000g, 5 minutes, 10 µL of supernatant was removed, pippeted in duplicate into a 96-well plate and 250 µL of DMB solution (Dimethylmethylene blue) was added. Sample absorbance was measured with microplate reader at OD 530 nm. Chondroitin 6-sulfate C sodium salt was used to prepare the standard curve.

2.7. HISTOLOGY AND IMMUNOHISTOCHEMISTRY

10% formalin was used to fix samples for 1 day, and further dehydrated with graded ethanol washes. Samples were embedded in paraffin, sectioned to 5 µm and mounted on glass slides. To proceed to distinct stainings, sections were deparaffinized with Clearite and rehydrated with a graded series of ethanol washes.

Safranin O and Alcian Blue staining were performed to detect articular cartilage extracellular matrix components, such as mucopolysaccharides and glycosaminoglycans, respectively. Briefly, safranin O stain was performed by staining with Weigert's iron hematoxylin, 10 min followed by running in tap water for 10 min. Slides were then immersing in 0.02% fast green solution during 5 min and rinsed 10-15 sec in 1% acetic acid. Finally, samples were stained with 0.1% safranin O solution for 5 min. Regarding alcian blue staining, slides were immersed 30 min in 0.01 g/mL alcian blue solution, and washed in running tap water for 2 min. A

counterstain with nuclear fast red was performed for 5 min. Upon stainings, sections were washed in running tap water, dehydrated with a graded series of ethanol, cleared with Clearite and mounted with resinous mounting media.

For immunohistochemistry sections were blocked with normal horse serum (NHS), stained sequentially with primary antibody (rabbit anti-human collagen type II polyclonal antibody, abcam ab34712 and rabbit anti-human collagen type I polyclonal antibody, abcam ab292; NHS for negative control), secondary antibody (Vectastain Universal Elite ABC Kit, PK-6200 Vector Laboratories) and developed with biotin-avidin system (DAB substrate kit SK-4100 Vector Laboratories).

2.8. QUANTITATIVE REAL TIME RT-PCR (QRT-PCR)

For RNA extraction, constructs were added to 800 µL of Trizol (Invitrogen 15596-026) and disintegrated by mortar and pestle. Suspensions were centrifuged at 12,000 g for 10 min at 4°C to remove tissue debris and extracted with chloroform (JMGS C/4960/17). Colorless aqueous phase, containing RNA was removed and mixed with equal volume of isopropanol (Laborspirit 33539). Suspensions were again centrifuged at 12,000 g for 8 min at 4°C, supernatant discarded, and RNA pellet washed with 75% ethanol. Samples were centrifuged at 7,500 g for 5 min at 4°C, supernatant removed, pellet air-dried, and dissolved with RNAase-free water (Invitrogen 10977035). RNA was quantified using Nanodrop® ND-1000. Approximately 1 µg of RNA was reversely transcribed with random hexameres using qScript™ cDNA Synthesis Kit (Quanta Biosciences 95047). Collagen type II, aggrecan, Sox-9 and the housekeeping gene glyceraldehyde-3-phosphatedehydrogenase (GAPDH) expression were quantified using PerfeCTa™ SYBR® Green FastMix™ (Quanta Biosciences 95072, Gaithersburg, MD, USA) and the Mastercycler ep *realplex*⁴ (Eppendorf, Hauppauge, NY, USA). Primer sequences and amplicon size are described on Table I. The expression data were normalized to GAPDH and presented as average values for each group (n=3 ± SD).

Table I. Primers used for qRT-PCR

Gene	Primer Forward	Primer Reverse	Amplicon
Collagen type II	5'GACAATCTGGCTCCCAAC	5'ACAGTCTTGCCCCACTTA	257 bp
Aggrecan	5'TGAGTCCTCAAGCCTCCTGT	5'TGGTCTGCAGCAGTTGATTC	129 bp
Sox-9	5'TACGACTACACCGACCACCA	5'TTAGGATCATCTCGGCCATC	256 bp
GAPDH	5'ACAGTCAGCCGCATCTTCTT	5'ACGACCAAATCCGTTGACTC	94 bp

bp – base pairs; GAPDH - Glyceraldehyde 3-phosphate dehydrogenase

2.9. STATISTICAL ANALYSIS

Data are presented as average (n=3) ± standard deviation. Statistical significance was determined using analysis of variance (ANOVA) followed by Tukey's HSD (honestly significant difference) test using Prism software (Prism 4.0c, GraphPad Software Inc., San Diego, CA, USA).

3. RESULTS

3.1. CELL PROLIFERATION AND VIABILITY

Human Nasal Chondrocyte (HNC) metabolic activity was quantified by the reduction of MTS reagent at the beginning and end of culture (Fig. 3A). No significant differences were obtained from day 1 to week 3 of culture, or among experimental groups. Live/Dead imaging of HNC encapsulated in gellan gum hydrogels corroborate with MTS data, as green viable cells are visualized by fluorescence microscopy.

DNA contents of human adipose stem cells (hASC) encapsulated in gellan gum hydrogels, was quantified at beginning and end of culture. hASC cultured in static conditions proliferated more than those cultured in 5 MPa HP ($p<0.05$) and was the only group that significantly increased cell number relatively to beginning of culture ($p<0.01$). Live/Dead viability assay allowed the observation, by fluorescence microscopy, of green viable cells which enzymatically converted nonfluorescent cell-permeant calcein AM into the intensely fluorescent calcein (Fig. 3B).

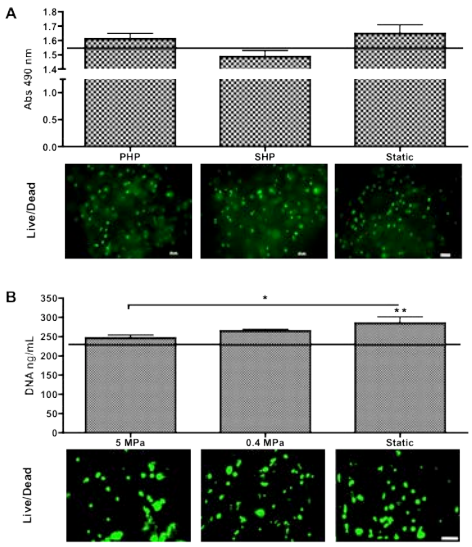

Figure 3. Cell viability and proliferation assessment. A) HNC study Top: Cell metabolic activity evaluated by MTS reduction. Horizontal line indicates day 1 values. n=3, no statistically significant differences between groups. Bottom) Live/Dead imaging of constructs after 3 weeks of culture. Scale

bar = 50 µm. B) hASC study Top: Cell proliferation evaluated by DNA concentration. Horizontal line indicates day 1 values. n=3, *p<0.05; **p<0.01 to day 1. Bottom) Live/Dead imaging of constructs after 4 weeks of culture. Scale bar = 50 µm.

3.2. CARTILAGE TISSUE DEVELOPMENT

3.2.1. HNC STUDY

Cartilage tissue developed by HNC-GG cultured under 0.4 MPa pulsatile or steady hydrostatic pressure was evaluated after 3 weeks, and compared with static culturing. Cartilage extracellular matrix components, namely collagen type II (Col II) and glycosaminoglycans (GAGs) were localized in cross-sections of constructs (Fig. 4). Safranin O and Alcian Blue stainings reveal the presence of negatively charged glycosaminoglycans (GAGs) in cultured constructs.

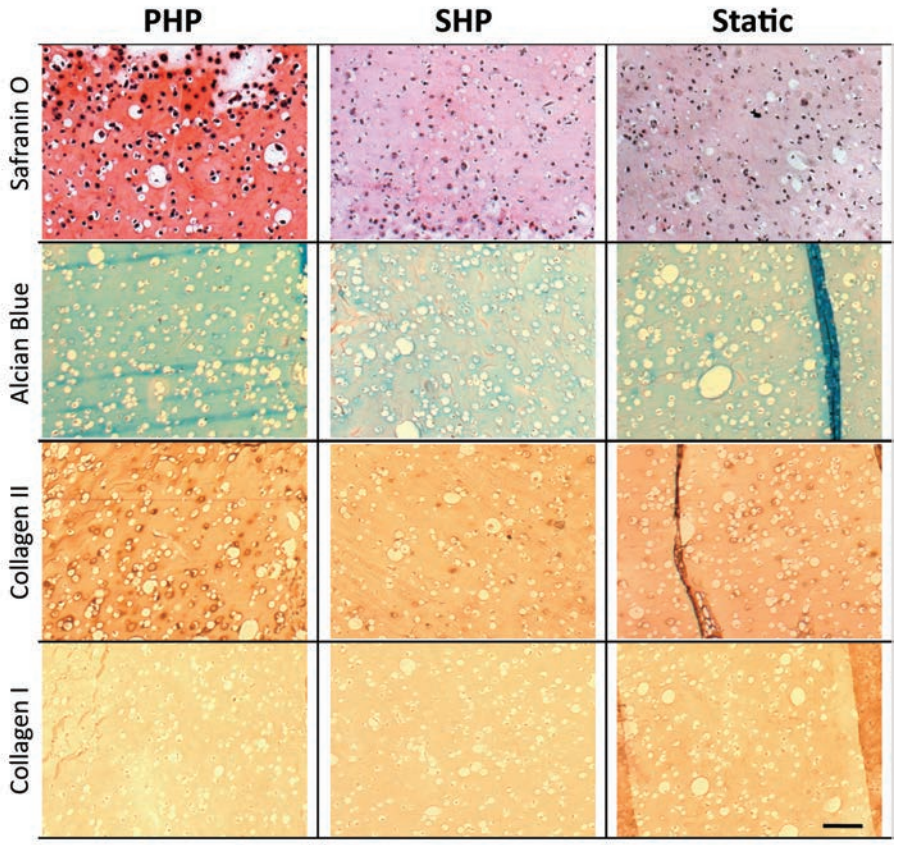

Figure 4. HNC study: Cartilage development evaluation after 3 weeks of culture. 1st & 2nd row) Histological stainings of cartilage extracellular matrix, namely Glycosaminoglycans (by Safranin O and Alcian Blue); 3rd & 4th row) Immunohistochemical localization of Collagen type II and Collagen type I. Scale bar = 100 µm. PHP – Pulsatile Hydrostatic Pressure; SHP – Steady Hydrostatic Pressure.

We observed that pulsatile hydrostatic pressure (PHP) induced a great increase in GAG deposition as shown by intense Safranin O staining and higher Alcian Blue staining, as compared to constructs cultured under steady hydrostatic pressure (SHP), or under static culturing conditions. Also, deposition of collagen type II, the major component of articular cartilage, was increased in the PHP group, while the least deposition was observed for the SHP group. Collagen type I, was not detected in any of the experimental groups, which is a positive marker of development of healthy articular cartilage (Fig.4). Gene expression profile corroborate with these observations (Fig.5). Collagen type II relative gene expression was over-expressed in cells cultured under PHP conditions, significantly different ($p<0.05$) than SHP or Static groups. Sox-9 gene expression, an important transcription factor in chondrogenesis, was also up-regulated in the PHP group, statistically different than SHP and Static groups. Among these, SHP culturing did not improve either Collagen type II nor Sox-9 relative gene expression over Static culturing. Aggrecan gene expression, though, was significantly inferior ($p<0.05$) in cells cultured under SHP as compared to Static conditions.

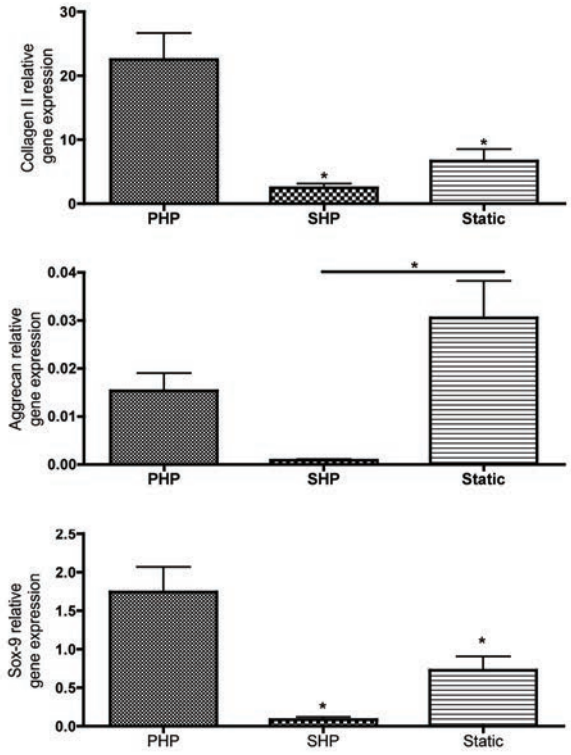

Figure 5. HNC study: Relative gene expression obtained after culture. Collagen II, aggrecan and sox-9 gene expression relative to GAPDH. n = 3, *$p<0.05$. PHP – Pulsatile Hydrostatic Pressure; SHP – Steady Hydrostatic Pressure.

3.2.2. hASC STUDY

Safranin O and Alcian Blue stainings were performed to detect glycosaminoglycans (GAGs) in hASC-GG constructs cultured under high (5 MPa) or low (0.4 MPa) pulsatile hydrostatic pressure (PHP), and compared to static culture conditions (Fig.6). Both dyes stained intensely the glycosaminoglycans present in constructs cultured under 5 MPa of PHP. Moreover, it was evident the presence of cells in lacunae, characteristic of articular cartilage tissue. Less stain intensity was observed for constructs cultured under 0.4 MPa of PHP in comparison to 5 MPa group, yet higher than the one observed for constructs cultured under static conditions. The same trend was observed for immunolocalization of collagen type II (Fig.6): higher deposition of this articular cartilage protein was observed in constructs of group 5 MPa, relatively to constructs of 0.4 MPa group, which per se, demonstrated higher collagen II deposition than constructs that were not mechanically stimulated (Static group).

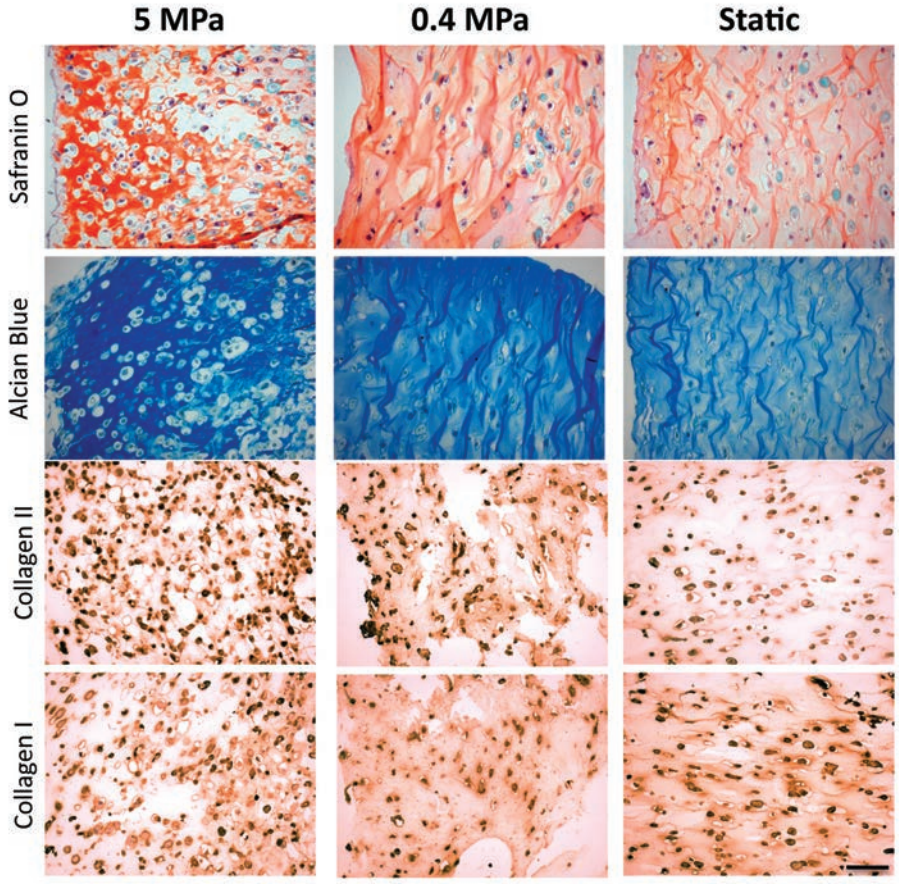

Figure 6. hASC study: Cartilage development evaluation after 4 weeks of culture. 1st & 2nd row) Histological stainings of cartilage extracellular matrix, namely Glycosaminoglycans (by Safranin O and Alcian Blue); 3rd & 4th row) Immunohistochemical localization of Collagen type II and Collagen type I. Scale bar = 100 µm.

Regarding collagen type I, the opposite trend was observed: constructs of Static group demonstrated deposition of this protein to a higher extent than constructs cultured under low PHP (0.4 MPa group). Constructs of 5 MPa group demonstrated the smaller deposition of collagen type I. The increased deposition of Collagen type II and low deposition of Collagen type I are indicative of the development of mature and healthy articular cartilage. The relative expression of genes encoding for major articular cartilage extracellular matrix components, such as collagen II and aggrecan, were determined by qRT-PCR and found to be consistent with histology staining (Fig.7). Aggrecan relative gene expression (GE) of cells exposed to 5 MPa PHP was significantly higher ($p<0.05$) than GE quantified for both 0.4 MPa and Static groups. Regarding collagen type II, the highest expression was obtained for cells exposed to 0.4 MPa, which was found to be significantly different from GE quantified for both 5 MPa and Static groups. Regarding gene expression of Sox-9 transcription factor, no significant differences were detected between culturing groups. The extracellular matrix components were also directly quantified by biochemical assays. The amount of quantified glycosaminoglycans in the constructs was superior for the 5 MPa group, and found to be significantly different ($p<0.05$) than those observed for static culturing (Fig.8).

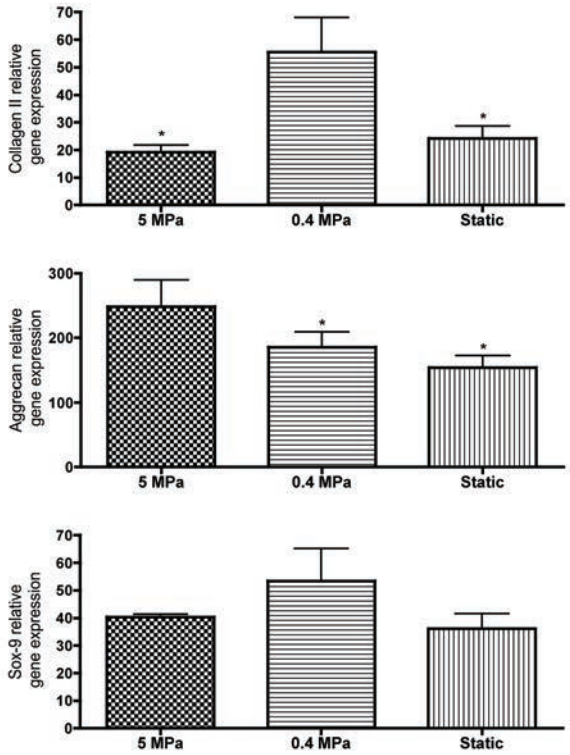

Figure 7. hASC study: Relative gene expression obtained after culture. Collagen II, aggrecan and sox-9 gene expression relative to GAPDH. n = 3, * $p<0.05$.

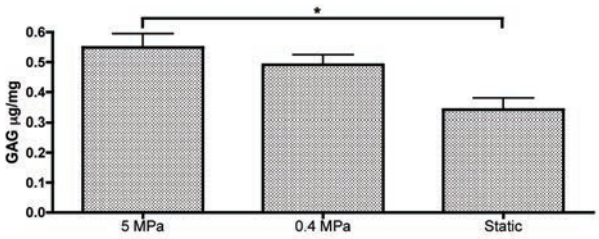

Figure 8. hASC study: Glycosaminoglycan quantification obtained after 4 weeks of culture. n = 3, *p<0.05.

4. DISCUSSION

Dynamic culturing has long been adopted [55-57] as a strategy to improve the development of cartilage tissue *in vitro* as opposed to standard static culturing techniques. We understand dynamic culturing, as the use of biomechanical stimuli that are relevant to the tissue being engineered. Articular cartilage tissue in joints such as the hip or the knee, is subjected to intermittent cyclic stress that can either be compressive or shear [2]. However, major joint load is supported by interstitial fluid pressurization [3, 58]. Hydrostatic pressure is so essential for cartilage homeostasis that joint immobilization or decreased loading results in cartilage thinning [59, 60]. Hydrostatic pressure is a fundamental mechanical stimulus governing the normal functioning of articular cartilage, which has justified its broad exploitation in our study. Two custom bioreactor systems were developed, being capable of generating and applying this mechanical stimulation to 3D tissue engineering constructs (Fig.1). These systems are novel and distinguish themselves from other systems described in the literature by several features, namely: a) the possibility to long term culture and stimulate cell-encapsulated / cell-seeded constructs in the same device up to 4 weeks (maximum evaluated). Other studies have explored HP pressurization for shorter periods, such as a few hours (1, 4 or 24h) [19-21, 23, 24, 27], or up to two weeks [18, 22, 25, 26]. Carver *et al* 1999 [17], and lately, Gunja and co-workers 2010 [61], cultured constructs up to 5 and 4 weeks respectively although requiring higher technical complexity. Our devices are user-friendly, and can be operated inside standard hoods and incubators during complete experimental periods, which is a feature not commonly observed in other studies [19, 21, 23, 24, 26, 27, 61].

In order to validate the purpose of using hydrostatic pressure to improve cartilage tissue development *in vivo*, we performed a preliminary study, using healthy chondrocytes from hyaline cartilage source (nasal septum cartilage). Nasal septum was chosen as alternative model of healthy articular cartilage as HNC have proven to respond to mechanical stimulation

[28]. In our study, very positive outcomes were obtained, even under low level of hydrostatic pressure (0.4 MPa). This finding supported the subsequent study using human adipose derived stem cells (hASCs). Our major aim was to understand if hASCs respond positively to this mechanical stimulation and develops cartilage tissue with increased properties than those obtained under standard culturing conditions, for similar culturing periods. Furthermore, we questioned if higher level of HP within the physiological range found in human joints (5–6 MPa for gait) [13, 14], would improve cartilage formation. In both studies, gellan gum hydrogel [50] was used for cell encapsulation due to its proven performance on supporting cartilage tissue development *in vitro* [50, 51] and *in vivo* [53] with chondrocytes and adipose stem cells[53]. For both studies, cell viability was assessed. We observed that hydrostatic pressure amplitudes of 0.4 MPa under both pulsatile and steady state regimes were not deleterious for human nasal chondrocytes, as no significant differences were obtained as compared to static conditions (Fig.3A). Furthermore, for the hASC study, DNA content for all groups measured at the end of culture was superior than the initial, which demonstrated that both 0.4 and 5 MPa pulsatile loading regimes were not harmful to cells (Fig.3B). Though, only hASC cultured under static conditions proliferated ($p<0.01$ to day 1 values), indicating that lack of HP allowed higher cell division in detriment of chondrogenic differentiation stimulation.

Hydrostatic pressure culturing induced chondrogenic matrix deposition. In the HNC study, more than questioning if HP would improve cartilage tissue development by these cells, we questioned whether pulsatile or steady loading would provide increased tissue formation. Therefore, HNC-GG were cultured under 0.1 Hz or 0 Hz, 0.4 MPa HP loading. Higher extracellular matrix production and deposition, identified by increased GAG staining by Safranin O and Alcian Blue, as well as Collagen type II immunolocalization was obtained for pulsatile culturing (PHP group). Moreover, steady HP culturing (SHP group) seemed to suppress any chondrogenic development, once very low histological detection and gene expression was obtained for this group, even lower than for static culturing (Fig.4 and 5). To our knowledge, HNC response to HP mechanical stimulation has not been yet fully explored. In the context of mechanical stimulation, Candrian and colleagues [28] evaluated HNC response to distinct compression loading regimens, and observed that these expressed collagen II, aggrecan and hyaluronan to different extents as response to those specific regimes. Bouchet *et al* [62] cultured HNC in spinner flasks, demonstrating that this stimulation improved aggrecan and collagen type II gene expression and deposition on Cellagen^{TM} beads. Although we have used HNC as a cell model, we also recognize its interest as a possible heterologous approach for the treatment of cartilage focal lesions. In fact, the use of HNC 1) avoids the need of biopsy

harvesting of hyaline cartilage from non-bearing articular sites; and 2) allows good cell response to mechanical stimuli that are physiological relevant, anticipating a good adaptation of the engineered tissue to the implantation site environment. From this preliminary study, we conclude that: 1) HNC respond to hydrostatic pressure mechanical stimulation by increasing cartilage formation outcome as compared to engineered constructs cultured under static conditions; 2) Pulsatile HP stimulated HNC to secrete cartilaginous ECM, while SHP appears to suppress cartilage development. Therefore, pulsatile hydrostatic pressure at 0.4 MPa was chosen to stimulate hASC in gellan gum hydrogels towards chondrogenic differentiation and hyaline cartilage tissue formation. Herein, more than hypothesizing the ability of hASC to sense and respond to pulsatile HP mechanical stimulation at 0.4 MPa, by increasing chondrogenic differentiation and improving cartilage tissue development, we also questioned the influence of physiologic levels of HP (5 MPa) on the magnitude of these outcomes. Both hypotheses were proven. Data shown demonstrates increased aggrecan gene expression, intense GAG staining and correspondent increased GAG quantification for the 5 MPa group, relatively to both 0.4 MPa and Static groups (Fig. 6, 7 and 8). Moreover, same outputs were found greater for 0.4 MPa group as compared to Static group, indicating an amplitude-related response of hASC to HP, since cartilage related outputs were found to vary proportionally to the HP magnitude: 5 MPa > 0.4 MPa > Static. Our results are additive to those obtained by Ogawa and co-workers [39], which remains, to our knowledge, the only study that previously explored the response of hASC to HP. In this work, hASC were exposed to pulsatile low HP (0.5 MPa) for 1 week, followed by 3 weeks of static culturing, and evidenced increased collagen II, aggrecan and sox-9 gene expression and ECM staining in the pressurized group, as compared to the static group. We suggest that physiologic levels of HP (10x higher), and longer loading periods provide a more mature tissue, which is better adapted to the environment found *in vivo*. Given this, we conclude that 1) hASC sense and respond to pulsatile hydrostatic pressure stimulation at both low (0.4 MPa) and physiologic (5 MPa) pressure amplitudes; 2) Physiologic HP amplitudes promoted a higher and better tissue matrix distribution, which resembles native articular cartilage.

5. CONCLUSIONS

By aiming the improvement of *in vitro* engineering of cartilage tissue, two custom-made bioreactor systems were developed, being capable of generating and applying, in a controlled manner, hydrostatic pressure (HP) as biomechanical stimuli - at high and low magnitudes - to

3D tissue engineering constructs. In addition, HNC and hASC were encapsulated in gellan gum hydrogels (ASC-GG), and cultured under several HP regimens in order to evaluate cartilaginous tissue formation. We observed that HNC enhance secretion of cartilaginous ECM when cultured under pulsatile low HP, while same levels of HP (0.4 MPa) applied continuously inhibit ECM secretion. Moreover, hASC cultured under same pulsatile low HP (0.4 MPa) secrete less chondrogenic ECM than under pulsatile physiologic levels of HP (5 MPa). We conclude that hASC not only sense and respond to HP loading, but also respond in different proportions in accordance to magnitude of loading applied. Further experimental studies are needed to understand the mechanotransduction mechanisms occurring that lead to the observed cell response.

Acknowledgments

We gratefully acknowledge funding support of this work by the FCT PhD grant (SFRH/BD/42316/2007 to CC). The authors thank Doctor Emílio Valls and Clínica Luso-Espanhola, Porto for providing adipose tissue, and Professor Nuno Neves and Hospital S. Marcos, Braga for providing cartilage tissue, both used in experiments.

References

1. Lippiello, L., et al., *Invitro Metabolic Response of Articular-Cartilage Segments to Low-Levels of Hydrostatic-Pressure.* Connective Tissue Research, 1985. 13(2): p. 99-107.
2. Grodzinsky, A.J., et al., *Cartilage tissue remodeling in response to mechanical forces.* Annu Rev Biomed Eng, 2000. 2: p. 691-713.
3. Mow, V. and X.E. Guo, *Mechano-electrochemical properties of articular cartilage: Their inhomogeneities and anisotropies.* Annual Review of Biomedical Engineering, 2002. 4: p. 175-209.
4. Seidel, J.O., et al., *Long-term culture of tissue engineered cartilage in a perfused chamber with mechanical stimulation.* Biorheology, 2004. 41(3-4): p. 445-58.
5. Davisson, T., et al., *Static and dynamic compression modulate matrix metabolism in tissue engineered cartilage.* J Orthop Res, 2002. 20(4): p. 842-8.
6. Wang, P.Y., et al., *Dynamic Compression Modulates Chondrocyte Proliferation and Matrix Biosynthesis in Chitosan/Gelatin Scaffolds.* Journal of Biomedical Materials Research Part B-Applied Biomaterials, 2009. 91B(1): p. 143-152.
7. Xie, J., Z.Y. Han, and T. Matsuda, *Mechanical compressive loading stimulates the activity of proximal region of human COL2A1 gene promoter in transfected chondrocytes.* Biochemical and Biophysical Research Communications, 2006. 344(4): p. 1192-1199.
8. Bueno, E.M., B. Bilgen, and G.A. Barabino, *Wavy-walled bioreactor supports increased cell proliferation and matrix deposition in engineered cartilage constructs.* Tissue Eng, 2005. 11(11-12): p. 1699-709.
9. Chen, H.C., et al., *A novel rotating-shaft bioreactor for two-phase cultivation of tissue-engineered cartilage.* Biotechnol Prog, 2004. 20(6): p. 1802-9.
10. Gooch, K.J., et al., *Effects of mixing intensity on tissue-engineered cartilage.* Biotechnol Bioeng, 2001. 72(4): p. 402-7.
11. Saini, S. and T.M. Wick, *Concentric cylinder bioreactor for production of tissue engineered cartilage: effect of seeding density and hydrodynamic loading on construct development.* Biotechnol Prog, 2003. 19(2): p. 510-21.
12. Alves da Silva, M.L., et al., *Chitosan/polyester-based scaffolds for cartilage tissue engineering: assessment of extracellular matrix formation.* Acta Biomater, 2010. 6(3): p. 1149-57.
13. Hodge, W.A., et al., *Contact pressures in the human hip joint measured in vivo.* Proc Natl Acad Sci U S A, 1986. 83(9): p. 2879-83.
14. Rushfeldt, P.D., R.W. Mann, and W.H. Harris, *Improved Techniques for Measuring Invitro the Geometry and Pressure Distribution in the Human Acetabulum .2. Instrumented Endoprosthesis Measurement of Articular Surface Pressure Distribution.* J Biomech, 1981. 14(5): p. 315-&.
15. Mow, V.C., A. Ratcliffe, and A.R. Poole, *Cartilage and diarthrodial joints as paradigms for hierarchical materials and structures.* Biomaterials, 1992. 13(2): p. 67-97.
16. Eckstein, F., et al., *In vivo morphometry and functional analysis of human articular cartilage with quantitative magnetic resonance imaging--from image to data, from data to theory.* Anat Embryol (Berl), 2001. 203(3): p. 147-73.
17. Carver, S.E. and C.A. Heath, *Increasing extracellular matrix production in regenerating cartilage with intermittent physiological pressure.* Biotechnol Bioeng, 1999a. 62(2): p. 166-74.
18. Mizuno, S., et al., *Hydrostatic fluid pressure enhances matrix synthesis and accumulation by bovine chondrocytes in three-dimensional culture.* J Cell Physiol, 2002. 193(3): p. 319-27.
19. Toyoda, T., et al., *Hydrostatic pressure modulates proteoglycan metabolism in chondrocytes seeded in agarose.* Arthritis Rheum, 2003. 48(10): p. 2865-72.
20. Wenger, R., et al., *Hydrostatic pressure increases apoptosis in cartilage-constructs produced from human osteoarthritic chondrocytes.* Front Biosci, 2006. 11: p. 1690-5.
21. Nakamura, S., et al., *Hydrostatic pressure induces apoptosis of chondrocytes cultured in alginate beads.* Journal of Orthopaedic Research, 2006. 24(4): p. 733-739.
22. Heyland, J., et al., *Redifferentiation of chondrocytes and cartilage formation under intermittent hydrostatic pressure.* Biotechnology Letters, 2006. 28(20): p. 1641-1648.

23. Sharma, G., R.K. Saxena, and P. Mishra, *Differential effects of cyclic and static pressure on biochemical and morphological properties of chondrocytes from articular cartilage.* Clin Biomech (Bristol, Avon), 2007. 22(2): p. 248-55.
24. Mio, K., J. Kirkham, and W.A. Bonass, *Possible role of extracellular signal-regulated kinase pathway in regulation of Sox9 mRNA expression in chondrocytes under hydrostatic pressure.* J Biosci Bioeng, 2007. 104(6): p. 506-9.
25. Gavenis, K., et al., *Effects of cyclic hydrostatic pressure on the metabolism of human osteoarthritic chondrocytes cultivated in a collagen gel.* Artif Organs, 2007. 31(2): p. 91-8.
26. Wagner, D.R., et al., *Hydrostatic pressure enhances chondrogenic differentiation of human bone marrow stromal cells in osteochondrogenic medium.* Ann Biomed Eng, 2008. 36(5): p. 813-20.
27. Sakao, K., et al., *Induction of chondrogenic phenotype in synovium-derived progenitor cells by intermittent hydrostatic pressure.* Osteoarthritis Cartilage, 2008. 16(7): p. 805-14.
28. Candrian, C., et al., *Engineered cartilage generated by nasal chondrocytes is responsive to physical forces resembling joint loading.* Arthritis Rheum, 2008. 58(1): p. 197-208.
29. Wachsmuth, L., et al., *Immunolocalization of matrix proteins in different human cartilage subtypes.* Histol Histopathol, 2006. 21(5): p. 477-85.
30. Idrus, R.B.H., et al., *Tissue engineered cartilage with different human chondrocyte sources: articular, auricular and nasal septum* Medical Journal of Islamic World Academy of Sciences, 2005. 15(1): p. 5-12.
31. Jiang, Y.Z., et al., *Cell transplantation for articular cartilage defects: principles of past, present, and future practice.* Cell Transplantation, 2011. 20(5): p. 593-607.
32. Zheng, M.H., et al., *Matrix-induced autologous chondrocyte implantation (MACI (R)): Biological and histological assessment.* Tissue Engineering, 2007. 13(4): p. 737-746.
33. Gimble, J.M., F. Guilak, and B.A. Bunnell, *Clinical and preclinical translation of cell-based therapies using adipose tissue-derived cells.* Stem Cell Research & Therapy, 2010. 1.
34. Gimble, J.M., et al., *Concise Review: Adipose-Derived Stromal Vascular Fraction Cells and Stem Cells: Let's Not Get Lost in Translation.* Stem Cells, 2011. 29(5): p. 749-754.
35. Schaffler, A. and C. Buchler, *Concise review: adipose tissue-derived stromal cells--basic and clinical implications for novel cell-based therapies.* Stem Cells, 2007. 25(4): p. 818-27.
36. Rada, T., R.L. Reis, and M.E. Gomes, *Adipose Tissue-Derived Stem Cells and Their Application in Bone and Cartilage Tissue Engineering.* Tissue Engineering Part B-Reviews, 2009. 15(2): p. 113-125.
37. Malafaya, P.B., et al., *Chitosan particles agglomerated scaffolds for cartilage and osteochondral tissue engineering approaches with adipose tissue derived stem cells.* J Mater Sci Mater Med, 2005. 16(12): p. 1077-85.
38. Mahmoudifar, N. and P.M. Doran, *Chondrogenic differentiation of human adipose-derived stem cells in polyglycolic acid mesh scaffolds under dynamic culture conditions.* Biomaterials, 2010. 31(14): p. 3858-3867.
39. Ogawa, R., et al., *The effect of hydrostatic pressure on three-dimensional chondroinduction of human adipose-derived stem cells.* Tissue Eng Part A, 2009. 15(10): p. 2937-45.
40. Awad, H.A., et al., *Chondrogenic differentiation of adipose-derived adult stem cells in agarose, alginate, and gelatin scaffolds.* Biomaterials, 2004. 25(16): p. 3211-3222.
41. Guilak, F., et al., *Clonal analysis of the differentiation potential of human adipose-derived adult stem cells.* J Cell Physiol, 2006. 206(1): p. 229-37.
42. Erickson, G.R., et al., *Chondrogenic potential of adipose tissue-derived stromal cells in vitro and in vivo.* Biochem Biophys Res Commun, 2002. 290(2): p. 763-9.
43. Crawford, A., Dickson, S. C., ed. *Chondrocyte Isolation, Expansion and Culture on Polymer Scaffolds*. Methods in Molecular Biology, ed. A.P. Hollander, P. V. Hatton Vol. 238, Biopolymer Methods in Tissue Engineering. 2004, Humana Press Inc.: Totowa, NJ.
44. McIntosh, K., et al., *The immunogenicity of human adipose-derived cells: Temporal changes in vitro.* Stem Cells, 2006. 24(5): p. 1246-1253.
45. Mitchell, J.B., et al., *Immunophenotype of human adipose-derived cells: Temporal changes in stromal-associated and stem cell-associated markers.* Stem Cells, 2006. 24(2): p. 376-385.

46. Grasdalen, H. and O. Smidsrod, *Gelation of Gellan Gum.* Carbohydrate Polymers, 1987. 7(5): p. 371-393.
47. Silva NA, S.A., Sousa RA, Oliveira JT, Pedro AJ, Mastronardi F, Mano J.F., Neves N.M., Sousa N, Reis RL, *Development and Characterization of a Novel Hybrid Tissue Engineering Based Scaffold for Spinal Cord Injury Repair.* Tissue Eng, 2009. accepted for publication.
48. Silva-Correia, J., et al., *Gellan gum-based hydrogels for intervertebral disc tissue-engineering applications.* J Tissue Eng Regen Med, 2010.
49. Silva-Correia, J., et al., *Photo-crosslinked gellan gum-based hydrogels: methods and uses thereof.* 2010.
50. Oliveira, J.T., et al., *Gellan gum: A new biomaterial for cartilage tissue engineering applications.* Journal of Biomedical Materials Research Part A, 2010. 93A(3): p. 852-863.
51. Oliveira, J.T., et al., *Gellan gum injectable hydrogels for cartilage tissue engineering applications: in vitro studies and preliminary in vivo evaluation.* Tissue Eng Part A, 2010. 16(1): p. 343-53.
52. Oliveira JT , S.R., Reis RL, *Gellan Gum Based Hydrogels for Regenerative Medicine and Tissue Engineering Applications, Its System, and Processing Devices Devices / Hidrogéis À Base De Goma Gelana Para Utilização Em Medicina Regenerativa e Engenharia De Tecidos, Seu Sistema E Dispositivos De Processamento*, in *INPI, EPO, submitted*. 2008.
53. Oliveira, J.T., et al., *Injectable Gellan Gum Hydrogels with Autologous Cells for the Treatment of Rabbit Articular Cartilage Defects.* Journal of Orthopaedic Research, 2010. 28(9): p. 1193-1199.
54. Oliveira, J., R. Sousa, and R. Reis, *Gellan gum based hydrogels for regenerative medicine and tissue engineering applications, its system, and processing devices* 2008.
55. Schulz, R.M. and A. Bader, *Cartilage tissue engineering and bioreactor systems for the cultivation and stimulation of chondrocytes.* Eur Biophys J, 2007. 36(4-5): p. 539-68.
56. da Silva, M.L.A., et al., *Chondrogenic differentiation of human bone marrow mesenchymal stem cells in chitosan-based scaffolds using a flow-perfusion bioreactor.* Journal of Tissue Engineering and Regenerative Medicine, 2011. 5(9): p. 722-732.
57. Goncalves, A., et al., *Effect of flow perfusion conditions in the chondrogenic differentiation of bone marrow stromal cells cultured onto starch based biodegradable scaffolds.* Acta Biomater, 2011. 7(4): p. 1644-52.
58. Soltz, M.A. and G.A. Ateshian, *Experimental verification and theoretical prediction of cartilage interstitial fluid pressurization at an impermeable contact interface in confined compression.* J Biomech, 1998. 31(10): p. 927-34.
59. Beaupre, G.S., S.S. Stevens, and D.R. Carter, *Mechanobiology in the development, maintenance, and degeneration of articular cartilage.* J Rehabil Res Dev, 2000. 37(2): p. 145-51.
60. Urban, J.P., *The chondrocyte: a cell under pressure.* Br J Rheumatol, 1994. 33(10): p. 901-8.
61. Gunja, N.J. and K.A. Athanasiou, *Effects of hydrostatic pressure on leporine meniscus cell-seeded PLLA scaffolds.* Journal of Biomedical Materials Research Part A, 2010. 92A(3): p. 896-905.
62. Bouchet, B.Y., et al., *Beta-1 integrin expression by human nasal chondrocytes in microcarrier spinner culture.* J Biomed Mater Res, 2000. 52(4): p. 716-24.

Section 4.

CHAPTER V

Development of silk-based scaffolds for tissue engineering of bone from human adipose derived stem cells

---

This chapter is based on the following publication: Correia C, Bhumiratana S, Yan LP, Oliveira AL, Gimble JM, Rockwood D, Kaplan DL, Sousa RA, Reis RL, Vunjak-Novakovic G, 2011, *Development of silk-based scaffolds for tissue engineering of bone from human adipose derived stem cells* - submitted.

Abstract

Silk fibroin is a potent alternative to other biodegradable biopolymers for bone tissue engineering, because of its tunable architecture and mechanical properties, and demonstrated ability to support bone formation, in vitro and in vivo. In this study, we investigated a range of silk scaffolds for bone tissue engineering using human adipose-derived stem cells (hASCs), an attractive cell source for engineering autologous bone grafts. Our goal was to understand the effects of scaffold architecture and biomechanics and to use this information to optimize silk scaffolds for bone tissue engineering applications. Silk scaffolds were fabricated using different solvents (aqueous vs. hexafluoro-2-propanol - HFIP), pore sizes (250-500μm vs. 500-1000μm) and structures (lamellar vs. spherical pores). Four types of silk scaffolds combining the properties of interest were systematically compared with respect to bone tissue outcomes with decellularized trabecular bone included as a "gold standard". The scaffolds were seeded with hASC and cultured for 7 weeks. The porous HFIP silk scaffold with 400-600 μm pores performed better than any other scaffold, while the lamellar scaffolds performed better than spherical-pore scaffolds. Based on the collected data, we propose a conceptual model describing the effects of silk scaffold design on bone tissue formation.

1. INTRODUCTION

Numerous approaches have been made towards development of an "ideal" scaffold for bone tissue engineering[1, 2]. Silk fibroin, obtained from silk-worms, demonstrates great biocompatibility along with outstanding mechanical properties [3] and proteolytic degradation [4]. In tissue engineering, silk fibroin has been extensively used for multiple types of scaffolds [5-8]. Various modifications of silk scaffolds have been fabricated with a wide range of chemical, structural and biomechanical modifications [6, 9, 10]. Silk sponges have been used for cartilage [11-13], fat [14, 15], silk tubes for blood vessels [16] and silk fibers for ligaments [17, 18]. Porous sponge scaffolds were suitable for bone tissue formation, by enhancing cell attachment, proliferation and migration. In addition, the high porosity (92-98%)[19-21] facilitates nutrient and waste transport into and out of the scaffolds.

Porous silk sponges can be fabricated using porogens, gas foaming, or lyophilization methods [22, 23]. Among these, NaCl salt leaching is among the simplest and most effective fabrication methods, resulting in scaffolds with spherical-shaped pores and different morphologies. Silk scaffolds are generally fabricated using two different silk preparation methods: aqueous- and solvent (HFIP)-based. HFIP does not solubilize salt particles, therefore pore sizes in these

sponges reflect the size of the porogen used in the process [22, 23]. On the other hand, aqueous-based silk sponges demonstrate pore sizes 10-20% smaller than the size of salt crystals. This is due to partial solubilization of the surface of the salt particles during supersaturation of the silk solution before solidification [3, 24]. This partial solubilization results in rougher surfaces of the pores, which improved cell attachment [22, 25]. For comparison, aqueous-based processing results in sponges with higher porosity [22, 25], and higher degradation rates [22, 25].

Besides silk sponges with spherical-shaped pores, our laboratory developed a novel silk scaffold fabrication method to produce lamellar-like structure using a freeze drying technique [26]. This structure mimics bone lamellae structure. Human bone marrow mesenchymal stem cells, cultured on osteogenic media, attached, proliferated and assembled new extracellular matrix on this patterned structure [26].

Tissue engineers have explored silk scaffolds for bone regeneration by using bone marrow mesenchymal stem cells (BM-MSC) as the preferred cell source with superior outcomes validated with both aqueous-based [19, 26, 27] and HFIP-derived scaffolds [6, 21, 28]. Human adipose derived stromal/stem cells (hASCs), on the other hand, present features comparable to BM-MSC and are a promising alternative for cell based therapies [29] such as bone tissue regeneration. ASCs may be easily isolated from adipose tissue with a high yield of cells per unit tissue volume [30]. Furthermore, ASCs proliferate quickly, and their osteogenic potential is comparable to that of bone marrow mesenchymal stem cells [31]. Our research group has engineered half-centimeter–sized bone constructs *in vitro* by using human adipose-derived stem cells (hASCs) that were seeded in decellularized bone scaffolds and cultured dynamically in perfusion bioreactors [32].

Still, silk scaffold and hASCs are two potential components for bone tissue engineering applications, which have not been yet investigated in combination. In this study, five different scaffolds were investigated: 1) aqueous, spherical-pore structure, small pores (250-500 μm), and 2) aqueous, spherical-pore structure, large pores (500-1000 μm); 3) aqueous, lamellar structure, 4) HFIP, medium pore sizes (400-600 μm), and 5) decellularized bovine trabecular bone used as a “gold standard”, to evaluate hASCs osteogenic responses and bone tissue development.

2. MATERIALS AND METHODS

2.1. PREPARATION OF SILK FIBROIN SCAFFOLDS

All chemicals were purchased from Sigma-Aldrich (St. Louis, MO) unless otherwise stated. Silk scaffolds were prepared according to Figure 1. Silk fibroin from silkworm (*Bombix mori*) cocoons was extracted with 0.02 M sodium carbonate (Na_2CO_3) solution, rinsed in distilled water, dissolved in a 9.3 M lithium bromide (LiBr) solution and dialyzed for 48h against distilled water in benzoylated dialysis tubing (Sigma D7884). Dissolved silk fibroin was centrifuged for 20 min at 9000 rpm (4ºC). The resulting solution was determined by weighing the remaining solid after drying, yielding a 6-wt % aqueous silk fibroin solution.

Aqueous-derived silk fibroin porous sponges were prepared by salt leaching methods. NaCl salt was sieved with metal mesh to obtain particle size distributions between 250–500 μm (Aq-250), or 500–1000 μm (Aq-500), and added into silk fibroin aqueous solution at a 2:1 (w/v) ratio, in disk-shaped containers. The container was covered and left at room temperature. After 24h, the container was immersed in water to extract NaCl salt for 2 days with water changes.

Aqueous-derived silk fibroin lamellar scaffolds (Aq-Lam) were prepared by pouring silk fibroin aqueous solution into silicon tubing (6 mm i.d.), frozen at -80ºC, lyophilized for 1 day, and autoclaved to induce the formation of β-sheet structure and insolubility in aqueous solution.

HFIP-derived silk fibroin scaffolds (HFIP-400) were prepared as previously described [25]. Silk fibroin aqueous solution was lyophilized and further dissolved with HFIP, resulting in a 17-wt % HFIP-derived silk fibroin solution. Granular NaCl particles (400–600 μm) were added to 2 mL of silk fibroin in HFIP at 2:1 (w/v) ratio. The containers were covered overnight to reduce evaporation of HFIP and to provide sufficient time for homogeneous distribution of the solution. Subsequently, the solvent was evaporated at room temperature for 3 days. The matrices were then treated in 90% (v/v) methanol for 30 min, to induce the formation of the β-sheet structure, followed by immersion in water for 2 days to remove NaCl porogens. Porous silk scaffolds were then freeze-dried. All scaffolds were cut and cored into cylinders of 4 mm in diameter and 2 mm thickness.

2.2. PREPARATION OF TRABECULAR BONE SCAFFOLDS

Trabecular bone scaffolds were decellularized as in our studies [32, 33]. Trabecular bone cylinders (4 mm diameter) were cored from the subchondral region of carpometacarpal joints of bovine calves, and washed with a high velocity stream of water to remove bone marrow from

pore spaces. Scaffolds were further washed for 1h in phosphate-buffered saline (PBS) with 0.1% ethylenediamine tetraacetic acid (EDTA) at room temperature (RT), followed by sequential washes in hypotonic buffer (10 mM Tris and 0.1% EDTA) overnight at 4º C, in detergent (10 mM Tris and 0.5% sodium dodecyl sulfate) for 24 h at RT, and in enzyme solution (100 U/mL DNAse, 1 U/mL RNAse, and 10 mM Tris) for 6 h at 37º C, to fully remove cellular material. Scaffolds were then rinsed in PBS, freeze-dried, and cut into 2 mm thick cylindrical plugs. The scaffolds within the density range of 0.28–0.38 mg/mm^3 (calculated based on the dry weights and exact dimensions) were selected for experiments.

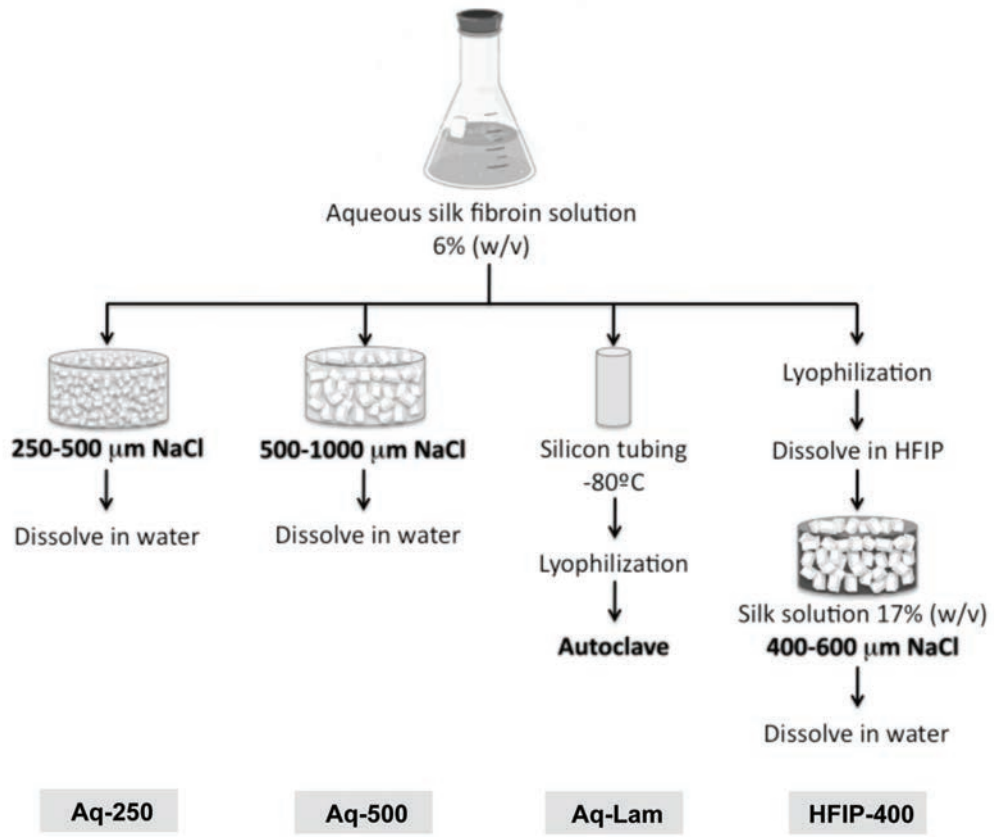

Figure 1. Silk scaffold development. Silk fibroin is extracted from silk worm cocoons into an aqueous solution. Aqueous-based spherical pore scaffolds (Aq-250 and Aq-500) are produced by salt-leaching method, where small (250-500 μm) or large (500-1000 μm) NaCl particles are used as porogen. Aqueous-based lamellar scaffolds (Aq-Lam) are produced by lyophilizing the frozen aqueous silk solution cast in a silicon tube. HFIP-derived porous scaffolds (HFIP-400) are developed by dissolving the lyophilized aqueous silk solution in HFIP solvent, to which NaCl particles (400-600 μm) are added to form the porous structure. NaCl particles used in salt-leaching method are further dissolved in water. Bold text represent step where ß-sheet formation occur.

2.3. ISOLATION, CHARACTERIZATION AND EXPANSION OF HASCS

hASCs were isolated according to previously described methods [34] from liposuction aspirates obtained from the Pennington Biomedical Research Center, under protocols approved by the Institutional Review Board. hASC were expanded to the fourth passage in high-glucose Dulbecco's modified Eagle's medium (DMEM) supplemented with 10% fetal bovine serum (FBS), penicillin–streptomycin (1%), and 1 ng/mL basic fibroblast growth factor (bFGF).

Passage zero (P0) cells were examined for surface marker expression using flow cytometry. The presence of specific antigens such as CD29, CD105, CD45, CD34, CD44, CD73 and CD90 were analyzed, as previously published [34, 35]. hASCs were confirmed for their differentiation capacity into the adipogenic and osteogenic lineages in monolayer cultures following induction with adipogenic and osteogenic inductive medium for up to 14 days and histochemical analysis of neutral lipid (Oil Red O) or mineralization (Alizarin Red) staining as published [36].

2.4. CONSTRUCT SEEDING AND CULTURE

All scaffolds were sterilized in 70% ethanol overnight, washed in PBS and incubated in culture medium prior to seeding. Expanded P4 hASCs were suspended in culture medium at $30x10^6$ cells/mL. A 20 μL aliquot of cell suspension was pipetted into blot-dried scaffolds, and pipetted up and down to ensure even distribution of cells. After 15 minutes in the incubator, scaffolds were rotated 180º, and 10 μL of cell-free medium was added to maintain hydration. This process was repeated four times, to achieve uniform cell distribution, after which, osteogenic media (low glucose DMEM, 10% FBS, 1% penicillin–streptomycin, 10 mM sodium-b-glycerophosphate, 10 mM HEPES, 100 nM dexamethasone and 50 μg/mL ascorbic acid-2-phosphate) was added and cultured for 7 weeks.

2.5. LIVE/DEAD ASSAY

LIVE/DEAD Viability/Citotoxicity kit (Molecular Probes, OR/USA) was used to evaluate cell viability. Live cells (indicated by calcein AM) and dead cells (indicated by ethidium homodimer-1) were observed and imaged through a confocal microscope (Leica, Germany). Optical surfaces were taken from the surface up until 160 μm deep, with 10 μm intervals. All images are presented as vertical projections.

2.6. BIOCHEMICAL CHARACTERIZATION

Constructs were harvested, washed in PBS, cut in half and weighed. For DNA assay, one-half was added to 1 mL of digestion buffer (10 mM Tris, 1 mM EDTA, 0.1% Triton X-100, 0.1 mg/mL proteinase K) and incubated overnight at 56ºC for digestion. After centrifugation at 3000g, during 10 minutes, the supernatants were removed, diluted, pippeted in duplicate into a 96-well plate and 1:1 ratio (v/v) of Picogreen solution (Quant-iT™ PicoGreen ® dsDNA Kit, Invitrogen) was added. Sample fluorescence was measured with fluorescent plate reader at excitation of ~480 nm, emission of ~520 nm. Lambda DNA was used to prepare the standard curve. Based on previous studies [32], 5 pg DNA/cell was used as the conversion factor to determine the cell number. For calcium quantification, one-half of constructs were incubated in 1 mL TCA 5% (trichloroacetic acid 5% v/v) and calcium was extracted by disintegrating the construct using steel balls and MinibeadBeater™ (Biospec, Bartlesville, OK/USA). Calcium content and standard were quantified using StanbioTotal Calcium Liquicolor® (Stanbio Laboratory/USA). Sample optical density was measured at 575 nm using a microplate reader. Alkaline Phosphatase (AP) activity was determined by adding cell lysis solution to one-half of each scaffold, and these were disintegrated using steel balls and MinibeadBeater™. After centrifugation, 50 μL of supernatant were incubated with 50 μL *p*NPP (p-nitrophenyl-phosphate) substrate solution, at 37ºC for 20 min. The reaction was stopped with 50 μL of stop solution, and absorbance was read at 405 nm. p-Nitrophenol at known concentrations was used to prepare the standard curve. All solutions were components of SensoLyte® *p*NPP Alkaline Phosphatase Complete Kit (Cell Biolabs, CBA-302).

2.7. HISTOLOGY AND IMMUNOHISTOCHEMISTRY

After harvest, the samples were fixed in 4% formaldyhyde solution for 1 day. Bone scaffolds were decalcified with immunocal solution (Decal Chemical, Tallman, NY) for 1 day, and further dehydrated with graded ethanol washes, concurrently with remaining silk constructs. Samples were embedded in paraffin, sectioned to 5-μm slices and mounted on glass slides. For staining, sections were deparaffinized with CitriSolv and rehydrated with a graded series of ethanol washes. Samples were stained using standard hematoxylin and eosin. Immunohistochemistry was performed on sections as follows: sections were blocked with normal horse serum (NHS), stained sequentially with primary antibody (rabbit anti-human Osteopontin (OPN) polyclonal antibody, Chemicon ab1870; rabbit anti-bone sialoprotein (BSP) polyclonal antibody, Millipore ab1854; mouse monoclonal to Collagen I, Abcam ab6308; NHS

for negative control), secondary antibody (Vectastain Universal Elite ABC Kit, PK-6200 Vector Laboratories) and developed with biotin-avidin system (DAB substrate kit SK-4100 Vector Laboratories).

2.8. MICROCOMPUTED TOMOGRAPHY (μCT) ANALYSIS

μCT was performed using the protocol described by Liu et al [37]. Samples were aligned in a 2 mL screw-cap centrifuge tube, which was clamped in the specimen holder of a vivaCT40 system (SCANCO Medical AG, Basserdorf, Switzerland). The 2 mm length of the scaffold was scanned at 21 μm isotropic resolution. A global thresholding technique, which only detects mineralized tissue, was applied to obtain the bone volume (BV) of samples.

2.9. SCANNING ELECTRON MICROSCOPY (SEM)

Samples were washed in PBS and then fixed in 2% glutaraldehyde in sodium cacodylate buffer for 2 h. Constructs were washed in buffer and freeze-dried overnight. The samples were coated with gold and palladium and imaged in SEM machine (JEOL, JAPAN).

2.10. MECHANICAL TESTING

Young's modulus upon compression of constructs after culture was determined under unconfined compression in wet conditions using a modification of an established protocol [38]. An initial tare load of 0.2 N was applied and was followed by a stress-relaxation step where specimens were compressed at a ramp velocity of 1% per second up to 10% strain and maintained at the position for 1800 s. The Young's modulus was obtained from the equilibrium forces measured at 10% strain.

2.11. STATISTICAL ANALYSIS

Data are presented as average (n=3) ± standard deviation. Statistical significance was determined using analysis of variance (ANOVA) followed by Tukey's HSD (honestly significant difference) test using Prism software (Prism 4.0c, GraphPad Software Inc.).

3. RESULTS

3.1. CHARACTERIZATION OF UNDIFFERENTIATED HASCS

The immunophenotype of undifferentiated hASCs was evaluated using flow cytometry (Fig. 2A). The antigen expression profile observed was consistent with our previous study [39]: expression of adhesion molecules integrin b1 (CD29) and endoglin (CD105), high expression of ecto 5' nucleotidase (CD73) surface enzyme as well as extracellular matrix proteins such as Thy-1 (CD90) and glycoprotein CD34. Hyaluronate (CD44) receptor molecule was less expressed than expected, however, expression of hematopoietic marker CD45 was accordingly very low. Multilineage potential of hASCs was evaluated by cultivation of cell monolayers in adipogenic or osteogenic medium. The isolated hASCs exhibited multi lineage differentiation as shown with formation of Oil Red O staining lipid droplets (Fig. 2C) and Alizarin Red staining extracellular mineralization (Fig. 2D).

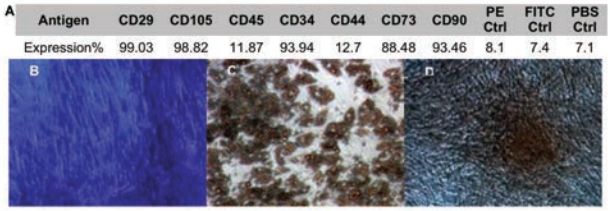

Figure 2. Phenotypic characterization and evaluation of multipotency of human adipose stem cells. A) Percentage of antigen expression in primary hASCs, B) Toluidine blue staining of undifferentiated stromal cells, C) Oil red O staining for adipogenesis, D) Alizarin red staining for osteogenesis.

3.2. CELL VIABILITY AND PROLIFERATION

Cell seeding efficiency, calculated as a fraction of the initial cells detected in the scaffold after seeding, ranged from 60 to 75% in all five groups, without statistically significant differences (Fig. 3A). DNA assay (Fig. 3B) demonstrated that, after two weeks of culture, proliferation occurred to the same extent (approximately 1.6-fold increase in cell numbers) in all spherical porous silk sponges, either aqueous or HFIP-based (Aq-250, Aq-500, HFIP-400). In contrast, the lamellar structure maintained the initial cell numbers throughout the culture period. In aqueous scaffolds, the cell numbers achieved by week 2 were maintained through week 7. In HFIP scaffold group, the cell number increased continuously. In the decellularized bone group, the cell numbers decreased at the end of culture period. Live/Dead assay confirmed cell viability and attachment throughout all scaffolds (Fig. 3C).

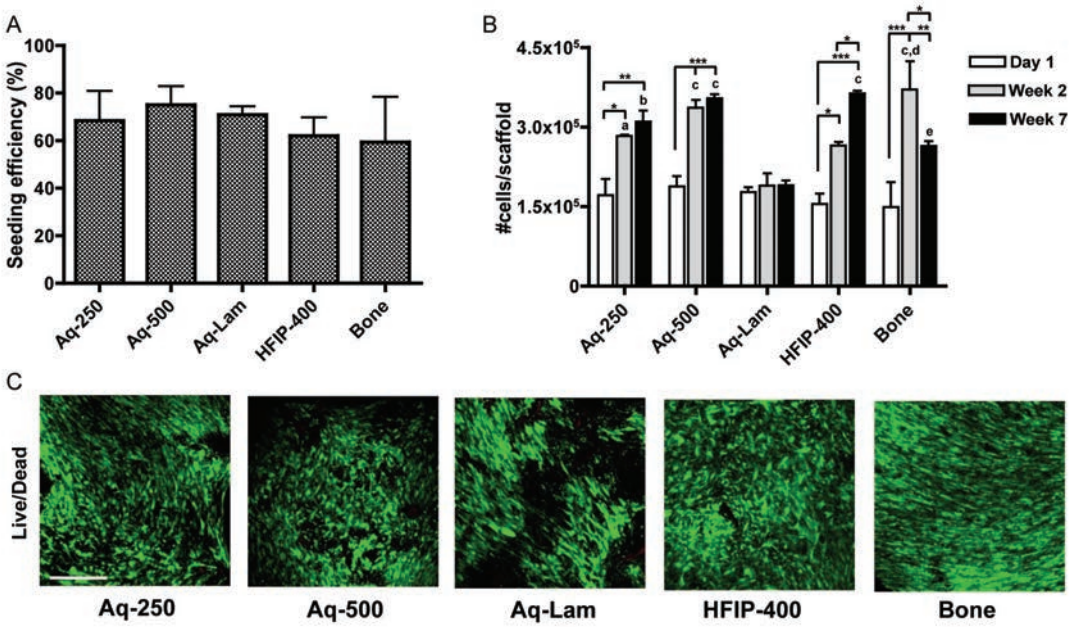

Figure 3. Cell viability and proliferation. A) Cell seeding efficiency. No significant differences were observed between groups. B) Cell proliferation evaluated by changes in the number of cells per scaffold. *p<0.05, **p<0.01, ***p<0.001; a p<0.05, b p<0.01, c p<0.001 to Aq-Lam; d p<0.05 to Aq-250 and HFIP-400; e p<0.05 to Aq-500 and HFIP-400; C) Cell viability (Live/Dead assay) after 7 weeks of culture. Scale bar = 200 μm.

Good distribution of cells at periphery and center of the constructs was observed through H&E staining in all groups (Fig. 4 top). Cells attached to scaffold surfaces, and filled the pore spaces. Rough pore surfaces were observed by H&E staining (Fig. 4 top) and SEM (Fig. 4 middle) in aqueous spherical-pore scaffolds in contrast to smooth pore surfaces in HFIP scaffolds. Matrix density appeared greater in aqueous porous scaffolds (Aq-250 and Aq-500) and the trabecular bone scaffold than in HFIP-derived scaffolds.

3.3. BONE TISSUE DEVELOPMENT

Distribution of bone tissue matrix was evaluated through immunolocalization of bone matrix proteins after 7 weeks of culture in osteogenic media. The expression of osteopontin (OPN), bone sialoprotein (BSP) and collagen type I (Col I) were similar in both small (Aq-250) and large (Aq-500) pore size aqueous silk sponges (Fig. 5). These bone matrix markers were distributed throughout the decellularized bone scaffold. The most robust groups were the aqueous lamellar and HFIP-derived sponges, with high intensity of immunolocalization of OPN and BSP, and somewhat lower intensity of collagen type I.

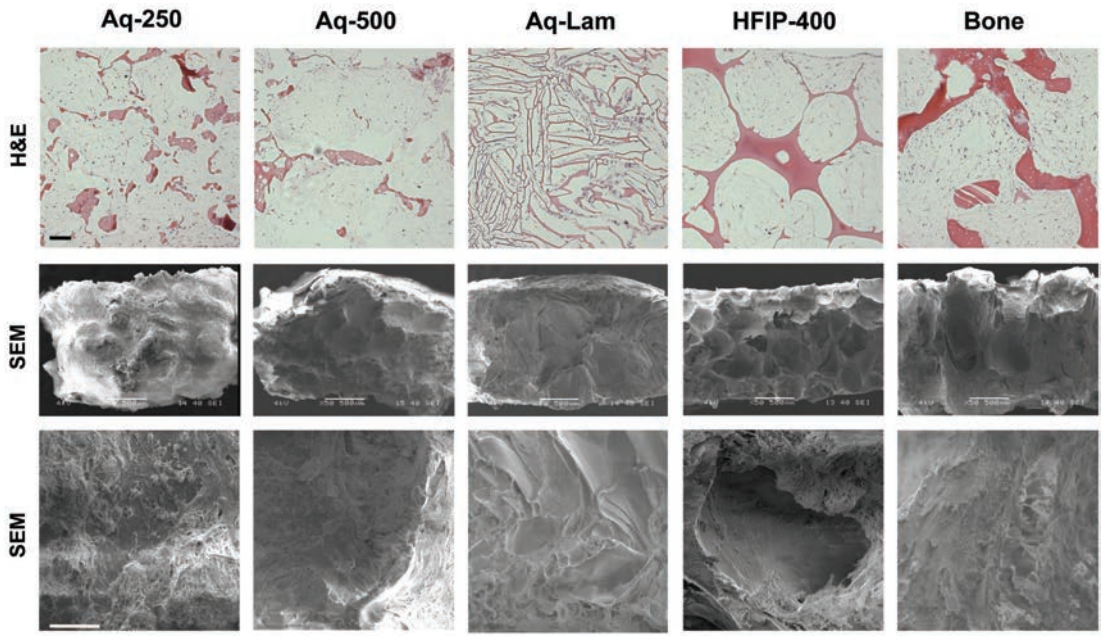

Figure 4. Scaffold structure. Constructs were analyzed after seven weeks of culture. Top row: Hematoxylin & Eosin (H&E) staining, scale bar = 200 μm; Middle row: Scanning electron microscope (SEM) images 50x, scale bar = 500 μm. Bottom row: SEM images 400x, scale bar = 50 μm.

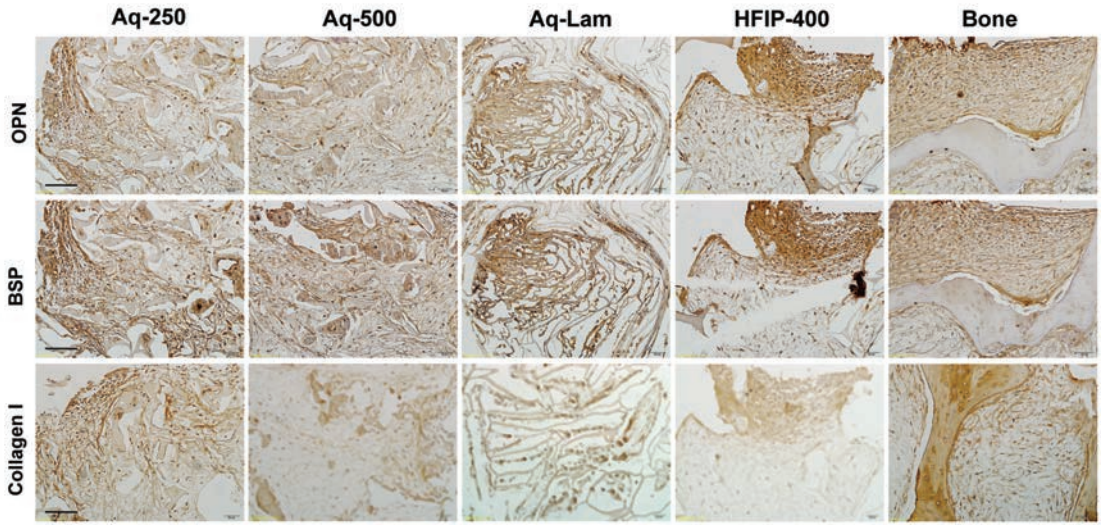

Figure 5. Accumulation of bone matrix proteins in tissue constructs. Data are shown after 7 weeks of culture. Top row: Osteopontin (OPN); Middle row: Bone Sialoprotein (BSP); Bottom row: Collagen type I. Scale bar = 100 μm.

3.4. Quantification of bone differentiation parameters

Alkaline phosphatase (AP) activity, an early marker of osteoblastic phenotype peaked after 2 weeks of culture, as expected, at similar levels in all groups, except for the significantly higher expression in the Aq-Lam group (Fig. 6A). As an indicator of ECM maturation and calcification,

AP activity levels decreased by seven weeks of culture. The calcium deposition increased in parallel to the decrease in AP activity, between weeks 2 and 7, with significantly higher levels in HFIP and decellularized bone scaffolds than in other groups (Fig. 6B). Consistent with the biochemically measured calcium levels, the bone volume (BV) detected by μCT analysis was also higher is HFIP than aqueous scaffolds and the highest in the decellularized bone group (Fig 6C). Although not significantly different, HFIP-derived sponges (HFIP-400) demonstrated increased bone volume relative to aqueous-based groups. The equilibrium modulus of the constructs was also highest for the decellularized bone group, and higher for the HFIP than aqueous porous scaffolds (Fig. 6D). Interestingly, the aqueous-based silk fibroin lamellar structure (Aq-Lam) was 3x stiffer than the corresponding aqueous-based porous silk sponges (Aq-250 and Aq-500) ($p<0.01$). This is evidence of the importance of the scaffold architecture for the resulting mechanical properties of engineered tissue. Furthermore, the mineralized tissue was better distributed in HFIP-400 group (Fig. 6E), where small spherical-like structures were observed, whereas in aqueous groups, mineral deposited less uniformly throughout the construct, forming plate-like structures.

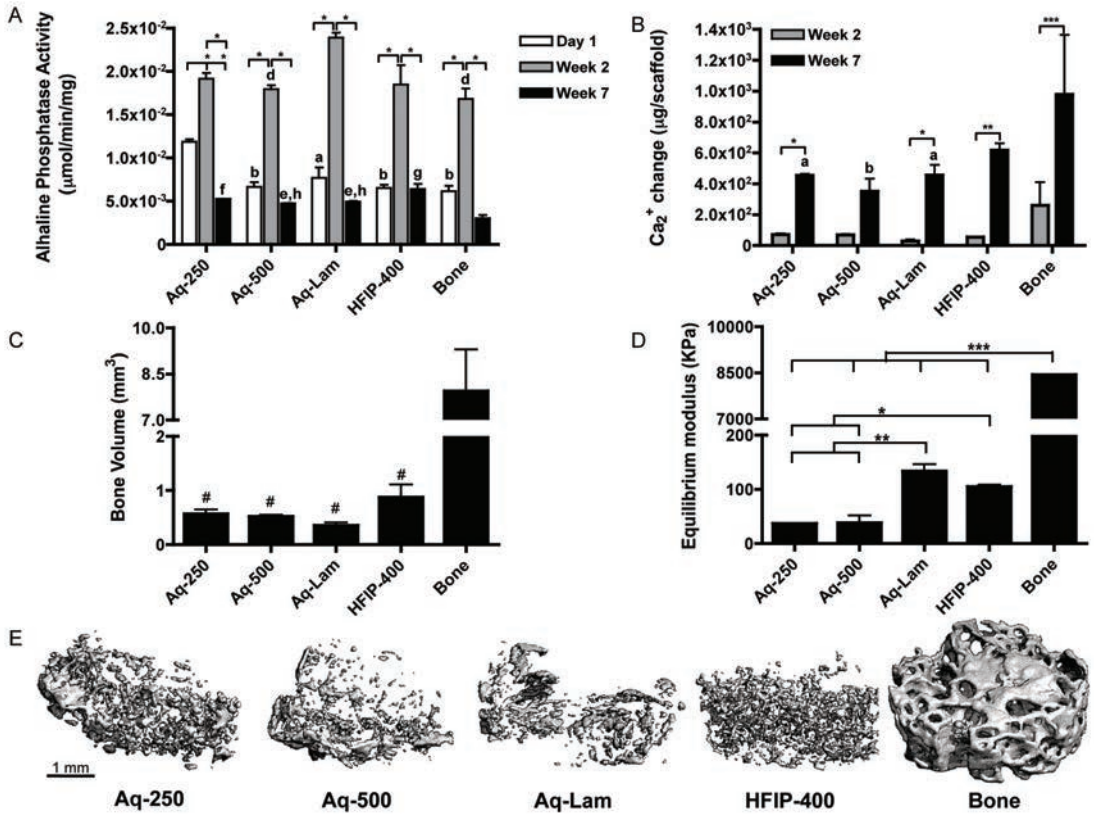

Figure 6. Biochemical and mechanical characterization of constructs. A) Alkaline phosphatase activity *p<0.001; a p<0.05, b p<0.01 to Aq-250; d p<0.05 to Aq-Lam; e p<0.05, f p<0.01, g p<0.001 to

Bone. B) Calcium change from day 1 measured at two and seven weeks of culture, *p<0.05, **p<0.01, ***p<0.001; a p<0.05, b p<0.01 to Bone. C) Bone volume (BV) of constructs at week 7 # p<0.05 to Bone. D) Equilibrium modulus at week 7 *p<0.05, **p<0.01, ***p<0.001. E) μCT reconstruction images of constructs after 5 weeks of culture. Scale bar = 1 mm.

4. DISCUSSION

In this study, we investigated different types of silk-based scaffolds varying in fabricated composition, chemistry, and structure as a potential material of choice for bone tissue engineering applications [19, 26], with focus on hASCs as a cell source. Notably, the hASCs showed expression patterns of surface markers characteristic for mesenchymal stem cell ($CD105^+$, $CD73^+$, $CD90^+$, $CD45^-$, $CD44^-$) (Fig. 2A) consistent with that of the BM-MSCs, which have been successfully used for engineering of bone [40]. The multi-lineage differentiation capability (adipogenic and osteogenic) was also verified and similar to that observed for BM-MSCs (Fig. 2B-D). Our previous studies confirmed the maintenance of high expression of the surface markers for hASC stemness and differentiation capability over several passages [32].

Four different types of silk scaffolds were investigated. Aqueous-based silk fibroin sponges were produced with three distinct pore size and morphology; Aq-250 resembled the pore size of native trabecular bone, Aq-500 was the scaffold successfully used by Kim et al (2005) [19], and Aq-Lam, while scaffold architecture developed by Oliveira et al (2008) [26] resembled the lamellar microstructure of bone. In addition to aqueous-based scaffold, HFIP-400, another silk scaffold, which previously demonstrated rapid bone formation when cultured with BM-MSCs was also studied [21]. The decellularized trabecular bone was used as a “gold standard”. The hASC osteogenic activity and bone formation among different scaffolds were directly compared.

The differences in silk chemistry, composition, pore size, and structure did not affect the hASCs seeding efficiency (Fig.3A) suggesting insignificant effect of silk chemistry and structure on hASCs attachment. After cultivation for 7 weeks, cell number increased in all groups except Aq-Lam (Fig.3B). Based on histology and SEM (Fig.4), the significant structural difference of Aq-Lam was likely the cause, as cells fully occupied the pore spaces.

Over 7 weeks, hASCs differentiated and expressed osteogenic markers in all groups but with different intensity. Bone tissue development for aqueous-based scaffolds, both small and large pore size (Aq-250 and Aq-500), was found to be similar. Pore size did not influence seeding efficiency or cell proliferation. Cell viability, morphology (Fig.3C), and distribution throughout individual pores or entire scaffold were very similar between the two groups (Fig.4 top). Bone

proteins, such as osteopontin, bone sialoprotein and collagen type I, were produced and retained in the form of extracellular matrix in an analogous extent (Fig.5). In addition, pore size did not affect amount of alkaline phosphatase production, calcium deposition and bone volume. Equilibrium moduli of Aq-250 and Aq-500 were also similar. We postulate that while smaller pores promote increased mechanical strength, on the other hand, the larger pores were associated with a more homogenous matrix [25], characteristics that may compensate the compressive capacity. Among all four silk scaffold groups in this study, both Aq-250 and Aq-500 were inferior.

Lamellar aqueous-based silk fibroin scaffolds (Aq-Lam) showed some interesting features. The equilibrium modulus was the highest among all silk scaffold groups which due to the small inter-lamellar distance (25-100μm). Furthermore, the cells of Aq-Lam group expressed the most alkaline phosphatase activity at week 2 of culture (Fig.6A), showing enhancement of osteogenic differentiation. This was confirmed by increased deposition of bone proteins such as OP, BSP and Col I (Fig.5). Calcium deposition and mineralization did not follow the same trend with amounts similar to those observed for Aq-250 and Aq-500 groups (Fig. 6B, 6C). This result may not be surprising as the native lamellar bone is generated more slowly than woven bone and is less mineralized [41].

Out of the four silk scaffold groups, HFIP-derived sponge supported superior hASCs osteogenic induction and bone-like formation. The similarity of cell proliferation and morphology to aqueous-based scaffolds demonstrated that the higher silk concentration and HFIP solvent did not alter the abilities for hASCs to adhere and proliferate. The equilibrium modulus of HFIP-based silk scaffold was superior to aqueous-based constructs with spherical pore, possibly due to the higher concentration of silk material (Fig. 6D). More importantly, HFIP-derived scaffolds enhanced hASCs deposition of matrix proteins (OPN, BSP, Col I) and mineralization, quantified by calcium retention in scaffold and mineralized bone volume (BV). According to microCT image (Fig. 6E), the bone formation was equally distributed throughout the scaffold in this group showing homogenous osteogenic activity of hASCs. The decellularized trabecular bone scaffolds have been used successfully in bone tissue engineering [32, 33, 42]. Although bone-forming structure and mechanical properties of the silk scaffolds were inferior to the trabecular bone scaffold, the osteogenic cellular activities in Aq-250 and Aq-500 groups were similar to bone scaffold and were enhanced in Aq-Lam and HFIP-400 groups (Fig.5 and 6A).

Taken together, data collected in this study are consistent with the conceptual model shown in Fig. 7. Two distinguishable scaffold properties – scaffold architecture and mechanical stiffness – appear to affect bone formation (Fig. 7). First, scaffold stiffness is positively correlated with

osteogenic differentiation of ASCs resulting in an increase in bone ECM secretion (Fig. 7A). The importance of mechanical properties in bone tissue engineering has been well established [19, 43]. Similar to previous findings, HFIP-derived silk fibroin scaffolds, which exhibited higher stiffness as compared to aqueous-based silk fibroin scaffolds, appear to provided a better platform for bone formation. Second, scaffold structure appears to alter cellular activities as well as bone tissue formation. Lamellar porous morphology is postulated to benefit ASC osteogenic differentiation into lamellar bone, which contains fewer cells, but higher mechanical properties once it is highly organized, while a spherical porous structure leads to the development of woven bone, which contains higher cellularity and mineral density but is far less organized [41, 44] (Fig. 7B).

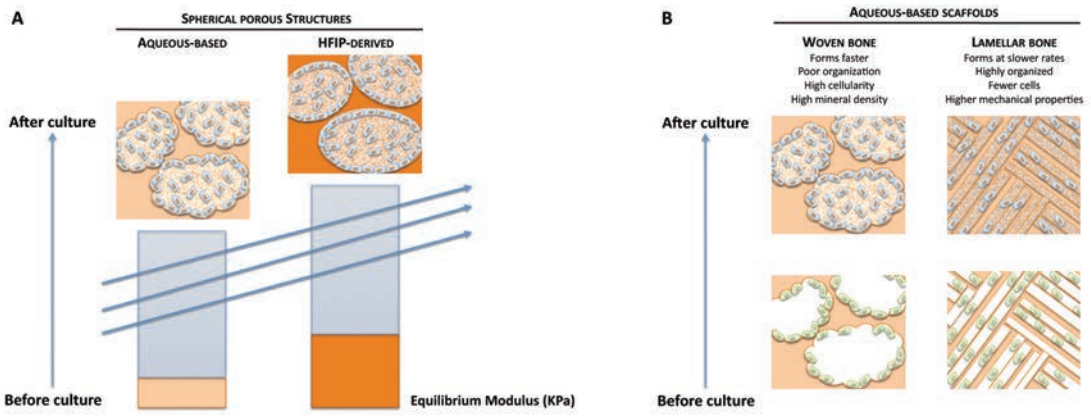

Figure 7. Proposed mechanism of regulation of bone formation by scaffold architecture and stifness. A) Scaffold mechanics. Mechanically stronger HFIP-derived silk scaffolds promote osteogenic differentiation of hASCs to result in increased bone volume (BV), calcium content and bone protein deposition, as compared to aqueous-based scaffolds. B) Scaffold architecture. Sponge like architecture with spherical pores serves as a template for the formation of woven bone, while a lamellar porous architecture serves as a template for the formation of lamellar bone.

5. Conclusion

This study demonstrated the optimization potential of silk scaffolds in terms of structure (porosity, pore dimensions, geometry and alignment) and biomechanics for bone tissue engineering applications. We demonstrated that human adipose derived stem cells (hASCs) interpret the extracellular environment, by responding differently to silk scaffolds' architecture, and producing bone-like extracellular matrix in a manner that appears to depend on structure and stiffness of scaffolds. Based on collected data, we have proposed a conceptual model that

correlates bone tissue formation with architecture and stiffness of silk scaffolds, which emphasizes the importance of appropriate scaffold design when engineering bone.

Acknowledgements

We gratefully acknowledge funding support of this work by the NIH (DE161525 and EB02520 to GVN), and the FCT PhD grant (SFRH/BD/42316/2007 to CC).

References

1. Puppi, D., et al., *Polymeric materials for bone and cartilage repair.* Progress in Polymer Science, 2010. 35(4): p. 403-440.
2. Salgado, A.J., O.P. Coutinho, and R.L. Reis, *Bone tissue engineering: state of the art and future trends.* Macromol Biosci, 2004. 4(8): p. 743-65.
3. Kim, H.J., et al., *Processing windows for forming silk fibroin biomaterials into a 3D porous matrix.* Australian Journal of Chemistry, 2005. 58(10): p. 716-720.
4. Horan, R.L., et al., *In vitro degradation of silk fibroin.* Biomaterials, 2005. 26(17): p. 3385-3393.
5. Saitow, C., D.L. Kaplan, and J.J. Castellot, *Heparin stimulates elastogenesis: Application to silk-based vascular grafts.* Matrix Biology, 2011. 30(5-6): p. 346-355.
6. Bhumiratana, S., et al., *Nucleation and growth of mineralized bone matrix on silk-hydroxyapatite composite scaffolds.* Biomaterials, 2011. 32(11): p. 2812-20.
7. Chao, P.H.G., et al., *Silk hydrogel for cartilage tissue engineering.* Journal of Biomedical Materials Research Part B-Applied Biomaterials, 2010. 95B(1): p. 84-90.
8. Yan, L.P., et al., *Macro/micro Porous Silk Fibroin Scaffolds with Potential for Articular Cartilage and Meniscus Tissue Engineering Applications.* Acta Biomaterialia, 2011. Accepted for publication.
9. Wang, Y.Z., et al., *Stem cell-based tissue engineering with silk biomaterials.* Biomaterials, 2006. 27(36): p. 6064-6082.
10. Murphy, A.R. and D.L. Kaplan, *Biomedical applications of chemically-modified silk fibroin.* Journal of Materials Chemistry, 2009. 19(36): p. 6443-6450.
11. Hofmann, S., et al., *Cartilage-like tissue engineering using silk scaffolds and mesenchymal stem cells.* Tissue Engineering, 2006. 12(10): p. 2729-2738.
12. Wang, Y.Z., et al., *In vitro cartilage tissue engineering with 3D porous aqueous-derived silk scaffolds and mesenchymal stem cells.* Biomaterials, 2005. 26(34): p. 7082-7094.
13. Wang, Y.Z., et al., *Cartilage tissue engineering with silk scaffolds and human articular chondrocytes.* Biomaterials, 2006. 27(25): p. 4434-4442.
14. Mauney, J.R., et al., *Engineering adipose-like tissue in vitro and in vivo utilizing human bone marrow and adipose-derived mesenchymal stem cells with silk fibroin 3D scaffolds.* Biomaterials, 2007. 28(35): p. 5280-5290.
15. Kang, J.H., J.M. Gimble, and D.L. Kaplan, *In Vitro 3D Model for Human Vascularized Adipose Tissue.* Tissue Engineering Part A, 2009. 15(8): p. 2227-2236.
16. Lovett, M., et al., *Tubular silk scaffolds for small diameter vascular grafts.* Organogenesis, 2010. 6(4): p. 217-224.
17. Altman, G.H., et al., *Silk matrix for tissue engineered anterior cruciate ligaments.* Biomaterials, 2002. 23(20): p. 4131-4141.
18. Chen, J.S., et al., *Human bone marrow stromal cell and ligament fibroblast responses on RGD-modified silk fibers.* Journal of Biomedical Materials Research Part A, 2003. 67A(2): p. 559-570.
19. Kim, H.J., et al., *Influence of macroporous protein scaffolds on bone tissue engineering from bone marrow stem cells.* Biomaterials, 2005. 26(21): p. 4442-4452.
20. Meinel, L., et al., *Engineering bone-like tissue in vitro using human bone marrow stem cells and silk scaffolds.* Journal of Biomedical Materials Research Part A, 2004. 71A(1): p. 25-34.
21. Marolt, D., et al., *Bone and cartilage tissue constructs grown using human bone marrow stromal cells, silk scaffolds and rotating bioreactors.* Biomaterials, 2006. 27(36): p. 6138-6149.
22. Vepari, C. and D.L. Kaplan, *Silk as a biomaterial.* Progress in Polymer Science, 2007. 32(8-9): p. 991-1007.
23. Nazarov, R., H.J. Jin, and D.L. Kaplan, *Porous 3-D scaffolds from regenerated silk fibroin.* Biomacromolecules, 2004. 5(3): p. 718-726.
24. Kim, U.J., et al., *Structure and properties of silk hydrogels.* Biomacromolecules, 2004. 5(3): p. 786-792.
25. Kim, U.J., et al., *Three-dimensional aqueous-derived biomaterial scaffolds from silk fibroin.* Biomaterials, 2005. 26(15): p. 2775-2785.

26. Oliveira, A.L., et al., *Designing silk-based 3D architectures with controlled lamellar morphology.* Tissue Engineering Part A, 2008. 14(5): p. 718-719.
27. Park, S.H., et al., *Relationships between degradability of silk scaffolds and osteogenesis.* Biomaterials, 2010. 31(24): p. 6162-6172.
28. Rockwood, D.N., et al., *Ingrowth of human mesenchymal stem cells into porous silk particle reinforced silk composite scaffolds: An in vitro study.* Acta Biomaterialia, 2011. 7(1): p. 144-151.
29. Gimble, J.M., F. Guilak, and B.A. Bunnell, *Clinical and preclinical translation of cell-based therapies using adipose tissue-derived cells.* Stem Cell Res Ther, 2010. 1(2): p. 19.
30. Zuk, P.A., et al., *Multilineage cells from human adipose tissue: implications for cell-based therapies.* Tissue Eng, 2001. 7(2): p. 211-28.
31. Schaffler, A. and C. Buchler, *Concise review: adipose tissue-derived stromal cells--basic and clinical implications for novel cell-based therapies.* Stem Cells, 2007. 25(4): p. 818-27.
32. Frohlich, M., et al., *Bone Grafts Engineered from Human Adipose-Derived Stem Cells in Perfusion Bioreactor Culture.* Tissue Engineering Part A, 2010. 16(1): p. 179-189.
33. Grayson, W.L., et al., *Effects of initial seeding density and fluid perfusion rate on formation of tissue-engineered bone.* Tissue Eng Part A, 2008. 14(11): p. 1809-20.
34. McIntosh, K., et al., *The immunogenicity of human adipose-derived cells: Temporal changes in vitro.* Stem Cells, 2006. 24(5): p. 1246-1253.
35. Mitchell, J.B., et al., *Immunophenotype of human adipose-derived cells: Temporal changes in stromal-associated and stem cell-associated markers.* Stem Cells, 2006. 24(2): p. 376-385.
36. Yu, G., et al., *Yield and characterization of subcutaneous human adipose-derived stem cells by flow cytometric and adipogenic mRNA analyzes.* Cytotherapy, 2010. 12(4): p. 538-46.
37. Liu, X.W.S., et al., *Quantification of the roles of trabecular microarchitecture and trabecular type in determining the elastic modulus of human trabecular bone.* Journal of Bone and Mineral Research, 2006. 21(10): p. 1608-1617.
38. Mauck, R.L., et al., *Functional tissue engineering of articular cartilage through dynamic loading of chondrocyte-seeded agarose gels.* Journal of Biomechanical Engineering-Transactions of the Asme, 2000. 122(3): p. 252-260.
39. Gimble, J.M., A.J. Katz, and B.A. Bunnell, *Adipose-derived stem cells for regenerative medicine.* Circulation Research, 2007. 100(9): p. 1249-1260.
40. Gimble, J.M., et al., *Concise Review: Adipose-Derived Stromal Vascular Fraction Cells and Stem Cells: Let's Not Get Lost in Translation.* Stem Cells, 2011. 29(5): p. 749-754.
41. McKenzie, J.A. and M.J. Silva, *Comparing histological, vascular and molecular responses associated with woven and lamellar bone formation induced by mechanical loading in the rat ulna.* Bone, 2011. 48(2): p. 250-258.
42. Grayson, W.L., et al., *Regenerative Medicine Special Feature: Engineering anatomically shaped human bone grafts.* Proc Natl Acad Sci U S A, 2009.
43. Thomson, R.C., et al., *Polymer Scaffold Processing*, in *Principles of Tissue Engineering*. 2000, Academic Press.
44. Martin, R.B., D.B. Burr, and N.A. Sharkey, *Skeletal tissue mechanics*. 1998: Springer-Verlag New York, Inc.

CHAPTER VI

Sequential application of steady and pulsatile medium perfusion enhanced the formation of engineered bone

---

This chapter is based on the following publication: Correia C, Bhumiratana S, Sousa RA, Reis RL, Vunjak-Novakovic G, 2011, *Sequential application of steady and pulsatile medium perfusion enhanced the formation of engineered bone* - submitted.

Abstract

In native bone, cells experience fluctuating shear forces that are induced by pulsatile interstitial flow associated with habitual loading. We hypothesized that the formation of engineered bone can be augmented by replicating such physiologic stimuli to osteogenic cells cultured in porous scaffolds using bioreactors with medium perfusion. To test this hypothesis, we investigated the effect of fluid flow regime on *in vitro* bone formation by human adipose stem cells (hASCs) cultivated on porous three-dimensional silk fibroin scaffolds. To this end, we varied the sequential relative durations of steady flow (SF) and pulsatile flow (PF) of culture medium applied over a period of 5 weeks, and evaluated their effect on bone tissue formation. Porous silk-fibroin scaffolds (400-600 μm pore size) were seeded with hASCs ($30x10^6$ cells/mL) and cultured in osteogenic medium under four distinct fluid flow regimes: (1) PF for 5 weeks; (2) SF for 1 week, PF for 4 weeks; (3) SF for 2 weeks, PF for 3 weeks; 4) SF for 5 weeks. The PF was applied in 12 hours intervals, with the interstitial velocity fluctuating between 400μm/s and 1200μm/s at a 0.5 Hz frequency for 2h, followed by 10h of SF. In all groups, SF was applied at 400μm/s. The best tissue development was achieved for the sequence of 2 weeks of SF and 3 weeks of PF, as evidenced by gene expression (including the PGE2 mechanotransduction marker), construct compositions, histomorphologies and biomechanical properties. We thus propose that osteogenesis in hASCs and the subsequent bone formation involve a mechanism, which detects and responds to the level and duration of hydrodynamic shear forces.

1. INTRODUCTION

The development and function of native bone largely depends on the balance between the endocrine drive towards bone resorption (by a number of biochemical and hormonal factors), and the mechanically-induced drive towards bone formation [1, 2]. A healthy balance between these two opposing factors is based on the biological mechanotransduction mechanisms, which may include streaming and piezoelectric potentials, damage to the extracellular matrix, and direct transduction of matrix strain [3]. The most widely accepted stimulator of bone cells *in vitro* has been the fluid flow, similar to that generated by loading-induced pressure gradients that stimulate the flow of interstitial fluid through the lacuno-canalicular porosities [4-6].

Beneficial effects of flow on osteogenic differentiation and bone cells have been observed already in cell monolayers [7-9]. The promising results of cell monolayer studies inspired the application of fluid flow in bone tissue engineering, with the aim to improve quality of tissue, and/or reduce the time of culture. Both primary osteoblasts and bone marrow mesenchymal

stem cells, known to have strong osteogenic properties, improved bone-tissue formation when cultured under flow conditions as compared to static culture [10-14]. Human adipose tissue derived stem cells (hASCs) were also used to engineer bone with the application of interstitial fluid flow [15, 16].

In recent years, hASCs have been generating a great deal of interest in the fields of tissue engineering and regenerative medicine. Multiple independent studies have proven their ability to selectively differentiate into chondrogenic, osteogenic and adipose cell lineages [17], and that this differentiation potential was not different from that observed fro the bone-marrow derived mesenchymal stem cells (BM-MSC) [16]. ASCs offer several advantages that make them a promising cell source for bone tissue engineering: adipose tissue is abundant, rapidly accessible, with possibility of repeated accessibility; the isolation process is simple, enzyme-based, and results in high yield of cells per unit tissue volume [16, 17], and - with the increased incidence of obesity, - high volumes of adipose tissue resulting from liposuction procedures may be potentially used for cell based therapies [18].

While fluid flow has been successfully used as stimulator for *in vitro* bone tissue development, the long-term differential effects of steady versus fluctuating shear stress on osteogenesis and bone tissue formation were not investigated. Physiologic shear stresses acting on the cells are generated by flow of interstitial fluid, and are intrinsically dynamic. According to Bacabac et al (2004), the frequency spectra of the forces acting on the human hip reach 1–3 Hz for walking and 8–9 Hz for running cycles [19]. Regarding the effect of shear stress on cell monolayers, Jacobs et al 1998, demonstrated that pulsing flow was a much higher stimulator than oscillating flow [3]. Jaasma et al 2008, using a tissue engineering approach, proved that intermittent flow proved advantageous for mechanically stimulating osteoblasts [20]. Several studies have utilized primary osteoblasts and osteocytes [21, 22], and cell lines [7, 8, 20] to demonstrate advantage of dynamic over steady shear stress. Taken together, these studies suggest that differentiated bone cells are capable of sensing environmental shear stresses [23, 24].

In this context, it is of great interest to investigate the temporal responsiveness of stem cells differentiation to such environments, over periods of time that are relevant to the formation of bone. We hypothesized that the formation of bone by osteogenic hASCs can be augmented by a sequence of steady and fluctuating shear stress that mediate osteogenic differentiation and subsequent assembly of bone matrix. To test this hypothesis, we investigated the application of steady and pulsatile perfusion combinations, with different relative durations of both regimes, and evaluated the effect of these regimes on osteogenic differentiation of hASCs cultivated in silk fibroin scaffolds.

2. MATERIALS AND METHODS

2.1. PREPARATION OF SILK FIBROIN SCAFFOLDS

All chemicals were purchased from Sigma-Aldrich (St. Louis, MO, USA) unless otherwise stated. HFIP-derived silk fibroin scaffolds were prepared as previously described [25]. Silk fibroin from silkworm (*Bombix mori*) cocoons was extracted with 0.02 M sodium carbonate (Na_2CO_3) solution, rinsed in distilled water, dissolved in a 9.3 M lithium bromide (LiBr) solution and dialyzed for 48h against distilled water in benzoylated dialysis tubing (Sigma D7884). Dissolved silk fibroin was centrifuged for 20 min at 9000 rpm (4°C). The resulting solution was determined by weighing the remaining solid after drying, yielding a 6-wt % aqueous silk fibroin solution. Silk fibroin aqueous solution was lyophilized and further dissolved with HFIP (hexafluoro-2-propanol), resulting in a 16-wt % HFIP-derived silk fibroin solution. 4 g of granular NaCl, particle size 500–600 μm, were added to 2 mL of silk fibroin in HFIP. The containers were covered overnight to reduce evaporation of HFIP and to provide sufficient time for homogeneous distribution of the solution. Subsequently the solvent was evaporated at room temperature for 3 days. The matrices were then treated in 90% (v/v) methanol for 30 min, to induce the formation of β-sheet structure, followed by immersion in water for 2 days to remove NaCl. The porous silk scaffolds were then freeze-dried, and cored into cylinder of 4 mm in diameter and 4 mm thick.

2.2. ISOLATION, CHARACTERIZATION AND EXPANSION OF HASCS

hASCs were isolated according to previously established methods [26] from liposuction aspirates of subcutaneous adipose tissue, that were obtained from the Pennington Biomedical Research Center under a protocol approved by the Institutional Research Board. hASC were expanded to the fourth passage (P4) in high-glucose Dulbecco's Modified Eagle's Medium (DMEM) (Gibco 11965) supplemented with 10% fetal bovine serum (FBS) (Gibco 26140), penicillin–streptomycin (1%) (Gibco 15140) and 1 ng/mL basic fibroblast growth factor (bFGF) (Peprotech 100-18B). p0 cells were examined for surface marker expression using flow cytometry. The presence of specific antigens such as CD29, CD105, CD45, CD34, CD44, CD73 and CD90 were analyzed, as previously published [26, 27]. hASCs were tested for their differentiation capacity into the osteogenic, chondrogenic and adipogenic lineages.

2.3. CELL SEEDING OF SILK SCAFFOLDS

Scaffolds were sterilized in 70% (v/v) ethanol overnight, washed in PBS and incubated in culture media prior to seeding. Expanded hASCs at passage 4 were suspended at $30x10^6$ cells/mL. A 40 μL aliquot of cell suspension was pipetted to the top of blot-dried scaffods, pipetted up and down to ensure even distribution of cells. After 15 minutes in the incubator, scaffolds were rotated 180º, and 10 μL of cell-free medium was added to prevent these to dry. This process was repeated four times, to allow uniform cell distribution, after which, osteogenic media (low glucose DMEM, 10% FBS, 1% penicillin–streptomycin, 10 mM sodium-b-glycerophosphate, 10 mM HEPES, 100 nM dexamethasone and 50 μg/mL ascorbic acid-2-phosphate) was added. Scaffolds were then cultured in static conditions (well-plate) for 3 days to allow cell attachment.

2.4. BIOREACTOR CULTIVATION OF TISSUE CONSTRUCTS

Cell-seeded scaffolds were transferred into the perfusion bioreactors using a set-up already described in previous works [10-12, 15]. The perfusion bioreactor system has the dimensions of a 10-cm glass Petri dish, and the glass cover of this dish serves as the removable bioreactor cover. It allows culturing multiple scaffolds (4 to 10 mm in diameter and up to 4 mm high) and imaging capabilities. Scaffolds are placed into six wells arranged in a radial pattern, press-fit in place into a layer of polydimethylsiloxane (PDMS). Each bioreactor enabled simultaneous cultivation and uniform perfusion of the six scaffolds. Culture medium enters the bioreactor through a central port from where it flows to the center of the bioreactor and is evenly distributed into six channels leading to the scaffolds. A multi-channel peristaltic pump (Ismatec, USA) is used to maintain re-circulating flow. The flow rate was determined by the cross-sectional area of the tube as the length of the column of fluid being pumped and the rate of pumping remained constant among groups. Four experimental groups were established by varying the relative durations of steady flow (SF) and pulsatile flow (PF) as follows: S_0P_5: PF for 5 weeks; S_1P_4: SF for 1 week, PF for 4 weeks; S_2P_3: SF for 2 weeks, PF for 3 weeks; S_5P_0: SF for 5 weeks. Pulsatile fluid flow regime was composed of flow velocities following a sinus curve between the amplitudes of 400 μm/s (1.64 mL/min) and 1200 μm/s (4.92 mL/min), at 0.5 Hz frequency for 2h, followed by 10 hrs of SF. In all groups, SF was applied at a flow velocity of 400 μm/s. The experimental design is schematically shown in Fig.1.

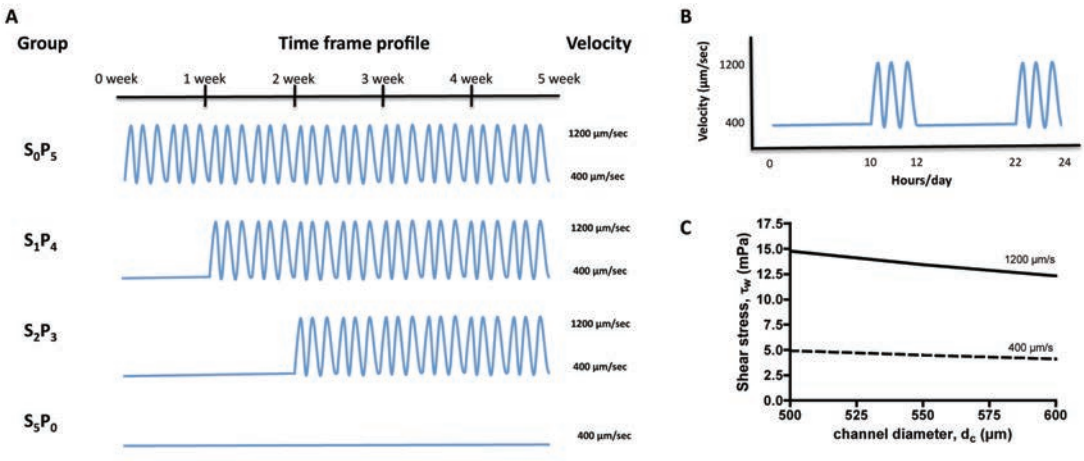

Figure 1. Experimental design. Bone tissue constructs were engineered by cultivation of adipose-derived human mesenchymal stem cells in porous silk fibroin scaffolds with medium perfusion through the forming tissue. A) The following perfusion regimes were applied: S_0P_5 (Pulsatile perfusion for 5 weeks); S_1P_4 (Steady perfusion for 1 week, Pulsatile perfusion for 4 weeks); S_2P_3 (Steady perfusion for 2 weeks, Pulsatile perfusion for 3 weeks); S_5P_0 (Steady perfusion for 5 weeks); B) Pulsatile perfusion profile; C) Estimated maximum and minimum shear stress generated in scaffold pores (500 – 600 µm diameter), at the fluid flow velocities of 400 and 1200 µm/sec.

2.5. LIVE/DEAD ASSAY

LIVE/DEAD Viability/Citotoxicity kit (Molecular Probes, OR/USA) was used to evaluate cell viability. Live cells (indicated by Calcein AM) and dead cells (indicated by Ethidium homodimer-1, EthD-1) were imaged through a confocal microscope (Leica, Germany). Optical sections were made parallel to the external surface in 10 µm intervals up to 160 µm deep, and presented as vertical projections.

2.6. BIOCHEMICAL CHARACTERIZATION

Constructs were harvested at timed intervals, washed in PBS, dry blotted, cut in half and weighed. For DNA assay, one-half was added to 1 mL of digestion buffer (10 mM Tris, 1 mM EDTA, 0.1% Triton X-100, 0.1 mg/mL proteinase K) and incubated overnight at 56ºC for digestion. After centrifugation at 3,000g for 10 minutes, the supernatants were removed, diluted, pipetted in duplicate into a 96-well plate and a 1:1 ratio of Picogreen solution (Quant-iT™ PicoGreen ® dsDNA Kit, Invitrogen, USA) was added. Sample fluorescence was measured with fluorescent plate reader at excitation ~480 nm, and emission ~520 nm. Lambda DNA was used to prepare the standard curve. For calcium quantification, one-half of constructs

were incubated in 1 mL TCA 5% (trichloroacetic acid 5% v/v) and calcium was extracted by disintegrating the construct using steel balls and MinibeadBeater™ (Biospec, Bartlesville, OK/USA). The supernatant were transferred in duplicate into 96-well plate and calcium binding reagent was added at 1:10 ratio (StanbioTotal Calcium Liquicolor®, Stanbio Laboratory/USA). Sample optical density was measured using a microplate reader set to 575 nm. Calcium standard was used to prepare the standard curve.

2.7. Immunohistochemistry

Samples were fixed in 10% formalin for 1 day, embedded in paraffin, sectioned to 5 μm and mounted on glass slides. Sections were deparaffinized with CitriSolv and rehydrated in a graded series of ethanol washes. For immunohistochemistry, sections were blocked with normal horse serum (NHS), stained sequentially with primary antibody (rabbit anti-human Osteopontin - OPN - polyclonal antibody, Chemicon ab1870; rabbit anti-bone sialoprotein - BSP - polyclonal antibody, Millipore ab1854; NHS for negative control), secondary antibody (Vectastain Universal Elite ABC Kit, PK-6200 Vector Laboratories, USA) and developed with biotin-avidin system (DAB substrate kit SK-4100 Vector Laboratories, USA).

2.8. Microcomputed tomography (μCT) analysis

μCT analysis was performed using an established protocol [28]. Samples were aligned in a 2 ml screw-cap centrifuge tube that was clamped in the specimen holder of a vivaCT40 system (SCANCO Medical AG, Basserdorf, Switzerland). 4 mm length of each scaffold was scanned at 21 μm isotropic resolution. A global thresholding technique, which only detects mineralized tissue, was applied to obtain the bone volume (BV) of samples.

2.9. Real-Time RT-PCR

For RNA extraction, one-half of constructs were added to 800 μL of Trizol (Invitrogen 15596-026, USA) and disintegrated by using steel balls and MinibeadBeater™ (Biospec, Bartlesville, OK/USA). Suspensions were centrifuged at 12,000 g for 10 min at 4°C to remove tissue debris and extracted with chloroform (Sigma C2432). Colorless aqueous phase, containing RNA was removed and mixed with equal volume of isopropanol (Sigma I9516). Suspensions were again centrifuged at 12,000 g for 8 min at 4°C, supernatant discarded, and RNA pellet washed with 75% ethanol. Samples were centrifuged at 7,500 g for 5 min at 4°C, supernatant removed,

pellet air-dried, and dissolved with DEPC-water (Applied Biosystems AM 9920). RNA was quantified using Nanodrop® ND-1000. Approximately 1 μg of RNA was reversely transcribed with random hexameres using High Capacity cDNA Reverse Transcription Kit (Applied Biosystems 4368814).

Osteopontin (OPN), bone sialoprotein (BSP), prostaglandin E2 synthase (PGE_2S) and the housekeeping gene glyceraldehyde-3-phosphatedehydrogenase (GAPDH) expression were quantified using a 7500 Fast Real-Time PCR System (Applied Biosystems, USA). Gene expression assay ID, probe and amplicon size and are described on Table I. All TaqMan® Gene Expression Assays were purchased from Applied Biosystems. The expression data were normalized to GAPDH and presented as average values for each group.

Table I. Primers used for qRT-PCR

Gene	GEA ID	Probe	Amplicon
Osteopontn	Hs00167093_m1	FAM	65 bp
Bone Sialoprotein	Hs00173720_m1	FAM	95 bp
Prostaglandin E_2 synthase	Hs00228159_m1	FAM	66 bp
GAPDH	Hs99999905_m1	FAM	122 bp

bp – base pairs; GEA – gene expression assay; GAPDH - Glyceraldehyde 3-phosphate dehydrogenase

2.10. MECHANICAL TESTING

The equilibrium Young's modulus of constructs was determined before and after culturing, under unconfined compression in wet conditions using a modification of an established protocol [29]. An initial tare load of 0.2 N was applied to each sample. Specimens were compressed at a strain rate of 1%/s up to 10% strain and subsequently maintained at this strain for 1800 s. The Young's modulus was obtained from the equilibrium stress measured at 10% strain.

2.11. STATISTICAL ANALYSIS

Data are presented as average ± standard deviation (n=3). Statistical significance was determined using analysis of variance (ANOVA) followed by Tukey's HSD (honestly significant difference) test using Prism software (Prism 4.0c, GraphPad Software Inc., USA).

3. RESULTS

3.1. CELL PROLIFERATION AND VIABILITY

After 5 weeks of dynamic bioreactor cultivation, the amounts of DNA increased over initial values in all groups, reaching levels that were slightly but not significantly different among the experimental groups (Fig. 2 - top). Live/Dead viability assay allowed the observation, by confocal microscopy, of green viable cells which enzymatically converted nonfluorescent cell-permeant calcein AM into the intensely fluorescent calcein, and dead cells identified by bright red fluorescense of EthD-1 bound to nucleic acids of cells with damaged membranes (Fig. 2 - bottom). Viable cells at scaffold surfaces were observed in all experimental groups.

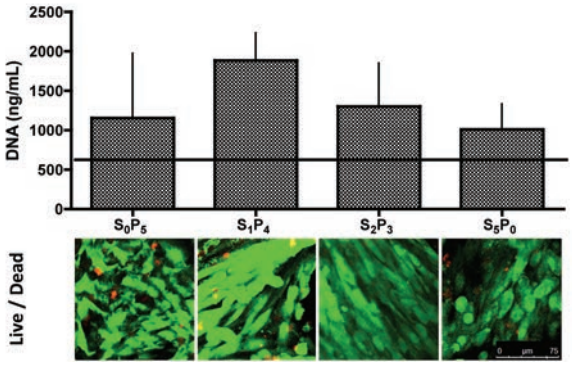

Figure 2. Cell proliferation and viability. Top: Amount of DNA in tissue constructs at the end of the 5-week culture period; the horizontal line indicates day 1 value (n = 3). Bottom: Live/Dead imaging of constructs after 5 weeks of culture. Scale bar = 75 μm.

3.2. BONE TISSUE DEVELOPMENT

Bone extracellular matrix proteins osteopontin (OPN) and bone sialoprotein (BSP) were immunolocalized in cross-sections of constructs harvested after 5 weeks of culture (Fig. 3). OPN deposition was clearly enhanced in all groups subjected to pulsatile fluid flow (PF) in comparison to the experimental group cultured under steady fluid flow (SF). The same trend was observed for the deposition of BSP. Among the three groups subjected to PF, we observed increased bone protein deposition (both OPN and BSP) in S_2P_3 group, where cell-seeded scaffolds were cultured under steady fluid flow (SF) for 2 weeks, before the application of pulsatile fluid flow (PF) during 3 weeks. Constructs cultured under any regimen of PF demonstrated increased deposition and more uniform distribution of mineral throughout the scaffold as compared to constructs cultured exclusively under SF, as evidenced by μCT reconstruction (Fig. 3 – bottom row). Among the three pulsatile regimens, S_2P_3 was the one

that stimulated best mineralization of hASC, as shown by compact mineral deposition detected by µCT.

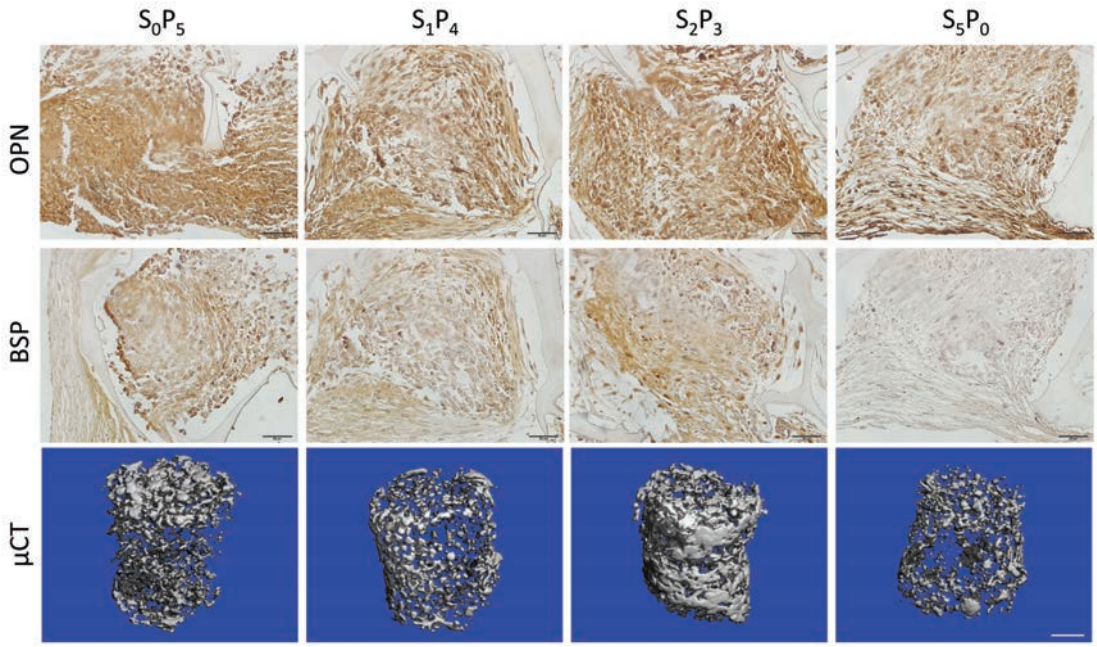

Figure 3. Bone tissue development. Top row: Immunohistochemical localization of osteopontin (OPN); Middle row: Immunohistochemical localization of bone sialoprotein (BSP). Scale bars = 50 µm. Bottom row: µCT reconstruction images of mineralized tissue matrix. Scale bar = 1 mm.

OPN gene expression profiles corroborates measured bone protein deposition (Fig. 4 - top), with highest OPN gene expression quantified for the S_2P_3 group and lowest OPN gene expression for S_5P_0 group. These values were significantly different ($p<0.05$). OPN gene expression (GE) progressively increased with the increase of osteogenic pre-differentiation period before application of pulsatile regimen – OPN GE_{S0P5} < OPN GE_{S1P4} < OPN GE_{S2P3}. BSP gene expression was not different among the groups studied.

Gene expression of prostaglandin E2 synthase (PGE_2S) was also quantified, since prostaglandin E 2 (PGE_2) release is stimulated by shear stress in a dose-dependent manner [30] (Fig. 4 - bottom). This paracrine factor was also highly expressed by hASCs cultured in S_2P_3 pulsatile regimen, and significantly different ($p<0.05$) from the S_5P_0 group, that was not subjected to pulsatile fluid flow during culture. As observed for OPN, PGE_2S GE progressively increased with the increase of osteogenic pre-differentiation period, and before application of a pulsatile regimen: PGE_2S GE_{S0P5} < PGE_2S GE_{S1P4} < PGE_2S GE_{S2P3}.

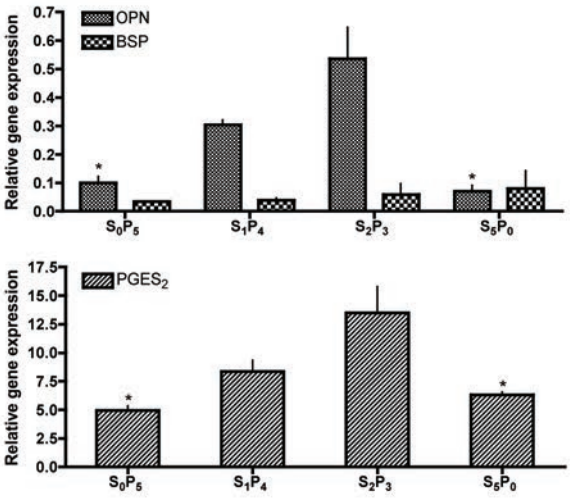

Figure 4. Gene expression after 5 weeks of culture. Top: Osteopontin (OPN) and Bone Sialoprotein (BSP) gene expression normalized to GAPDH (n = 3) * $p<0.05$ relatively to S_2P_3. Bottom: Prostaglandin E 2 synthase ($PGES_2$) gene expression normalized to GAPDH (n = 3) *$p<0.05$ relative to S_2P_3.

Mineralization was assessed through calcium quantification, and bone volume normalized by tissue volume (BV/TV) (Fig. 5). The highest amount of calcium was obtained in the S_2P_3 culturing regimen, again significantly different ($p<0.05$) from S_5P_0 group where the lowest amount was quantified (Fig. 5 - top). BV/TV ratio corroborates calcium data and μCT reconstruction images, where S_2P_3 present the highest ratio, and S_5P_0 the lowest (Fig. 5 - bottom).

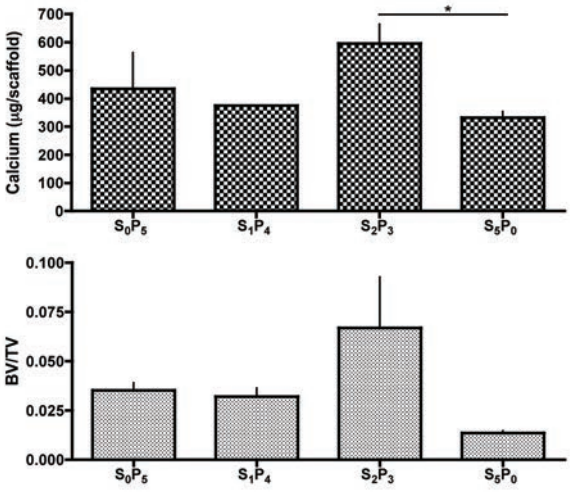

Figure 5. Deposition of mineralized tissue after 5 weeks of culture. Top: Amount of calcium (n = 3), * $p<0.05$. Bottom: Ratio of bone volume (BV) to tissue volume (TV) (n=3).

Mechanical properties of cultured constructs are presented in Fig. 6. After culture, scaffolds became stiffer, although no statistical difference was detected among groups. In average, an increase of equilibrium modulus of 1.8 times at the end of culture.

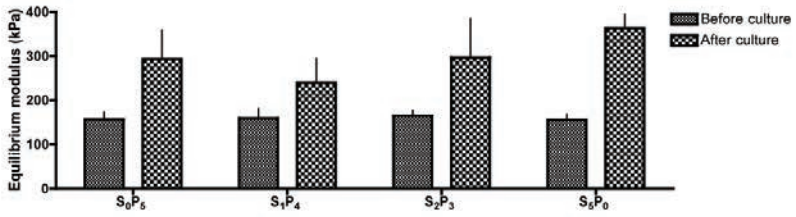

Figure 6. Biomechanical properties of tissue constructs. Equilibrium modulus measured after 5 weeks of culture is compared to the initial value measured for the scaffold.

4. DISCUSSION

Perfusion bioreactors have been used in tissue engineering with the main purpose to improve gas transfer, nutrient supply and waste removal between tri-dimensional constructs and culture medium by reducing diffusional distances [31, 32]. Several studies have explored the use of perfusion to improve osteogenic differentiation and bone tissue formation with primary osteoblasts, bone marrow mesenchymal stem cells [11-14], and human adipose stem cells [15]. In the present work, we aimed to augment bone tissue formation by hASC osteogenic differentiation, in porous silk scaffolds, under a sequence of steady and pulsatile flows. We also aimed to understand the importance of osteogenic pre-differentiation of hASC in the achievement of this goal. Our aim was accomplished, as all pulsatile flow regimes improved bone tissue development over steady flow, and the best tissue was obtained for 2 weeks of osteogenic pre-differentiation preceding pulsatile regime.

In native bone, the cells experience dynamic mechanical shear force[4, 33] due to the flow of interstitial fluid resulting from physical movement [9, 34, 35]. Ideally, bone tissue engineering should mimic such physiologic environment in which medium flow is dynamic and, hence, shear stress is variable. Previous studies demonstrated the positive effect of static shear force on osteogenic differentiation and tissue engineered bone formation[10-12, 15]; however, the physiologic shear force is not static[23, 35]. We hypothesized that osteogenic cells do not only respond to shear force but also to time and dynamic range of shear force application. In this study, we explored the dynamic flow paradigm by applying a sequence of steady and pulsatile

fluid flows, SF and PF respectively, to human adipose stem cells (hASCs) in silk fibroin scaffolds, in the context of bone tissue engineering.

In order to estimate the hydrodynamic shear stress acting at cells within scaffolds, we have modeled the interconnected pore network of scaffolds as a bundle of parallel, cylindrical channels with an average diameter of 550 μm. In this model, we have considered a sufficient number of channels that assures a porosity of 90%, as in one of our previous studies[12]. According to our estimates, the calculated shear stress within tissue constructs ranged from to 4.48 mPa (0.045 dyn/cm^2) to 13.44 mPa (0.134 dyn/cm^2) at flow velocities of 400 μm/s to 1200 μm/s, respectively. According to the theoretical model proposed by Weinbaum et al (1994), the magnitude of the fluid induced shear stresses *in vivo* is in the range of 8 - 30 dyn/cm^2. In our study, we did not reach these high levels of shear stress associated with the mature bone, but instead attempted to mimic the in vivo pulsatile profile for developing bone. To this end, we varied shear stress at a lower level, with a three-fold difference between the minimum and maximum shear stress levels (0.045 - 0.134 dyn/cm^2) (Fig.1). In terms of frequency, we have used a regimen (0.5 Hz) that resembles the dynamic force spectra applied to the human hip during slow walking [19].

As one of the drawbacks in perfusion culturing is the possibility of cell "wash out" from the scaffold, we assessed cell viability and proliferation and observed viable cells attached to the scaffold surface for all studied groups, as well as an increase in cell numbers at the end of culture (Fig.2). No significant differences were detected between groups, suggesting that proliferation occurred to a similar extent despite differences in fluid flow regimen.

The constructs subjected to pulsatile fluid flow during 5 weeks demonstrated superior bone development in terms of bone protein deposition (Fig.3 – top and middle row) and gene expression (Fig.4 - top) of both osteopontin (OPN) and bone sialoprotein (BSP). Notably, OPN is a mechanosensitive gene, encoding the extracellular bone matrix protein osteopontin, which has been used to asses bone cell mechanoresponsiveness[36-38]. Bone sialoprotein mRNA expression has also been used to prove bone formation induced by mechanical signals[39]. Increased expression of PGE_2S (Fig.4 - bottom), corroborate the hASCs response to dynamic mechanical stimulation, once PGE_2 is one of the most important markers of mechanically induced bone formation [7, 20, 40]. In addition to gene expression and protein deposition, constructs cultured under dynamic shear stress (PF) increased mineralization as compared to constructs cultured under steady flow (SF) (Fig.3 – bottom row; Fig.5). Therefore, the pulsatile fluid flow culture improves human adipose stem cells (hASCs) osteogenic

differentiation and tissue engineered bone formation in contrast to conventional steady fluid flow.

Furthermore, we determined the temporal development of the sensing mechanism for the exerted pulsatile forces in hASCs osteogenic differentiation. It was previously suggested that communicating osteocytes are the bone cells responsible for sensing small strains in the calcified matrix components of bone, through their osteocytic processes and not through the cell body [23, 24]. Human adipose stem cells lack these processes, which may lead to failure to response to mechanical stimuli. Therefore, we assumed that hASC should be first differentiated into the osteogenic lineage in order to be capable to sense the pulsatile fluid flow applied by dynamic culture of hASCs seeded silk scaffolds. Therefore, cells were cultured in osteogenic medium, first under steady fluid flow and then under pulsatile fluid flow for the remaining culture period (starting at 0, 1, 2 weeks, or maintaining SF throughout the culture). The best bone tissue development was achieved for hASC pre-differentiated for 2 weeks under SF, and only then subjected to the PF regime. Under these conditions, highest increases in bone protein deposition (both osteopontin and bone sialoprotein) and the corresponding gene expression, calcification and bone volume were detected.

Mechanical loading is known to induce expression of prostaglandin E_2 (PGE_2), an important early stage bone formation marker [40, 41]. Thus, we looked into gene expression of PGE_2 synthase to assess if this marker would be differently expressed as response to changes in shear force. Interestingly, we have observed the following progression of PGE_2 synthase and osteogenic differentiation: $S_0P_5 < S_1P_4 < S_2P_3$. These data are in support of our hypothesis that there is a temporal development of the sensing mechanism to the exerted shear stresses upon hASC differentiation, which makes cells to sense differently steady and pulsatile flow and hydrodynamic shear. Therefore, the mechanisms and key factors involved in mechanotransduction are interesting targets for modulating osteogenic differentiation of hASCs under dynamic shear stress.

5. CONCLUSION

A bone tissue engineering model consisting of human adipose stem cells cultured in porous silk fibroin scaffolds in a bioreactor with perfusion (interstitial flow) of culture medium was used to investigate the effects of pulsatile vs steady medium flow. Our hypothesis was that a sequence of steady flow followed by pulsatile flow will be optimal for supporting bone development, first by stimulating osteogenic cell differentiation and, second, by promoting

expression of bone tissue matrix. Pulsatile flow ranging from 400 μm/s to 1200 μm/s, at 0.5 Hz, associated with fluctuating shear stresses (0.045 – 0.134 dyn/cm^2) improved bone formation in comparison to steady flow at 400 μm/s. Furthermore, cell response to pulsatile fluid flow was progressively enhanced with the increase of steady flow culturing time, being maximum for 2 weeks of culture. These data are consistent with the notion that osteogenic hASCs gradually developed a mechanism to detect and respond to changes in shear stress.

Acknowledgements

We gratefully acknowledge funding support of this work by the NIH (DE161525 and EB02520 to GVN), and the FCT PhD grant (SFRH/BD/42316/2007 to CC).

References

1. Martin, A.D. and R.G. McCulloch, *Bone dynamics: Stress, strain and fracture.* Journal of Sports Sciences, 1987. 5(2): p. 155-163.
2. Jones, H.H., et al., *Humeral Hypertrophy in Response to Exercise.* Journal of Bone and Joint Surgery-American Volume, 1977. 59(2): p. 204-208.
3. Jacobs, C.R., et al., *Differential effect of steady versus oscillating flow on bone cells.* Journal of Biomechanics, 1998. 31(11): p. 969-976.
4. Burger, E.H. and J. Klein-Nulend, *Mechanotransduction in bone--role of the lacuno-canalicular network.* FASEB J, 1999. 13 SuppI: p. S101-12.
5. Hung, C.T., et al., *Real-Time Calcium Response of Cultured Bone-Cells to Fluid-Flow.* Clinical Orthopaedics and Related Research, 1995(313): p. 256-269.
6. Reich, K.M. and J.A. Frangos, *Effect of Flow on Prostaglandin-E2 and Inositol Trisphosphate Levels in Osteoblasts.* American Journal of Physiology, 1991. 261(3): p. C428-C432.
7. Donahue, T.L.H., et al., *Mechanosensitivity of bone cells to oscillating fluid flow induced shear stress may be modulated by chemotransport.* Journal of Biomechanics, 2003. 36(9): p. 1363-1371.
8. Santos, A., et al., *Pulsating fluid flow modulates gene expression of proteins involved in Wnt signaling pathways in osteocytes.* J Orthop Res, 2009. 27(10): p. 1280-7.
9. Knippenberg, M., et al., *Adipose tissue-derived mesenchymal stem cells acquire bone cell-like responsiveness to fluid shear stress on osteogenic stimulation.* Tissue Engineering, 2005. 11(11-12): p. 1780-1788.
10. Grayson, W.L., et al., *Optimizing the Medium Perfusion Rate in Bone Tissue Engineering Bioreactors.* Biotechnology and Bioengineering, 2011. 108(5): p. 1159-1170.
11. Grayson, W.L., et al., *Effects of initial seeding density and fluid perfusion rate on formation of tissue-engineered bone.* Tissue Eng Part A, 2008. 14(11): p. 1809-20.
12. Bhumiratana, S., et al., *Nucleation and growth of mineralized bone matrix on silk-hydroxyapatite composite scaffolds.* Biomaterials, 2011. 32(11): p. 2812-20.
13. Gomes, M.E., et al., *Influence of the porosity of starch-based fiber mesh scaffolds on the proliferation and osteogenic differentiation of bone marrow stromal cells cultured in a flow perfusion bioreactor.* Tissue Eng, 2006. 12(4): p. 801-9.
14. Martins, A.M., et al., *Combination of enzymes and flow perfusion conditions improves osteogenic differentiation of bone marrow stromal cells cultured upon starch/poly(epsilon-caprolactone) fiber meshes.* J Biomed Mater Res A, 2010. 94(4): p. 1061-9.
15. Frohlich, M., et al., *Bone Grafts Engineered from Human Adipose-Derived Stem Cells in Perfusion Bioreactor Culture.* Tissue Engineering Part A, 2010. 16(1): p. 179-189.
16. Scherberich, A., et al., *Three-dimensional perfusion culture of human adipose tissue-derived endothelial and osteoblastic progenitors generates osteogenic constructs with intrinsic vascularization capacity.* Stem Cells, 2007. 25(7): p. 1823-1829.
17. Gimble, J.M.B., B. A. , *Adipose-derived stem cells: Methods and protocols*. Methods in Molecular Biology, ed. J.M. Walker. Vol. 702. 2011, LLC: Springer Science+Business Media.
18. Gimble, J.M., A.J. Katz, and B.A. Bunnell, *Adipose-derived stem cells for regenerative medicine.* Circulation Research, 2007. 100(9): p. 1249-1260.
19. Bacabac, R.G., et al., *Nitric oxide production by bone cells is fluid shear stress rate dependent.* Biochemical and Biophysical Research Communications, 2004. 315(4): p. 823-829.
20. O'Brien, F.J. and M.J. Jaasma, *Mechanical stimulation of osteoblasts using steady and dynamic fluid flow.* Tissue Engineering Part A, 2008. 14(7): p. 1213-1223.
21. Sikavitsas, V.I., et al., *Mineralized matrix deposition by marrow stromal osteoblasts in 3D perfusion culture increases with increasing fluid shear forces.* Proceedings of the National Academy of Sciences of the United States of America, 2003. 100(25): p. 14683-14688.
22. Bancroft, G.N., et al., *Fluid flow increases mineralized matrix deposition in 3D perfusion culture of marrow stromal osteoblasts in a dose-dependent manner.* Proc Natl Acad Sci U S A, 2002. 99(20): p. 12600-5.

23. Weinbaum, S., S.C. Cowin, and Y. Zeng, *A Model for the Excitation of Osteocytes by Mechanical Loading-Induced Bone Fluid Shear Stresses.* Journal of Biomechanics, 1994. 27(3): p. 339-360.
24. Anderson, E.J., et al., *Nano-microscale models of periosteocytic flow show differences in stresses imparted to cell body and processes.* Annals of Biomedical Engineering, 2005. 33(1): p. 52-62.
25. Kim, U.J., et al., *Three-dimensional aqueous-derived biomaterial scaffolds from silk fibroin.* Biomaterials, 2005. 26(15): p. 2775-2785.
26. McIntosh, K., et al., *The immunogenicity of human adipose-derived cells: Temporal changes in vitro.* Stem Cells, 2006. 24(5): p. 1246-1253.
27. Mitchell, J.B., et al., *Immunophenotype of human adipose-derived cells: Temporal changes in stromal-associated and stem cell-associated markers.* Stem Cells, 2006. 24(2): p. 376-385.
28. Liu, X.W.S., et al., *Quantification of the roles of trabecular microarchitecture and trabecular type in determining the elastic modulus of human trabecular bone.* Journal of Bone and Mineral Research, 2006. 21(10): p. 1608-1617.
29. Mauck, R.L., et al., *Functional tissue engineering of articular cartilage through dynamic loading of chondrocyte-seeded agarose gels.* Journal of Biomechanical Engineering-Transactions of the Asme, 2000. 122(3): p. 252-260.
30. Reich, K.M. and J.A. Frangos, *Effect of Flow on Prostaglandin-E2 and Inositol Trisphosphate Levels in Osteoblasts.* Am J Physiol Cell Physiol, 1991. 261(3): p. C428-C432.
31. Coletti, F., S. Macchietto, and N. Elvassore, *Mathematical modeling of three-dimensional cell cultures in perfusion bioreactors.* Industrial & Engineering Chemistry Research, 2006. 45(24): p. 8158-8169.
32. Martin, I., D. Wendt, and M. Heberer, *The role of bioreactors in tissue engineering.* Trends in Biotechnology, 2004. 22(2): p. 80-86.
33. Klein-Nulend, J., et al., *Sensitivity of osteocytes to biomechanical stress in vitro.* FASEB J, 1995. 9(5): p. 441-5.
34. Piekarski, K. and M. Munro, *Transport mechanism operating between blood supply and osteocytes in long bones.* Nature, 1977. 269(5623): p. 80-2.
35. Knothe Tate, M.L. and U. Knothe, *An ex vivo model to study transport processes and fluid flow in loaded bone.* Journal of Biomechanics, 2000. 33(2): p. 247-54.
36. Klein-Nulend, J., et al., *Mechanical stimulation of osteopontin mRNA expression and synthesis in bone cell cultures.* J Cell Physiol, 1997. 170(2): p. 174-81.
37. Mullender, M., et al., *Mechanotransduction of bone cells in vitro: mechanobiology of bone tissue.* Med Biol Eng Comput, 2004. 42(1): p. 14-21.
38. Toma, C.D., et al., *Signal transduction of mechanical stimuli is dependent on microfilament integrity: identification of osteopontin as a mechanically induced gene in osteoblasts.* J Bone Miner Res, 1997. 12(10): p. 1626-36.
39. Tong, L., et al., *Focal adhesion kinase expression during mandibular distraction osteogenesis: evidence for mechanotransduction.* Plast Reconstr Surg, 2003. 111(1): p. 211-22; discussion 223-4.
40. Nauman, E.A., et al., *Osteoblasts respond to pulsatile fluid flow with shortterm increases in PGE(2) but no change in mineralization.* Journal of Applied Physiology, 2001. 90(5): p. 1849-1854.
41. Murakami, M., et al., *Regulation of prostaglandin E-2 biosynthesis by inducible membrane-associated prostaglandin E-2 synthase that acts in concert with cyclooxygenase-2.* Journal of Biological Chemistry, 2000. 275(42): p. 32783-32792.

Section 5.

CHAPTER VII

Human adipose stem cells can serve as a single cell source for the in vitro cultivation of vascularized bone grafts

---

This chapter is based on the following publication: Correia C, Grayson WL, Eton R, Gimble JM, Sousa RA, Reis RL, Vunjak-Novakovic G, 2011, *Human adipose derived cells can serve as a single cell source for the in vitro cultivation of vascularized bone grafts,* Journal of Tissue Engineering and Regenerative Medicine – in press.

Abstract

Orthopedic surgery often requires bone grafts to correct large defects resulting from congenital defects, surgery or trauma. Great improvements have been made in tissue engineering of bone grafts. However, these grafts lack the vascularized component that is critical for their survival and function. From a clinical perspective, it would be ideal to engineer vascularized bone grafts starting from one single cell harvest obtained from the patient. To this end, we explored the potential of human adipose derived mesenchymal stem cells (hASC) as a single cell source for osteogenic and endothelial differentiation and the assembly of bone and vascular compartments within the same scaffold. hASC were encapsulated in fibrin hydrogel as a angioinductive material for vascular formation, combined with a porous silk fibroin sponge to support osteogenesis, and subjected to sequential application of growth factors. Three strategies were evaluated by changing spatio-temporal cues: 1) induction of osteogenesis prior to vasculogenesis, 2) induction of vasculogenesis prior to osteogenesis, or 3) simultaneous induction of osteogenesis and vasculogenesis. By 5 weeks of culture, bone development was evidenced by the deposition of bone matrix proteins, alkaline phosphatase activity and calcium deposition, along with the formation of vascular networks evidenced by endothelial cell surface markers, such as CD31 and von Willebrand factor, and morphometric analysis. Most robust development of the two tissue compartments was achieved by sequential induction of osteogenesis followed by the induction of vasculogenesis. Taken together, the collected data strongly support the utility of hASC as a single cell source for the formation of vascularized bone tissue.

1. INTRODUCTION

Bone vascularization has been a major hurdle for engineering viable and functional bone grafts. Several approaches have been proposed to reach this goal. The co-operation of endothelial cells (either EPCs - endothelial progenitor cells or HUVECs - human umbilical cord endothelial cells) and osteoblasts / osteo-progenitors have been the most studied [1-4]. Previous work of our own group [5], where HUVECs and hMSCs (human bone marrow mesenchymal stem cells) were co-cultured in decellularized bone scaffolds has demonstrated that vascular development was increased when vasculogenesis is induced prior to osteogenesis, and that the addition of fresh hMSCs (human bone marrow mesenchymal stem cells) at the osteogenic induction stage improved both tissue outcomes. The *in vitro* developed networks successfully anastomosed with the host vessels when implanted sub-cutaneously in

nude mice. In an alternate *in vivo* approach, Tsigkou *et al*. 2010 used a mouse model to develop a two-stage protocol for generating vascularized bone grafts using HUVECs and hMSC. Endothelial cells formed networks throughout the bone scaffold 4-7 days after implantation, which anastomosed with nude mice vasculature after 11 days. Vasculature was mature upon 4 weeks, at which time evidence of mineral deposition was also revealed [2]. Koob and co-workers 2011, also developed a completely *in vivo* approach, where HUVECs formed complex three-dimensional networks of perfused human neovessels in critical-sized calvarial defects in SCID mice. However, this neovasculature did not seem to improve MSC-triggered bone regeneration [4].

All these approaches combined osteogenic and vasculogenic cells from different sources, which limits their clinical utility. An ideal tissue engineering solution would use a complete autologous procedure (minimizing host rejection), and one single cell source (reducing therapy complexity and patient discomfort caused by multiple biopsy procedures) for the development of both independent structures – bone and vasculature.

In the present study, we propose the use of human adipose derived stem cells (hASC) as single cell source to generate both the bone tissue matrix and the associated vascular network. Adipose tissue represents an attractive cell source for tissue engineering for several reasons. These cells can be used in an autologous fashion, as tissue is harvested from the patient at a dedicated or non-dedicated liposuction surgery. Adipose tissue can be obtained repeatedly in large quantities under local anesthesia and with a minimum of patient discomfort. Additionally, the simple enzyme-based isolation procedure results in very high cell yield, ~404 000 cells/mL of lipoaspirate [6]. Moreover, hASC are fairly well characterized, including their intrinsic potential to differentiate into osteogenic lineages – and thereby develop bone tissue [7-9] – and endothelial lineages, to form capillaries [10-16].

Herein, we hypothesize that a sequential application of osteogenic and endothelial growth factors to hASC cultured on biomaterial scaffolds, with different timing of addition of fresh cells can support the development of bone-like tissue containing an integrated vascular network. The experiments were performed by culturing hASC in porous silk fibroin scaffolds designed for bone tissue development in combination with fibrin-encapsulated hASC, to provide an environment conducive to the formation of capillary-like networks.

2. MATERIALS AND METHODS

2.1. PREPARATION OF SILK FIBROIN SCAFFOLDS

Silk fibroin from silkworm (*Bombix mori*) cocoons was extracted with 0.02 M sodium carbonate (Na_2CO_3) solution, rinsed in distilled water, dissolved in a 9.3 M lithium bromide (LiBr) solution and dialyzed for 48h against distilled water in benzoylated dialysis tubing (Sigma D7884). Dissolved silk fibroin was centrifuged for 20 min at 9000 rpm (4°C). The resulting solution was determined by weighing the remaining solid after drying, yielding a 6-wt % aqueous silk fibroin solution. HFIP-derived silk fibroin scaffolds were prepared as previously described [17]. Silk fibroin aqueous solution was lyophilized and further dissolved with HFIP (hexafluoro-2-propanol), resulting in a 17-wt % HFIP-derived silk fibroin solution. 4 g of granular NaCl, particle size 400–600 μm, were added to 2 mL of silk fibroin in HFIP. The containers were covered overnight to reduce evaporation of HFIP and to provide sufficient time for homogeneous distribution of the solution. Subsequently the solvent was evaporated at RT for 3 days. The matrices were then treated in 90% (v/v) methanol for 30 min, to induce the formation of the β-sheet structure, followed by immersion in water for 2 days to remove the NaCl. The porous silk scaffolds were then freeze-dried.

2.2. ISOLATION, CHARACTERIZATION AND EXPANSION OF HASC

hASC were isolated according to previously described methods [18] from liposuction aspirates of subcutaneous adipose tissue, at the Pennington Biomedical Research Center under protocols approved by the Institutional Review Board with informed patient consent. hASC were expanded to the third passage in high-glucose Dulbecco's modified Eagle's medium (DMEM) (GIBCO 11965) supplemented with 10% fetal bovine serum (FBS) (GIBCO 26140), penicillin–streptomycin (1%) (GIBCO 15140) and 1 ng/mL basic fibroblast growth factor (bFGF) (Peprotech 100-18B). Passage 0 (P0) cells were examined for surface marker expression using flow cytometry. The presence of specific antigens such as CD29, CD105, CD45, CD34, CD44, CD73 and CD90 were analyzed, and reproducibility of cells was confirmed from various donors [14, 18]. hASC were confirmed for their differentiation capacity into the adipogenic and osteogenic lineages in monolayer cultures following induction with adipogenic and osteogenic inductive medium for up to 14 days and histochemical analysis of neutral lipid (Oil Red O) or mineralization (Alizarin Red) staining as published [19].

2.3. CELL ENCAPSULATION AND SCAFFOLD SEEDING

Silk scaffolds were cut into 2mm thick, 4mm diameter cylinders, sterilized in 70% (v/v) ethanol overnight, washed in PBS and incubated in culture media prior to seeding, as in our previous studies [20]. Expanded hASC were suspended at $20x10^6$ cells/mL and seeded into silk scaffolds according to a well-established procedure [9, 21, 22]: 20 μL aliquot of cell suspension was pipetted to the top of blot-dried scaffods, pipetted up and down to ensure even distribution of cells. After 15 minutes in the incubator, scaffolds were rotated 180º, and 10 μL of cell-free medium was added to prevent drying. This process was repeated four times to allow uniform cell distribution, after which, constructs were incubated overnight to allow cell attachment (Fig.1). hASC attached to silk fibroin scaffolds were intended for bone formation. At day 1, fibrinogen (Sigma F8630) was prepared at a concentration of 5 mg/mL and thrombin (Sigma T6200-1KU) was used at 10 Units/mL. Fibrin has been extensively used to create vascularized tissue constructs (bone, adipose tissue, skin, cardiovascular tissue) due to its excellent pro-angiogenic properties [23]. Moreover, in a skin regeneration context, fibrin has proven to control ASC differentiation toward vascular cell types [24]. In our study, expanded hASC intended to form vasculature networks within the engineered bone tissue, were encapsulated in fibrin at a density of $20x10^6$ cells/mL. Thrombin was added to cross-link the gel, giving a final fibrin concentration of 4 mg/mL. Before cross-linking occurred, 20 μl of cell/gel suspension was pipetted into blot-dried scaffolds to allow uniform cell seeding throughout the scaffolds. Before the gels became cross-linked fully, they were aspirated under a light vacuum so that they coated the walls of the scaffolds but did not fill the pore spaces. This step was performed on groups 1 to 5 at day 1, and on groups 6 and 7 only after 3 weeks of osteogenic culture (Fig.1).

2.4. IN VITRO CULTIVATION

Seven experimental groups of cell–biomaterial constructs were established as follows (Fig. 1), and the constructs were cultured for 5 weeks.

Group 1 served as osteogenic control, with constructs cultured in osteogenic medium (OM), which consisted of low glucose DMEM, 10% FBS, 1% Pen–Strep supplemented with osteogenic factors (all purchased from Sigma-Aldrich): 100 nM dexamethasone, 10 mM sodium-β-glycerophosphate, 10 mM HEPES and 50 μg/mL ascorbic acid-2-phosphate,

Group 2 served as vasculogenic control, where endothelial growth media-2 was used (EGM-2; Lonza CC-3162) to induce endothelial differentiation of hASCs as in prior studies [25]. This endothelial cell basal medium contains, among other important growth factors, VEGF (Vascular

endothelial growth factor) and FGF-b (basic fibroblast growth factor), known to stimulate endothelial differentiation, vasculogenesis and angiogenesis. Five further groups were chosen for growing vascularized bone constructs.

In Group 3, both osteogenic and vasculogenic supplements were provided simultaneously throughout the total period of culture by using cocktail medium composed by EGM and OM at 1:1 ratio (cocktail group).

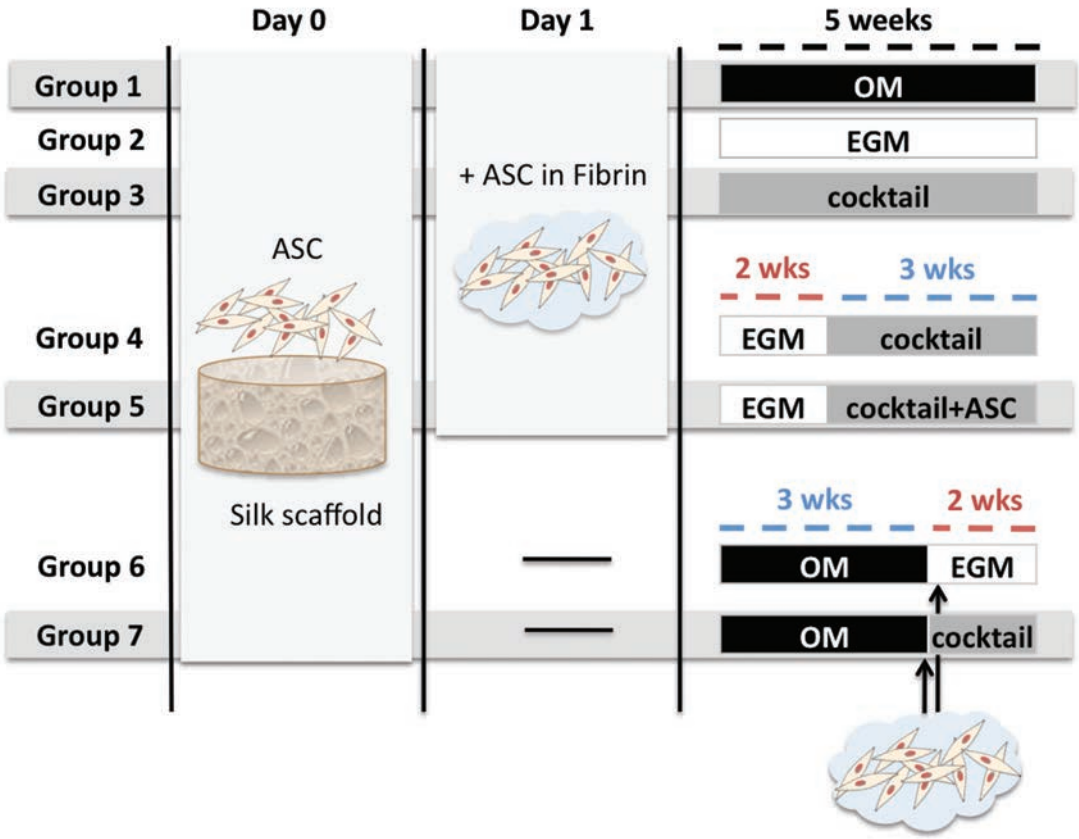

Figure 1. Experimental design. Groups 1 & 2 are controls, where constructs were provided osteogenic supplements (OM) or endothelial factors (EGM) for 5 weeks. Group 3 was cultured with a cocktail of both OM & EGM (1:1) for 5 weeks. In Groups 4 & 5, vascular differentiation was induced for 2 weeks before adding osteogenic factors in a cocktail medium (EGM|cocktail). Additional hASC were added into the pore spaces at this point in Group 5 (EGM|cocktail+ASC). Groups 6 & 7 were seeded with hASC to silk scaffold and osteogenic differentiation was induced for 3 weeks; only at this time point, hASC in fibrin were added to the scaffold for vascular development. Constructs were cultured in either EGM (Group 6 – OM|EGM) or cocktail media (Group 7 – OM|cocktail) for the remaining 2 weeks.

Further, two sequential approaches were established: a) induction of vasculogenesis prior to osteogenesis (groups 4 and 5), and b) the reverse: induction of osteogenesis prior to

vasculogenesis (groups 6 and 7). In both approaches, 2–week differentiation periods were chosen for vasculogenic induction, and 3 weeks for osteogenic differentiation. These time frames were based on prior studies: hASC cultured for 2 weeks in endothelial cell growth medium-2 (EGM-2) have demonstrated network formation of branched tube-like structures positive for CD31, CD144, and von Willebrand factor [25]. With respect to bone development, previous studies of our group have demonstrated osteogenic differentiation of hASCs and secretion of mineralized bone matrix as early as 2 weeks after osteogenic induction in this silk scaffold system [20], although 3 weeks was allowed for increased tissue development.

In Group 4, constructs were cultured in EGM for 2 weeks to induce endothelial differentiation, and in cocktail medium for the remaining 3 weeks (EGM|cocktail) for maintenance and augmentation of endothelial phenotype, while simultaneously inducing osteogenesis. In Group 5, the constructs were cultured exactly as in Group 4 except that fresh hASC were added into scaffold pore spaces at the 2-week time point, intended to respond more promptly to osteogenic cues. This is indicated as EGM|cocktail+ASC.

In Group 6 and Group 7, we 'reversed' the process and induced osteogenic differentiation first. hASC were seeded into the scaffolds and cultured in osteogenic media for 3 weeks. Subsequently, hASC in fibrin were added to the constructs and cultured either in EGM media (Group 6 - OM|EGM), or in cocktail medium (Group 7 - OM|cocktail).

2.5. LIVE/DEAD ASSAY

LIVE/DEAD Viability/Citotoxicity kit (Molecular Probes) was used to evaluate cell viability at the end of culture. Live cells (indicated by calcein AM) and dead cells (indicated by ethidium homodimer-1) were observed and imaged through a confocal microscope. Optical surfaces were taken from the surface up until 160 μm deep, in 10 μm intervals. All images are presented as vertical projections.

2.6. BIOCHEMICAL CHARACTERIZATION

Constructs were harvested, washed in PBS, cut in half and weighed.

For DNA assay, samples were added to 1 mL of digestion buffer (10 mM Tris, 1 mM EDTA, 0.1% Triton X-100, 0.1 mg/mL proteinase K) and incubated overnight at 56ºC. After centrifugation at 3000g for 10 minutes, the supernatants were removed, diluted and pippeted in duplicate into a 96-well plate and a 1:1 ratio of picogreen solution (Quant-iT™ PicoGreen ® dsDNA Kit, Invitrogen) was added. Sample fluorescence was measured with fluorescent plate

reader at excitation ~480 nm, emission ~520 nm. Lambda DNA was used to prepare the standard curve.

For calcium quantification, samples were incubated in 1 mL TCA 5% (trichloroacetic acid 5% v/v) and calcium was extracted by disintegrating the construct using steel balls and MinibeadBeater™. The supernatant were transferred in duplicate into 96-well plate and calcium binding reagent was added at 1:10 ratio (StanbioTotal Calcium Liquicolor®). Sample optical density was measured using a microplate reader set to 575 nm. Calcium standard was used to prepare the standard curve.

Alkaline Phosphatase (AP) activity was determined by adding cell lysis solution to one-half of each scaffold, and these were disintegrated using steel balls and MinibeadBeater™. After centrifugation, 50 µL of supernatant was incubated with 50 µL *p*NPP (p-nitrophenyl-phosphate) substrate solution, at 37ºC for 20 min. The reaction was stopped with 50 µL of stop solution and absorbance of was read at 405 nm. p-Nitrophenol at known concentrations was used to prepare the standard curve. All solutions were components of SensoLyte® *p*NPP Alkaline Phosphatase Complete Kit (Cell Biolabs, CBA-302).

2.7. Histology and Immunohistochemistry

Samples were fixed in 10% formalin for 1 day, dehydrated in graded ethanol washes, embedded in paraffin, sectioned to 5 µm and mounted on glass slides. Sections were deparaffinized with CitriSolv and rehydrated with a graded series of ethanol washes. For immunohistochemistry, sections were blocked with normal horse serum (NHS), stained sequentially with primary antibody (rabbit anti-human CD31 monoclonal antibody, Millipore 04-1074; rabbit anti-human von Willebrand factor (vWF), Sigma-Aldrich F3520; rabbit anti-human Osteopontin (OPN) polyclonal antibody, Chemicon ab1870; rabbit anti-bone sialoprotein (BSP) polyclonal antibody, Millipore ab1854; NHS for negative control), secondary antibody (Vectastain Universal Elite ABC Kit, PK-6200 Vector Laboratories) and developed with biotin-avidin system (DAB substrate kit SK-4100 Vector Laboratories).

2.8. Real-Time RT-PCR

For RNA extraction, samples were added to 800 µL of Trizol (Invitrogen 15596-026) and disintegrated by using steel balls and MinibeadBeater™. Suspensions were centrifuged at 12,000 g for 10 min at 4°C to remove tissue debris and extracted with chloroform (Sigma C2432). Colorless aqueous phase, containing RNA was removed and mixed with equal volume

of isopropanol (Sigma I9516). Suspensions were again centrifuged at 12,000 g for 8 min at 4°C, supernatant discarded, and RNA pellet washed with 75% ethanol. Samples were centrifuged at 7,500 g for 5 min at 4°C, supernatant removed, pellet air-dried, and dissolved with DEPC-water (Applied Biosystems AM 9920). RNA was quantified using Nanodrop® ND-1000. Approximately 1 μg of RNA was reverse-transcribed with random hexamers using High Capacity cDNA Reverse Transcription Kit (Applied Biosystems 4368814). CD31, von Willebrand factor (vWF) and the housekeeping gene glyceraldehyde-3-phosphatedehydrogenase (GAPDH) expression were quantified using the 7500 Fast Real-Time PCR System (Applied Biosystems). Primer sequences, probe, amplicon size and gene expression assay ID are described on table I. All TaqMan® Gene Expression Assay were purchased from Applied Biosystems. The expression data were normalized to GAPDH and presented as average values for each group (n=3 ± standard deviation).

Table I. Information about gene expression assays used for real time RT-PCR

Gene	GEA ID	Probe	Amplicon size
CD31	Hs00169777_m1	FAM	65 bp
von Willebrand factor	Hs00169795_m1	FAM	79 bp
GAPDH	Hs99999905_m1	FAM	122 bp

bp – base pairs; GAPDH - glyceraldehyde-3-phosphatedehydrogenase; GEA ID – Gene Expression Assay Identification

2.9. Statistical analysis

Data are presented as mean ± standard deviation (n=3). Statistical significance was determined using analysis of variance (ANOVA) followed by Tukey's HSD (honestly significant difference) test using Prism software (Prism 4.0c, GraphPad Software Inc.). $p < 0.05$ were considered statistically significant.

3. Results and discussion

3.1. Cell viability and proliferation

The DNA content of constructs (Fig. 2A) revealed that cells within constructs cultured in EGM for the total 5 weeks proliferated significantly more than any other group, even osteogenic control group ($p<0.05$). This result is coherent with studies performed by Suga and colleagues, where ASC cultured with EGM-2 proliferated 10^5 times more in 2 weeks than those cultured with DMEM [26]. It is interesting to notice that, in a study performed by our group, where

HUVECs and hMSC (bone marrow derived) were used to develop a vascularized bone model, the opposite outcomes were obtained: these co-cultured cells proliferated better in OM rather than EGM media [5]. The mixture of OM and EGM to 1:1 ratio (group 3 - cocktail) resulted in significantly lower cell proliferation ($p<0.05$) than EGM alone. DNA contents obtained in group 6 - OM|EGM and group 7 - OM|cocktail support this proliferative effect of EGM, once cells cultured with EGM after osteoinduction (OM for 3 weeks) proliferated 1.84x more than the corresponding constructs cultured in cocktail medium. Clearly, growth factors present in EGM enhance proliferation, and their effects are diminished after dilution to 1:1 ratio with osteogenic media. Accordingly, group 4 - EGM|cocktail show less DNA content than constructs of group 2 (EGM alone), showing that replacement of EGM by cocktail media at week 3, resulted in less cell proliferation. Unexpectedly, the addition of fresh cells after 3 weeks of culture, when culture medium was switched from EGM to cocktail, did not increase DNA contents (group 5 - EGM|cocktail+ASC, Fig. 2A). Live/Dead imaging (Fig. 2B) show considerable cell viability in all experimental groups, with some cell debri found in group 7.

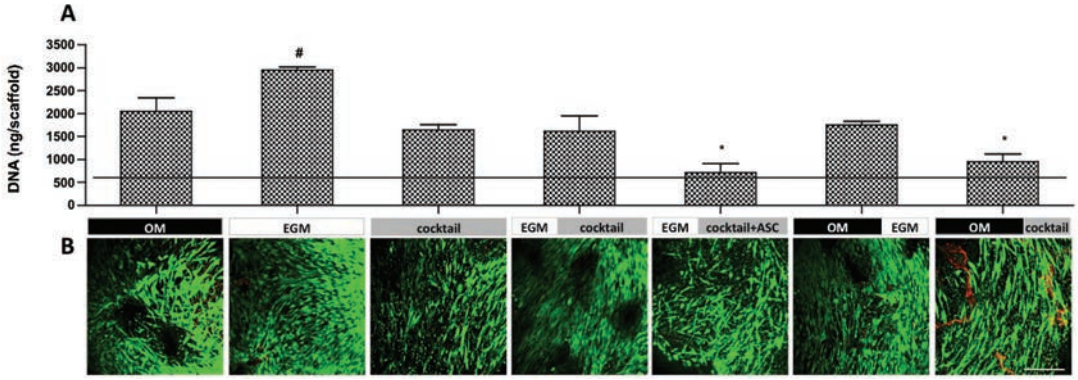

Figure 2. Cell proliferation and viability after 5 weeks of culture. A) DNA quantification. Horizontal line indicates day 1 values. Data are shown as Ave ± SD (n=3), *$p<0.001$ to EGM group, #$p<0.05$ to all other groups; B) Live/Dead assay. Scale bar = 200 μm.

3.2. VASCULAR DEVELOPMENT

Endothelial cell markers - CD31 adhesion molecule and von Willebrand factor (vWF) - were used to identify and characterize specific endothelial cell types and evaluate vascular development in cultured tissues.

Both the gene expression (GE) (Fig. 3) and protein deposition (Fig. 4) of endothelial cell markers were assessed. CD31 gene expression (Fig. 3A) in groups 1 through 4 - OM, EGM,

cocktail and EGM|cocktail respectively, was comparable to that observed at day 1 (horizontal line). In contrast, statistically significant increases in CD31 GE was shown by group 5 - EGM|cocktail+ASC ($p<0.01$), group 6 – OM|EGM ($p<0.05$) and group 7 – OM|cocktail ($p<0.01$), relatively to day 1. The addition of fresh hASCs in all these groups at later stages of culture appears crucial for enhanced endothelial cell differentiation. After 5 weeks of culture, group 5 - EGM|cocktail+ASC expressed significantly higher CD31 ($p<0.01$) than groups 1 through 4. CD31 protein deposition (Fig. 4) correlates with the expression profile of the CD31 gene, with the groups 1 through 4 showing weak deposition and groups 5 and 6 showing strong protein deposition. Additionally, we observe that culture conditions at group 6 – OM|EGM promoted the development of elongated and circumferential structures, corresponding to vascular lumen (indicated by arrow). In contrast, protein staining in group 7 – OM|cocktail, was relatively weak, although CD31 GE was relatively high. Though, it is not uncommon for protein and mRNA levels to differ [27]. vWF protein deposition was consistent with CD31 protein deposition, with very weak staining in group 7, and good staining in groups 5 and 6. Again, elongated structures were stained for vWF at group 6 – OM|EGM.

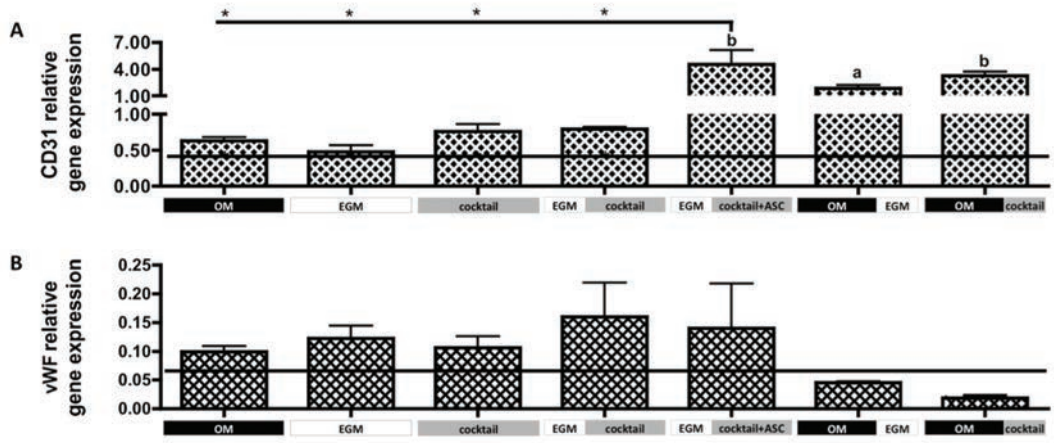

Figure 3. Gene expression of endothelial markers after culture. A) CD31 and B) vWF gene expression relative to GAPDH. Horizontal line indicates day 1 values. Data are shown as Ave ± SD (n=3), *$p<0.01$ to EGM|cocktail+ASC group.

Groups 1 through 5 had comparable vWF gene expression (GE), which was upregulated relatively to day 1, although not significantly different. The same was not observed for groups 6 and 7, where vWF GE was downregulated relative to day 1. No significant differences were obtained between groups. Regarding vWF protein detection by immunohistochemistry (Fig.4),

positive staining was obtained for groups 2 (EGM control), 3, 5 and 6. Among these, more elongated stained structures are observed in group 6, what is not observed in other experimental groups.

Overall, the cultivation system comprised of hASC adhered to silk scaffold surface, and encapsulated in fibrin hydrogel, was not sufficient to support the formation of robust tube like structures in the vasculogenic control group (group 2 – EGM), as no lumens were detected despite positive staining for CD31 and vWF. Previous work developed by Heydarkhan-Hagvall and colleagues demonstrated formation, by hASC, of branched tube-like structures positive for these endothelial markers as early as 2 weeks cultured in same endothelial media [25]. Miranville obtained similar observations when culturing in endothelial growth media supplemented with VEGF and IGF [10], as well as Planat-Bernard in methylcellulose medium [11] and Rehman when cultured ASC in EGM-2MV media [12]. In the current study, we observed that sequential nourishment of growth factors was most beneficial to vascular development, specifically when osteogenesis was induced before vasculogenesis, consisting of the addition of hASC with EGM media at the 3 week time point. Elongated structures were identified positive for both CD31 and vWF, in association with what appeared to be small lumen in histological sections (Fig.4, black arrow).

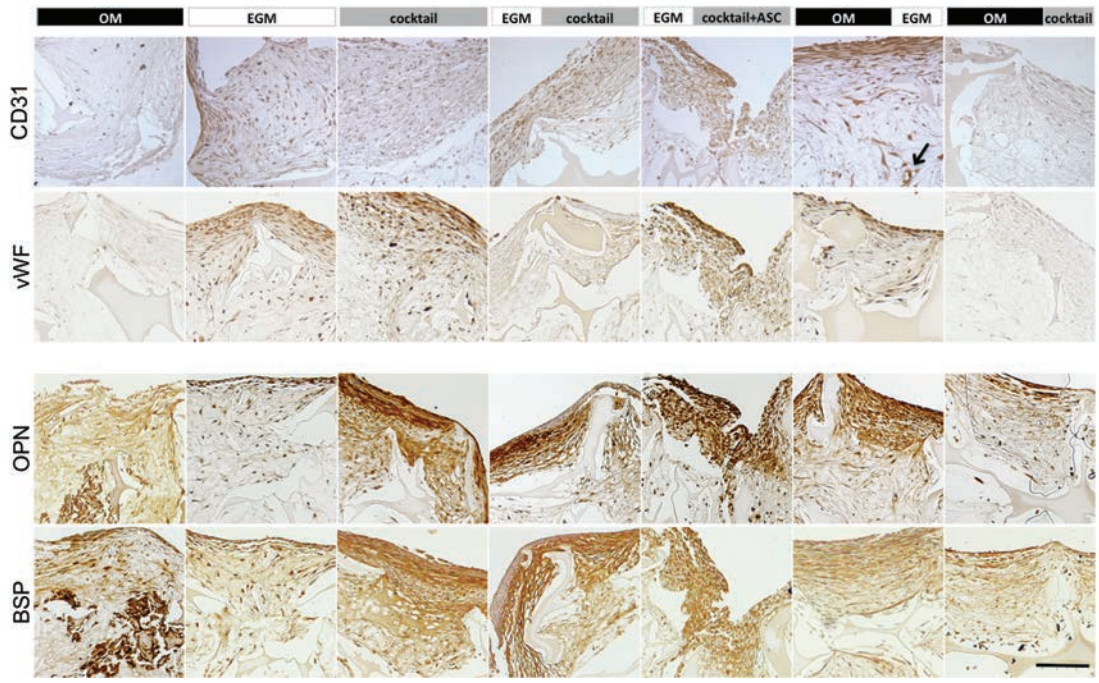

Figure 4. Immunohistological analysis of constructs after 5 weeks. The expression of vascular and osteogenic proteins was evaluated. CD31 and von Willebrand Factor (vWF) were expressed in

endothelial control group (EGM) as well as in both groups where endothelial differentiation was firstly induced (EGM|cocktail & EGM|cocktail+ASC). These proteins were also detected in the group where EGM was supplemented after osteogenic differentiation (OM|EGM). Osteopontin (OPN) and bone sialoprotein (BSP) were expressed in the matrix of all groups with exception to EGM group, where these proteins were detected only at a cellular level. Scale bar = 100 μm.

It is known that osteoblasts secrete not only VEGF but also BMPs, which induce endothelial migration, filopodia and tube formation (via activation of the transcription factor Id1 through SMADs or ERK signaling) [28, 29]. The osteogenic differentiation of hASC at a first stage may lead to the secretion of these growth factors (GF) as the BMPs have been detected at the mRNA level in previous studies [30]. Furthermore, hASC added to the system after 3 weeks are immediately in close proximity to the GF-secreting osteogenic induced cells. Consequently, these paracrine relationships may be playing an important role in stimulating the freshly delivered hASC into the endothelial lineage. Given the concurrent outcomes evaluated, we propose that culturing conditions provided in group 6 – OM|EGM are the most promising for vascular development in this synergistic approach to engineer vascularized bone.

3.3. BONE TISSUE DEVELOPMENT

Bone tissue markers were assessed in order to evaluate bone development in the proposed vascularized bone tissue culture. Bone Sialoprotein II (BSP) and Osteopontin were detected in cultured grafts through immunolocalization on histological slides (Fig. 4). As expected, the EGM group was the least stained, as this group was not supplemented with osteogenic growth factors. The group that showed the strongest osteogenesis was the cocktail group. It seems that the simultaneous presence of osteogenic and vasculogenic growth factors over 5 weeks of culture improved bone protein deposition. We hypothesized that hASC cultured in endothelial media, triggered by angiogenic cues for 2 weeks, would commit to the endothelial cell lineage, and consequently be less able to respond to osteogenic cues provided at the second induction stage. The addition of fresh hASC at this time-point would potentially respond to the osteogenic growth factors present in cocktail media and develop bone tissue, but differences in staining intensity were not that evident: groups 4 and 5 - EGM|cocktail and EGM|cocktail+ASC respectively, demonstrated comparable bone protein deposition. From groups 6 – OM|EGM and 7 – OM|cocktail, that were subjected to osteogenic cues before vasculogenic induction, superior staining of bone proteins was observed in group 6.

Alkaline phosphatase (AP) activity was quantified as an early marker of osteogenic differentiation [31] (Fig. 5). Constructs cultured in OM exhibited a typical progression of osteogenic differentiation, as AP activity peaked at 3 weeks of osteogenic induction, and decreased by the end culture in all groups. Lower AP activity was detected in groups 6 and 7 (OM|EGM and OM|cocktail) as endothelial factors were provided at the last two weeks of culture. AP activity of cells cultured in EGM media the complete experimental period (EGM group) decreased throughout the 5-week culture period, while constructs cultured in cocktail media after endothelial media (groups 4 and 5), showed characteristic increases in AP activity, suggesting that osteogenesis still occur in these groups, but with delay. Constructs cultured during total 5 weeks in cocktail media demonstrated a decrease of AP activity after the first 2 weeks, increasing by the end of the culture period.

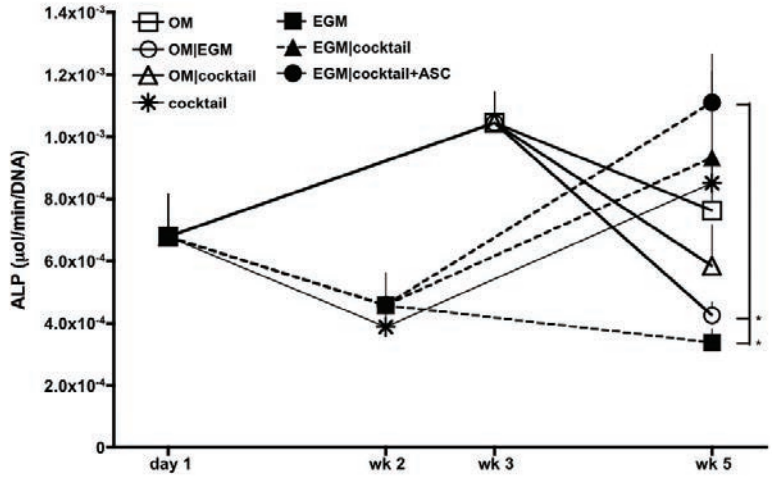

Figure 5. Alkaline phosphatase activity. n=3, *p<0.01 to EGM|cocktail+ASC.

Mineralization of engineered tissue was evaluated by calcium quantification (Fig. 6). After 5 weeks of culture, the osteogenic control group (OM) presented the highest amount of calcium, significantly different from all other groups ($p<0.001$), while the vasculogenic control presented the least. Among groups where sequential induction of both lineages were evaluated, group 7 - OM|cocktail presented the highest amount of calcium deposition, followed by group 6 – OM|EGM. Significant differences ($p<0.05$) were observed between these groups, suggesting that osteogenic growth factors present in cocktail media are essential to maintain bone development. Constructs from group 5 – EGM|cocktail+ASC demonstrated 1.7x higher

calcium content than group 4, suggesting that the addition of hASC at the osteogenic induction stage improved calcification of the overall system.

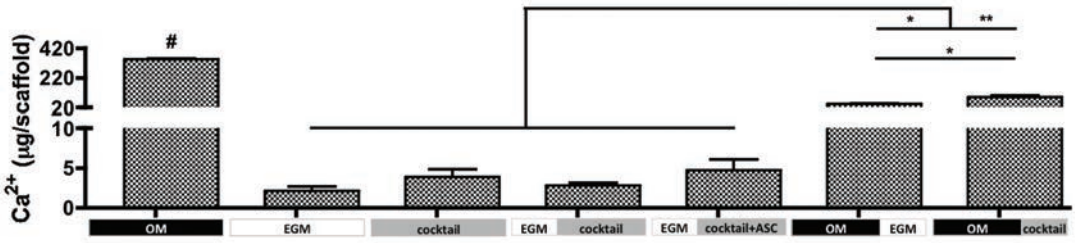

Figure 6. Mineralization of tissue engineered grafts after 5 weeks. Calcium content. n=3, #p<0.001 to all other groups, *p<0.01, **p<0.001.

Taken altogether, in accordance to collected data for bone development in the culturing conditions evaluated, we suggest that the combination tested in Group 6 – OM|EGM promoted the most promising synergistic deposition of calcium and bone proteins.

3.4. SYNERGISTIC DEVELOPMENT OF VASCULARIZED BONE

The establishment of an environment suitable for the *in vitro* development of vascularized bone from a single cell source presents a considerable challenge. In this study we proposed changing spatio-temporal cues by manipulating delivery of cells to scaffolds and/or timing of vasculogenic and osteogenic cues leading to the concomitant formation of the bone and vascular compartments in the same scaffold. The collected experimental data are consistent with the model presented in Fig. 7. We postulate that hASC adhered to the silk scaffold wall, sense its stiff surface, which, in combination with osteogenic cues, trigger cells to undergo osteogenic differentiation and secrete mineralized matrix. At a second stage, hASC-encapsulated in fibrin hydrogel sense the surrounding smooth environment and inherent vasculogenic properties, which in combination with vasculogenic growth factors such as VEGF and bFGF present in endothelial growth media, trigger undifferentiated hASC to undergo differentiation into endothelial cells.

The results obtained in this study are promising. However, fully developed networks within the bone compartment were not achieved. In a similar study performed by our group, where HUVECs and hMSC were co-cultured in order to develop a vascularized bone model, we obtained well-developed vasculature, with visible lumen formed after *in vitro* culture, which further anastomosed with host vasculature after 2 weeks of sub-cutaneous implantation in

nude mice. Vasculogenic induction with endothelial growth media was performed for 2 weeks, as in the present study, although HUVECs, a mature endothelial cell, were capable to successfully form tube-like structures and nourish the bone tissue [5]. This reinforces the hypothesis that a distinct approach may be needed to account for the undifferentiated state of the adipose stem cell. Actually, the fact that the opposite spatio-temporal application of cells and differentiation cues resulted in most promising outcomes is already an insight to guide future experiments.

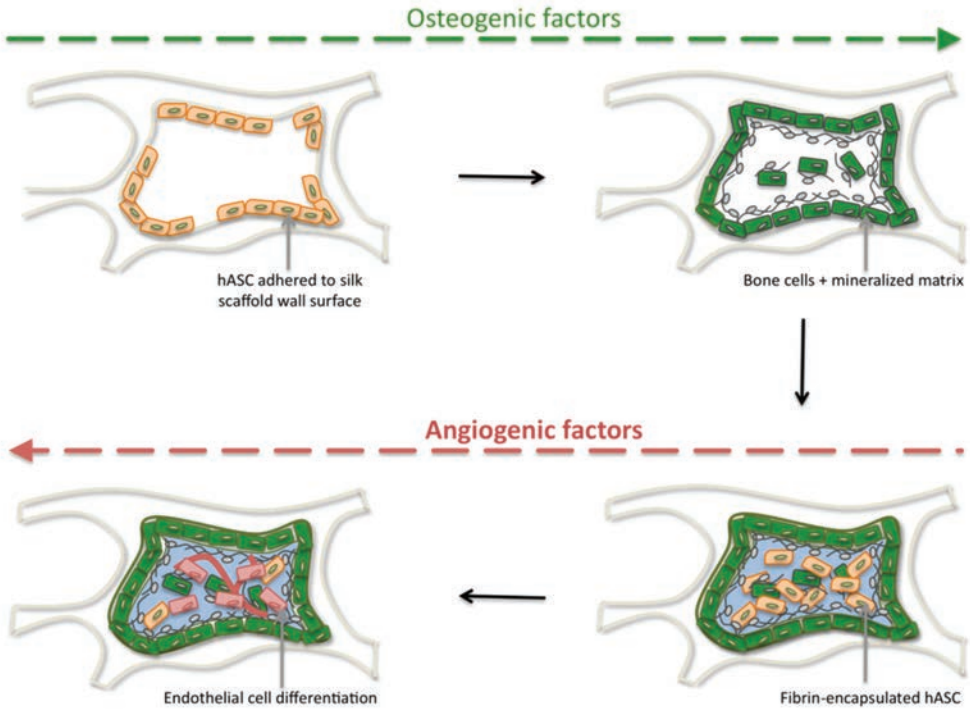

Figure 7. Model of *in vitro* coordination of bone and vascular tissue development. hASC (beige spindle-shape) adhered to silk scaffold wall, sense the hard surface and osteogenic factors provided, stimulate osteogenic differentiation (green cells) and deposition of mineralized matrix (grey). At a second stage, hASC encapsulated in fibrin hydrogel (light blue) are triggered by smooth vasculogenic surface growth factors provided, to undergo endothelial differentiation (red cells).

Moreover, our results are additive to those obtained by Gardin and co-workers, which remains, to our knowledge, the only study that previously explored the concurrent osteogenic and endothelial *in vitro* commitment of hASC [32]. In this work, hASC loaded to a fibronectin coated hydroxyapatite scaffold were exposed to either osteogenic induction only, vasculogenic induction only, or a mixture of both osteogenic and vasculogenic growth factors for 21 days, *in vitro*. In their hands, concurrent gene expression of both osteogenic markers osteopontin,

osteonectin, osteocalcin, collagen type I and vasculogenic markers CD31, von Willebrand Factor, VEGF was achieved. Our study extends the work by Gardin et al to design an engineered vascularized bone graft. We further explored the development of both tissues by investigating: 1) the sequential application of cells and/or osteogenic and vasculogenic growth factors to the system; and 2) evaluation of outcomes based on tissue formation where, besides gene expression, we also assessed the deposition of bone and endothelial specific proteins within the engineered graft, as well as mineralization of the tissue construct. Therefore, we may furthermore propose our approach as an *in vitro* model for studying and optimizing both spatial and temporal effects of cell and growth factor delivery.

4. CONCLUSIONS

This study supports the hypothesis that human adipose derived stem cells may be used as a single cell source for the formation of vascularized bone. Three culture approaches were tested in order to differentiate both osteogenic and endothelial lineage: 1) simultaneous construct nourishment with bone and vascular growth factors; 2) induction of vasculogenesis before osteogenesis; and 3) induction of osteogenesis before vasculogenesis, to show that the osteogenic induction was necessary before supplying the construct with fresh cells and growth factors for vascularization. This last combination, in particular the osteo-induction of hASC seeded to silk scaffold for 3 weeks, followed by addition (to the free pore spaces of the construct) of fibrin-encapsulated hASC to which vasculogenic cues were provided for 2 weeks, resulted in the most promising outcomes towards engineered vascularized bone grafts. Nevertheless, extensive research has yet to be performed in order to understand cell crosstalk and underlying mechanisms associated with multilineage cell differentiation of hASC and interactions responsible for the development of a robust functional vascularized bone graft useful for successful therapeutic applications.

Acknowledgements

We gratefully acknowledge funding support of this work by the NIH (DE161525 and EB02520 to GVN), and the FCT PhD grant (SFRH/BD/42316/2007 to CC). The authors gratefully thank Darja Marolt and Supansa Yodmuang for their help with the experiments, and David Kaplan for providing silk scaffolds used in this study.

References

1. Usami, K., et al., *Composite implantation of mesenchymal stem cells with endothelial progenitor cells enhances tissue-engineered bone formation.* J Biomed Mater Res A, 2009. 90(3): p. 730-41.
2. Tsigkou, O., et al., *Engineered vascularized bone grafts.* Proceedings of the National Academy of Sciences of the United States of America, 2010. 107(8): p. 3311-3316.
3. Unger, R.E., et al., *The rapid anastomosis between prevascularized networks on silk fibroin scaffolds generated in vitro with cocultures of human microvascular endothelial and osteoblast cells and the host vasculature.* Biomaterials, 2010. 31(27): p. 6959-6967.
4. Koob, S., et al., *Bone formation and neovascularization mediated by mesenchymal stem cells and endothelial cells in critical-sized calvarial defects.* Tissue Eng Part A, 2011. 17(3-4): p. 311-21.
5. Correia, C., et al., *In vitro model of vascularized bone: synergizing vascular development and osteogenesis.* PLoS ONE, 2011. in press.
6. Aust, L., et al., *Yield of human adipose-derived adult stem cells from liposuction aspirates.* Cytotherapy, 2004. 6(1): p. 7-14.
7. Gimble, J. and F. Guilak, *Adipose-derived adult stem cells: isolation, characterization, and differentiation potential.* Cytotherapy, 2003. 5(5): p. 362-9.
8. Malafaya, P.B., et al., *Chitosan particles agglomerated scaffolds for cartilage and osteochondral tissue engineering approaches with adipose tissue derived stem cells.* J Mater Sci Mater Med, 2005. 16(12): p. 1077-85.
9. Frohlich, M., et al., *Bone Grafts Engineered from Human Adipose-Derived Stem Cells in Perfusion Bioreactor Culture.* Tissue Engineering Part A, 2010. 16(1): p. 179-189.
10. Miranville, A., et al., *Improvement of postnatal neovascularization by human adipose tissue-derived stem cells.* Circulation, 2004. 110(3): p. 349-55.
11. Planat-Benard, V., et al., *Plasticity of human adipose lineage cells toward endothelial cells - Physiological and therapeutic perspectives.* Circulation, 2004. 109(5): p. 656-663.
12. Rehman, J., et al., *Secretion of angiogenic and antiapoptotic factors by human adipose stromal cells.* Circulation, 2004. 109(10): p. 1292-1298.
13. Cao, Y., et al., *Human adipose tissue-derived stem cells differentiate into endothelial cells in vitro and improve postnatal neovascularization in vivo.* Biochemical and Biophysical Research Communications, 2005. 332(2): p. 370-379.
14. Mitchell, J.B., et al., *Immunophenotype of human adipose-derived cells: Temporal changes in stromal-associated and stem cell-associated markers.* Stem Cells, 2006. 24(2): p. 376-385.
15. Fischer, L.J., et al., *Endothelial Differentiation of Adipose-Derived Stem Cells: Effects of Endothelial Cell Growth Supplement and Shear Force.* Journal of Surgical Research, 2009. 152(1): p. 157-166.
16. Scherberich, A., et al., *Adipose tissue-derived progenitors for engineering osteogenic and vasculogenic grafts.* J Cell Physiol, 2010. 225(2): p. 348-53.
17. Kim, U.J., et al., *Three-dimensional aqueous-derived biomaterial scaffolds from silk fibroin.* Biomaterials, 2005. 26(15): p. 2775-2785.
18. McIntosh, K., et al., *The immunogenicity of human adipose-derived cells: Temporal changes in vitro.* Stem Cells, 2006. 24(5): p. 1246-1253.
19. Yu, G., et al., *Yield and characterization of subcutaneous human adipose-derived stem cells by flow cytometric and adipogenic mRNA analyzes.* Cytotherapy, 2010. 12(4): p. 538-46.
20. Correia, C., et al., *Development of silk-based scaffolds for tissue engineering of bone from human adipose derived stem cells.* submitted, 2011.
21. Grayson, W.L., et al., *Optimizing the medium perfusion rate in bone tissue engineering bioreactors.* Biotechnol Bioeng, 2010.
22. Bhumiratana, S., et al., *Nucleation and growth of mineralized bone matrix on silk-hydroxyapatite composite scaffolds.* Biomaterials, 2011. 32(11): p. 2812-20.
23. Tian, L. and S.C. George, *Biomaterials to prevascularize engineered tissues.* J Cardiovasc Transl Res, 2011. 4(5): p. 685-98.

24. Natesan, S., et al., *A Bilayer Construct Controls Adipose-Derived Stem Cell Differentiation into Endothelial Cells and Pericytes Without Growth Factor Stimulation.* Tissue Engineering Part A, 2011. 17(7-8): p. 941-953.
25. Heydarkhan-Hagvall, S., et al., *Human adipose stem cells: A potential cell source for cardiovascular tissue engineering.* Cells Tissues Organs, 2008. 187(4): p. 263-274.
26. Suga, H., et al., *Rapid expansion of human adipose-derived stromal cells preserving multipotency.* Cytotherapy, 2007. 9(8): p. 738-45.
27. Ghazalpour, A., et al., *Comparative analysis of proteome and transcriptome variation in mouse.* PLoS Genet, 2011. 7(6): p. e1001393.
28. Valdimarsdottir, G., et al., *Stimulation of Id1 expression by bone morphogenetic protein is sufficient and necessary for bone morphogenetic protein-induced activation of endothelial cells.* Circulation, 2002. 106(17): p. 2263-2270.
29. Suzuki, Y., et al., *BMPs promote proliferation and migration of endothelial cells via stimulation of VEGF-A/VEGFR2 and angiopoietin-1/Tie2 signalling.* J Biochem, 2008. 143(2): p. 199-206.
30. Halvorsen, Y.D., et al., *Extracellular matrix mineralization and osteoblast gene expression by human adipose tissue-derived stromal cells.* Tissue Eng, 2001. 7(6): p. 729-41.
31. Beck, G.R., B. Zerler, and E. Moran, *Phosphate is a specific signal for induction of osteopontin gene expression.* Proceedings of the National Academy of Sciences of the United States of America, 2000. 97(15): p. 8352-8357.
32. Gardin, C., et al., *In vitro concurrent endothelial and osteogenic commitment of adipose-derived stem cells and their genomical analyses through CGH array: novel strategies to increase the successful engraftment of tissue engineered bone grafts.* Stem Cells and Development, 2011. in press.

CHAPTER VIII

In vitro model of vascularized bone: synergizing vascular development and osteogenesis

---

This chapter is based on the following publication: Correia C, Grayson WL, Park M, Hutton D, Zhou B, Guo XE, Niklason L, Sousa RA, Reis RL and Vunjak-Novakovic G, 2011, *In vitro model of vascularized bone: synergizing vascular development and osteogenesis*, PLoS ONE, 6(12): e28352.

Abstract

Tissue engineering provides unique opportunities for regenerating diseased or damaged tissues using cells obtained from tissue biopsies. Tissue engineered grafts can also be used as high fidelity models to probe cellular and molecular interactions underlying developmental processes. In this study, we co-cultured human umbilical vein endothelial cells (HUVECs) and human mesenchymal stem cells (MSCs) under various environmental conditions to elicit synergistic interactions leading to the colocalized development of capillary-like and bone-like tissues. Cells were encapsulated at the 1:1 ratio in fibrin gel to screen compositions of endothelial growth medium (EGM) and osteogenic medium (OM). It was determined that, to form both tissues, co-cultures should first be supplied with EGM followed by a 1:1 cocktail of the two media types containing bone morphogenetic protein-2. Subsequent studies of HUVECs and MSCs cultured in decellularized, trabecular bone scaffolds for 6 weeks assessed the effects on tissue construct of both temporal variations in growth-factor availability and addition of fresh cells. The resulting grafts were implanted subcutaneously into nude mice to determine the phenotype stability and functionality of engineered vessels. Two important findings resulted from these studies: (*i*) vascular development needs to be induced prior to osteogenesis, and (*ii*) the addition of additional hMSCs at the osteogenic induction stage improves both tissue outcomes, as shown by increased bone volume fraction, osteoid deposition, close proximity of bone proteins to vascular networks, and anastomosis of vascular networks with the host vasculature. Interestingly, these observations compare well with what has been described for native development. We propose that our cultivation system can mimic various aspects of endothelial cell – osteogenic precursor interactions *in vivo,* and could find utility as a model for studies of heterotypic cellular interactions that couple blood vessel formation with osteogenesis.

1. INTRODUCTION

In native bone, synergistic interactions between osteoblasts/osteogenic precursors and endothelial cells enable coordinated development of vasculature and mineralized tissue. In the process of intramembranous ossification during craniofacial bone growth, this cell coupling results in close spatial relationships between the two tissues in newly forming bone, with the vascular network serving as a 'template' for bone mineral deposition [1]. A synergy between the two cell populations has also been observed during endochondral ossification. A murine model was used to demonstrate that when the HIF-1α protein was constitutively activated in

osteoblasts by conditional deletion of the *Vhl* gene, the result was higher vascularity in long bones with complementary increases in bone volumes [2]. In a recent study, it was shown that osteoblast precursors occupy pericytic locations as they invade the cartilage template along with blood vessels to form new trabecular bone during ossification of long bones [3]. Still, many of the mechanisms guiding interactions between endothelial cells and osteogenic precursors remain largely unknown due to the complexity of the *in vivo* environment.

The need to vascularize tissue engineered bone grafts, during culture and following implantation, has led to studies between endothelial cells and osteoblasts/osteo-progenitors [4-7]. Interestingly, despite the preponderance of evidence linking vascular development and osteogenesis *in vivo*, it has been decidedly difficult to simultaneously form capillary-like networks and mineralized deposits *in vitro,* within a single culture environment. Whereas beneficial effects of osteogenic precursors on vascular network formation have been demonstrated [7, 8], adequate formation of bone-like tissue within the same constructs has not been achieved. The effect of endothelial population on osteogenesis remains conflicting: some studies have indicated a positive effect of endothelial cells on mineral deposition [6, 9-12], while other studies have described molecular pathways via which endothelial cells inhibited osteogenesis [13, 14]

Recently, one group circumvented the difficulty of inducing adequate vascular development and osteogenic differentiation by seeding mesenchymal stem cells (MSCs) into polymer scaffolds and inducing osteogenesis prior to seeding MSCs and human umbilical vein endothelial cells (HUVECs) into a gel substrate [15]. When these constructs were implanted subcutaneously into the dorsum of nude mice, developed vascular networks anastomosed to the host vasculature, while after eight weeks of *in vivo* cultivation evidence of mineral deposition was revealed. Several other groups have shown that implanting biomaterial constructs with a mixture of mesenchymal and vascular or hematopoietic progenitor cells enabled the development of vascularized tissues *in vivo* [12, 16-18]. However, realistic *in vitro* cultivation models are required to elucidate the mechanistic interactions of both cell populations during the formation of vascularized bone.

In this study, we hypothesize that the sequential application of growth factors, to firstly induce the formation of stable vasculature and subsequently initiate osteogenic differentiation, could provide a biologically-inspired *in vitro* model of bone vascularization. HUVECs and human MSCs were cultured in decellularized trabecular bone constructs using fibrin as a cell carrier to provide an environment conducive to the formation of capillary-like networks. Coordinated development of the two tissue compartments was evaluated over a two-stage procedure (6

weeks *in vitro* culture followed by a 2 week sub-cutaneous implantation), to establish an alternative model for engineering bone-like constructs containing vascular networks (Fig. 1).

2. MATERIALS & METHODS

2.1. MATERIALS

Fetal bovine serum (FBS), Dulbecco's Modified Eagle Medium (DMEM), Penicillin–Streptomycin (Pen–Strep), HEPES and trypsin/EDTA were obtained from Invitrogen (Carlsbad, CA). Ascorbic acid-2-phosphate, dexamethasone, sodium-β-glycerophosphate, Triton X-100, fibrinogen and thrombin were obtained from Sigma-Aldrich (St. Louis, MO). Basic fibroblast growth factor (bFGF) and bone morphogenetic protein 2 (BMP2) were obtained from Peprotech (Rocky Hill, NJ). Endothelial Growth Medium-2 (EGM) was obtained from Lonza (Walkersville, MD). Phosphate buffered saline (PBS) and proteinase K were obtained from Fisher Scientific (Pittsburgh, PA). All other substances were of analytical or pharmaceutical grade and obtained from Sigma-Aldrich.

2.2. HUMAN MESENCHYMAL STEM CELLS (MSCS)

Bone marrow-derived human mesenchymal stem cells (MSCs) were isolated from the mononuclear fraction of a bone marrow aspirate obtained from a commercial source (Cambrex, CA) based on their attachment to tissue culture plastics [19] , expanded in high glucose DMEM supplemented with 10 % FBS, 1 % Pen–Strep and 1 ng/mL basic fibroblast growth factor (bFGF) to the 3rd passage. These cells have been characterized for their ability to differentiate into osteogenic, chondrogenic, and adipogenic phenotypes *in vitro* and for their ability to give rise to new bone formation *in vitro* and *in vivo* [19-21]. Three independent series of experiments were performed, each with triplicates of samples for each experimental group, data point and analytical method.

2.3. HUMAN UMBILICAL VEIN ENDOTHELIAL CELLS (HUVECS)

Fresh umbilical veins were obtained from the neonatal unit at Columbia University following an approved IRB protocol (IRBAAAC4839). To isolate HUVECs, the vein was flushed with HEPES buffer to remove residual blood and treated with trypsin for 15 minutes to remove the endothelial cells. Cells were flushed from the vein with HEPES and collected in centrifuge tubes. The suspension was centrifuged at 300 g for 5 minutes and the supernatant was

discarded. Cells were resuspended in EGM and cultured in tissue culture flasks. Non-adherent cells were washed out after 1 day. When the HUVECs grew to confluence, they were trypsinized, counted and cryopreserved.

2.4. MEDIUM SCREENING STUDIES

In this study, HUVECs were expanded in EGM to the 4th passage. HUVECs used in preliminary screening studies were suspended in serum-free medium at 1 × 10^6 cells/mL and then incubated with 10 ml/mL of Vybrant DiI (Molecular Probes) for 30 minutes at 37 ºC. The cells were washed of excess dye three times prior to mixing with hMSCs in a 1:1 ratio, and encapsulation in fibrin hydrogel in the wells of a 96-well plate and cultured for 4 weeks *in vitro*. A 1:1 ratio was chosen in pilot studies (data not shown) as it provided robust and stable vascular networks while enabling bone formation. The hydrogels were divided into five groups depending on the various growth medium provided the constructs. These included osteogenic medium (OM) containing low glucose DMEM, 10% FBS, 1% Pen–Strep supplemented with osteogenic factors: 100 nM dexamethasone, 10 mM sodium-β-glycerophosphate, and 50 μg/mL ascorbic acid-2-phosphate. The other groups were provided EGM or a cocktail of OM and EGM in a 1:1 ratio. The temporal sequence was investigated by providing the cells EGM only for 2 weeks followed by cocktail for the subsequent two weeks or cocktail medium supplemented with 10 ng/ml of BMP-2. The development of vascular structures was imaged with a Zeiss 510 confocal microscope using an image stack 200 μm thick with 10 μm spacing between slices.

2.5. DECELLULARIZED BONE SCAFFOLDS

Bone plugs (4 mm diameter × 2 mm high) were prepared as in our previous studies [22]. Briefly, trabecular bone was cored from the subchondral region of carpometacarpal joints of 2-week to 4-month old bovine calves, washed with high velocity stream of water to remove the marrow from the pore spaces, followed by sequential washes in PBS, hypotonic buffer, detergent and enzymatic solution to remove any remaining cellular material. At the end of the process, decellularized bone plugs were rinsed repeatedly in PBS, freeze-dried and cut into scaffolds for cell cultivation. The dry weight and exact length of each plug was measured and used to calculate the scaffold density and porosity. Scaffolds were sterilized in 70% ethanol for one day and incubated in culture medium overnight prior to cell seeding.

2.6. CELL ENCAPSULATION AND SEEDING

To induce bone formation, 20 µl suspension of MSCs at a density of 10 × 10^6 cells/mL was seeded into blot-dried scaffolds, divided into five groups, and incubated overnight to allow cell attachment as shown in Fig. 1. At day 1, the solutions of fibrinogen (5 mg/mL) and thrombin (10 Units/mL) were prepared. In Groups 1 – 4, HUVECs and MSCs, intended to form stable vasculature network, were encapsulated in fibrin at a 2:1 ratio and a density of 30 × 10^6 cells/mL. Thrombin was added to crosslink the gel, giving a final fibrin concentration of 4 mg/mL. Before crosslinking occurred, 20 µl of cell/gel suspension was pipetted into blot-dried scaffolds to allow uniform cell seeding throughout the scaffolds. Before the gels became fully cross-linked, they were aspirated under a light vacuum so that the fibrin gel coated the walls of the scaffolds, but did not fill the pore spaces. In Group 5, this same step was performed on MSC-seeded scaffolds after 4 weeks of osteogenic culture.

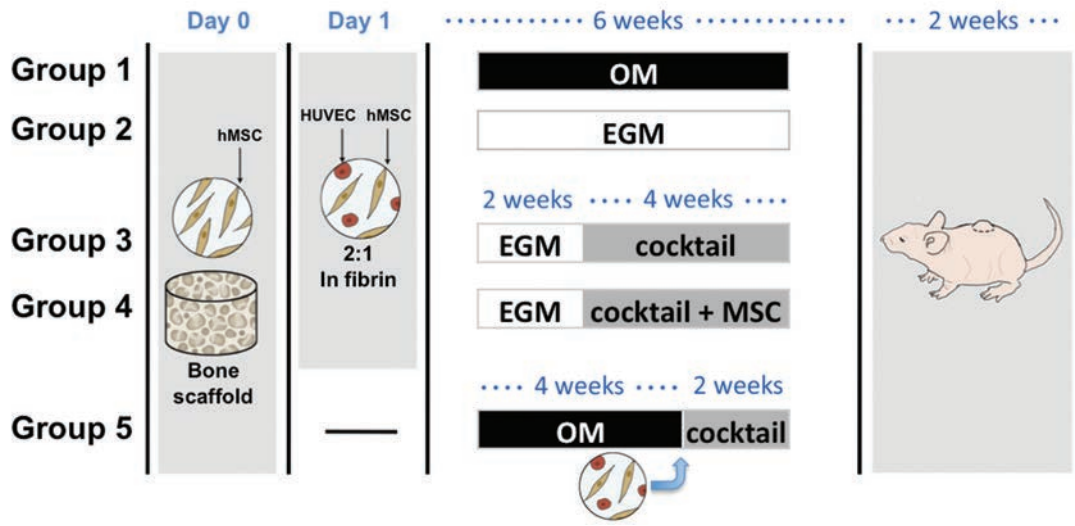

Figure 1. Schematic of experimental approaches. Groups 1 & 2 are 'controls' where constructs were provided osteogenic supplements (OM) or endothelial factors (EGM) for 6 weeks. In Groups 3 & 4, vascular differentiation was induced for 2 weeks before adding osteogenic factors in a cocktail medium (EGM+OM at 1:1 ratio). No additional cells were added at this point in Group 3 (EGM|cocktail), while osteo-induced MSCs were seeded into the pore spaces in Group 4 (EGM|cocktail+MSCs). These were compared with cultures in Group 5 where only MSCs were added initially and cultured in OM for 4 weeks. A co-culture of HUVECs and MSCs were then added and constructs cultured in cocktail medium (OM|cocktail) for remaining 2 weeks. Constructs of all groups were implaneted sub-cutaneously in nude mice for additional 2 weeks.

2.7. IN VITRO CULTURE

Five experimental groups were established to study vascularized bone constructs, including three main groups and two controls (Fig. 1). Group 1 (control for osteogenic conditions) utilized osteogenic medium (OM) throughout the culture, containing low glucose DMEM, 10% FBS, 1% Pen–Strep supplemented with osteogenic factors: 100 nM dexamethasone, 10 mM sodium-β-glycerophosphate, and 50 μg/mL ascorbic acid-2-phosphate, supplemented with BMP-2 (at 10 ng/mL) for 6 weeks. Group 2 (control for vasculogenic conditions) utilized endothelial growth medium (EGM) throughout the culture. Group 3 utilized EGM for 2 weeks and then a cocktail medium composed by EGM and OM at 1:1 ratio (EGM|cocktail) for 4 weeks. Group 4 was designed exactly as Group 3 except that osteo-induced MSCs were added into scaffold pore spaces at the 2-week time point (EGM|cocktail+MSC). In Group 5, MSCs only were seeded into the scaffolds and cultured in osteogenic medium for 4 weeks, at which point HUVECs and MSCs in fibrin were added to the constructs and cultured in cocktail medium for an additional 2 weeks (OM|cocktail).

2.8. IN VIVO IMPLANTATION

After 6 weeks of *in vitro* culture, constructs of all groups were evaluated for 2 weeks in a subcutaneous implantation nude mouse model *in vivo.* NOD SCID mice (NOD.CB17-*Prkdc*^{scid}/NCrHsd, Harlan) were anaesthetized by a subcutaneous injection of ketamine (80-100 mg/kg) and xylazine (5-10 mg/kg). Analgesia was provided with buprenorphine (0.05-0.1 mg/kg). Constructs were implanted into separate subcutaneous dorsal pockets (one construct per pocket, two pockets per animal) according to an approved Columbia University Institutional Animal Care and Use Committee (IACUC) protocol. Implants were retrieved after 2 weeks for analysis of blood vessel anastomosis and bone growth.

2.9. DNA ASSAY

Constructs were washed in PBS, cut in half, placed into micro-centrifuge tubes and incubated overnight at 56°C in 1 mL of digestion buffer (10 mM Tris, 1mM EDTA and 0.1% Triton X-100) containing 0.1 mg/mL proteinase K. The supernatants were collected and diluted 10 times to bring into the linear range of the Picogreen assay. A standard curve was prepared from a solution of bacteriophage λ DNA obtained from Molecular Probes. Picogreen dye (Molecular

Probes, OR) was added to the samples in 96-well plates (100 μL dye into each 100 μL sample) and read in a fluorescent plate reader (excitation 485 nm, emission 528 nm).

2.10. LIVE-DEAD ASSAY

Constructs were cut in half, washed in PBS, incubated with calcein AM (indicating live cells) and ethidium homodimer-1 (indicating dead cells) according to manufacturer's protocol (LIVE/DEAD (R) Viability/Cytotoxicity Kit, Molecular Probes) and imaged on a confocal microscope. Optical slices were taken from the surface at 10 μm intervals, up to the depth of 160 μm and presented as a vertical projection.

2.11. IMMUNOHISTOCHEMISTRY

Constructs were washed in PBS and fixed in 10% formalin for 1 day. Samples were then decalcified for 2 days with Immunocal solution, dehydrated in graded ethanol washes, embedded in paraffin, sectioned to 5 μm and mounted on glass slides. Sections were deparaffinized with Citrisolv, rehydrated with a graded series of ethanol washes, blocked with normal serum, and stained with primary antibodies followed by the secondary antibody and development with a biotin/avidin system. Immunohistochemistry was performed for anti-human collagen I (Abcam ab6308), bone sialoprotein II (BSP) (Chemicon AB1854), CD31 (Millipore 04-1074) and von Willebrand factor (vWF) (Sigma-Aldrich F3520). Counterstaining was performed with hematoxylin. The serum, secondary antibody and developing reagents were obtained from Vector Laboratories and included in the Vector Elite ABC kit (universal) (PK6200) and DAB/Ni Substrate kit (SK-4100). Negative controls were performed by omitting the primary antibody incubation step.

2.12. MICRO COMPUTERIZED TOMOGRAPHY (μCT)

μCT was performed on all five cell-seeded groups after 6 weeks of *in vitro* culture. As a control, unseeded scaffolds were remained in OM throughout culturing period and analyzed at this time point. A modification of a previously developed protocol was used [23]. The samples were aligned along their axial direction and stabilized in a 2 mL centrifuge tube that was clamped within the specimen holder of a vivaCT 40 system (SCANCO Medical AG, Basserdorf, Switzerland). The 2 mm length of the scaffold was scanned at a 21 μm isotropic voxel size. The total bone volume (BV), accounting for the sum of the bone matrix in the scaffold and the

new mineralized bone, was obtained from the application of a global thresholding technique so that only the mineralized tissue is detected. The bone volume fraction (BV/TV) was calculated as the ratio of the BV and the total volume (TV) of the sample. Spatial resolution of this full voxel model was considered sufficient for evaluating the micro-architecture of the samples.

2.13. Evaluation of in vivo anastomosis and new bone formation

After 2 weeks of subcutaneous implantation in NOD SCID mice, samples were harvested, washed in PBS and macroscopic photographs were taken with the stereomicroscope. Samples were cut in half, and used for soft and hard tissue histology. Anastomosis of *in vitro* developed capillary networks with host vasculature was evaluated by immunolocalization of human CD31 (Millipore 04-1074) as described above. Counterstaining with hematoxylin was performed to detect mouse red blood cells within human capillary lumen. New bone formation was evaluated on undecalcified sections processed according to hard tissue histology methods: constructs were fixed in 10% formalin for 1 day and dehydrated with sequential washes in 70 % ethanol (2 days), 100 % ethanol (2 days with twice daily solution changes), and toluene (2 days with once daily solution change). Constructs were then washed in activated methyl methacrylate (MMA) with daily changes of MMA solution for four days at 4 °C, and then placed at 32 °C until the MMA cured. Plastic-embedded sections were sectioned to 8 μm on a Leica hard tissue microtome. Staining for the new osteoid formation was done using the traditional Goldner's Masson trichrome stain.

2.14. Statistics

Statistical analysis was performed using the GraphPad Prism 4.0c software. A one-way analysis of variance (ANOVA) with Tukey's multiple comparison post-hoc test was used to verify statistically significant differences among groups. $p < 0.05$ were considered statistically significant. Data is presented as mean±SD.

3. Results

3.1. Formation of vascular networks in fibrin hydrogels

We confirmed that capillary networks formed from HUVECs are stable *in vitro* only in the presence of MSCs (Fig. S1). Robust networks were observed in confocal microscopy within two weeks of culture in constructs cultured in endothelial growth media (Fig. S2 – EGM group)

and remained stable throughout the 6 weeks of cultivation. When OM was used at the beginning of the culture period (Fig. S2 – OM group), the cells did not form networks. Instead, significant amounts of 'debris' from the dil-stained HUVECs were observed by confocal (and used as a pseudo parameter for evaluating HUVEC viability). Cells in the cocktail medium (EGM+OM 1:1 ratio) formed vascular networks, as evidenced via confocal imaging of the pre-stained HUVECs, however high amount of cell debris was observed (Fig. S2 – cocktail group). Sequential induction was investigated in Group 3 and Group 4 constructs, using EGM first, since HUVECs did not survive well if OM was used first. In both groups, vascular networks that formed within the first two weeks were maintained for the duration of culture. However, supplementation of cocktail medium (EGM+OM 1:1 ratio) with BMP-2 (10 ng/mL) significantly decreased the amount of cell debris, suggesting that BMP-2 may help maintain the viability of the endothelial cell population (Fig. S2 – EGM|cocktail+BMP group).

The amount and pattern of mineral deposition also differed significantly when sequential induction was utilized (Groups 3 and 4) as compared to the osteogenic conditions applied throughout culture (Group 1). Notably, the new mineral deposition was observed mostly in the close spatial proximity to vascular networks, particularly in the EGM|cocktail+BMP2 group. From these studies, it was determined that sequential induction was needed to facilitate the development of both structures within single constructs for bone tissue engineering applications.

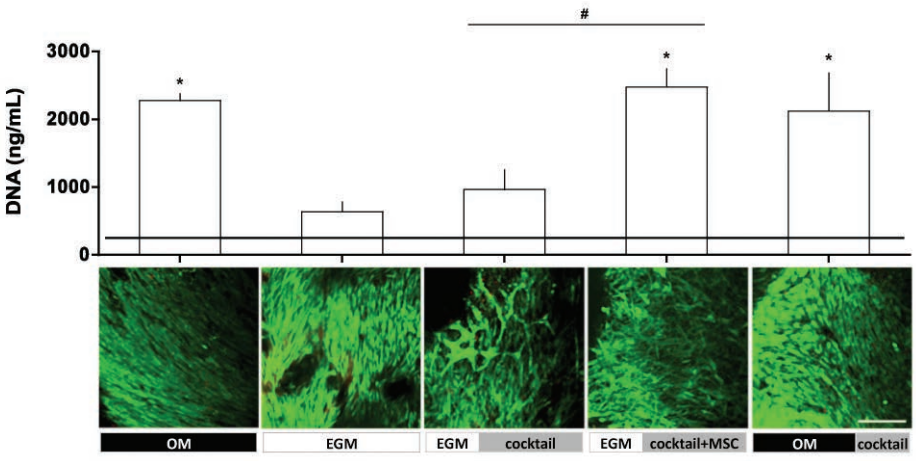

Figure 2. DNA contents of constructs after 6 weeks of *in vitro* culture. Upper: Horizontal line indicates day 1 values. n = 3; * indicate $p < 0.05$ in comparison to day 1 values. # indicate $p < 0.05$ among groups. Lower: Live/dead imaging of constructs after *in vivo* culture. Scale bar =200μm.

3.2. FORMATION OF BONE AND CAPILLARY NETWORKS IN SCAFFOLDS CULTURED IN VITRO

Based on the screening studies performed on fibrin gel, we chose to supplement all osteogenic medium with BMP-2 for its role in maintaining the viability of the endothelial population. HUVECs and hMSCs were seeded uniformly throughout the decellularized bone scaffold and located predominantly on the wall surfaces (Fig. S3). The DNA content of constructs revealed that OM enhanced cell proliferation considerably more than EGM ($p < 0.05$). This was clearly a specific cellular response to factors in the OM medium since EGM|cocktail also had more cells than EGM only. Not surprisingly, Group 4 (EGM|cocktail+MSC) and Group 5 (OM|cocktail) had the most cells (Fig. 2), given that more cells were added to these constructs. Confocal microscopy demonstrated cell viability in all groups (Live/Dead assay) and robust capillary networks, in Group 3 and Group 4 (calcein assay) (Fig. 2).

The two control groups, OM (Group 1, osteo-induction) and EGM (Group 2, vascular induction) were compared to Groups 3, 4 and 5 where vascular supplements were applied in sequence with osteogenic supplements. Anti-human CD31 and vWF staining demonstrated formation of vascular structures in all groups except for the OM (Group 1). Vascular structures were clearly most developed in EGM|cocktail (Group 3) and EGM|cocktail+MSC (Group 4). While there were CD31 and vWF positive cells in the OM|cocktail groups, the vascular networks did not show signs of maturity as evidenced by the sizes of lumens in the structures (Fig. 3).

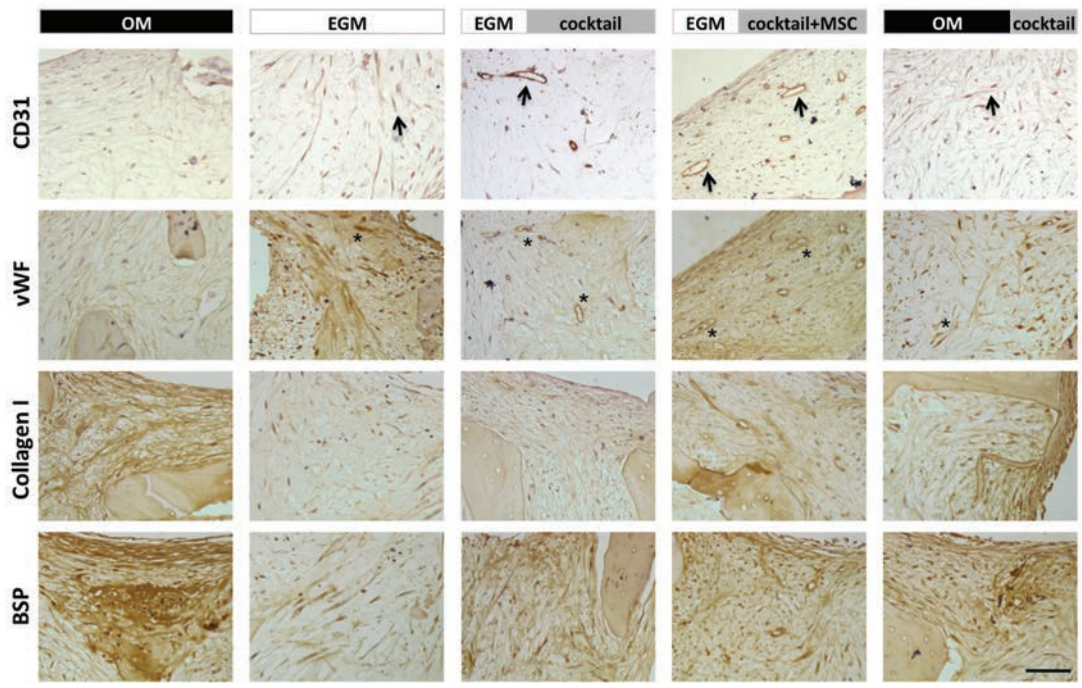

Figure 3. Immunohistological analysis of constructs cultured *in vitro*. Engineered bone grafts were evaluated for the expression of vascular and osteogenic proteins. CD31 (black arrows) and vWF

(indicated by *) expression was observed in constructs from all groups. Vascular structures were most developed in EGM|cocktail and EGM|cocktail+MSC groups. Collagen I & BSP were readily apparent in the OM group. Expression was observed in individual cells in EGM group, but not distributed through matrix. Both collagen I & BSP were observed in all other groups. In EGM|cocktail+MSC group, BSP appeared in close proximity to the vascular structures. Scale bar = 20 µm.

The OM group stained most intensely for collagen I and bone sialoprotein II (BSP), which are indicative of osteogenic differentiation, with incorporation of both collagen and BSP into the new tissue matrix. In contrast, the osteogenic markers in the EGM group were confined to individual cells. In the EGM|cocktail+MSC group, high expression of BSP was observed in spatial proximity to lumenal structures (Fig. 3). BV/TV of tissue constructs, determined by µCT, demonstrated a concordant trend: constructs that were cultured for 6 weeks in osteogenic medium showed the highest BV/TV, while those cultured in endothelial growth medium, show the lowest BV/TV that was close to that observed for unseeded scaffolds. In all other groups, the BV/TV was comparable to that in the OM group, being highest for the EGM|cocktail+MSC group (Fig. 4).

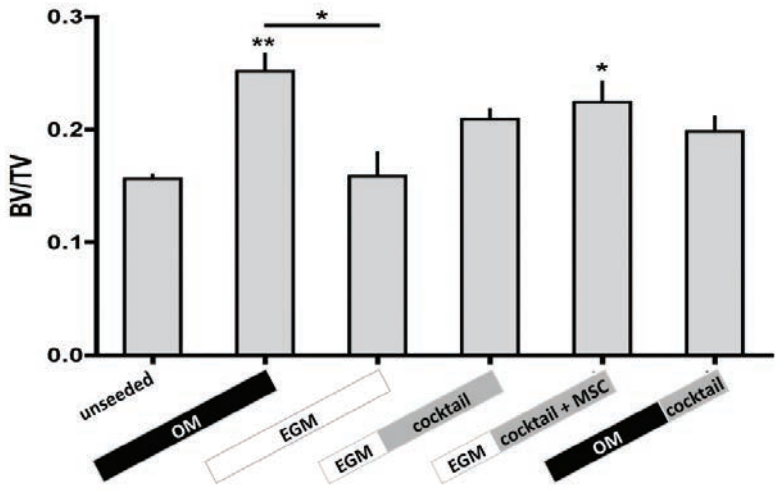

Figure 4. Ratio of bone material volume over tissue volume (BV/TV) of constructs after *in vitro* culture. n = 3; * indicate $p < 0.05$ and ** indicate $p < 0.001$ in comparison to unseeded group. # indicate $p < 0.05$ among both groups.

3.3. PROPERTIES OF CAPILLARY NETWORKS IN VIVO

Macroscopic photographs taken with the stereomicroscope indicated in-growth of large, well-developed blood vessels into each of the constructs (Fig. 5). In some groups, blood perfusion

through microvascular network structures was also observed. Only a few capillaries were seen in the OM group, as compared to a higher vascular density in the EGM group. Groups 3 and 4, where vasculogenesis was induced prior to osteogenic differentiation, showed the development of the most robust capillary networks.

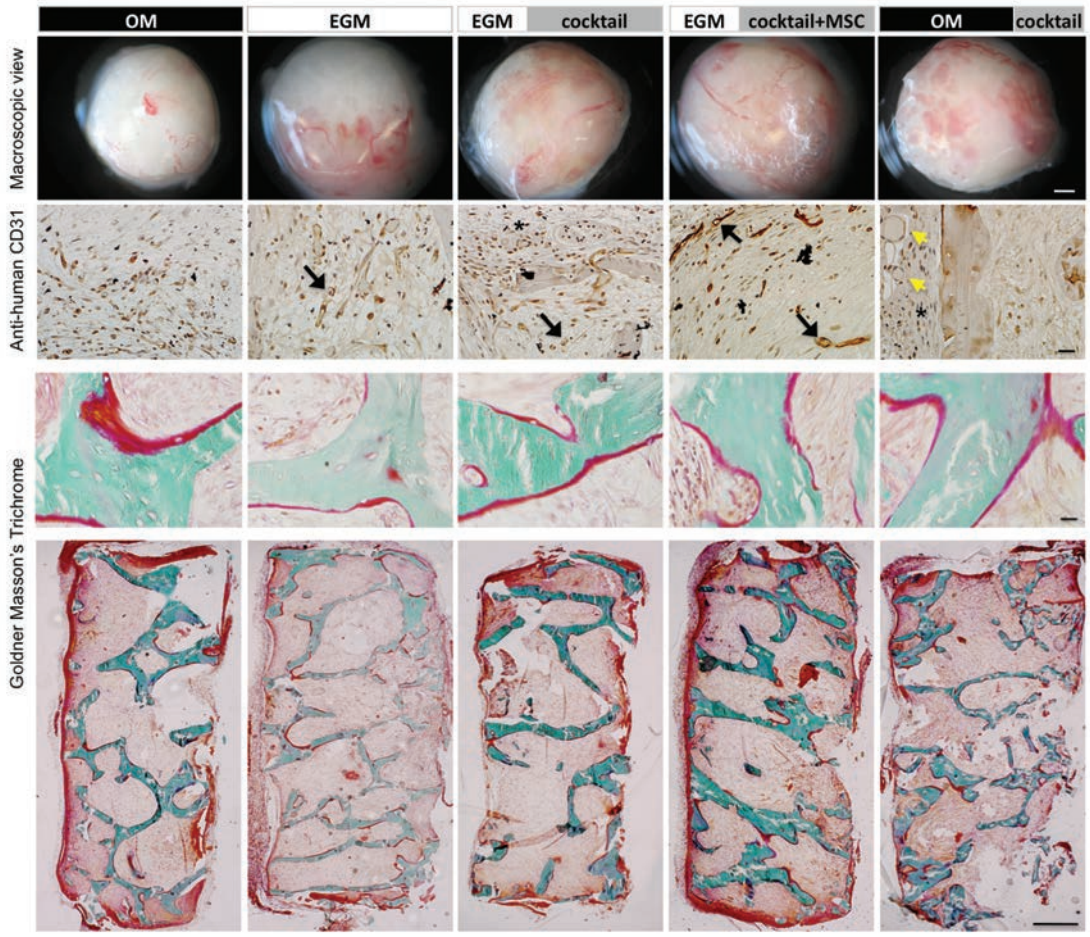

Figure 5. Composition of engineered grafts. Top row: Gross images of constructs post-harvest showing the translucent capsule and the in-growth of blood vessels. Constructs are perfused to different extents in different experimental groups. The large blood vessels also seem to anastomose to engineered microvasculature resulting in blood flow through capillary-like networks. This is particularly evident in EGM|cocktail and EGM|cocktail+MSC groups. Scale bar = 500 μm. Second row: Constructs were stained with anti-human CD31. Capsular region filled with mouse cells are shown with asterisks (*). In EGM|cocktail and EGM|cocktail+MSC groups, lumen (stained with anti-human CD31) are larger and well-developed (black arrows) with red blood cells inside (stained with hematoxylin). In OM|cocktail group, there is little evidence of human-derived vascular tissue. Large vessel-like structures in the capsular region are not stained with anti-human CD31 mAb and are probably of mouse origin (yellow arrow heads). Scale bar = 50 μm. Rows 3 and 4: *In vivo* bone development. Goldner's Masson trichrome staining of non-decalcified constructs indicate distinct levels of osteoid formation among groups (red stains). Third row: scale bar = 20 μm, Bottom row: scale bar = 500 μm.

Decalcified constructs were stained with anti-human CD31 to confirm that the vascular networks present prior to implantation remained viable and functional *in vivo*. Positively stained structures were found with cells inside, in all groups where vasculogenesis was induced prior to osteogenesis (Groups 3 and 4) suggesting that the perfused microvasculature might be of human origin (Fig. 5 and Fig. S4). Although there were positively stained cells in the OM|cocktail group, these vessels were not well developed and there was no evidence of perfusion. Non-decalcified grafts harvested from *in vivo* studies were stained with Goldner's Masson Trichrome to visualize osteoids, which were observed to a higher extent in the OM and EGM|cocktail+MSC groups. Clearly, the least osteoid formation was observed in the EGM group.

3.4. PROPOSED MODEL OF THE DEVELOPMENT OF VASCULARIZED BONE IN VITRO

In initial hydrogel studies, we found that providing osteogenic medium to co-cultures of HUVECs and hMSCs was detrimental to vascular formation. As a result, subsequent studies induced robust vascular development through the application of EGM for two weeks. Early studies demonstrated that the capillary-like structures were formed by HUVECs within a couple days and were only stable in the presence of hMSCs. This suggests that the hMSCs may be playing a pericyte-like role in this system (Figure 6).

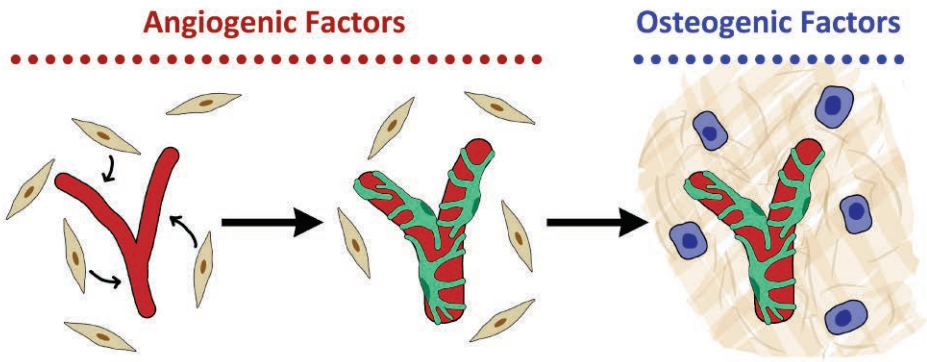

Figure 6. Model of *in vitro* coordination of vascular and bone tissue development. In a co-culture of ECs and hMSCs (beige, spindle-shaped cells), angiogenic supplements provide cues to stimulate the formation of primitive vascular networks (red) by the ECs (dispersed ECs are not shown in the model). These, in turn, recruit hMSCs into a pericyte-like role (green) that enables the vascular network to remain stable when osteogenic cues are provided. These cues induce osteoblast formation (blue cells) and deposition of mineralized matrix (beige).

One prevailing view in the literature is that the process of perivascular cell migration and recruitment is mediated by PDGFR signaling [24-26]. Sequential addition of osteogenic factors to the EGM, and potential BMP expression by EC's [27] facilitated *de novo* bone formation by undifferentiated hMSCs over a period of several weeks. The bone formation was augmented when osteo-induced MSCs were added to the bone scaffolds at the same time as the osteogenic supplements. Moreover, several studies have shown that BMP stimulate VEGF expression in osteoblasts, and VEGF up-regulate BMP-2 mRNA and protein expression in microvascular endothelial cells [27, 28].

4. DISCUSSION

The major goal of this study was to test the hypothesis that the sequential application of growth factors, to first induce the formation of stable vasculature and then initiate osteogenic differentiation, could provide a biologically-inspired *in vitro* model of bone vascularization. To this end, we systematically studied cultivation conditions that give rise to both functional vascular structures and robust osteogenesis using HUVEC-MSC co-cultures in conjunction with previously developed tissue engineering and bioreactor methods [19, 20, 29]. We propose that the system used in this study might provide a high-fidelity tissue engineering model of vascularized bone for mechanistic studies of heterotypic cell-cell interactions between endothelial cells and osteo-progenitors. In fact, a recent study showing that vascular endothelial cells may possess an intrinsic capability of transitioning to mesenchymal progenitors [30] opens tremendous possibilities for the role of endothelial cells in this model.

In our model, the MSCs have two major roles: as pericytes stabilizing vascular networks and as osteogenic progenitors forming mineralized bone matrix. Several published studies show that bone marrow-derived MSCs adopt pericyte-like locations during *in vitro* co-culture with mature endothelial cells [15, 31, 32] or when co-delivered *in vivo* with mature endothelial cells [24, 33, 34]. Our study supports these previous observations as the capillary-like structures formed by HUVECs were only stable in the presence of hMSCs (Fig. S1).

The ability of MSCs to respond with spatial and temporal specificity to differentiation cues was key in gel studies where all cells were seeded at the beginning of culture and no cells could be introduced at later stages of culture (supplemental data). From these preliminary studies, several key outcomes were identified that determined the selection of experimental groups for the subsequent scaffold study: (i) a sequential-induction approach enabled vascular-osteogenic outcomes within the same culture space, with the need for endothelial growth factors to be

provided prior to osteogenic induction, and (ii) the role of BMPs as a vascular promoter was confirmed [35] even during *in vitro* culture. Mineralization of the tissue matrix was evident in the groups containing vascular networks, although to limited extent as cells were exposed to osteo-inductive medium for only two weeks. Thus, a longer osteo-induction period was adopted during scaffold studies.

Trabecular bone scaffolds also provided great versatility of the *in vitro* co-culture system and enabled the evaluation of concurrent supplementation of growth factors and fresh MSCs responding to these growth factors. We also investigated the hypothesis of MSCs losing their ability to respond to osteogenic factors during the two-week exposure to vascular supplements, by comparing Group 4 (EGM|cocktail+MSC, in which osteo-induced MSCs were added along with cocktail medium) with the Group 3 (EGM|cocktail, in which the same MSCs present at the beginning of culture were exposed to cocktail medium). Data suggests that fresh MSCs enhance bone formation, as verified by increased bone volume fraction (Fig. 4), osteoid deposition (Fig. 5), and spatial proximity of bone proteins to vascular networks (Fig. 3). However the addition of additional MSCs is not critical, as bone formation also occurred in Group 3 (EGM|cocktail). This suggests that MSCs may act initially as pericytes [15, 31, 32], but maintain the ability to undergo osteogenesis, which is arguably consistent with the prior evidence that osteoblasts take up pericytic locations *in vivo* [3].

By adding HUVECs at the latter stages of culture, it was possible to evaluate osteogenesis that has been induced in the scaffolds prior to providing vascular cells and growth factors, an approach similar to that taken by Tsigkou et al [15]. This approach to improve vascularized bone tissue development (OM|cocktail group) was moderately successful: we observed reasonable osteogenic development as evidenced by deposition of bone protein, osteoid formation and the BV/TV ratio. However, two-week exposure to vascular growth factors was not sufficient to develop robust vascular structures, as evidenced by the sizes of vessel lumens that were smaller than those observed in Groups 3 and 4. In these two groups, not only lumen were evident after *in vitro* cultivation, they also anastomosed well during *in vivo* implantation, which is consistent with the earlier reports that well-developed vascular networks are necessary for functional anastomosis [36-39], although recent studies suggest that is also possible to obtain functional network formation without extensive *in vitro* cultivation [8, 15]. These studies open several under-explored areas of investigation. For example, the DNA content was considerably higher in the OM group relative to the EGM group, suggesting that HUVECs may have survived better as a result of BMP2 supplementation in osteogenic media (Fig. 4).

In future studies, it might be relevant to distinguish whether HUVECs and MSCs are equally stimulated in this group and to decipher the role of cell proliferation in tissue development. Also, despite promising results, our studies suggest that alternative cocktails (e.g. EGM|OM or increased vascular growth factor concentration in OM|cocktail group) could be tested to synergistically improve mineralization with vascular network formation. Likewise, further studies are needed to optimize the temporal stages of culture, as the two-week period of vascular induction was selected based on the robust network structures observed for fibrin gel studies.

Overall, by providing temporal variation of the culture environment, we were able to demonstrate the ability to derive vascular networks and induce *bona fide* osteogenic differentiation within single tissue grafts during *in vitro* cultivation. Notably, functional vascular networks and viable osteoid formation were detected post-implantation. The most successful approach involved induction of vasculogenesis prior to osteogenesis, with the addition of osteo-induced MSC further improving tissue outcomes. Finally, while the focus of our study was to evaluate 'functional' outcomes such as vessel formation and matrix mineralization, significantly more work is needed to elucidate the underlying mechanisms that regulate heterotypic interactions and understand the interactive roles of multiple growth factors.

In summary, it has long been accepted that vascularization is essential for the advancement of tissue-engineered bone grafts to clinical application [40]. Due to the close interaction between MSCs and HUVECs in co-culture systems, it may be possible to utilize the proposed tissue engineering model as a controllable experimental tool to elucidate other molecular mechanisms regulating the heterotypic cell-cell interactions. Such studies could have relevance for gaining further insights into developmental processes [41] and cellular interactions under conditions of disease.

Acknowledgements

We gratefully acknowledge funding support of this work by the NIH (DE161525 and EB02520 to GVN), the ORS Career Development Award (to WG), and the FCT PhD grant (SFRH/BD/42316/2007 to CC). The authors thank Sarindr Bhumiratana, and George Eng for their help with the experiments.

References

1. Mikos, A.G., et al., *Engineering complex tissues.* Tissue Engineering, 2006. 12(12): p. 3307-3339.
2. Wang, Y., et al., *The hypoxia-inducible factor a pathway couples angiogenesis to osteogenesis during skeletal development.* Journal of Clinical Investigation, 2007. 117(6): p. 1616-1626.
3. Maes, C., et al., *Osteoblast Precursors, but Not Mature Osteoblasts, Move into Developing and Fractured Bones along with Invading Blood Vessels.* Developmental Cell, 2010. 19(2): p. 329-344.
4. Hofmann, A., et al., *The effect of human osteoblasts on proliferation and neo-vessel formation of human umbilical vein endothelial cells in a long-term 3D co-culture on polyurethane scaffolds.* Biomaterials, 2008. 29(31): p. 4217-4226.
5. Choong, C.S.N., D.W. Hutmacher, and J.T. Triffitt, *Co-culture of bone marrow fibroblasts and endothelial cells on modified polycaprolactone substrates for enhanced potentials in bone tissue engineering.* Tissue Engineering, 2006. 12(9): p. 2521-2531.
6. Kaigler, D., et al., *Endothelial cell modulation of bone marrow stromal cell osteogenic potential.* Faseb J, 2005. 19(6): p. 665-7.
7. Rouwkema, J., J. De Boer, and C.A. Van Blitterswijk, *Endothelial cells assemble into a 3-dimensional prevascular network in a bone tissue engineering construct.* Tissue Engineering, 2006. 12(9): p. 2685-2693.
8. Unger, R.E., et al., *The rapid anastomosis between prevascularized networks on silk fibroin scaffolds generated in vitro with cocultures of human microvascular endothelial and osteoblast cells and the host vasculature.* Biomaterials, 2010. 31(27): p. 6959-6967.
9. Villanueva, J.E. and M.E. Nimni, *PROMOTION OF CALVARIAL CELL OSTEOGENESIS BY ENDOTHELIAL-CELLS.* Journal of Bone and Mineral Research, 1990. 5(7): p. 733-739.
10. Villars, F., et al., *Effect of HUVEC on human osteoprogenitor cell differentiation needs heterotypic gap junction communication.* Am J Physiol Cell Physiol, 2002. 282(4): p. C775-85.
11. Bidarra, S.J., et al., *Phenotypic and proliferative modulation of human mesenchymal stem cells via crosstalk with endothelial cells.* Stem Cell Res, 2011. 7(3): p. 186-97.
12. Grellier, M., et al., *The effect of the co-immobilization of human osteoprogenitors and endothelial cells within alginate microspheres on mineralization in a bone defect.* Biomaterials, 2009. 30(19): p. 3271-8.
13. Meury, T., S. Verrier, and M. Alini, *Human endothelial cells inhibit BMSC differentiation into mature osteoblasts in vitro by interfering with osterix expression.* Journal of Cellular Biochemistry, 2006. 98(4): p. 992-1006.
14. Clarkin, C.E., et al., *Heterotypic contact reveals a COX-2-mediated suppression of osteoblast differentiation by endothelial cells: A negative modulatory role for prostanoids in VEGF-mediated cell: cell communication?* Exp Cell Res, 2008. 314(17): p. 3152-61.
15. Tsigkou, O., et al., *Engineered vascularized bone grafts.* Proceedings of the National Academy of Sciences of the United States of America, 2010. 107(8): p. 3311-3316.
16. Usami, K., et al., *Composite implantation of mesenchymal stem cells with endothelial progenitor cells enhances tissue-engineered bone formation.* Journal of Biomedical Materials Research Part A, 2009. 90A(3): p. 730-741.
17. Koob, S., et al., *Effect of endothelial and mesenchymal stem cell co-seeding on healing of critical-sized defects in murine calvarial bone.* British Journal of Surgery, 2010. 97: p. S55-S56.
18. Moioli, E.K., et al., *Synergistic Actions of Hematopoietic and Mesenchymal Stem/Progenitor Cells in Vascularizing Bioengineered Tissues.* Plos One, 2008. 3(12): p. -.
19. Grayson, W.L., et al., *Engineering anatomically shaped human bone grafts.* Proc Natl Acad Sci U S A, 2010. 107(8): p. 3299-304.
20. Grayson, W.L., et al., *Optimizing the Medium Perfusion Rate in Bone Tissue Engineering Bioreactors.* Biotechnology and Bioengineering, 2011. 108(5): p. 1159-1170.
21. Bhumiratana, S., et al., *Nucleation and growth of mineralized bone matrix on silk-hydroxyapatite composite scaffolds.* Biomaterials, 2011. 32(11): p. 2812-20.
22. Grayson, W.L., et al., *Effects of initial seeding density and fluid perfusion rate on formation of tissue-engineered bone.* Tissue Eng A, 2008. 14(11): p. 1809-1820.

23. Liu, X.W.S., et al., *Quantification of the roles of trabecular microarchitecture and trabecular type in determining the elastic modulus of human trabecular bone.* Journal of Bone and Mineral Research, 2006. 21(10): p. 1608-1617.
24. Au, P., et al., *Bone marrow-derived mesenchymal stem cells facilitate engineering of long-lasting functional vasculature.* Blood, 2008. 111(9): p. 4551-8.
25. Hirschi, K.K., S.A. Rohovsky, and P.A. D'Amore, *PDGF, TGF-beta, and heterotypic cell-cell interactions mediate endothelial cell-induced recruitment of 10T1/2 cells and their differentiation to a smooth muscle fate.* J Cell Biol, 1998. 141(3): p. 805-14.
26. Lindahl, P., et al., *Pericyte loss and microaneurysm formation in PDGF-B-deficient mice.* Science, 1997. 277(5323): p. 242-5.
27. Bouletreau, P.J., et al., *Hypoxia and VEGF up-regulate BMP-2 mRNA and protein expression in microvascular endothelial cells: implications for fracture healing.* Plast Reconstr Surg, 2002. 109(7): p. 2384-97.
28. Deckers, M.M., et al., *Bone morphogenetic proteins stimulate angiogenesis through osteoblast-derived vascular endothelial growth factor A.* Endocrinology, 2002. 143(4): p. 1545-53.
29. Grayson, W.L., et al., *Spatial regulation of human mesenchymal stem cell differentiation in engineered osteochondral constructs: effects of pre-differentiation, soluble factors and medium perfusion.* Osteoarthritis and Cartilage, 2010. 18(5): p. 714-723.
30. Medici, D., et al., *Conversion of vascular endothelial cells into multipotent stem-like cells.* Nature Medicine, 2010. 16(12): p. 1400-U80.
31. Koob, S., et al., *Bone formation and neovascularization mediated by mesenchymal stem cells and endothelial cells in critical-sized calvarial defects.* Tissue Eng Part A, 2011. 17(3-4): p. 311-21.
32. Klein, D., et al., *Vascular wall-resident CD44+ multipotent stem cells give rise to pericytes and smooth muscle cells and contribute to new vessel maturation.* Plos One, 2011. 6(5): p. e20540.
33. Ozerdem, U. and W.B. Stallcup, *Early contribution of pericytes to angiogenic sprouting and tube formation.* Angiogenesis, 2003. 6(3): p. 241-9.
34. Rajantie, I., et al., *Adult bone marrow-derived cells recruited during angiogenesis comprise precursors for periendothelial vascular mural cells.* Blood, 2004. 104(7): p. 2084-6.
35. Zhang, F.J., et al., *Sustained BMP Signaling in Osteoblasts Stimulates Bone Formation by Promoting Angiogenesis and Osteoblast Differentiation.* Journal of Bone and Mineral Research, 2009. 24(7): p. 1224-1233.
36. Koike, N., et al., *Creation of long-lasting blood vessels.* Nature, 2004. 428(6979): p. 138-139.
37. Rouwkema, J., N.C. Rivron, and C.A. van Blitterswijk, *Vascularization in tissue engineering.* Trends in Biotechnology, 2008. 26(8): p. 434-441.
38. Chen, X.F., et al., *Prevascularization of a Fibrin-Based Tissue Construct Accelerates the Formation of Functional Anastomosis with Host Vasculature.* Tissue Engineering Part A, 2009. 15(6): p. 1363-1371.
39. Levenberg, S., et al., *Engineering vascularized skeletal muscle tissue.* Nature Biotechnology, 2005. 23(7): p. 879-884.
40. Laschke, M.W., et al., *Angiogenesis in tissue engineering: Breathing life into constructed tissue substitutes.* Tissue Engineering, 2006. 12(8): p. 2093-2104.
41. Ingber, D.E. and M. Levin, *What lies at the interface of regenerative medicine and developmental biology?* Development, 2007. 134(14): p. 2541-2547.

Supporting Information

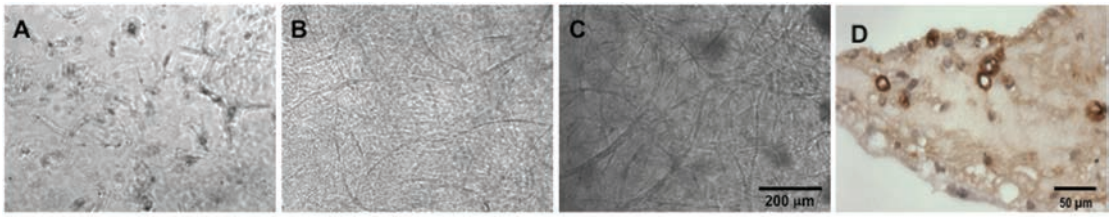

Figure S1: Gel cultivation. A: HUVECs only at 3 weeks in EGM-2. Co-culture of HUVECs with MSCs (1:1) enables formation of stable micro-vasculature networks at 3 weeks in EGM-2 (B) that last up to 12 weeks (C) during *in vitro* culture. D: von Willebrand Factor (vWF) staining of lumen.

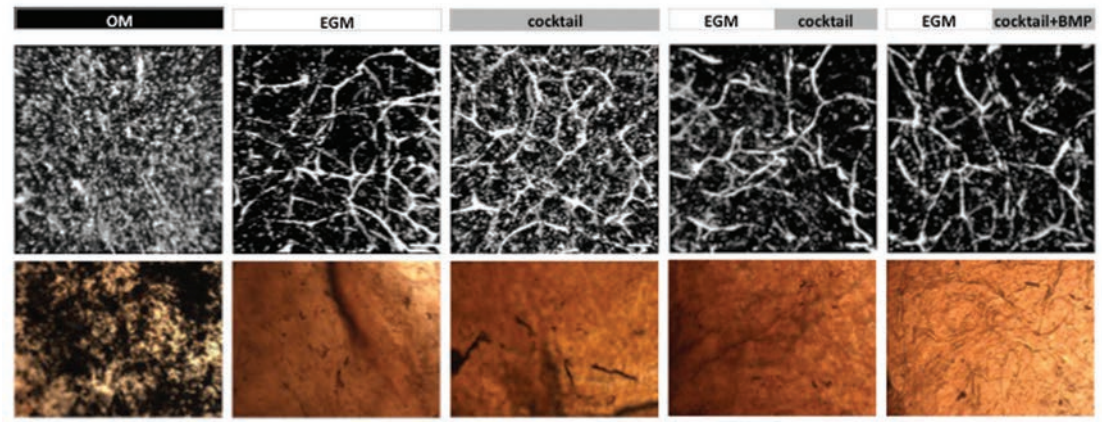

Figure S2: Gel screening studies. HUVECs (pre-stained with Di-I) and MSCs were encapsulated in fibrin hydrogels (1:1 ratio) and cultured in small wells for 4 weeks to determine cellular responses to different medium conditions. Confocal images were used to evaluate vascular network formation and provide a read-out on HUVEC viability (cellular debris). Scale bar= 50 µm. Bottom row: von Kossa staining of mineral deposition within the gel regions. Mineral is shown as black/dark brown stains within the gels.

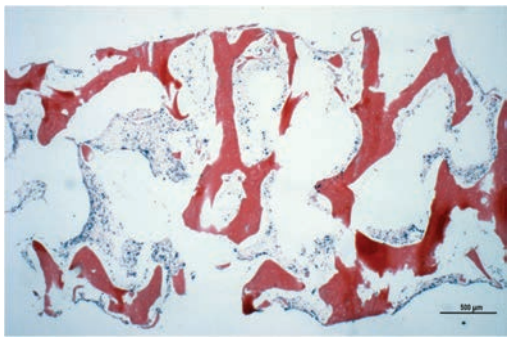

Figure S3: H&E staining of constructs at day 1. Cells are uniformly distributed throughout the scaffold upon seeding. Cells are located predominantly on the wall surfaces of scaffolds but grow into pore spaces subsequently.

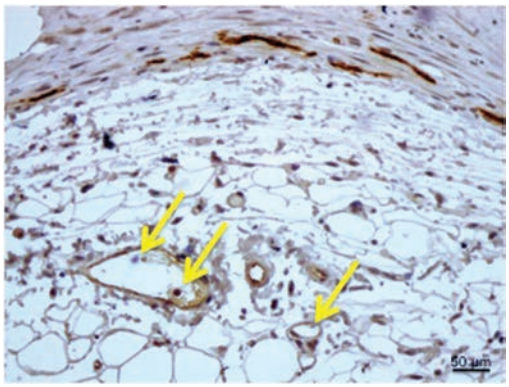

Figure S4: EGM|cocktail+MSC group stained with anti-human CD31 mAb. Human origin lumen, with red blood cells inside (stained with hematoxylin) are pointed with yellow arrows.

Section 6.

CHAPTER IX

Major conclusions and future perspectives

Major conclusions

Tissue engineering has proven its potential on providing valuable solutions to overcome the clinical need for regeneration and replacement of diseased tissues.

In the orthopaedic field, joint ailments are one of the major drawbacks causing physical disability, limited activity, pain and reduced quality of life. In addition, joint ailments affect population of all ages, at a global scale, and are usually lifetime enduring.

Among the distinct pathologies affecting joints, osteochondral lesions – where articular cartilage and underlying bone are damaged - present particular challenges to be overcome:

- Osteochondral tissue is composed by a layer of hydrated soft cartilagineous tissue, composed of one cell type in a dense matrix; and the bone compartment, a dynamic, stiff and complex tissue, composed of a highly organized structure, several cell types, which demand an impregnated vascular network for survival.
- The hierarchical structure, composition and mechanical properties specific of this tissue require the design of particular tools and strategies, by combining living cells, biomaterial scaffolds as templates, biochemical cues and bioreactors, this later providing precise environmental control and physical stimuli which mimic their unique physiologic biomechanical context.

Aimed at improving current knowledge on *in vitro* engineering of cartilage and bone tissues, this thesis gathers a set of experimental approaches focused on the use of adipose tissue derived stem cells as single cell source to engineer both cartilaginous and osteogenic components, including the vasculogenic compartment of bone. To this end, we have additionally explored biomechanical cues, such as hydrostatic pressure stimulation for cartilage and flow perfusion for bone, and biochemical cues, such as chondrogenic, osteogenic and endothelial growth factors, alone or in combination, to better engineer cartilaginous and osteogenic tissues.

Adipose stem cells of human origin (hASC) were used in this thesis as single cell source for the development of both tissues. The potential of these adult mesenchymal stem cells was extensively explored, due to their unique characteristics that makes them attractive for the purpose of osteochondral tissue engineering:

1. Adipose tissue harvesting and processing procedures, leading to stem cell isolation, are simple and expedite, which are advantageous aspects towards clinical application;

2. hASC differentiation capacity into the chondrogenic and osteogenic lineages was confirmed, and their potential use for vasculogenesis was further suggested and supported;
3. Not only differentiation capacity was confirmed, but also robust and viable 3D tissues were developed by hASC culturing;
4. Biomechanical stimulation of hASC-scaffold constructs demonstrated that hASC detect physical forces of distinct nature (hydrostatic pressure and shear stress), magnitude and frequency, by responding diversely in terms of gene expression and matrix deposition.

On what concerns the improvement of *in vitro* engineered cartilage tissue, two custom-made bioreactor systems were developed, being capable of generating and applying, in a controlled manner, hydrostatic pressure (HP) as biomechanical stimuli - at high and low magnitudes - to 3D tissue engineering constructs. These devices hold key characteristics such as:

1. Capacity of long term culturing (several weeks) of 3D constructs of distinct size and shape, in standard biohazard hood and CO_2 incubator, in compliance with good cell culturing practices;
2. Tunable loading parameters, namely HP magnitude (0-0.4 MPa for low HP bioreactor and 1.5-10 MPa for high HP bioreactor), and frequency (0-1 Hz). Specific device design leads to minimal need for operator manipulation.

In this particular study, hASC were encapsulated in gellan gum hydrogels (ASC-GG), a biomaterial previously developed by our research group, which has proven adequate properties, such as biomechanical performance and structural versatility. More than hypothesizing the ability of hASC to sense and respond to pulsatile HP mechanical stimulation at 0.4 MPa, by increasing chondrogenic differentiation and improving cartilage tissue development, we have questioned the influence of physiologic levels of HP (5 MPa) on the magnitude of these outcomes. Both hypotheses were proven:

1. hASC sense and respond to pulsatile hydrostatic pressure stimulation at low (0.4 MPa) and physiologic (5 MPa) pressure ranges;
2. Physiologic HP amplitudes promoted a higher and better tissue matrix distribution, which resembles native articular cartilage.

This approach may be proposed as an alternative strategy to current chondrocyte-based therapies for the repair of focal cartilage lesions. It benefits from a cell source that is abundant

and rapidly accessible, provides very high yields per volume of tissue, and may therefore minimize or even avoid lengthy cell expansion periods.

Maintaining hASCs as cell source, potential templates for bone tissue engineering were further investigated. Different types of silk-based scaffolds were fabricated varying in soluble reagent (aqueous vs. hexafluoro-2-propanol (HFIP)), pore size (250-400μm vs. 400-600μm) and porous structure:

1. aqueous, spherical-pore structure, small pores (250-500 μm);
2. aqueous, spherical-pore structure, large pores (500-1000 μm);
3. aqueous, lamellar structure,
4. HFIP-derived, medium pore sizes (400-600 μm), and

After 7 weeks of static culturing with osteogenic cues, HFIP-derived silk fibroin scaffolds, which exhibited higher stiffness as compared to aqueous-based silk fibroin scaffolds, appeared to provide a better platform for bone formation, in terms of deposition of matrix proteins (OPN, BSP, Col I), mineralization and mechanical properties of engineered constructs. The bone formation was equally distributed throughout the scaffold showing homogenous osteogenic activity of hASCs.

Despite the encouraging results achieved using static culturing, we aimed to further augment bone tissue formation by hASC osteogenic differentiation using this porous silk scaffold, by applying a sequence of steady (400 μm/s) and pulsatile flows (ranging from 400 μm/s to 1200 μm/s, at 0.5 Hz), associated with fluctuating shear stresses (0.045 – 0.134 dyn/cm^2). We aimed to understand the importance of osteogenic pre-differentiation of hASC for the achievement of this goal – 1 or 2 weeks of pre-differentiation culturing was performed under steady perfusion. Our aim was accomplished, as all pulsatile flow regimes improved bone tissue development over steady flow - the prevalent regime adopted by literature. Cell response to pulsatile fluid flow was progressively enhanced with the increase of steady flow culturing time, being maximum for 2 weeks of culture. These findings are consistent with the notion that osteogenic hASC gradually develops mechanisms to detect and respond to changes in shear stress.

The same cell-scaffold system was further used to engineer vascularized bone, under static conditions, by managing spatio-temporal cues. Three strategies were evaluated:

1. induction of osteogenesis prior to vasculogenesis,

2. induction of vasculogenesis prior to osteogenesis, or
3. simultaneous induction of osteogenesis and vasculogenesis.

After 5 weeks of culture, bone development was evidenced by the deposition of bone matrix proteins, alkaline phosphatase activity and calcium deposition, along with the formation of vascular networks evidenced by endothelial cell surface markers, such as CD31 and von Willebrand factor, and morphometric analysis. The most robust development of the two tissue compartments was achieved by sequential induction of osteogenesis followed by the induction of vasculogenesis. Taken together, the collected data strongly supports the utility of hASC as a potential single cell source for the formation of vascularized bone tissue.

In parallel, an original *in vitro* model was also developed, where HUVECs and hMSC were co-cultured in order to grow vascularized bone under temporal variation of the culture environment. We were able to derive vascular networks and induce *bona fide* osteogenic differentiation within single tissue grafts *in vitro*. Functional vascular networks and viable osteoid formation were detected post-implantation in Severe Combined Immunodeficiency (SCID) mice. The most successful approach was achieved with induction of vasculogenesis prior to osteogenesis, for which the addition of osteo-induced MSC further improved tissue outcomes. Due to the close interaction between MSCs and HUVECs in co-culture systems, the proposed tissue engineering model may be useful as a controllable experimental tool to elucidate other molecular mechanisms regulating heterotypic cell-cell interactions.

As conclusion of this thesis, new approaches are proposed to engineer fully developed and functional cartilage and vascularized bone tissue that can be used individually or in combination to restore and/or regenerate osteochondral lesions: Experimental data demonstrates that hASC cultured in gellan gum hydrogels under physiological hydrostatic pressure loading differentiate into the chondrogenic lineage and secrete dense cartilaginous extracellular matrix, while, if cultured in a silk fibroin-based porous scaffold with adequate mechanical properties, under shear stress forces, hASC differentiate into the osteogenic lineage, producing a calcified robust bone-like tissue. Moreover, when the appropriate spatial and temporal nourishment of growth factors where provided to hASC, both osteogenic and vascular compartments of bone tissue were identified, which add strength to the proposal of using hASC as single cell source to fully engineer osteochondral tissues.

Future perspectives

Although results obtained prove successful use of human adipose stem cells for osteochondral tissue engineering, research in three additional directions are considered fundamental to consolidate the merits of such approach, namely:

1) Exploitation of fluid perfusion as a biomechanical stimulation route of hASC endothelial differentiation in order to optimize blood vessel formation;
2) Research regarding concurrent development of both bone and vessel compartments using hASC, in terms of timing and nature of biochemical and mechanical stimulation;
3) Combination of both cartilaginous and osteogenic compartments into an integral, viable and functional osteochondral graft for further *in vivo* evaluation in animal models where relevant osteochondral pathologies are truly replicated so that:
    a. Surgical procedures and rehabilitation procedures can be jointly developed and tested;
    b. Long-term tissue integration can be properly evaluated.